Paleoproterozoic Snowball Earth?
Sedimentology and Geochemistry of a Huronian Glacial Cycle

Sophie Kurucz

Supervised by: Dr. Philip Fralick

Thesis Submitted in Partial Fulfillment of the
Requirements for the Degree of
Master of Science (Geology)
2019

Lakehead
UNIVERSITY

In the
Department of Geology
Faculty of Science and Environmental Studies
Lakehead University

ABSTRACT

The study discusses new sedimentological and geochemical results for the Paleoproterozoic Bruce glacial cycle, which represents the second of three glacial cycles within the Huronian Supergroup. This Bruce glacial event is unique for its cap carbonate, the Espanola Formation, which directly overlies glacial diamictites of the Bruce Formation. Cap carbonates are ubiquitous overlying glacial sediments in Neoproterozoic successions and are believed to be precipitated as a direct result of deglaciation. An investigation of the Bruce glacial cycle has led to a summary of the depositional history, wherein the Bruce ice sheet was grounded as it entered the Huronian basin and overrode outwash of the Mississagi Formation. It quickly delaminated, and deposited a uniform blanket of diamict before retreating, followed by the development of a glacial rebound sequence within the Espanola and Serpent Formations.

The upper Mississagi Formation directly underlies the glacial diamictites of the Bruce Formation and consists predominantly of planar and trough cross-stratified sandstones. These sandstones were deposited in a distal braided fluvial to deltaic system immediately prior to the advent of the local Bruce ice sheet advance. The Bruce ice sheet was grounded as it entered the basin, which is indicated by the typically sharp contact with the Mississagi Formation and the erosional uptake of Mississagi sands into the base of the Bruce. Delamination of the Bruce ice sheet and development of a floating ice shelf is illustrated by the dominance of massive, laterally continuous diamictites and evidence for current winnowing and iceberg rafting. These units, which constitute the majority of the Bruce Formation, were deposited beneath floating ice. Partial digestion of a carbonate-rich laminated dropstone lithofacies in the uppermost Bruce Formation for $\delta^{13}C_{carb}$ analysis produced highly negative values that are derived from a

methane seepage signature. These same samples also have REE patterns with consistent negative Eu anomalies that are the result of remobilizing reduced Eu^{2+} via the highly reducing fluids sourced from methane seepage.

The Espanola Formation, the cap carbonate which overlies the Bruce Formation glacial deposits, is typically separated from the underlying Formation by a 0.5-3m thick laminated rain-out siltstone unit. Overlying this unit, the stratigraphy of the Espanola Formation records a gradual shallowing upwards sequence, with the lower, offshore facies being dominated by laminated carbonate and siltstone with abundant contortion and slumping, and the middle and upper stratigraphy dominated by ripple and hummocky cross-lamination and intraformational conglomerate beds deposited in a higher energy nearshore environment. An upward trend, from ~-4‰ to -2.5‰ over approximately 110m, occurs in the $\delta^{13}C_{carb}$ of the carbonate fraction of the middle and upper stratigraphy in drill hole E150-2. These samples produce patterns that have a 'hat-shaped' distribution with middle REE-enrichment that is similar to patterns of some Neoproterozoic cap carbonates. These patterns are suggested to be a reflection of influence by both seawater and freshwater signatures.

The stratigraphy of the upper Espanola Formation gradually transitions into the lower Serpent Formation, another sandstone-dominated Formation that represents the completion of the glacial rebound cycle. Environments of deposition for the lower Serpent Formation are variable, but range from storm- tide- and wave-influenced nearshore settings to fluviodeltic with varying tidal influence. This sequence concludes the glacial rebound cycle of the Bruce ice sheet in the Huronian Supergroup.

ACKNOWLEDGEMENTS

I would like to extend my utmost gratitude to my thesis supervisor Dr. Philip Fralick for his guidance and mentorship over the years and throughout the development of this thesis. This project would also not have been possible without the help of field and drill core logging assistants Amy Cleaver and Teegan Ojala. I would also like to thank Greg Kepka at the Lakehead University Instrumentation Laboratory and Anne Hammond and Kristi Tavener at the Lakehead University Lapidary Facility for their work in preparing thin sections, polished slabs, and geochemical analytical work. Thank you to the analytical staff at the Pôle Spectométrie Océan in Brest for running the stable isotopic data, which contributed immensely to the findings of this study. Lastly, I would like to thank the students and faculty of the Department of Geology for providing an atmosphere of growth and challenge and to friends and family for all of their support.

TABLE OF CONTENTS

LIST OF FIGURES

1 INTRODUCTION

1.1 BACKGROUND

The focus of this study is the Paleoproterozoic Bruce glacial event, represented in the Quirke Lake Group of the Huronian Supergroup, a package of predominantly sedimentary rocks deposited on the margin of Superior craton (Figure 1). The Quirke Lake Group is the third of four Groups within the greater Huronian Supergroup and is believed to have been deposited by the second of three complete glacial advance-retreat cycles preserved (Frarey and Roscoe, 1971; Young, 1973a). While all three cycles contain a similar sequence of basal diamictite, overlain by fine-grained sedimentary rocks, and in turn overlain by coarser-grained clastics (Robertson et al., 1969; Eggertson, 1975), the Quirke Lake Group is unique in that it contains a carbonate-bearing sequence, the Espanola Formation, within the finer-grained sediments overlying the glacial tillite of the Bruce Formation (Frarey and Roscoe, 1971; Bekker et al., 2005). The presence of the Espanola Formation has led to numerous studies being completed on its geochemistry and sedimentary structures in an effort to shed light on the conditions that led to deposition of a carbonate unit above only one of three glacial units within the Huronian Supergroup (e.g. Eggertson, 1975; Veizer et al., 1992; Bekker et al., 2005; Young, 2013a).

Despite the abundance of research that has been conducted upon the Huronian Supergroup, and on the Espanola Formation in particular, a comprehensive study outlining the depositional environment leading into the Bruce glacial event, deposition of tillites during glaciation, and changes in environment during glacial retreat, is sorely lacking. Recent studies hypothesizing the Bruce glacial event as a possible Paleoproterozoic ‘Snowball Earth Event’ and

a suggested possible association with a rise in atmospheric oxygen (Kirschvink et al., 2000; Bekker et al., 2005; Hoffman, 2013) necessitates that the Bruce glacial event be described in its entirety. This may aid in reaching some conclusions as to whether or not the Bruce glacial event and the Espanola Formation reflect conditions that can be inferred to be global in their extent, or if the Espanola Formation was deposited through isolated conditions that reflect little else but the environment in which the Huronian Supergroup was deposited. These are deeply complicated questions, and this study may hopefully provide useful context that will assist in drawing conclusions as to the implications of the Bruce glacial event in the development of Paleoproterozoic atmospheric composition.

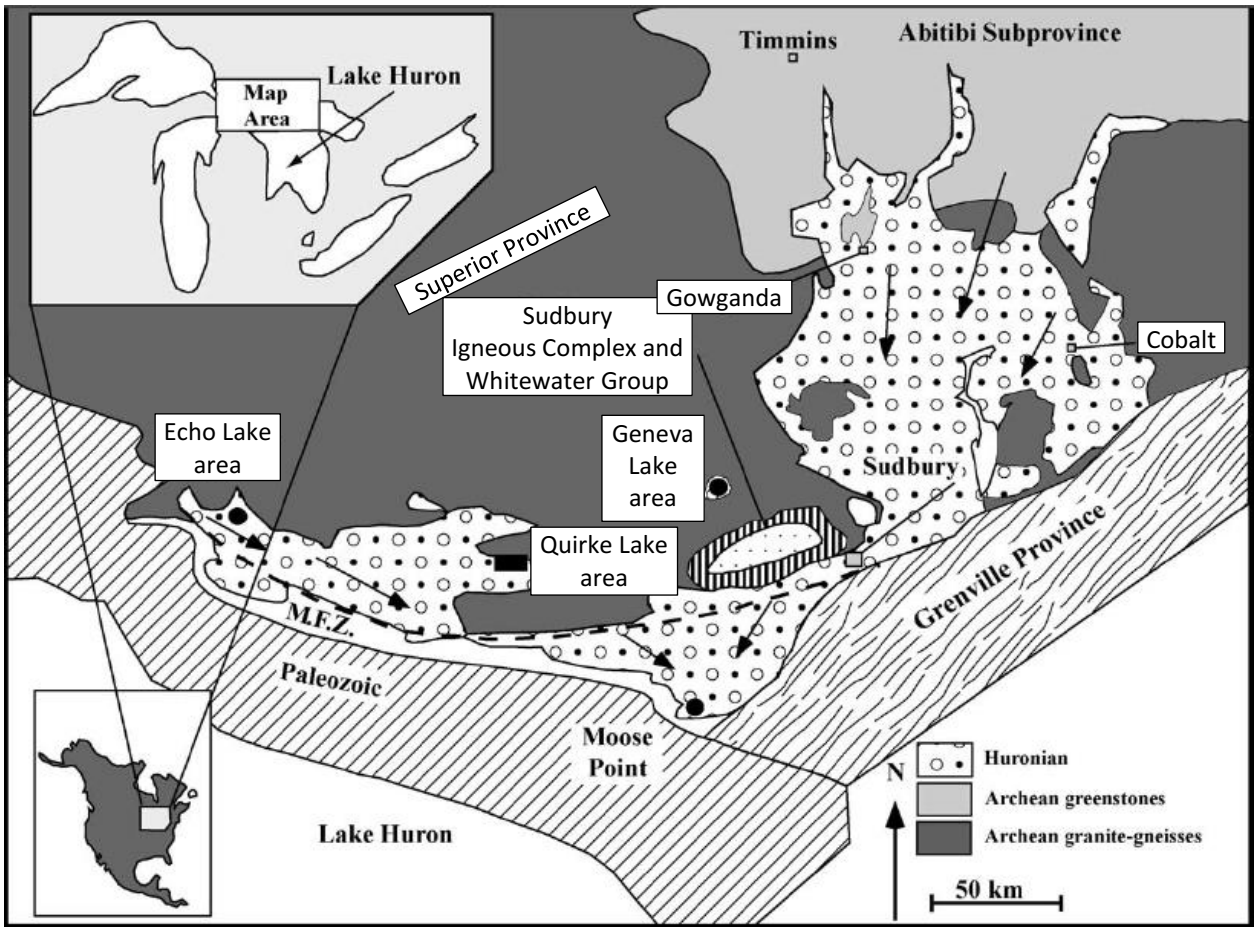

Figure 1: Map showing the outcrop extent and location of the Huronian Supergroup. Arrows depict average paleocurrent directions for the Huronian sediments. From Bekker et al. (2005).

1.2 PROTEROZOIC GLACIATIONS

The beginning and end of the Proterozoic Eon (2.5 Ga-542 Ma) represent unique periods in Earth's history when climatic changes preserved glacial cycles within the sedimentary rock record (Young, 2013b). Sedimentary evidence for glacial activity is ubiquitous in deposits from the Paleoproterozoic and Neoproterozoic, with at least 13 glacially deposited formations recognized from Paleoproterozoic rocks, and 90 formations in Neoproterozoic rocks, suggesting that glacial ice cover was extensive (Evans, 2003; Hoffman and Li, 2009; Evans and Raub, 2011; Hoffman, 2013). What has made the presence of the Proterozoic glacial events of even greater interest are observations of the Neoproterozoic glacial deposits made by early researchers such as Mawson (1949) and Harland (1964) who noted the presence of glacial deposits with paleomagnetic results that suggested they had been deposited at low paleoaltitudes. A hypothesis put forth by Williams (1975) to explain the presence of seemingly near-equatorial glacial deposits was that the Earth had a high obliquity in the Proterozoic. This theory was considered to be an inadequate explanation because of a lack of a known mechanism to cause this phenomena, an association of carbonate belts with glacial deposits, and studies conducted on heliotropic stromatolites that showed that the Earth's obliquity 800 Ma was comparable to that of today (Vanyo and Awramik 1982, 1985; Awramik and Vanyo 1986; Vanyo et al. 1986; Kirchvink, 1992). The rejection of the high-obliquity hypothesis for the low paleolatitudes of the glacial deposits led to a tentative acceptance of the possibility that ice house conditions did indeed prevail in near-equatorial areas at certain times during the Neoproterozoic. This observation was then built upon by Kirchvink (1992) and Hoffman et al. (1998) who interpreted that for such glacial deposits to have been found near the paleoequator, the planet must have

experienced global glacial conditions, in events referred to as 'Snowball Earth', during which most of the ocean's surface was ice covered.

More recently, the concept of glacial ice cover that was global in extent has been suggested to have occurred during the Paleoproterozoic glaciations as well (Kirschvink et al., 2000; Kopp et al., 2005). Within the Huronian Supergroup glacial deposits this is based largely on paleolatitude data collected from the Coleman Member of the Gowganda Formation and Firstbrook Member of the Lorrain Formation that indicate deposition occurred within 11˚ of the paleoequator (Williams and Schmidt, 1997). The results of this study have come into contention however, with the Gowganda, the third glacial event preserved within the Huronian Supergroup, having been suggested to have uncertain paleolatitude origins due to secondary results obtained from a fold test (Hilburn et al., 2005). Furthermore, paleolatitude data collected from the 2.45 Ga Matachewan dykes provide a latitude of ~5.5˚ but there is an unknown break in time between the emplacement of the dykes and the first glaciation (Bates and Halls, 1990; Young et al., 2001; Kopp et al., 2005). Thus, caution must be taken when interpreting and drawing conclusions from the Huronian sediments being deposited at near-equatorial latitudes, as there is still uncertainty regarding the paleolatitude of the Huronian glacial deposits.

There have been a number of theories surrounding the cause of the Proterozoic glaciations including that both the Neoproterozoic and the Paleoproterozoic glacial events are associated with supercontinent assembly, rifting, and subsequent divergent margins (Aalto, 1981; Eisbacher, 1981; Hiscott, 1981; Anderton, 1982; Karlstrom et al., 1983; Fralick, 1985; Eyles et al., 1985; Young, 1988, 2013b). It has been suggested that the formation of the late

Archean supercontinent Kenorland prior to the Paleoproterozoic glaciations would have resulted in a drawdown of atmospheric CO_2 through increased weathering, leading to atmospheric cooling and glaciations (Williams et al., 1991; Kirschvink et al., 2000; Kopp et al., 2005; Young, 2013a). There has also been a great deal of work suggesting that the advent of photosynthesizing bacteria and the Great Oxidation Event (GOE) may have played a large role in triggering the Paleoproterozoic glaciations through oxidation of reduced greenhouse gases (Pavlov et al., 2000; Catling and Claire, 2005; Kopp et al., 2005; Kasting and Ono, 2006; Zahnle et al., 2006; Kirschvink and Kopp, 2008). In the instance of a 'Snowball Earth' it is believed that the ocean would be completely cut off from the atmosphere due to extensive ice-cover. Termination of global ice-house conditions would occur through volcanic outgassing causing a build-up of atmospheric CO_2 until concentrations were high enough to facilitate warming (Hoffman et al., 1998). One strong counterarguement to the 'Snowball Earth' hypothesis is the evidence for an active hydrologic cycle and high sediment discharges during the supposed global glaciations, which indicates that the Neoproterozoic glacial epochs were perhaps climatically pulsed (Allen and Etienne, 2008). Likewise, investigations of fossil records from the Neoproterozoic indicate the presence of photosynthesizing benthic eukaryotes during glacial periods (Ye et al., 2015). These microbes would require light and open water and their presence similarly supports the notion of open water during the Neoproterozoic glaciations (Corsetti, 2015). Furthermore, the deposition of glacial diamictites within tectonically active rift basins in the Neoproterozoic has been suggested to indicate that the location of ice centers was determined by rift-related topographic uplift during the break-up of Rodinia (Eyles and Januszczak, 2004).

While there are strong similarities between the Neoproterozoic and Paleoproterozoic glacial events in terms of their association with supercontinent assembly and disintegration, there are some obvious differences, including the ubiquity of carbonates overlying diamictites in Neoproterozoic successions, which are rarely present in association with the Paleoproterozoic glacial deposits (Young, 1988; Bekker et al., 2005). The uniformity of carbonate-bearing facies overlying glacially-deposited diamictites is important as the presence of carbonates directly overlying glacial deposits (termed 'cap carbonates') is believed to be the conclusion to a 'Snowball Earth' event, when melting of ice allows for the high CO_2 atmosphere to regain contact with the ocean and drive precipitation of carbonate (Hoffman et al., 1998). Precipitation would be further perpetuated by the large influx of additional alkalinity provided by increased weathering on the continents (Hoffman et al., 1998). In the case of a 'Snowball Earth', these processes would all have occurred on a global scale, which is observed in the Neoproterozoic, where cap carbonates are ubiquitous with glacial deposits (Bekker et al., 2005).

The Espanola Formation, a carbonate-bearing formation that directly overlies the second of three glacial Formations within the Huronian Supergroup, has been suggested as a possible cap carbonate associated with the Paleoproterozoic glaciations (Bekker et al., 2001, 2005; Hoffman, 2013). Aside from the Espanola Formation there are also the carbonate-bearing Vagner and Bottle Creek Formations of the Snowy Pass Supergroup in the Medicine Bow Mountains and Sierra Madre, which are believed to be lateral extensions of the Espanola Formation (Bekker et al., 2001, 2005; Hoffman, 2013). Recent research has also disclosed another possible Paleoproterozoic cap carbonate in India that is correlative with the Espanola

Formation (Mohanty et al., 2015; Sarangi et al., 2017). Therefore, these localized developments of possible cap carbonates in the Paleoproterozoic give rise to speculation as to whether or not there was a 'Snowball Earth' event in the Paleoproterozoic, as it may be presumptuous to extrapolate global conditions from localized carbonate deposits (Young, 2013a).

The Espanola Formation and the Bruce glacial event are unique compared to the later Neoproterozoic glaciations on account of their proposed direct correlation to a rise of atmospheric oxygen (Hoffman, 2013). Evidence for this is provided by the presence of indicators of anoxic conditions within the Huronian stratigraphy prior to and during the Bruce glacial event. These include the drab colour of their sediments indicating iron was not oxidized during weathering, the presence of detrital pyrite and uraninite, and paleosols that exhibit an upward increase in iron (Prasad and Roscoe, 1996; Frarey and Roscoe, 1971). In comparison, the Cobalt Group, higher in the stratigraphy than the Bruce glacial event, contains red beds and iron oxides suggesting that oxygen was present at the time of its deposition (Prasad and Roscoe, 1996; Frarey and Roscoe, 1971). Other evidence that correlates the Bruce glacial event to a rise in atmospheric oxygen is from a ~1.5m siltstone-sandstone layer that separates the Bruce Formation from the overlying Espanola carbonates (Sekine et al., 2011; Hoffman, 2013). This transitional unit contains a higher concentration of radiogenic osmium that is believed to be the result of weathering of continental rocks in an atmosphere with oxygen greater than or equal to 10^{-4} present atmospheric levels (Sekine et al., 2011; Hoffman, 2013). Lastly, evidence for a shift in atmospheric oxygen content at the time of the Bruce glacial event is supported by its association with loss of the mass independent fractionation (MIF) sulfur signature in the marine record (Papineau et al., 2007). Prior to a rise in the concentration of atmospheric

oxygen, photochemical atmospheric reactions preserved a MIF sulfur signal within sulfates and sulfides, but an increase in free oxygen in the atmosphere is believed to have shut down the chemical reactions that generate sulfur with anomalous isotopic compositions (Farquhar et al., 2000). This shift in the MIF sulfur signal occurs immediately preceding the Bruce glacial event, indicating a rise in atmospheric oxygen that was sustained thereafter (Figure 2); (Papineau et al., 2007). Thus, one of the most interesting features that distinguishes the Bruce glacial event from others is its direct association with the GOE.

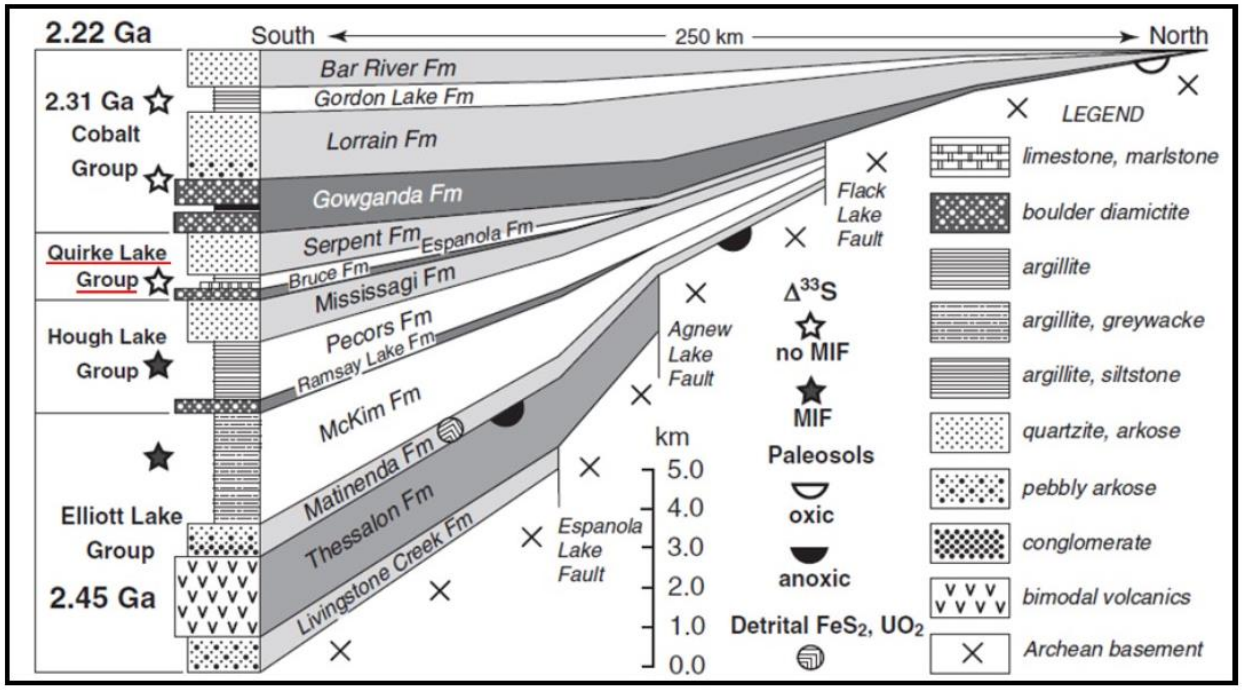

Figure 2: Diagram outlining the loss of the mass independent fractionation isotope signal that occurs within the Espanola Formation. This loss is suggested to be the result of a change in the atmospheric levels of oxygen, and is supported by the presence of anoxic indicators such as detrital pyrite and uraninite in the groups underlying the Quirke Lake Group, and the presence of oxic indicators, such as red beds in the overlying Cobalt Group. The Quirke Lake Group is underlined in red. From Hoffman (2013).

1.3 REGIONAL GEOLOGY

The ~2.5 to 2.2 Ga Huronian Supergroup located along the southern margin of the Superior craton is a sedimentary and volcanic sequence that is wedge-shaped and up to 12km thick (Sims et al., 1981; Bennett et al., 1991; Young et al., 2001; Bekker et al., 2005; Bennett, 2006; Ketchum et al., 2013). The Huronian sediments overlie the Thessalon volcanics and other igneous extrusive rocks with a maximum age of 2.49-2.44 Ga constrained by U-Pb age determinations on zircon (Van Schmus, 1965; Krough et al., 1984; Prasad and Roscoe, 1996; Hoffman, 2013). A minimum age date of 2.22 Ga for Huronian sediments is provided by U-Pb zircon data of the Nipissing Diabase bodies that intrude Huronian rocks (Corfu and Andrews, 1986; Noble and Lightfoot, 1992), but most of the sediments, including the three glacial intervals, are further constrained in age by ~2.31 Ga U-Pb dates collected from zircons in tuffaceous beds in the Gordon Lake Formation (Rasmussen et al., 2013). Deposition of the Huronian Supergroup sedimentary package is capped in the west by foredeep sediments deposited during the ~1.85 Ga Penokean Orogeny, which was the result of the southern margin of the Superior craton colliding with an island arc terrane (Hoffman, 1989; Bennet et al., 1991; Schulz and Cannon, 2007; Ketchum et al., 2013) or volcanism on the margin itself (Fralick et al., 2002).

The Huronian Supergroup is subdivided into four groups based on unconformities and on reoccurring depositional cycles within the uppermost three groups (Robertson et al., 1969; Zolnai et al., 1984). From base to top these groups are: Elliot Lake, Hough Lake, Quirke Lake, and Cobalt (Figure 3). The basal Elliot Lake Group is unique in that it contains metavolcanics and does not contain glacial diamictites. The uppermost three Groups represent triparte cycles

consisting of: a lower conglomeratic unit, a middle mudstone unit, and an overlying sandstone unit (Figure 4); (Robertson et al., 1969; Card et al., 1977; Young et al., 2001; Bekker et al., 2005; Ketchum et al., 2013; Young, 2014). These cycles are interpreted to be representative of glacial advances and retreats in non-marine to marginal marine environments with each cycle beginning as glacial ice sheets advanced, forming an erosive contact, and depositing diamictite units (Casshyap, 1969; Roscoe, 1969; Farey and Roscoe, 1970; Bennet et al., 1991; Ketchum et al., 2013; Young, 2014). Ice loading and subsequent marine transgression following glacial retreat result in marine sediments being deposited overtop of glacial deposits, and in turn these sediments are overlain by shallow water and fluvial deposits as isostatic rebound completes a regressive systems tract (Frarey and Roscoe, 1971; Bennet et al., 1991; Ketchum et al., 2013; Young, 2014). The Quirke Lake Group is the third Group in the Huronian succession and represents the middle glacial cycle. It consists of a lower conglomerate (Bruce Formation), a middle carbonate-siltstone-mudstone unit (Espanola Formation), and an overlying sandstone (Serpent Formation); (Card et al., 1977).

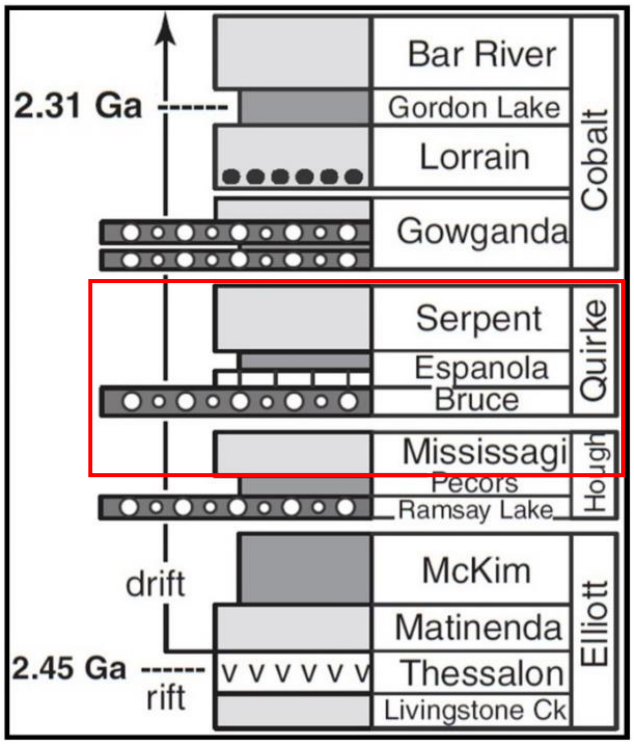

Figure 3: Stratigraphy of the Huronian Supergroup. The Bruce glacial cycle, which is the focus of this study, is highlighted by the red box. Modified from Hoffman (2013).

Group	Formation	Depositional Environment
Cobalt	Bar River	coastal—beach
	Gordon Lake	tidal flat
	Lorrain	fluvial to near-shore
	Gowganda	glacial to glaciomarine
Quirke Lake	Serpent	distal stream
	Espanola	fluvial through deltaic and shallow marine to deeper marine
	Bruce	glacial to glaciomarine
Hough Lake	Mississagi	deltaic, fluvial, and shallow marine
	Pecors	offshore
	Ramsay Lake	glacial to glaciomarine
Elliot Lake	McKim	offshore
	Matinenda	fluvial

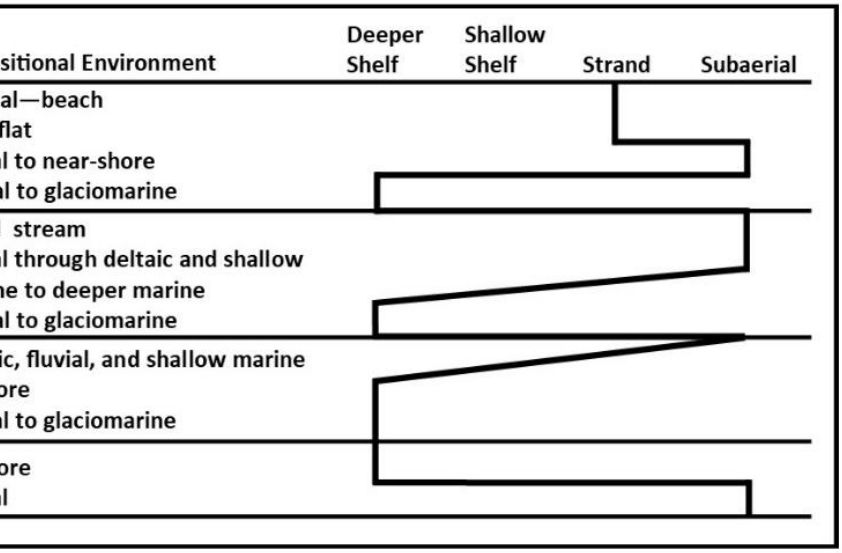

Figure 4: Table outlining the depositional environments of the Formations in each group of the Huronian Supergroup. The Quirke Lake Group, which preserves the Bruce glacial event and is the focus of this study, is highlighted with the red box. A rapid transgression occurs during the advance of the Bruce ice sheet, and a slow marine regression occurs during the interglacial period in which the Espanola and Serpent Formations were deposited. Modified from Fralick and Miall (1989).

Thickening of the Huronian Supergroup occurs towards the south as deposition of the sediments coincided with, and was controlled by, subsidence of the Archean basement during a period of extension and rifting followed by a gradual change to a passive margin environment (Figure 5); (Fralick and Miall, 1989; Young et al., 2001; Bennett et al., 2006; Young, 2013a, 2014). The extensional regime led to the development of east-trending and south-dipping half grabens that imparted the southward-thickening wedge shape to the Huronian sedimentary package and contemporaneous faulting affected deposition in the lower part of the Huronian Supergroup (Zolani et al., 1984; Jolly, 1987; Young et al., 2001; Ketchum et al., 2013).

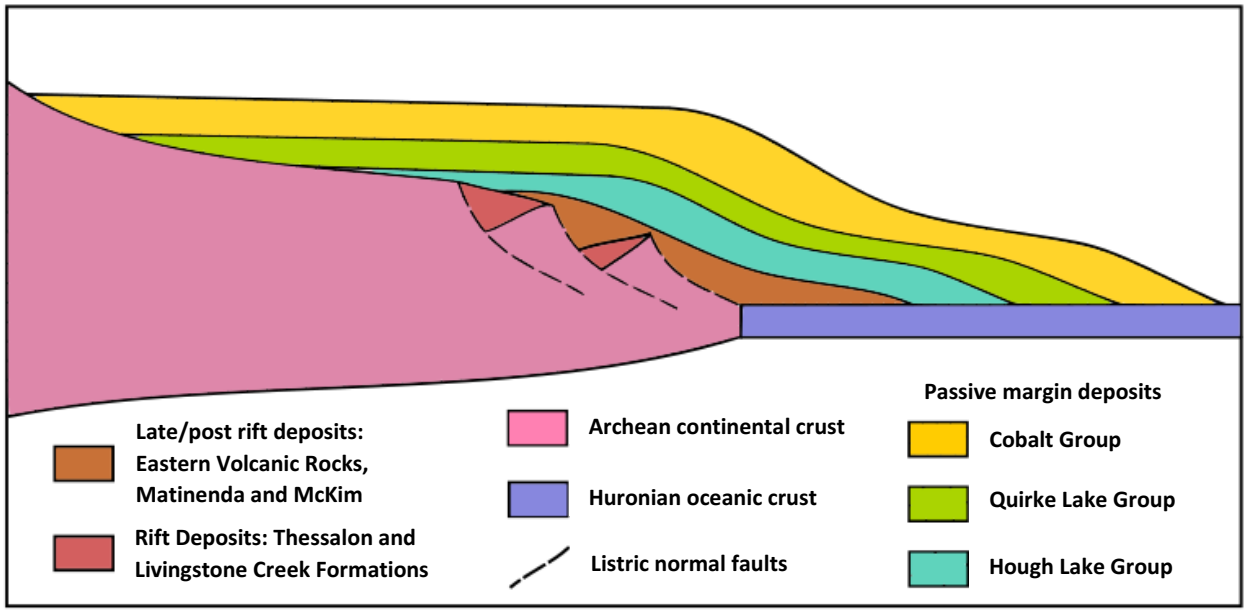

Figure 5: Schematic cross-section of the paleotectonic model for the earlier rift-drift transition in the Huronian stratigraphy. Modified from Bennet et al. (2006).

While it is generally accepted that the Huronian Supergroup was deposited in a rift environment that transitioned into a passive margin based on the wedge-shaped geometry, associated volcanic rocks, and thick package of sediments bounded by normal faults, the timing at which the transition from rift to drift occurred in relation to deposition of the Huronian

sediments is still in contention (Zolnai et al., 1984; Fralick and Miall, 1989; Young et al., 2001; Withjack et al., 2002; Allen and Allen, 2005; Al-Hashim, 2016). The division exists between those who believe that the transition occurred at the base of the Cobalt Group (Young, 2013a, 2014) and others who argue that the transition occurred much earlier than that, at the base of the Matinenda Formation (Fralick and Miall, 1989; Bennet et al., 1991; Hoffman, 2013). The lowermost two glacial deposits, preserved in the Hough Lake and Quirke Lake Groups have a restricted distribution relative to the much more laterally extensive glacial deposit of the Cobalt Lake Group and this is due to their confinement northward by the Flack Lake Fault which was overstepped by the Gowganda Formation (Frarey and Roscoe, 1971; Young and Nesbitt, 1985; Young et al., 2001; Young, 2014). This feature in particular has been argued as the basis for interpreting that the lower part of the Huronian Supergroup was deposited in a rift setting, and that the glacial advance of the Gowganda Formation marks the transition to a passive margin setting (Zolnai et al., 1984; Young and Nesbitt, 1985; Young et al., 2001; Young, 2004, 2014). An earlier rift-to-drift transition is supported by evidence of fluvial sediment transportation shifting to a consistent southward direction at the base of the Matinenda which is towards the inferred basin axis (Card et al., 1972; Fralick and Miall, 1989; Bennet et al., 1991; Hoffman, 2013). This change suggests a shift from an active rift arm sloping away from the elevated rim of the axis, to lithospheric cooling and subsidence (Bond et al., 1995; Hoffman, 2013). In this scenario, rift-related extensional faults would be reactivated as a result of heat dissipation and sediment loading driving subsidence of the basement, which would broadly control regional facies variations within the Huronian Supergroup sedimentary units (Zolnai et al., 1984; Bennet et al., 1991; Ketchum et al., 2013).

The ongoing discussion regarding the tectonic regime and timing of the rift-drift transition during deposition of the Huronian Supergroup is critical to the significance of the results of this study and to the implications of the Bruce glacial event and the Espanola Formation. The Quirke Lake Group is unique in that it contains the only considerable carbonate unit found in the Huronian Supergroup, and its direct placement upon the underlying Bruce diamictite has been used to suggest that it may be a cap carbonate (Young, 1973a; Bernstein and Young, 1990; Bekker et al., 2005; Hofmann, 2013). This interpretation is in contention however, as the later rift-drift transition hypothesis would suggest that the Espanola Formation formed in a restricted rift setting and thus would only be reflective of local conditions and cannot be extrapolated to represent global phenomena (Young, 2013a, 2014). The results of this study, in describing the sedimentology, geochemistry, and isotopic composition of the Quirke Lake Group, may aid in dispelling the uncertainty regarding its tectonic setting and facilitate further discussion of the significance of the Bruce glacial event.

1.4 METHODS

In an effort to compile a comprehensive, and as complete as possible dataset on the Quirke Lake Group, fieldwork was conducted in the summers of 2016 and 2017 and outcrops of the Bruce, Espanola, and Serpent Formations, as well as the transition from the underlying Mississagi sandstone to overlying mixtites were described in detail (Figure 6). Paleocurrent data were collected with the intention of recognizing shifts in flow direction, and these data were compared with previously collected paleocurrent data for the upper Mississagi and Serpent Formations (McDowell, 1957; Pienaar, 1963; Palonen, 1971, 1973; Long, 1976, 1977). Three drill holes; 150-1, 150-2, and 144-1 were logged at the Ministry of Northern Development and Mines Core Library in Sault Ste. Marie (Figure 7). Stratigraphic columns were then generated for the drill core and some of the more extensive field outcrops using SedLog. After creating basic logs using SedLog, the columns were then transferred to Inkscape, where detailed sedimentary structures and colour were added. To provide as much detail as possible in the stratigraphic sections, one legend was used for the Mississagi, Bruce, and Serpent Formation sections, and another legend was used for the Espanola Formation. These legends are provided in the appendices.

Approximately 75 samples of the Espanola Formation were collected from outcrop and drill core. Of these, 30 were chosen for petrographic analysis as well as 60 for geochemical and isotopic analysis. Petrographic analysis was used to examine mineralogy and microscopic sedimentary features in the hopes of gaining insight as to the type of precipitation. Outcrop sampling of carbonates was limited largely to the Elliot Lake and surrounding area due to the higher degree of metamorphism in the southern exposures. Samples collected at the outcrop

along Highway 108 5km north of Elliot Lake were also omitted from geochemical and isotopic analysis due to contact metamorphism by an adjacent intrusion.

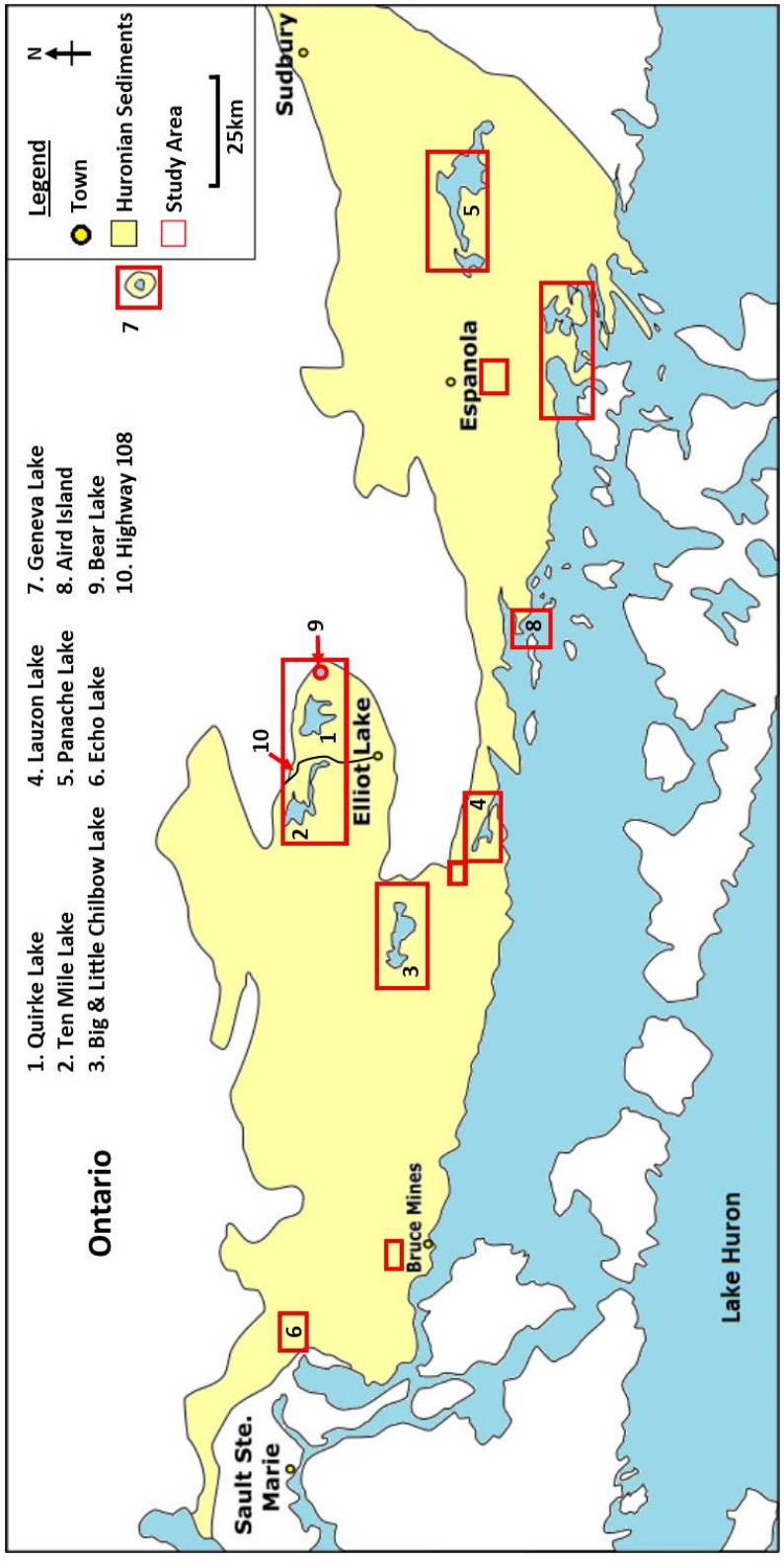

Figure 6: Generalized map detailing the extent of the Huronian Supergroup sediments in the Sault Ste. Marie-Elliot Lake and Espanola-Sudbury areas. Red boxes indicate the outcrop areas that were the focus of this study.

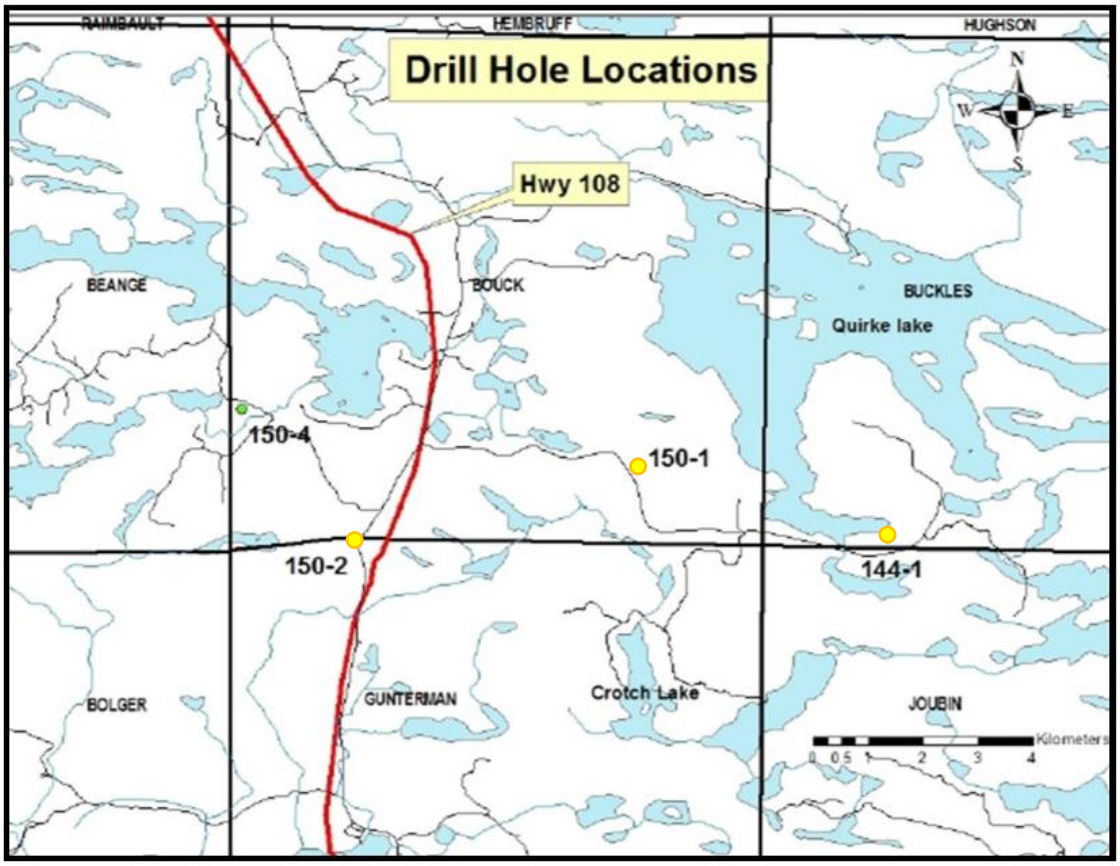

Figure 7: Map of the locations of the drill holes that were used in this study. The three cores logged in this study are highlighted with yellow points. From Al-Hashim (2017).

Samples for geochemical analysis were crushed and powdered in an agate mill, then underwent whole rock and partial digestion. Geochemical analysis was conducted on the prepared samples at Lakehead University Instrument Laboratory using ICP-AES and ICP-MS.

1.4.1 WHOLE ROCK ANALYSIS

Whole rock digestion was completed using 0.5g of powder placed in Teflon beakers. The samples underwent a series of acid baths that included a primary step of 5ml of nitric acid and 10ml of double distilled water to allow for controlled effervescence. After drying the samples on a hot plate at 90˚C, 5ml of hydrofluoric acid and 10ml of nitric acid were added to the beakers and left to evaporate again. This step was completed three times. Lastly, 2ml of nitric

acid was added to each beaker and left for approximately 10 minutes on the hot plate to allow for full dissolution of the remaining sample. The contents of each beaker were then placed into 100ml flasks and filled with double distilled water. From these solutions, 50ml polypropylene tubes were filled with a 200x dilution and a 1000x dilution of each sample to be used for ICP-AES and ICP-MS, respectively. Along with the Espanola samples, three standards and three blanks were prepared to quantify accuracy and contamination for each run of approximately 30 samples. The values for the standards (BHVO-2, 8-44A, and SR-16B) are provided in their respective appendices.

1.4.2 PARTIAL DIGESTIONS

Samples for partial digestion analysis began by weighing out 0.2g of powdered sample into Teflon beakers and adding 10mL of 5% acetic acid solution. This was allowed to sit for 1 hour as a pre-leach to remove materials loosely bound to siliciclastic particles. Pre-leach solutions were then removed from the beakers by eye dropper and discarded. Another 10mL of 5% acetic acid solution was added again to the original Teflon beakers and allowed to react for 24 hours. After 24 hours, the acetic acid solution was removed using an eye dropper and placed in clean Teflon beakers. The solutions were then placed on a hot plate at 90˚C to allow for evaporation. Once the samples were dried, the residua were then weighed to determine the amount of soluble material. This step was necessary for calculations of dilution factors during data processing. After weighing, the samples were dissolved in 2% nitric acid solutions for ICP-MS and ICP-AES analysis. Two standards and two blanks were prepared with the Espanola Formation samples to quantify accuracy and contamination by fluids. The values for the

standards (SR-22A and RL2-51 or SR-16B and 8-44A) are provided in their respective appendices.

Two carbonate standards were utilized for the partial digestion analysis. One standard is from Steep Rock and the second is from Red Lake. Due to an inability to assume that 100% of the carbonate fraction was put into solution during the partial digestion process, to constrain the accuracy of the analytical results the REE plots of the standard values were compared instead of the absolute values (Figure 8). True values of the standards are from Fralick and Riding (2015) Supplemental Data. The similarities of the patterns between the standards indicates that the analytical results are accurate and, as expected, typically fall slightly below the concentrations of the true standard whole rock values. REE plots are normalized to Post Archean Australian Shale (PAAS).

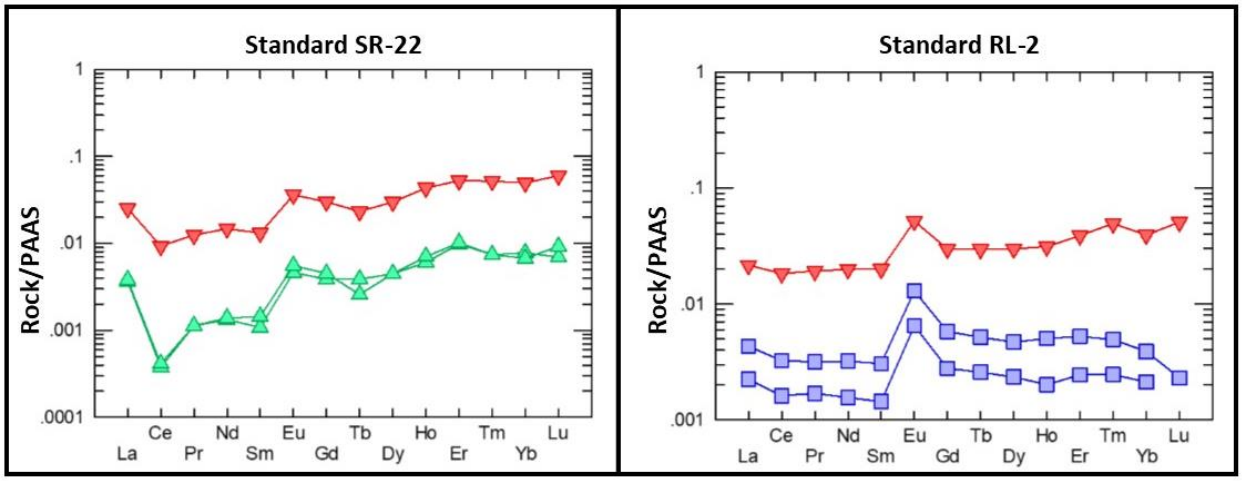

Figure 8: Two carbonate samples used as standards for partial digestions. SR-22 from Steep Rock, and RL-2 from Red Lake. Red patterns are the true values, while the green and blue patterns are those produced during the digestions performed in this study. Similarities in the patterns produced is used to determine the accuracy of the data, as total values will be different for the partial digestions. The patterns are similar but it is important to note that there is some deviation in the heavy REE of RL-2.

1.4.3 STABLE ISOTOPES

Stable isotope analysis was completed on 78 carbonate samples from the Espanola Formation. Samples were crushed and powdered in the lapidary facility at Lakehead University and shipped to France for analysis at the Pôle Spectométrie Océan in Brest. There, the powdered samples were placed in a Kiel IV automated carbonate preparation device, where 100% H_3PO_4 was added and allowed to react at 72˚C to release CO_2 from the powders. Samples were then analyzed in a Finnigan MAT 253 mass spectrometer. Results are reported against the Vienna Pee Dee Belemnite (V-PDB) standard with an analytical error (2σ) of 0.2‰ for $\delta^{18}O$ and 0.1‰ for $\delta^{13}C_{carb}$.

2 MISSISSAGI FORMATION

The Mississagi Formation is the upmost Formation of the Hough Lake Group and is a dominantly sandstone sequence that crops out from near Sault Ste. Marie to east of the Cobalt Embayment. It ranges in thickness from 1500m at its western extent up to 3000m in the southeast (Card and Lumbers, 1977; Frarey, 1977; Card, 1978; Bennet and Sawiuk, 1979; Sims et al., 1981; Debicki, 1990; Bennet et al., 1991). Thickness of the formation is less towards the north, with an average thickness of 500-600m (Robertson, 1968; Sims et al., 1981; Bennett et al., 1991). Sandstones are largely well-sorted, medium- and coarse-grained, and consist of arkose to subarkose, feldspathic to subfeldspathic arenites with minor quartz arenite (Card et al., 1977; Long, 1976; Bennet, 1982; Bennett et al., 1991). Conglomerate, wacke, and argillite occur as minor lithologies and, particularly near the contact with the Bruce diamictite, coarse arkosic sandstone becomes locally conglomeratic (Long, 1976; Card et al., 1977; Bennet, 1982; Bennett et al., 1991). Stratigraphy of the Mississagi Formation has a general trend of an upwards increase in sorting near the top of the formation (Long, 1976; Bennet et al., 1991). Furthermore, an upwards increase in grainsize has been observed in numerous studies, but it is not a uniform feature (Long, 1976; Card et al., 1977; Bennet, 1982; Bennet et al., 1991).

Studies of the lithological composition of the Mississagi Formation have determined that the mineralogy consists mostly of quartz, plagioclase, and potassium feldspars with abundant clays including chlorite and muscovite-sericite-illite in the fine-grained material (Parviainen, 1973). The presence of a high matrix component of the sandstones in the Mississagi Formation has been interpreted as the result of post-depositional weathering (Long, 1976). Weathering of plagioclase and alkali feldspars is also interpreted as the source of

carbonate in some of the Mississagi Formation, with the exception of a carbonate cement that is locally present and has been suggested to have been precipitated during diagenesis (Long, 1976). The sandstones of the Mississagi Formation are immature and are believed to be derived from granitic and gneissic rocks (Parviainen, 1973; Long, 1976).

In this section the lithofacies associations present in the Upper Mississagi Formation will be discussed as it pertains to the transition into the advance of the overlying Bruce glacial ice-sheet. Determining the periglacial environment prior to ice inundation is important for interpretation of genesis of the Bruce Formation glacial diamictites. This involves using the vertical lithofacies relationships with the underlying (and overlying) Formations to constrain a stratigraphic context. In this study I examined outcrops of the Mississagi Formation immediately below the contact with the Bruce diamictite in the Sudbury-Espanola and Sault Ste. Marie-Elliot Lake areas to interpret the depositional environment of the Mississagi Formation prior to glaciation and the nature of the contact with the overlying Bruce Formation.

The upper Mississagi Formation has been subdivided into three lithofacies associations based on the stratigraphic trends observed in outcrop. Lithofacies Association 1 dominates the stratigraphy along the north shore of Lake Huron where the Mississagi Formation is well preserved in outcrop and the high angle of bedding allows for mapping of continuous sections. This lithofacies association consists predominantly of cross-bedded sandstones and is best described from sections recorded along the north shore, including; west of West Sampson Point, 1km east of Birch Island, 1.5km east of Birch Island, Wells Island, and Aird Island (Figure 9). Approaching the overlying Bruce glacial deposits, there is a shift in stratigraphy to heterolithic lamination, clay drapes, and a decrease in sorting of sediment. The exception to

this transition is in the Lauzon Lake area, where a unique lithofacies association, Lithofacies Association 2, is indicated by parallel laminated calcareous sediments separating the Mississagi Formation from the Bruce in this locale.

Figure 9: Map depicting the locations of the Mississagi Formation stratigraphic sections generated from outcrop exposures. Image taken from Google Maps.

2.1 LITHOFACIES ASSOCIATION 1: CROSS-STRATIFIED SANDSTONES

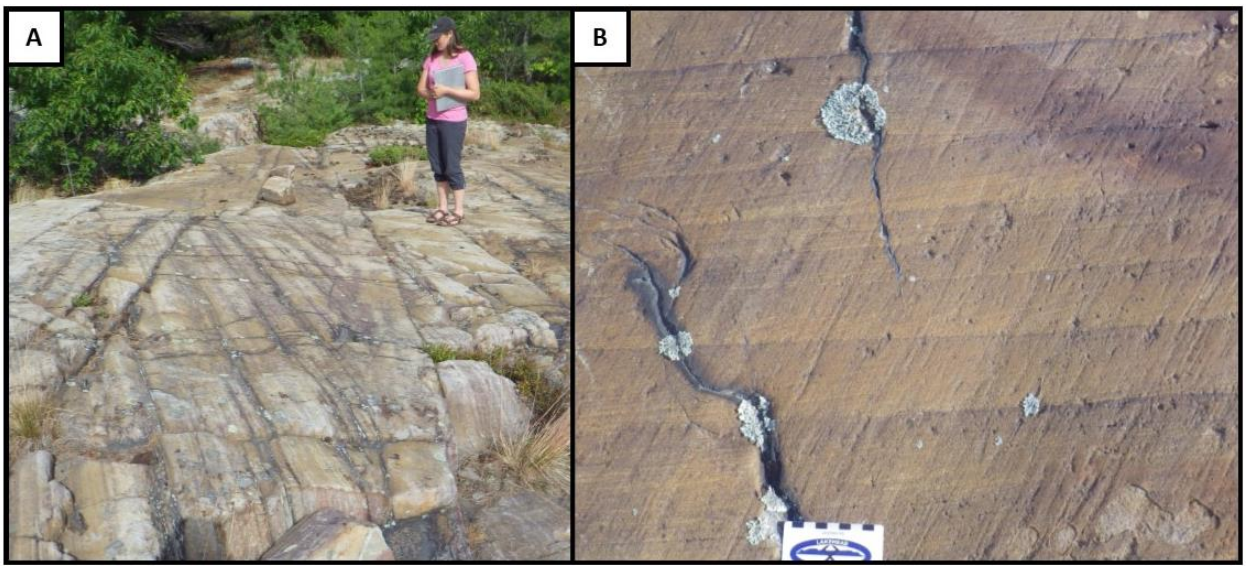

Figure 10: A: Large-scale, planar cross-stratified beds with abundant clay-rich laminae, the most common unit of the upper Mississagi Formation (up is towards the right). B: Set of small-scale, very low angle graded planar cross-stratified beds.

Planar cross-stratified sandstone is the most common unit of Lithofacies Association 1 and planar beds are typically large-scale (Figure 10A) (greater than 60cm in height) and of medium- to coarse-grained sand but also occur as sets of small-scale (Figure 10B) (up to 30cm in height) planar cross-stratification composed predominantly of medium-grained sand. Sets of small-scale, planar cross-stratification may be graded from medium-grained sand to fine-grained and more silt-rich sand at their tops. These graded beds average 4-8cm in thickness and have laminae that dip at angles ~10˚. Large-scale, planar cross-stratified units also commonly have laminae that dip at low angles. Contacts of planar cross-stratified units are sharp and may be erosively overlain by broad scours filled with small- to medium-scale, trough cross-stratification. Basal contacts of planar cross-stratified units are sharp as well and typically flat, but may be angled to give the appearance of a wedge-shaped geometry. Wedge-shaped planar cross-stratified sets occur at the Aird Island locality and preserve rare occurrences where

adjacent planar cross-beds have bimodal paleocurrents. Along the north shore of Lake Huron large-scale, planar cross-stratified beds are often in contact with one another and are more common than in the Elliot Lake, Chilbow Lake, and Lauzon Lake areas where large cross-beds are more typically isolated by massive and parallel laminated units. Deformation of large-scale, planar cross-stratified units is common and may manifest as: wavy to contorted lamination, overturning of bed laminae, and faulting of lamination (Figure 11A, B, C). Faulting of cross-lamination, contortion, and overturning of laminae are isolated to individual beds. Reactivation surfaces are present within large-scale, planar cross-stratified units and are sometimes accentuated by clay drapes.

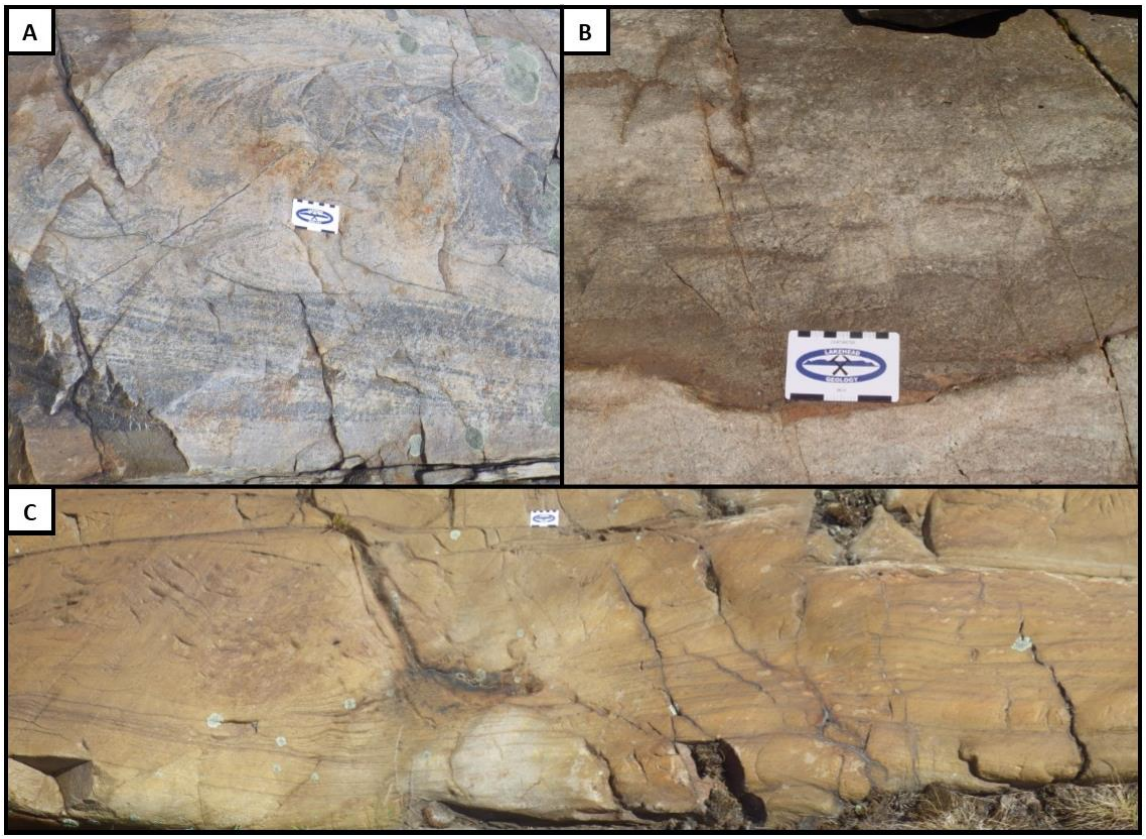

Figure 11: Various types of deformation structures observed in Lithofacies Association 1. A: Large-scale, planar-cross stratified unit that has laminae that are overturned and contorted. B: Faulted cross-lamination from a planar bed. C: Parallel bedded sandstone unit that is slumped and deformed in places.

Figure 12: A: Typical occurrence of a medium-scale, trough cross-bed erosively scouring down into the top of a large-scale, low angle planar cross-stratified unit. B: Set of bundled medium-scale, trough cross-beds that erosively scour into one another.

Trough cross-stratified sandstone is the second most common unit within Lithofacies Association 1 and occurs as single beds or bundled sets that are commonly separated by, or erode directly into, planar cross-stratified units (Figure 12A, B). Bundled sets of troughs and individual troughs are typically medium-scale but are also rarely large-scale or small-scale. Where in contact with an underlying planar cross-stratified unit the trough or troughs often erosively cut into it as broad scours (Figure 13). In turn, planar cross-stratified units also erosively truncate underlying trough cross-stratified beds. The grainsize of the trough cross-

stratified sandstone lithofacies is typically medium- to coarse-grained sand and some troughs contain coarse-grained sand at their base and roughly fine upwards. Additionally, some troughs contain heterolithic lamination composed of coarse and medium sand. Heterolithic laminated trough cross-stratification is a particularly common feature in closer proximity to the overlying diamictites of the Bruce Formation and is equally present in the Elliot Lake and north shore of Lake Huron areas. Bundles of troughs may also display polymodal paleocurrent directions.

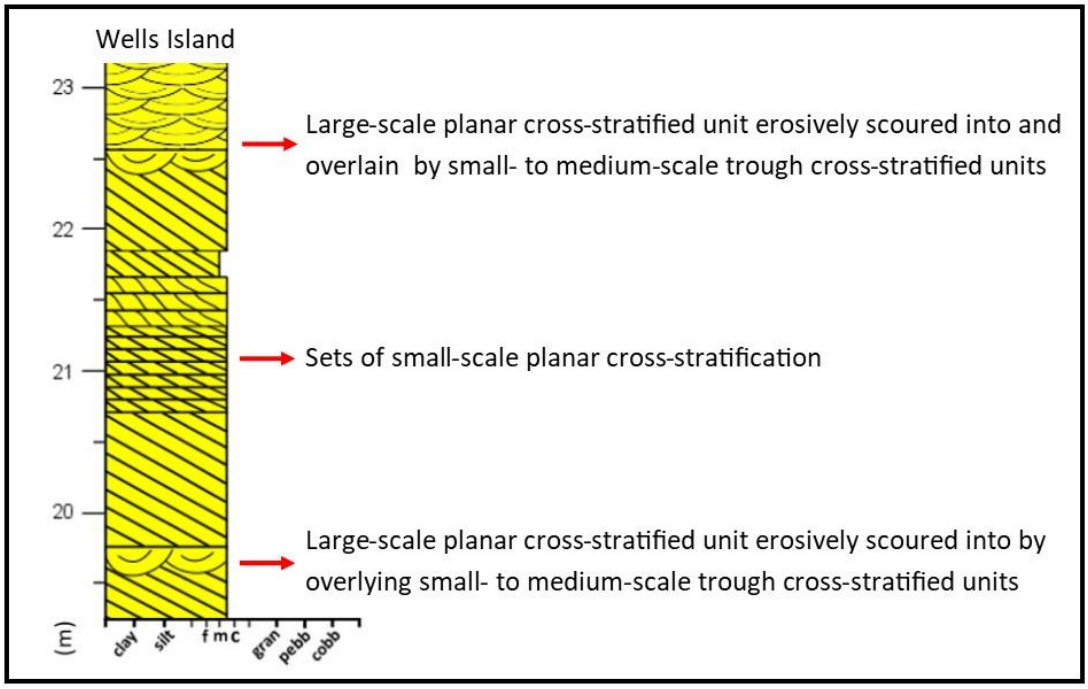

Figure 13: Section of stratigraphy outcropping at Wells Island. This provides an example of the predominance of cross-stratification and the typical relationships between units within Lithofacies Association 1. This section was taken from between 19 and 23m of the longer section from Wells Island in Appendix 1A.

Parallel lamination is a minor lithofacies within Lithofacies Association 1 and is most commonly finer-grained than the units it is in contact with. Grainsize of parallel laminated beds is highly variable and ranges from coarse- to fine-grained sandstone to siltstone and clay-rich siltstone. Lamination is distinguishable by differences in grainsize between laminae, including

upper flow regime fine-grained to medium-grained sand with coarse-sand laminae. Parallel laminated units are interbedded with various lithologies and have sharp contacts with adjacent units. Where in contact with cross-stratification, the contact is typically erosive but may be more gradational where in contact with massive sandstone beds. Thickness of laminae is variable and ranges from 1mm up to several centimeters. Generally lamination is planar and well preserved, but wispy and wavy to slightly contorted lamination does occur. At Wells Island, the sequence contains one fine-grained sand to silt unit that is parallel laminated and erosively scoured into by a planar cross-stratified layer, which in turn is scoured by overlying trough cross-stratified beds.

Grading of parallel laminated units is present at Aird Island and along Highway 108 and increase in abundance with proximity to the overlying diamictite. They usually occur in sets of multiple beds, commonly 8-14 cm thick and at Aird Island these sets of units are interbedded with cross-stratified beds that also fine upwards, grading from more medium-grained sand laminae at the base to more silt-rich laminae at the top (Figure 14). Grainsizes typically range from coarse- or very coarse-grained sand to fine-grained sand, silt, and clay at their tops. Parallel lamination is visible within the sandstone portions of the graded beds, while fine silt and clay tops have a massive appearance. Contacts between graded parallel-laminated beds and other facies are sharp and planar to slightly irregular.

Figure 14: An outcrop in the vicinity of Aird Island with two parallel laminated fining upwards beds, grading from medium sand to clay-rich silt that are overlain by two coarser, parallel laminated, normal graded coarse-grained and medium-grained sand to silt.

Rippled sandstones occur most commonly in the Chilbow Lake area, where a 10m outcrop of rippled sandstones underlies the Bruce diamictite. Both symmetrical wave ripples and asymmetrical current ripples are found interbedded with one another (Figure 15A). Both wave and current ripples are composed of fine- to medium-grained sand. Discrete layers with rippled tops can also show internal normal grading from a medium-grained sand to a fine sand with silt at the top. Individual beds range from approximately 0.5cm to 1.5cm thick on average (Figure 15B). Individual layers of current and wave ripples can be adjacent to one another and indicate alternating wave and current activity. Rare occurrences of rippled sandstones at other localities are typically associated with parallel lamination, with wave ripple lamination overlying and disturbing parallel lamination beneath it. At Wells Island, one planar cross-stratified bed contained a regressive climbing ripple on its topset.

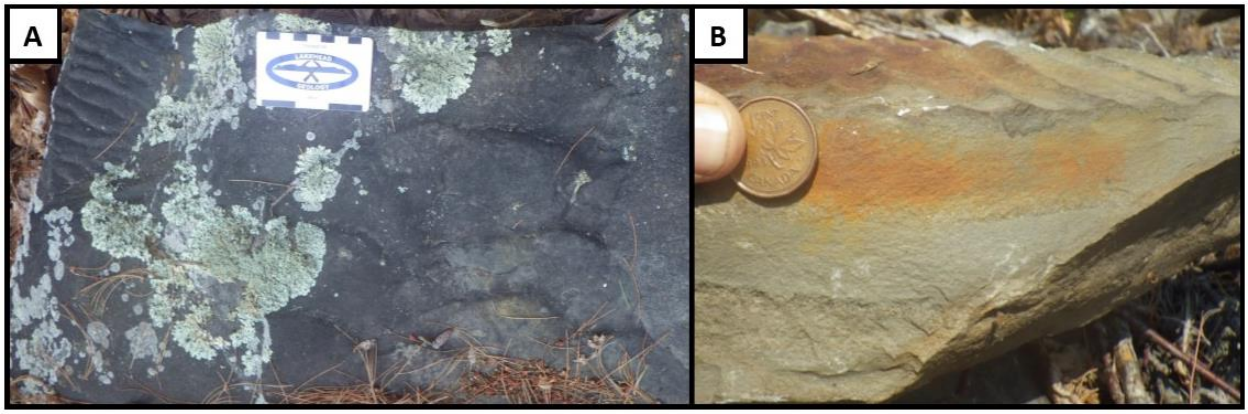

Figure 15: Rippled units that occur at the contact between the Bruce and Mississagi Formations at Big Chilbow Lake. A: Asymmetrical current-rippled layer (right) that directly overlies a symmetrical and bifurcating wave-rippled unit (left). B: Interbedded medium- to fine-grained sand with a wave-rippled surface.

2.2 LITHOFACIES ASSOCIATION 2: COARSE-GRAINED, POORLY-SORTED TRANSITIONAL SANDSTONE

Figure 16: Interstratified to interlaminated medium- to fine-grained sand and silty-clay immediately underlying the Bruce Formation east of Birch Island.

The most ubiquitous and consistent feature observed within the Upper Mississagi Formation approaching the contact with the overlying Bruce diamictite in the Sault Ste. Marie-

Elliot Lake and the north shore of Lake Huron areas is the shift from more well-sorted sands to generally coarser-grained and poorly sorted sands approaching the contact with the overlying Bruce diamictite. One exception to the coarsening upwards of sandstones directly at the contact with the Bruce Formation is in some of the extreme southern exposures along the north shore of Lake Huron in the Birch Lake area. Here, parallel lamination and finer-grained clay-rich beds occur directly underlying the contact and suggests a shift to an environment of lower energy at the end of the interglacial (Figure 16). This contact may extend further to the north in this area, as an approximately 20m thick clay-rich unit separates the Upper Mississagi Formation from the Bruce Formation immediately north of Espanola as well (Ginn, 1961).

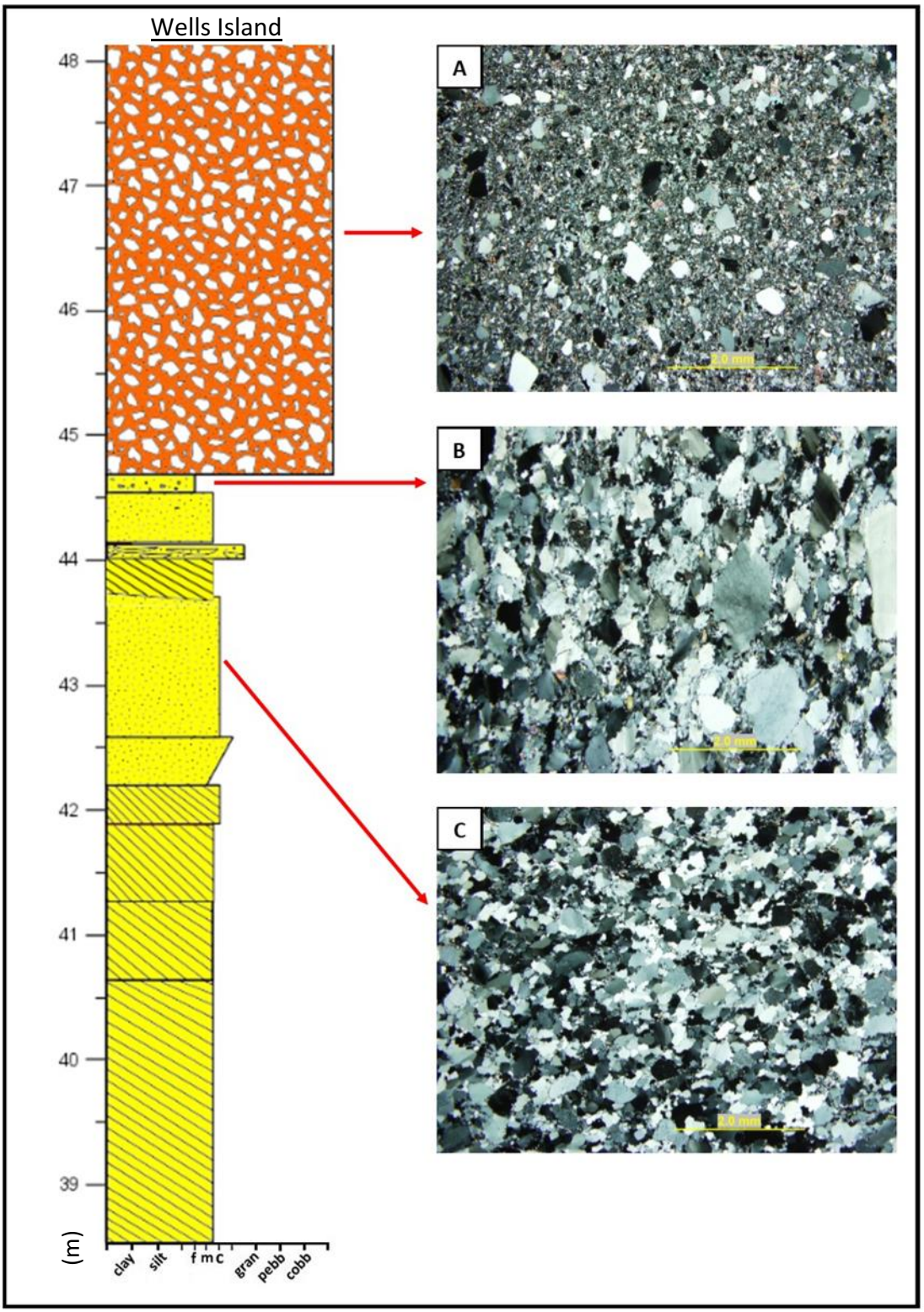

Figure 17: Petrographic analysis of the contact between Lithofacies Association 1 and the Bruce Formation at Wells Island. A: Poorly-sorted diamictite with a high-matrix content. B: Poorly-sorted sandstone from directly below the contact with the Bruce. C: Well-sorted sandstone from ~1.5m below the contact with the Bruce diamictite.

Other features that are commonly associated with the rapid transitional zone in the upper Mississagi Formation, prior to ice advance, include; an increase in massive and structureless sandstone units, an increase in soft-sediment deformation and faulting of beds, and the development of heterolithic lamination in large-scale, planar cross-stratified units. Massive sandstones range in grainsize from medium- to very coarse-grained sand and, particularly approaching the overlying diamictite, become very poorly sorted (Figure 17A, B, C). The coarsest grains within massive beds underlying the contact are often well-rounded quartz and they approach granule- to pebble-size within a very poorly sorted matrix. Lower down in the stratigraphy, where massive sandstones are interbedded with cross-bedded and laminated units, grainsize is usually well-sorted, medium- to coarse-grained sand. Generally contacts of massive sandstone units are sharp and planar surfaces.

Soft-sediment deformation and faulting is visible in laminated and cross-stratified units and are typically isolated to single beds in the case of cross-stratified units. These types of deformation increase in occurrence approaching the contact with the overlying diamictite and, in the Aird Island vicinity, a sandstone unit directly underlying the contact has been sheared. The massive and structureless upper Mississagi sands at Bear Lake also display evidence of soft sediment injection, with very poorly sorted and coarse-grained sands containing irregular intrusions of medium-grained sands with fairly sharp contacts (Figure 18A). This feature may have been caused by an increase in pressure during ice override. Heterolithic lamination in large-scale, planar cross-stratified units occurs as segregation of medium-grained sands and coarse- to very coarse-grained sands in alternating laminae. Furthermore, alternating heterolithic lamination may be between more well sorted medium- to coarse-grained laminae

and medium-grained laminae that are more poorly sorted and have a higher silt and clay concentration.

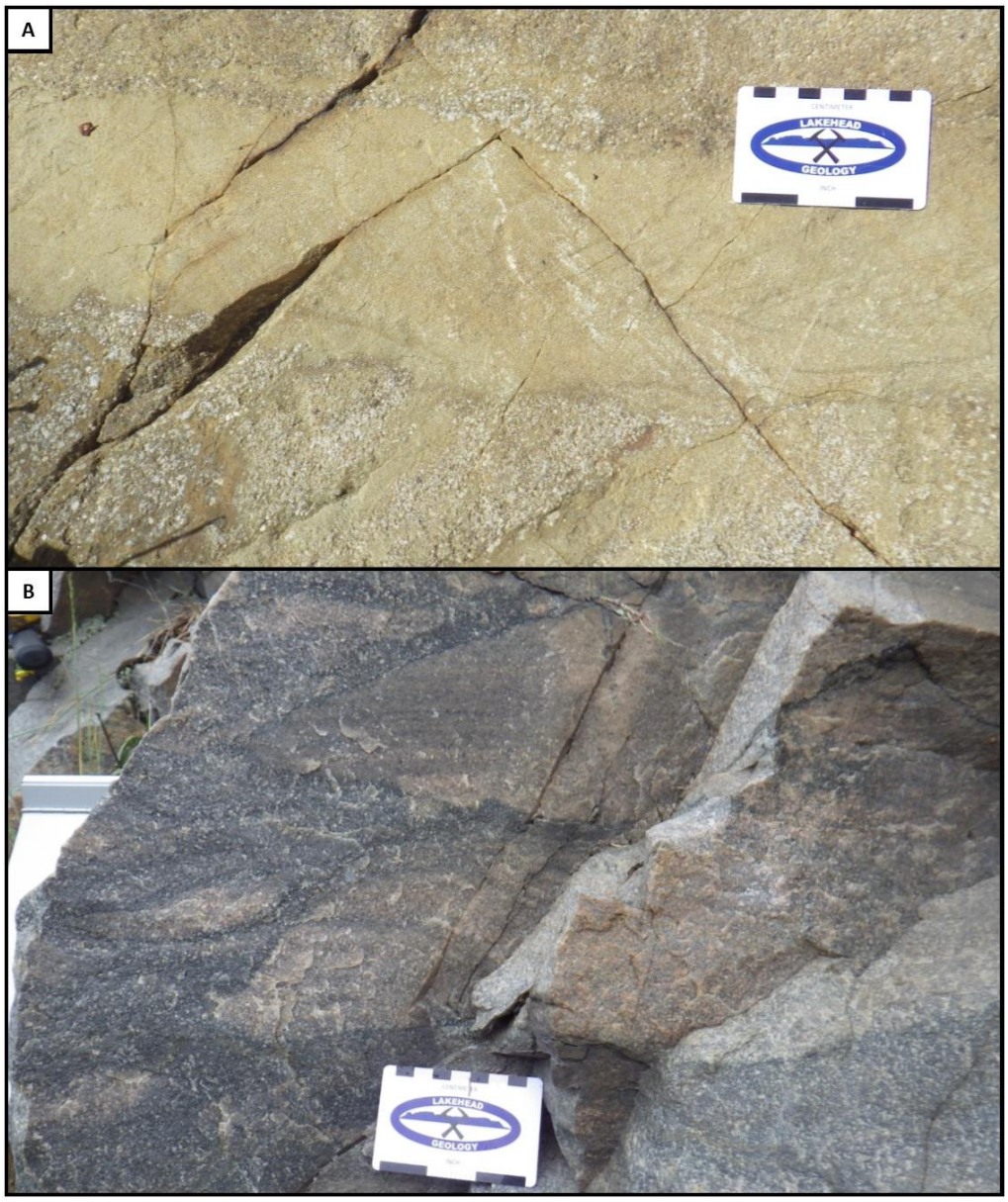

Figure 18: A: Injection of medium-grained sand (below scale card) into very coarse and very poorly sorted sandstone at Bear Lake. B: Sandstone lenses that occur within a more mud-rich and poorly sorted sandstone matrix near the upper contact of the Mississagi Formation.

Along Highway 108, the contact with the overlying Bruce is somewhat gradational, in that, there exists a transition zone over which diamictite and sandstone interlayer with one

another. At this location, fining upwards units are associated with heterolithic laminated cross-stratified beds that are separated by clay drapes and clay layers up to 1cm thick. At the immediate contact, the diamictite contains thin millimetric and discontinuous layering and lenses of fine-grained sandstone. Rapid changes in grainsize and sedimentary structures at this location further suggest that the Mississagi sandstone was deposited in a highly dynamic environment prior to deposition of the Bruce diamictite. This is also indicated by a noticeable change in the sandstone matrix. Near the base of the outcrop, the sandstone is a pure beige-pink colour, while near the upper contact the sandstone becomes more variable in colour and there is an increase in the silt and clay concentration of the matrix. There is also a unit near the contact that contains lenses of the more well-sorted beige-pink sand that have slumped into a matrix of the darker and more poorly sorted sand (Figure 18B). Sampling of the Mississagi Formation leading into the Bruce diamictite was conducted in an effort to assess this change. Three samples were taken from the sandstone: one from clean sandstone near the base of the outcrop, another from 30cm below the contact with the diamictite, and a third from 10cm below the contact with the diamictite. A sample of diamictite from above the contact was also collected for comparison. Petrographic analysis of these four samples show a systematic change from a well-sorted sandstone with a very minor silt and clay fraction, to a very poorly sorted diamictite with a clay- and silt-rich matrix surrounding rounded to subangular clasts (Figure 19A, B, C, D).

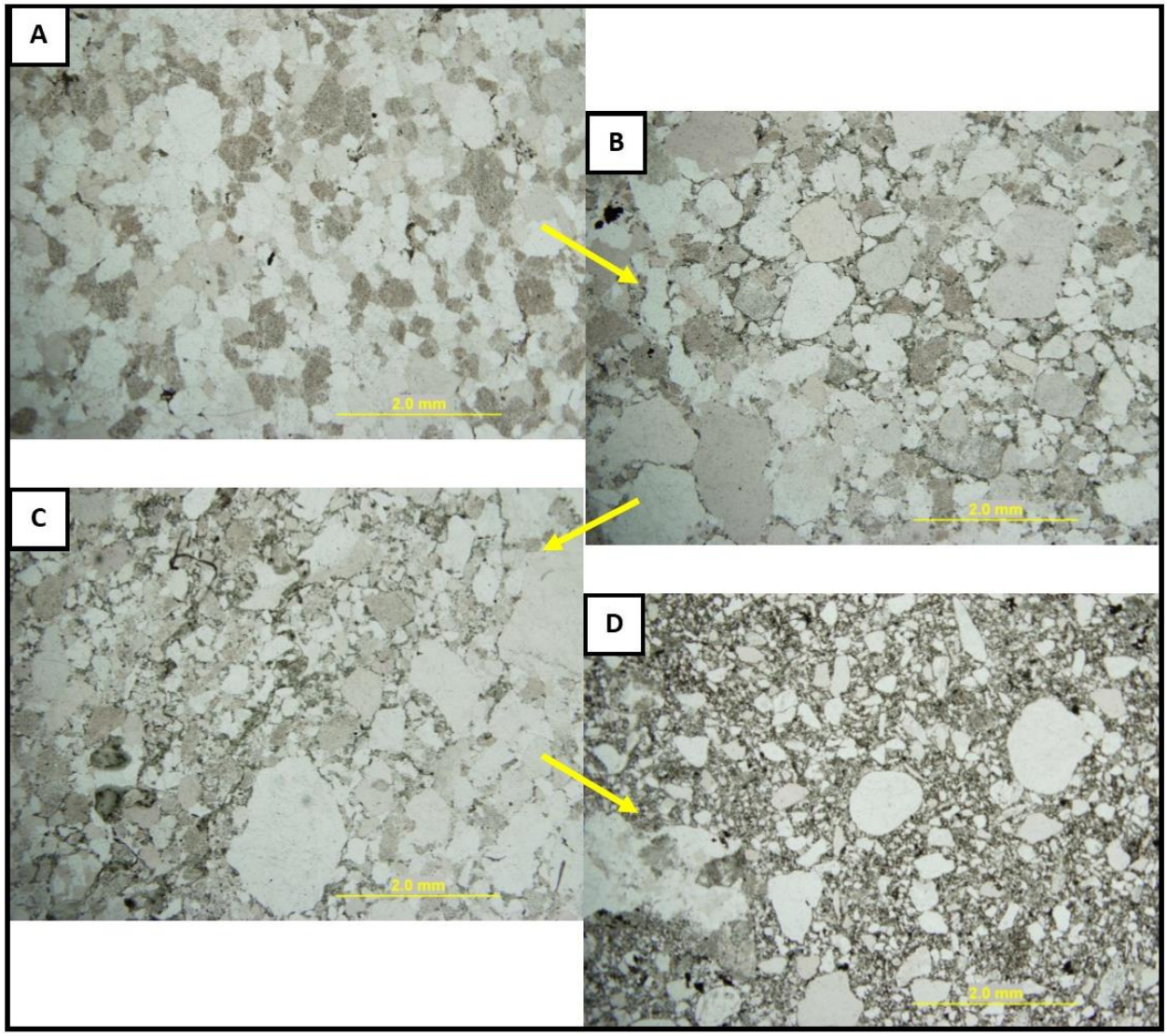

Figure 19: Samples of the upper Mississagi Formation and overlying Bruce Formation along Highway 108, 5km north of Elliot Lake. A) Typical Mississagi sandstone taken near the base of the outcrop. B) Sandstone 30cm below the contact with overlying diamictite. C) Sandstone 10cm below contact. D) Bruce diamictite containing round to angular clasts of a highly variable grainsize in a clay-rich matrix.

2.3 LITHOFACIES ASSOCIATION 3: CALCAREOUS LAMINATED SANDSTONE

At Lauzon Lake the contact between the Bruce and underlying upper Mississagi Formation is marked by features unique to this location. The typical increase in grainsize and decrease in sorting observed in other locations was present here with grainsize ranging from medium-grained sand to granules, but a unit of parallel laminated calcareous sand, approximately 2m thick is present below the contact with the diamictite (Figure 20A). Where directly underlying the Bruce diamictite, structure is lost, but parallel and wavy to contorted lamination is visible beneath the massive structureless sand of the contact. Laminations of the calcareous sandstone at Lauzon Lake are poorly sorted, range in thickness from several mm up to 1-2cm, have a low matrix content, and in places show variations in grainsize between very coarse sand layers and fine- to medium-grained sand layers with the fine- to medium-grained sand layers being more easily eroded and giving the rock a ribbed appearance (Figure 20B). The finer sand layers have a higher concentration of carbonate cement than the coarser sand layers, which causes the finer layers to erode more readily. In some places the more eroded layers are darker in appearance, indicating that the sand layers with more carbonate cement also contain a greater matrix content. The direct contact with the overlying diamictite is sharp and the Bruce Formation in this vicinity is unique in that there are a number of pink granite clasts in the diamictite near the lower contact.

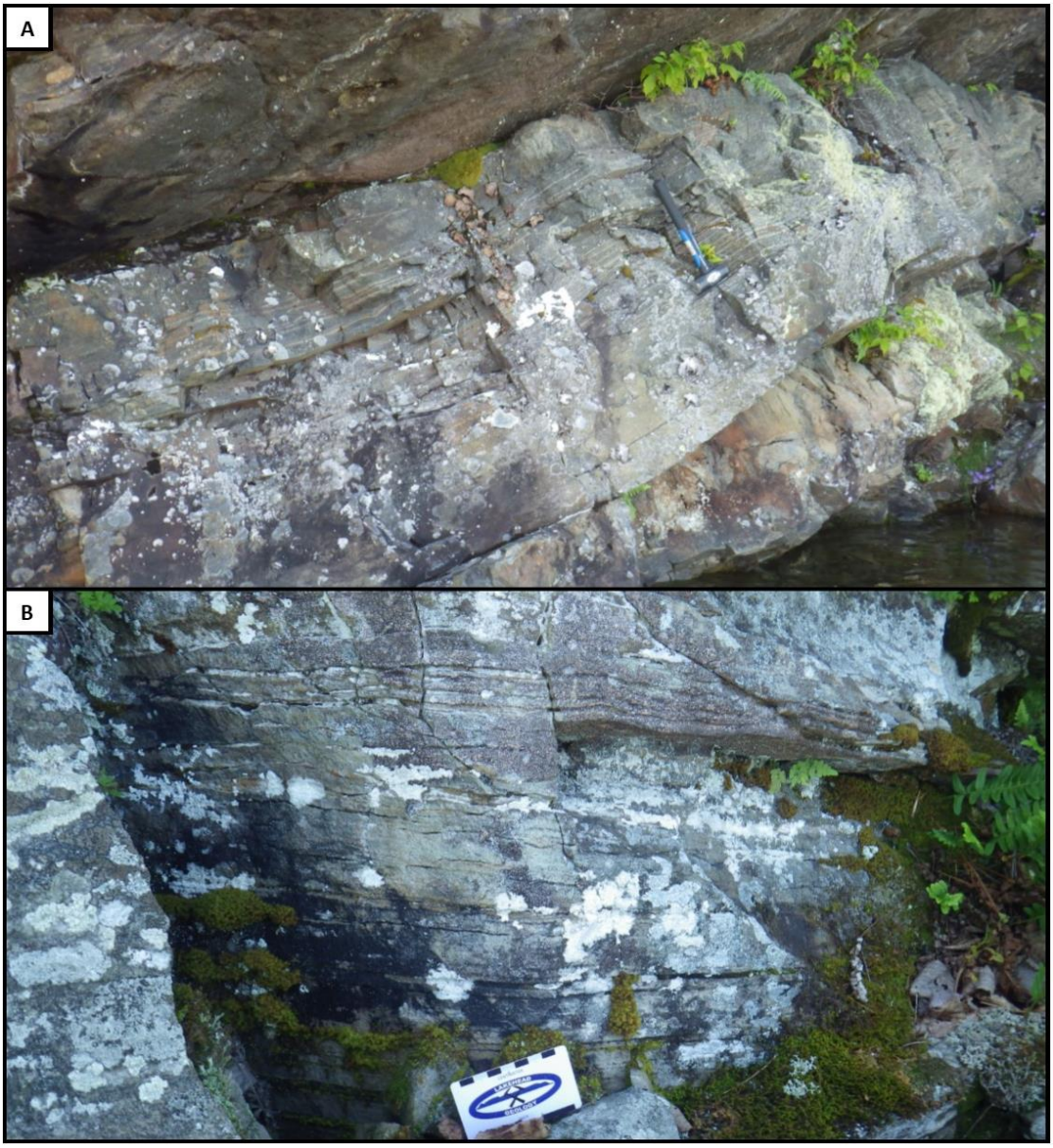

Figure 20: Laminated sandstones at Lauzon Lake A: Sharp contact between laminated sandstone of the upper Mississagi Formation and the overlying Bruce diamictite. B: Laminated sediments showing the ribbed appearance of the sandstones due to the difference in weathering of layers.

3 MISSISSAGI FORMATION DISSCUSSION

Previous studies of the Mississagi Formation have focused on whether the succession was deposited in a primarily fluvial or marine environment (Long, 1976, 1978). A marine depositional environment is inferred based on: a lack of fining upwards cycles, possible prograding marine cycles, and bimodal and polymodal paleocurrent distributions (Pettijohn, 1970; Card et al., 1977; Palonen, 1971, 1973; Bennet et al., 1991). Proponents of a fluvial environment of deposition use some of the same features to bolster their claim, such as a bimodal to polymodal paleocurrent distribution and a lack of fining upwards cycles, but also point to other evidence such as a lack of erosional features, the high-cross bedding azimuth variance values, an increase in silt layers towards the top of the formation, and an upwards decrease in cross-bed thickness and lowering of inclination of graded foreset beds (Visher, 1965; Young, 1966, 1969; Casshyap, 1967, 1969, 1971; Chandler, 1969; Frarey and Roscoe, 1971; Parviainen, 1973). There is also a general lack of extensive mudstone units, symmetrical and asymmetrical ripples, tidal bedding, and reactivation surfaces throughout the Mississagi stratigraphy, which further bolsters the suggestion that the Mississagi Formation was deposited in a non-marine environment (Long, 1976). The interpretation of a fluvial environment of deposition has been later built upon to include two major braided stream systems that is largely based on two distinct paleocurrent patterns that indicate separate fluvial systems sourced from the Sault Ste. Marie-Elliot Lake region, and the Cobalt region (Long, 1976, 1978). The area of coalescence for these systems was the southern Huronian area and the system continued flowing south from this intersection, with clastic material being derived from both sources (Long, 1976). The results of this study support the interpretation of the Upper

Mississagi Formation being deposited largely in a fluvial environment, as Lithofacies Association 1 has many features that strongly indicate non-marine origins that will be discussed in this section.

3.1 LITHOFACIES ASSOCIATION 1: DISTAL BRAIDED FLUVIAL SYSTEM

Lithofacies Association 1, which dominates the upper stratigraphy of the Mississagi Formation, is interpreted to represent a distal braided fluvial system and records features that are consistent with the previously completed interpretations by Parvianinen (1973) and Long (1976, 1978). These features include: a general lack of fining upwards cycles or any reliable form of cyclicity, presence of unimodal paleocurrent distributions, and absence of features that would point to a marine environment such as laterally extensive mudstone units and distinct tidal structures (Parvianinen, 1973; Long, 1976, 1978). The stratigraphy of the cross-stratified sandstones lithofacies association is highly similar to what was previously described by Long (1976, 1978) and is dominated by large-scale, planar cross-stratification with lesser small- and medium-scale planar and trough cross-stratification. A predominance of cross-stratified sandstones within Lithofacies Association 1 and the relationships between them is an indicator of a fluvial environment of deposition because sandy braided fluvial environments are characterised by repetitive hierarchies of superimposed dunes of different morphologies and scale, caused by variable discharge rates in these systems (Pretious and Blench, 1951; Neill, 1969; Allen and Collinson, 1974). In Lithofacies Association 1, large-scale planar cross-stratified units formed from well-sorted medium- and coarse-grained sands are interpreted to represent transverse bars. Evidence of contortion, slumping, and overturning of laminae within the upper parts of the foresets of large-scale planar units is a common feature within braided fluvial

environments and have been ascribed to probable rapid deposition causing a loss of strength in the bed (Allen and Banks, 1972; Hendry and Stauffer, 1977).

Trough cross-stratification is the second most common lithofacies and occurs usually as small-scale trough cross-stratified bundles erosively scouring into underlying planar cross-stratified beds. This is another common feature of fluvial environments where a decrease in water-level causes the tops of transverse bars to become exposed and transected by small chute channels that flow over their tops and deposit trough cross stratified sand (Smith, 1970). The tendency towards an upwards decrease in bed form size is also characteristic of fluvial environments (Potter, 1967; Thompson, 1970), and this is displayed commonly throughout the upper Mississagi Formation by the presence of small-scale trough cross-stratification overlying large-scale planar cross-stratification. Lastly, reactivation surfaces were observed in large scale planar cross-stratified units, and clay drapes were observed in places separating individual trough or planar cross-stratified beds or accentuating internal reactivation surfaces within cross-stratified beds. Reactivation surfaces and clay drapes, while typically ascribed to tidal activity, are not unheard of within fluvial environments and can be formed by fluctuations in water stage (Collinson, 1970; Smith, 1970).

Horizontal lamination is rare in Lithofacies Association 1 but may have similarly formed during waning water levels, as the presence of thin horizontally stratified sandstone beds overlying planar cross-stratified sandstone units has been observed in other fluvial environments and forms under lower depth and/or higher velocity conditions than cross-stratification (Smith, 1970). In instances where planar cross-stratified beds superimpose one another, this may be due to a sharp increase in depth, possibly during flood conditions (Jopling,

1966; Smith, 1970). The climbing ripples observed on a planar cross-stratified unit at Wells Island represent high sedimentation during a waning flood stage event (Stear, 1985).

In some instances the rare parallel laminated units show interlamination of finer and more silt and clay-rich layers and more well sorted coarser sand layers. This interlayering of the two may be the result of variations in flow velocity. During higher flow conditions, sands are transported in upper stage plane bed and finer material is transported away, whereas a slowing down of flow conditions allows for deposition of finer-grained micaceous material (Stear, 1985). The presence of platy particles has been shown to inhibit the formation of ripples (Manz, 1978), which may also provide some explanation as to why rippled bedding is uncommon to rare within the upper Mississagi Formation, as Long (1976) has previously identified a relatively high amount of mud-grade material within the matrix of the Mississagi sandstones. This feature is also another piece of evidence that Long (1976) used to interpret the fluvial nature of the Mississagi Formation, as mud and sand would tend to be separated in a marine environment through winnowing processes (Folk, 1968). Horizontal stratification was rare in nearly all outcrops observed and may further supplement the interpretation that the upper Mississagi Formation represents a downstream fluvial environment as horizontal stratification is typically rare in distal braided environments and usually is found overlying planar cross-stratified sand beds (Smith, 1970). An alternative interpretation for the source of the layering is that the interlamination of sand and silt and clay-rich layers represent heterolithic bedding and record the beginnings of tidal influence on the sediments. This would provide an ideal interpretation for the clay-infiltrated tops to the sand layers and may suggest a shift to a tide-influenced river channel.

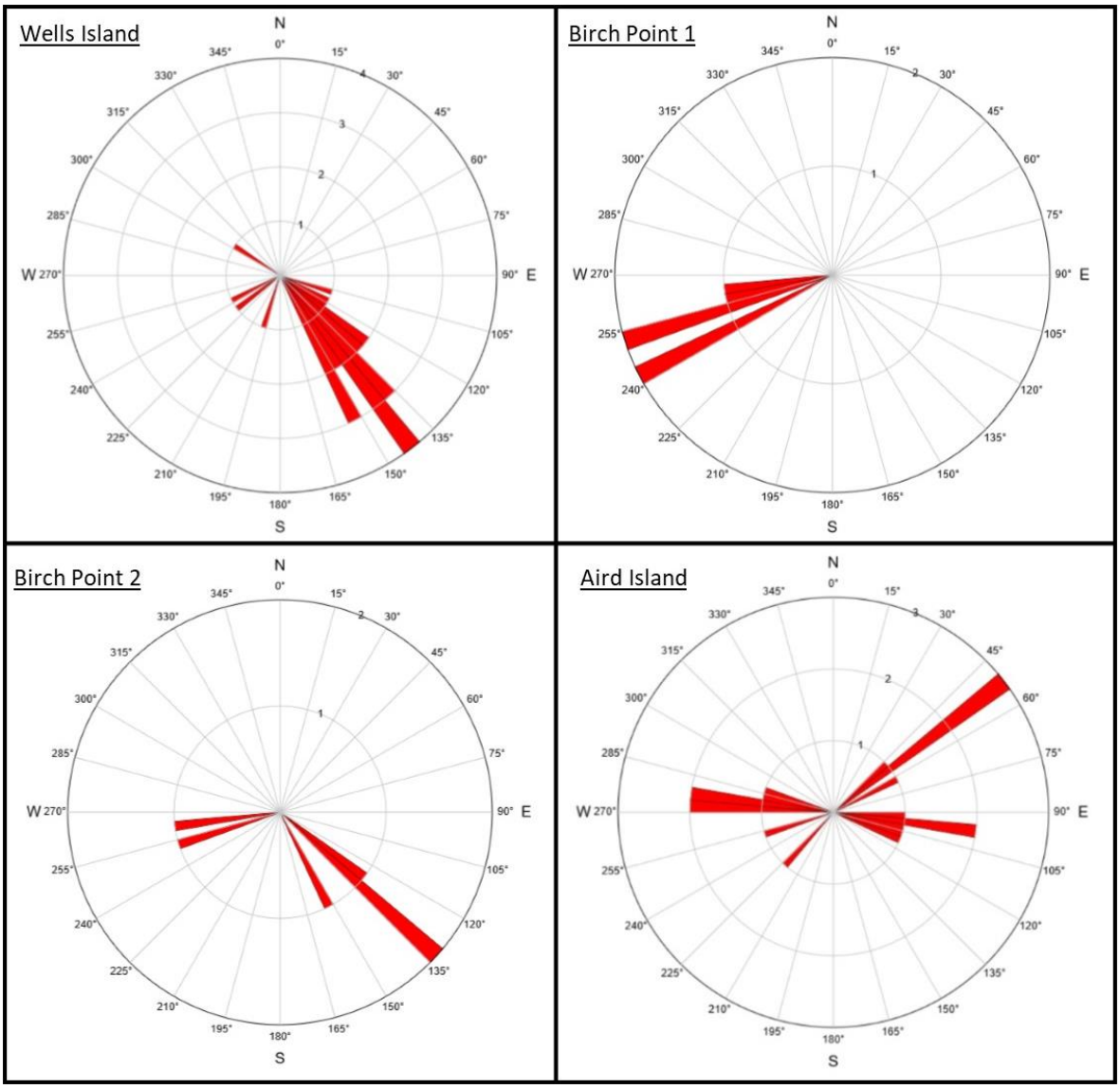

Figure 21: Rose diagrams depicting average paleocurrent directions for various outcrops of the upper Mississagi Formation. Birch Point 1 outcrops ~500m west of Birch Point 2.

Paleocurrent data collected from outcrops logged along the north shore of Lake Huron indicate that there is variability in predominant paleocurrent directions at each location (Figure 21). At Wells Island, the strongest paleocurrent direction was to the southeast, with a few other values scattered more towards the west and southwest. The two paleocurrent distributions generated 1km and 1.5km east of Birch Island are interesting because they show different paleocurrent directions despite only being located 500m apart. The outcrop located 1km from

Birch Island has unidirectional southwest paleocurrents, while the outcrop located only 500m farther to the east has a southeast transport direction but has a few beds that record a west-southwest direction similar to the more western outcrop. Rose diagrams generated from paleocurrent data collected at the four locations along the north shore of Lake Huron provide predominantly unidirectional current patterns, as would be expected in a fluvial environment (Figure 21). The exception to this is at Aird Island where two sets of bidirectional trends, one east-west, and another southwest-northeast, suggest that there may have been some tidally-influenced conditions at this location. The northeast trend is stronger in influence than the others and the east-west trends are of equal strength.

Several more extensive studies have been completed on the paleocurrent distributions of the Mississagi Formation and record a great deal of variability in transportation directions (cf. McDowell, 1957; Pienaar, 1963; Palonen, 1971, 1973; Long, 1976). This has resulted in several different conclusions for interpretations of the depositional environment. Long (1976, 1978) found two distinct patterns in the paleocurrent directions indicating separate fluvial systems sourced from the Sault Ste. Marie-Elliot Lake region and the Cobalt region. This interpretation is supported by other studies which found an easterly transport direction in the Bruce Mines area and a southwest direction of transport in the Sudbury area (McDowell, 1957; Frarey and Roscoe, 1970). Long (1976, 1978) argues that the dominance of unimodal distributions collected from the Mississagi Formation is evidence that the sands are fluvial in origin. A different analysis, made by Palonen (1971, 1973) is that the Mississagi Formation was deposited under mostly marine conditions based on bimodal distributions from the Panache Lake area and east-west counterclockwise rotation of principal current directions in the

southern exposures. The counterclockwise distribution of paleocurrent principal modes was interpreted to represent circulation patterns in a marine embayment. Furthermore, the unidirectional nature of paleocurrents collected from the areas around Elliot Lake and north-central exposures (McDowell, 1957; Pienaar, 1963) was suggested to be the result of sand waves migrating across a tidal flat (Palonen, 1973).

The varied results of the paleocurrent distributions collected in this study attest to the diverse and complicated nature of the sediment transport directions of the upper Mississagi Formation. Based on the sedimentological similarities between what was described by Long (1976, 1978) and the observations made in this study, the paleocurrent distributions for the upper Mississagi Formation are reasonable with regard to his interpretation of a largely braided fluvial environment. The distinct contact between the upper few meters of stratigraphy in the Mississagi Formation and the overlying Bruce Formation, which will be discussed next, does however point to the possibility of some marine/nearshore influence on the paleocurrent distributions. This is supported by the strong bimodal east-west distribution recorded at Aird Island. Therefore, it is suggested that the upper Mississagi Formation largely represents sediment transport in a fluvial system.

3.2 LITHOFACIES ASSOCIATION 2: GLACIODELTAIC OUTWASH

The upper few meters of stratigraphy of the Mississagi Formation directly below the contact with the Bruce Formation is distinct for its overall decrease in sorting and, typically, an overall increase in grainsize from medium- to coarse-grained sandstone to very coarse-grained

sandstone to gravel. While not a universal truth, this is most commonly the case and suggests an increase in energy, and energy fluctuations, in the environment heralding the advance of the Bruce ice sheet. The contact between the Bruce and the Mississagi Formations is typically sharp but can be gradational to transitional in places, usually represented as an erosional mixing or uptake of unconsolidated upper Mississagi sands into the base of the Bruce diamictite (Parviainen, 1973; Long, 1976, 2009). Furthermore, in several locations the upper few meters of stratigraphy of the Mississagi Formation contains greater amounts of mud layers and drapes and the development of heterolithic lamination within cross-stratified units. These variations from the remainder of the underlying stratigraphy suggest that the uppermost Mississagi Formation records a shift to a deltaic environment immediately prior to advance of the Bruce ice sheet.

A shift to heterolithic lamination, including very coarse-grained sand alternating with coarse- and medium-grained sand or mud- and silt-rich sand alternating with well-sorted sand laminae suggests greater fluctuations in flow velocity. The most common mechanism for heterolithic bedding is tidal current activity. The finer-grained layers would be deposited during high tide, slack-water conditions when flow over the offshore bar system is stalled and the lack of current allows for mud to be deposited as a layer on the upper surface of the sand (Goodbred and Saito, 2011). Thus, the presence of heterolithic bedding in units of the uppermost Mississagi Formation suggests a shift to a tide-dominated braid delta.

The distinct upper contact of the Mississagi Formation at Chilbow Lake, where a ~10m high outcrop of consecutive rippled sand layers underlies the contact with the Bruce Formation, indicates a probable shallow water environment. Current and wave rippled layers alternate and

are superimposed upon one another indicating that current and wave activity were active during their deposition, immediately prior to the advance of the Bruce ice sheet. This interpretation is supported by the presence of a clast supported conglomerate at the basal contact of the Bruce Formation which may be the result of winnowing.

The shift to an overall higher energy marine, thus deltaic, environment immediately prior to ice override, and the commonly sharp contact between the upper Mississagi Formation and the overlying Bruce Formation, suggests the Bruce ice sheet was mostly grounded as it entered the basin. In areas of the Quirke Lake Syncline, boulders of sandstone similar to the Mississagi have been observed in the overlying Bruce Formation indicating that the upper Mississagi may have been either frozen or semilithifed at the time of ice override (Robertson, 1961, 1962, 1963a; Parviainen, 1973; Long, 1976). While the upper Mississagi Formation was originally interpreted to have been semilithifed at the time of the Bruce ice advance, indicating a break in time before deposition of the Bruce diamictites, it has been more recently suggested that no break in time occurred and that the upper Mississagi was frozen prior to ice advance (Roscoe, 1969; Parviainen, 1973; Long, 1976). Furthermore, a previously proposed 'bleaching' of the uppermost 50-100cm of the Mississagi Formation during the hypothesized break in sedimentation has instead been determined to be a mineralogical shift to an increase in quartz content and a decrease in micaceous material (Roscoe, 1969, Parviainen, 1973). The interpretation of a mineralogical shift as opposed to a break in sedimentation is supported by the occurrence of granitic cobbles and pebbles akin to those of the Bruce Formation present within the uppermost Mississagi Formation (Parviainen, 1973).

The poorly sorted and very coarse-grained sands adjacent to the contact seldom display any evidence of internal structure and are massive. This has been suggested to possibly represent destruction of structures by shearing due to bed override (Long, 1976). The sheared sandstone unit located near the contact at Aird Island, as was observed in this study and others, would support this interpretation (Long, 1976). Other evidence that supports this theory is the incorporation of sand from the underlying Mississagi Formation at some locations into the overlying diamictite as probable frozen blocks or as dissagregated grains (Ginn, 1961; Robertson 1961, 1962, 1963; Parviainen 1973, Long 1976). The presence of blocks of sandstone near the contact with the Bruce diamictite was observed on Highway 108 where lenses of clean and well sorted sand are found within a matrix of muddy sand, which may have similarly been frozen and incorporated into the base of the Bruce ice sheet. In the case of disaggregated incorporation or places where internal structure of sand bodies is lost, these contacts have been suggested to be transitional in nature (Long, 1976).

3.3 LITHOFACIES ASSOCIATION 3: SUBAQUEOUS FLUVIAL OUTWASH

The environment of the Upper Mississagi Formation forming a 60km belt in the area of Lauzon Lake has a unique stratigraphy such that it has been referred to as a separate member; the Lauzon Member (Robertson, 1964, 1966b, 1970; Robertson and Fraser, 1964; Long, 1976). The uppermost laminated sediments observed in this study are merely the last remnant of a stratigraphic sequence that is representative of a distinct environment. Massive and parallel laminated medium-grained sands dominate this member, and it is separated from the

underlying remainder of the typical cross-bedded sandstones by a conglomeratic horizon with an erosive base (Long, 1976). Cross-bedded sandstones in this member occur usually as isolated planar cross-beds that are separated by massive and parallel laminated medium-grained sandstones (Long, 1976). Modal analysis of this conglomerate within the Lauzon Member indicates a resemblance to the Bruce Formation, excepting a predominance of red coloured clasts as opposed to the typical grey to white granite clasts of the Bruce diamictite (Parviainen, 1973; Long, 1976). In this study pink granitic clasts were also observed at the base of the Bruce Formation as well, which may indicate a unique source composition. The conglomerates of the Lauzon Member also contain argillite and conglomerate clasts that are lithologically akin to the Pecors and Ramsey Lake Formations. It has been suggested that the conglomeratic units that are common in the base of the Lauzon Member are the result of deposition through gravity flow that infilled a proximal fan environment that, upon becoming infilled, was overlain by a lacustrine or marine environment (Long, 1976). It has also been suggested that the conglomerates were at least partially deposited through glacio-deltaic conditions which is supported by the presence of a dropstone lithofacies observed at Lauzon Lake (Parviainen, 1973; Long, 1976). Both hypothesis are in agreement that deposition of the Lauzon Member represents subaqueous conditions, whether in a lacustrine or marine environment, and that the Lauzon Member is superseded by diamictites of the Bruce Formation (Parviainen, 1973; Long, 1976).

3.4 CONCLUSIONS

Based on the observations made in this study, along with previously completed work, it seems most likely that the upper Mississagi Formation was largely deposited in a braided fluvial environment, based on the repetitive nature of the stratification that is dominated by planar and trough cross-stratification with little evidence for large scale cyclicity (Long, 1976; cf., Pretious and Blench, 1951; Neill, 1969; Allen and Collinson, 1974). The biggest exception to this interpretation is the undoubtedly lacustrine or marine environment that deposited the Lauzon Member in the Lauzon Lake area. Here, a standing body of water allowed for the deposition of unique lithofacies such as calcareous laminated sandstones and laminated sediments with dropstones (Parvianinen, 1973; Long, 1976). The advance of the Bruce ice sheet is typically first observed as an increase in the presence of deformation of sedimentary structures and an increase in grainsize and decrease in sorting of sediments. This transitional zone is interpreted to represent a glaciodeltaic environment. The uptake of both consolidated and unconsolidated Mississagi sands into the Bruce diamictite suggests that ice advance occurred prior to lithification of the Mississagi Formation. The often sharp contact between the overlying diamictite and the underlying sandstone beds, and this incorporation of underlying sediments suggests that the Bruce glacial advance was grounded in places.

4 BRUCE FORMATION

The Bruce Formation is the lowermost Formation of the Quirke Lake Group and is typically described as conformably and gradationally overlying the Mississagi Formation (Ginn, 1961; Robertson, 1964). It is dominated by polymictic conglomerate that is largely matrix supported, massive, and uniform in appearance (Robertson, 1964; Parviainen, 1973; Card et al., 1977). Quartzite and siltstone lenses are also present, most commonly in the lower part of the formation, but laminated greywacke does occur in the upper part as well (Robertson, 1964; Parviainen, 1973). Thickness of the Bruce Formation is variable, though it occurs as a basin-wide sheet that reaches up to 460m thick (Ginn, 1961; Parviainen, 1973; Card et al., 1977). A general trend has been noted that the northern exposures of the Bruce Formation are more uniform in thickness and overall thinner than in the south, but it becomes thinner again at its southernmost extent (Parviainen, 1973; Young, 1981). The lower contact with the Mississagi Formation is conformable to disconformable, as has been discussed in the previous section, while the upper Bruce Formation directly below the contact with the Espanola Formation is conformable and marked in places with laminated sediments containing dropstones (Frarey and Roscoe, 1970).

Overall the Bruce contains a low clast content; however, clast-supported areas have been observed in the Sault Ste. Marie-Elliot Lake area, usually at the base of the formation, and are suggestive of a locally erosive contact (Robertson, 1964). Clasts consist largely of subrounded to subangular white granite with minor red granite, metavolcanics, gneiss, and diabase, as well as pebbles of quartz, feldspar, chert, and jasper (Robertson, 1964). The hypothesized source of the granite clasts is the Algoman granite based on mineralogical and

textural features (Robertson, 1964). These Algoman granites, along with most of the other stones found within the Bruce diamictite, are derived from Archean terrain to the north of the Huronian succession (Frarey and Roscoe, 1970; Young, 1981). The Birch Lake granites and Keewatin volcanic-schistose complex also provided some sediment to the Bruce from the north (Casshyap, 1969). The clast content of the Bruce is unique from the other diamictite bearing formations in the Huronian Supergroup in that it has a greater abundance of sedimentary rock fragments than other Huronian Formations (Parviainen, 1973). Clasts are most commonly pebble-sized and the proportion of clasts to matrix is most typically low with clasts averaging 20-30% of the rock (Frarey and Roscoe, 1970; Young, 1981).

The matrix of the Bruce Formation has been described as highly siliceous and contains quartz with lesser plagioclase, potassium feldspars, sheet silicates, and opaques (Ginn, 1961; Robertson, 1964; Parviainen, 1973). Sorting of the matrix is typically moderate to poor and a general trend has been noted that the Bruce is overall finer-grained towards the top of the Formation (Parviainen, 1973). The pyrite and carbonate content increases towards the top as well while the quartz and feldspar content decrease upwards (Parviainen, 1973). The most prevalent matrix component is rounded grains of quartz (Robertson, 1964). Carbonate occurs locally as a cement, at the top of the Formation in the east (Frarey and Roscoe, 1970; Young, 1981).

While overall homogenous and massive, the diamictite is rarely host to sedimentary structures including: graded bedding, cross bedding, ripple lamination, and evidence of pebbles distorting poorly laminated matrix (Ginn, 1961; Robertson, 1964; Frarey and Roscoe, 1970). Sandstone lenses may be massive, or can display cross-lamination and may be slightly

calcareous with associated secondary iron minerals (Ginn, 1961; Casshyap, 1969; Robertson, 1964; Card et al., 1977). Cross bedding can sometimes be observed within the sandstone bodies and foreset beds may be graded (Parvianinen, 1973). Sand layers may also display soft sediment deformation and graded bedding is present in sandstone and mudstone layers in the upper parts of the Formation (Parvianinen, 1973; Young, 1981; Long, 2009).

The Bruce Formation has been divided into five lithofacies associations based on the results of this study. Lithofacies Association 2, including both the sandy and silty massive diamictites, constitutes the overwhelming majority of the Bruce Formation stratigraphy and is present throughout its lateral extent. The second most common lithofacies association is the weakly stratified to stratified diamictite which outcrops predominantly along the north shore of Lake Huron east of Birch Island and in the vicinity of McGregor Bay. The siltstone lithofacies association is specific to a 1-3m thick siltstone bed that almost uniformly overlies the Bruce Formation diamictites and marks the contact with the Espanola Formation. Secondary and more isolated lithofacies associations including the clast-supported diamictite and the laminated carbonate-rich diamictite facies were only encountered in drill core and represent more localized conditions.

4.1 LITHOFACIES ASSOCIATION 1: CLAST-SUPPORTED DIAMICTITE

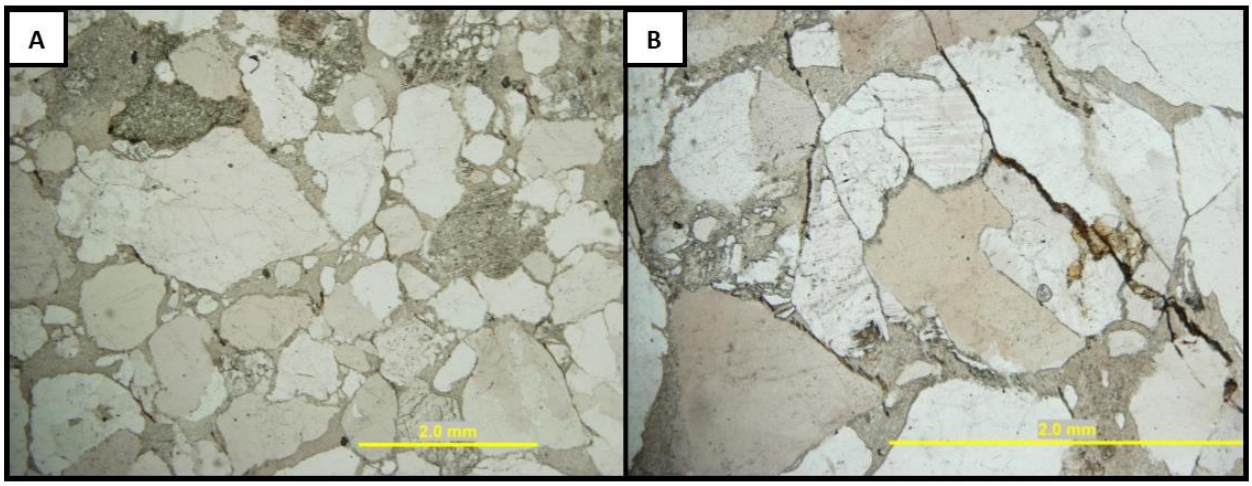

Figure 22: Plane-polarized light (PPL) image of clast-supported diamictite occurring at the lower contact of the Bruce Formation in drill hole 150-1. A: Clasts and grains are usually in contact with one another and grain shape and size is highly variable. B: Close-up of brittle fracturing occurring at the boundaries between clasts.

A clast supported diamictite is present at the base of the Bruce Formation in drill holes 150-1 and 150-2. The clasts are dominantly quartz, with lesser potassium feldspar and lithic fragments of granitic and mafic igneous compositions and plagioclase as an accessory mineral. Sorting of the clasts is very poor, ranging from granules and pebbles to rare cobbles, and no structure is present within the facies (Figure 22A). Clasts are randomly oriented within the matrix, and there is also a broad range in the angularity of clasts from highly angular to round. Some clasts have jagged or broken edges resulting in a brittle splintering of grains in extreme cases (Figure 22B). The matrix component constitutes ~10-15% of the diamictite and consists of very fine-grained sericite with accessory chlorite and a variable amount of sulfides. Sulfide minerals within the matrix are euhedral. In other areas the pyrite forms clusters of rounded frambiodal grains that range in size from silt up to a fine-grained sand. The contacts between this unit and the adjacent units are sharp and in both drill holes, 150-1 and 150-2, the clast supported diamictite is underlain by a very poorly sorted sandstone with rare layers up to

~10cm thick that contain pebbly clasts up to 3cm long. These conglomeratic layers have gradational contacts with the sandstone of the upper Mississagi Formation.

4.2 LITHOFACIES ASSOCIATION 2: MASSIVE SANDY AND SILTY DIAMICTITE

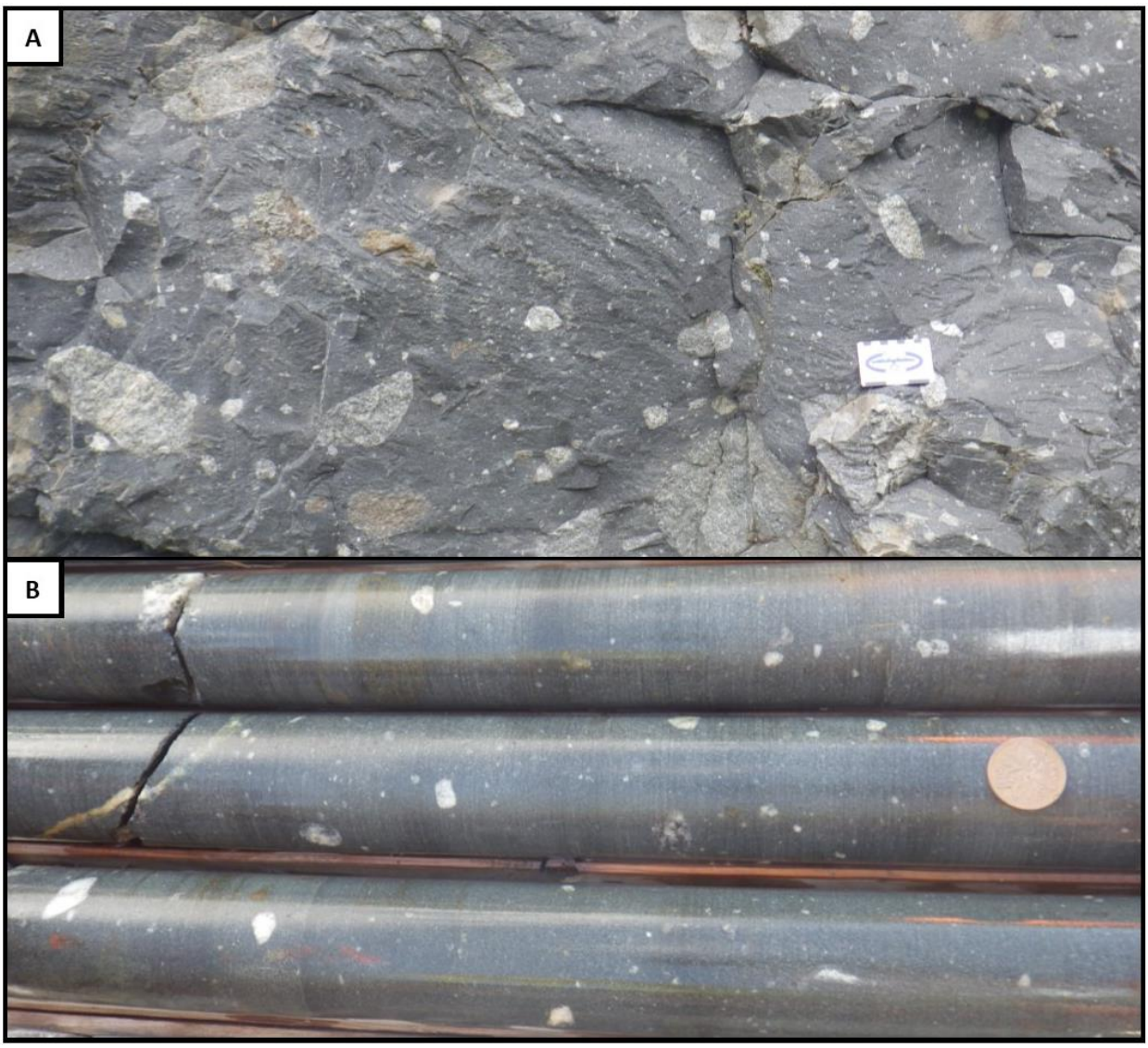

Figure 23: Comparison photos of the subtle differences between massive sandy diamictite and massive silty diamictite. A: Massive sandy diamictite outcrop is a lighter grey colour due to the higher quartz fraction. B: Massive silty diamictite in drill core. The matrix is slightly darker grey due to the higher silt-sized fraction and, in this instance, clasts are no larger than pebble-sized.

The massive sandy diamictite lithofacies constitutes the vast majority of the Bruce Formation deposits and is host to sand and silt layers and lenses that may be massive, parallel laminated, or cross-bedded. This lithofacies is present throughout the Sault Ste. Marie-Elliot Lake and Sudbury-Espanola areas. The matrix of this unit is unsorted to very poorly sorted, ranging from silt and clay to very coarse-grained sand and granules. In thin section the coarser matrix fraction is distinctly quartz-rich, with minor to rare potassium feldspar and plagioclase present. Quartz grains are typically subround, but may be round to angular, and along the north shore of Lake Huron where metamorphic grades are higher, some quartz grains begin to show grainsize reduction and serrated edges that may be sutured when two grains are adjacent to one another. The finer matrix component consists largely of sheet silicates, and occasionally carbonate is present as a cement. Clasts throughout the Bruce Formation are dominantly white, subrounded granitic rocks with pink granitic rocks present in lesser amounts. These granitic clasts are of a composition that is similar to the sand grains within the matrix component and have a mineralogy that is dominantly quartz and microcline. The massive silty diamictite is mineralogically similar to the sandy diamictite but contains a higher concentration of sheet silicates and is dominated by the clay- and silt-sized fraction (Figure 23A, B).

Siltstone layers, lenses, and soft sediment injections are present within the sandy diamictite facies (Figure 24A). These siltstone areas typically have fairly sharp to slightly gradational contacts with the surrounding or adjacent diamictite facies. Mineralogically the siltstone units are of similar composition to the adjacent diamictite facies as well, but almost entirely lack the sand-sized fraction of grains (Figure 24B).

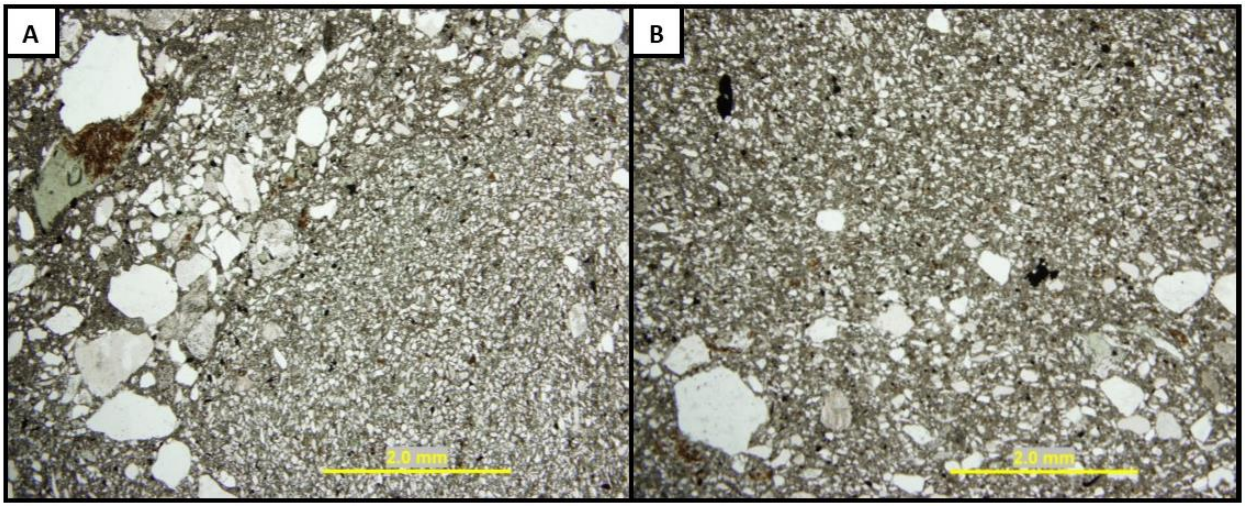

Figure 24: A: PPL image of a sandy diamictite unit in drill hole 150-1 with an injection of siltstone. B: PPL image of sandy diamictite adjacent to a layer of siltstone. The siltstone unit contains rare fine-grained sand-sized material.

Sandstone units of the Bruce Formation are typically contained within the massive diamictite facies as lenses and wisps (Figure 25A). Contacts between these two facies is usually sharp, particularly in the case of smaller wisps and lenses (Figure 25B). However, larger sandstone layers and lenses may have a slightly more dispersed contact. Sandstone layers, lenses, and wisps consist mostly of fine to medium-grained sand and are fairly well sorted, particularly in comparison to the sand-sized fraction of the adjacent diamictite facies. Mineralogy of the sandstone facies of the Bruce diamictite is similar to the sand fraction of the diamictite facies with quartz being the most predominant mineral and potassium feldspar being the next most common mineral and plagioclase present as a rare accessory.

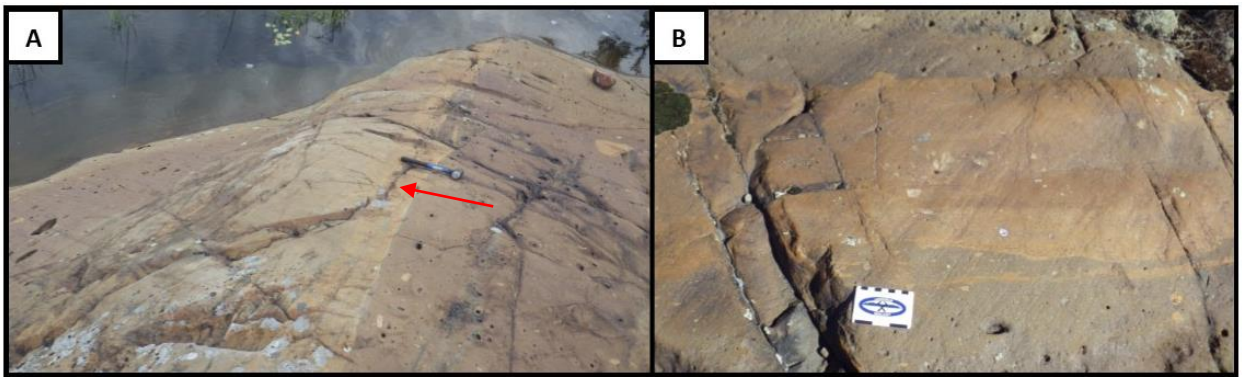

Figure 25: Fine-grained sand layers within the massive diamictite facies that outcrops along the north shore of Lake Huron in the McGregor Bay area. Sand units are devoid of clasts and have a much lower clay content than the adjacent diamictite A: Laterally continuous sand layer (red arrow) with sharp contacts in a massive diamictite unit. B: Close-up of a ~30cm thick sand layer with sharp, slightly irregular contacts.

In outcrop and drill core sandstone units may be massive, cross-stratified, or contain layering that is commonly partially or completely contorted. This contortion of sand layers can be present as faulting of laminae or as loading. Sometimes faulting and loading are present within the same unit as was the case with a sand unit outcropping at Bear Lake where the lower area of the sand unit is loaded and the upper part of the layer is faulted (Figure 26A, B). This sand unit is fine- to medium-grained, has a slightly gradational contact with a massive silty diamictite unit, and is well sorted. The mineral composition of sandstone units in the Bruce Formation is similar to the sand-sized fraction of the diamictite facies.

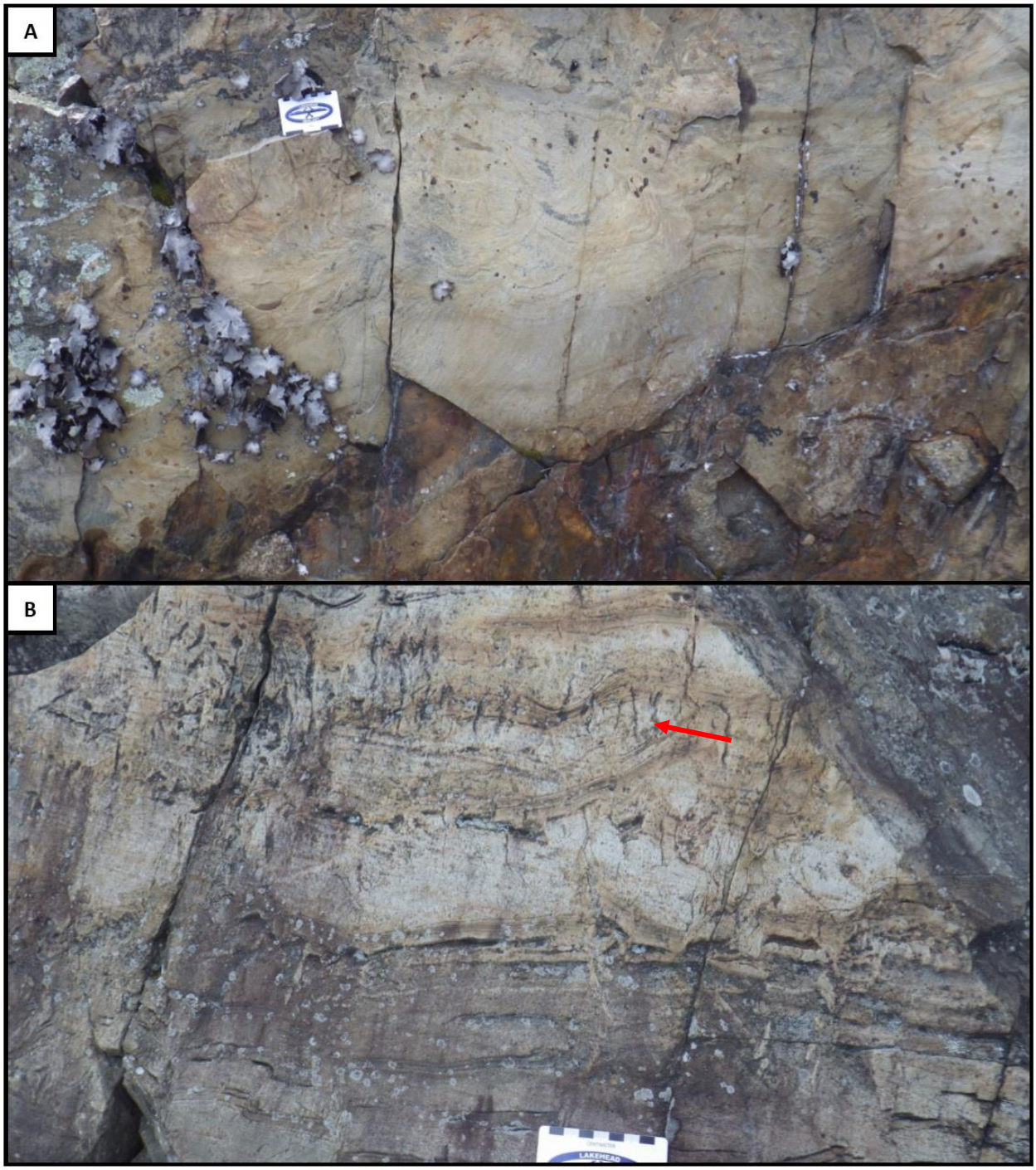

Figure 26: Clean, well-sorted medium-grained sandstone layer contained within a massive diamictite unit at Bear Lake. A: Layering of the sandstone is contorted and loaded. The contact with the underlying massive diamictite is slightly gradational. B: Further up within the same sandstone layer, loading and contortion at the base of the layer gradually transitions into faulted and slightly better preserved lamination at the top (red arrow).

The basal contact of the Bruce diamictite outcrop along Highway 108 contains a cobble-rich layer. The cobbles are typically well-rounded and are largely of white to pink granitic rock. Overlying the cobble-rich layer is a sandy diamictite that contains clasts of largely granitic composition with minor metavolcanics. Within this outcrop of the Bruce diamictite there are three sand lenses that range in thickness from 30cm to 50cm. These lenses are contorted and wispy in appearance and may show some evidence of soft-sediment loading. Overlying the diamictite with sandstone lenses is approximately 5m of typical clast-poor (~10%) diamictite with a sandy matrix and a clast content dominated by white granite clasts.

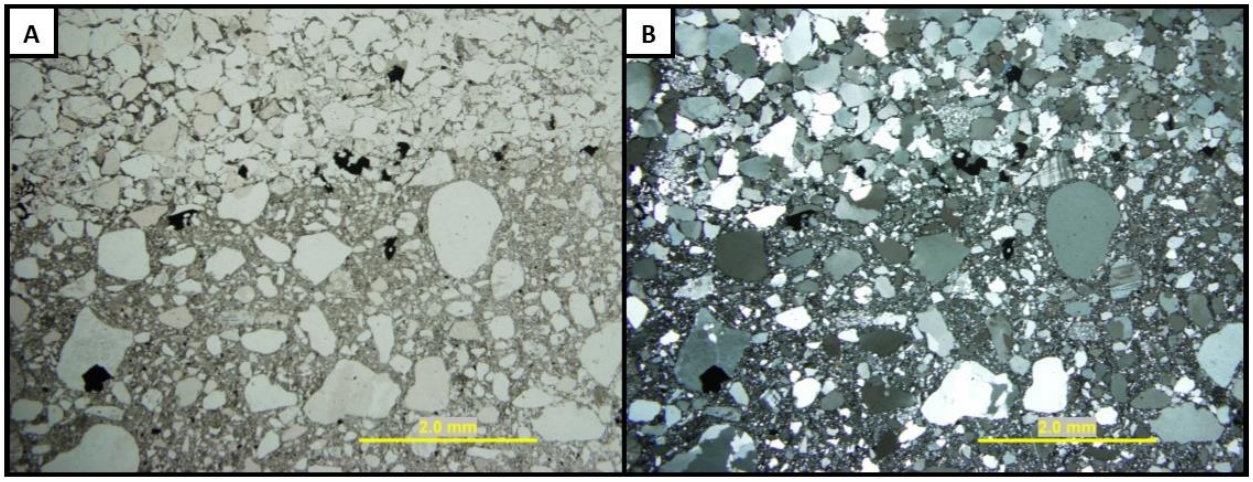

Figure 27: A: PPL image of a sandstone unit that sharply overlies a sandy diamictite unit. B: Cross-polarized light (XPL) image showing the similarities in mineralogy of the diamictite and sandstone. Both the sandstone and the sand fraction of the diamictite are dominated by quartz with lesser potassium feldspar.

In thin section a 57cm thick sandstone unit contained within the lowermost 5m of the Bruce diamictite in drill hole 150-1 is of a fine- to medium-grained sand that overlies the underlying diamictite with a sharp contact (Figure 27A). The mineralogy of the sandstone unit is similar to the sand fraction of the adjacent diamictite unit and consists of quartz with lesser potassium feldspar (mostly microcline) and rare plagioclase (Figure 27B). The angularity of the sand fraction is also similar for both the sandstone and the diamictite with a broad range from

angular to round, but with the average being subround. Sorting of the sand fraction is better in the sandstone unit ranging from fine- to medium-grained sand while grains in the diamictite can range up to coarse-grained sand and rare granules. In the sandstone unit grains are tightly packed with very little matrix material between them. The small amount of matrix material present is largely silt- and clay-sized chlorite.

4.3 LITHOFACIES ASSOCIATION 3: WEAKLY STRATIFIED TO STRATIFIED DIAMICTITE

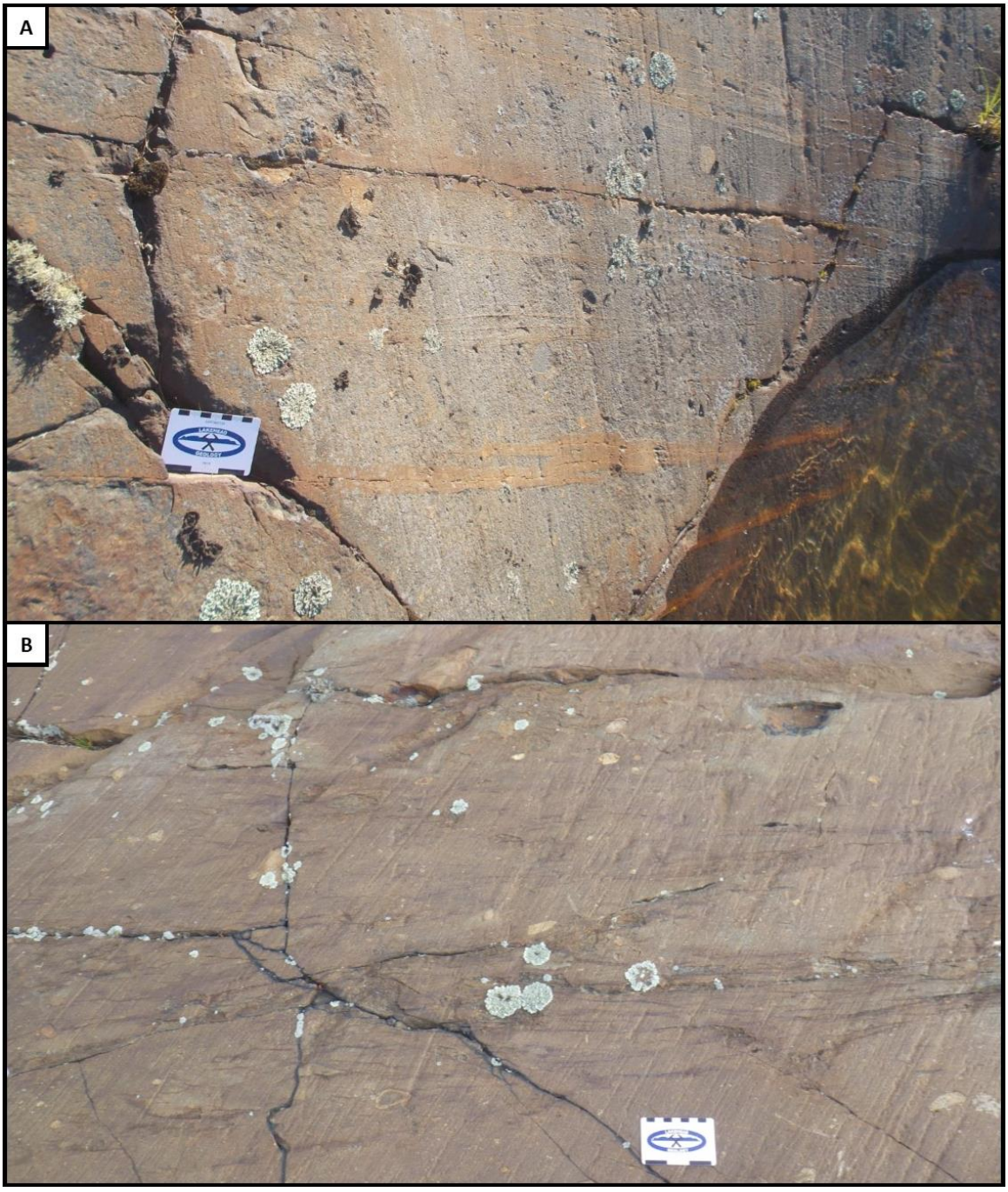

Figure 28: A: Weak horizontal stratification in a diamictite unit outcropping along East and West Channel southeast of Iroquois Bay. Stratification is defined by irregular and discontinuous fine-grained sand layers up to ~4cm in thickness. Clasts are rare within this facies and are rarely larger than cobble-sized B: Highly wispy and discontinuous horizontal lamination in a diamictite outcrop with a low clast content.

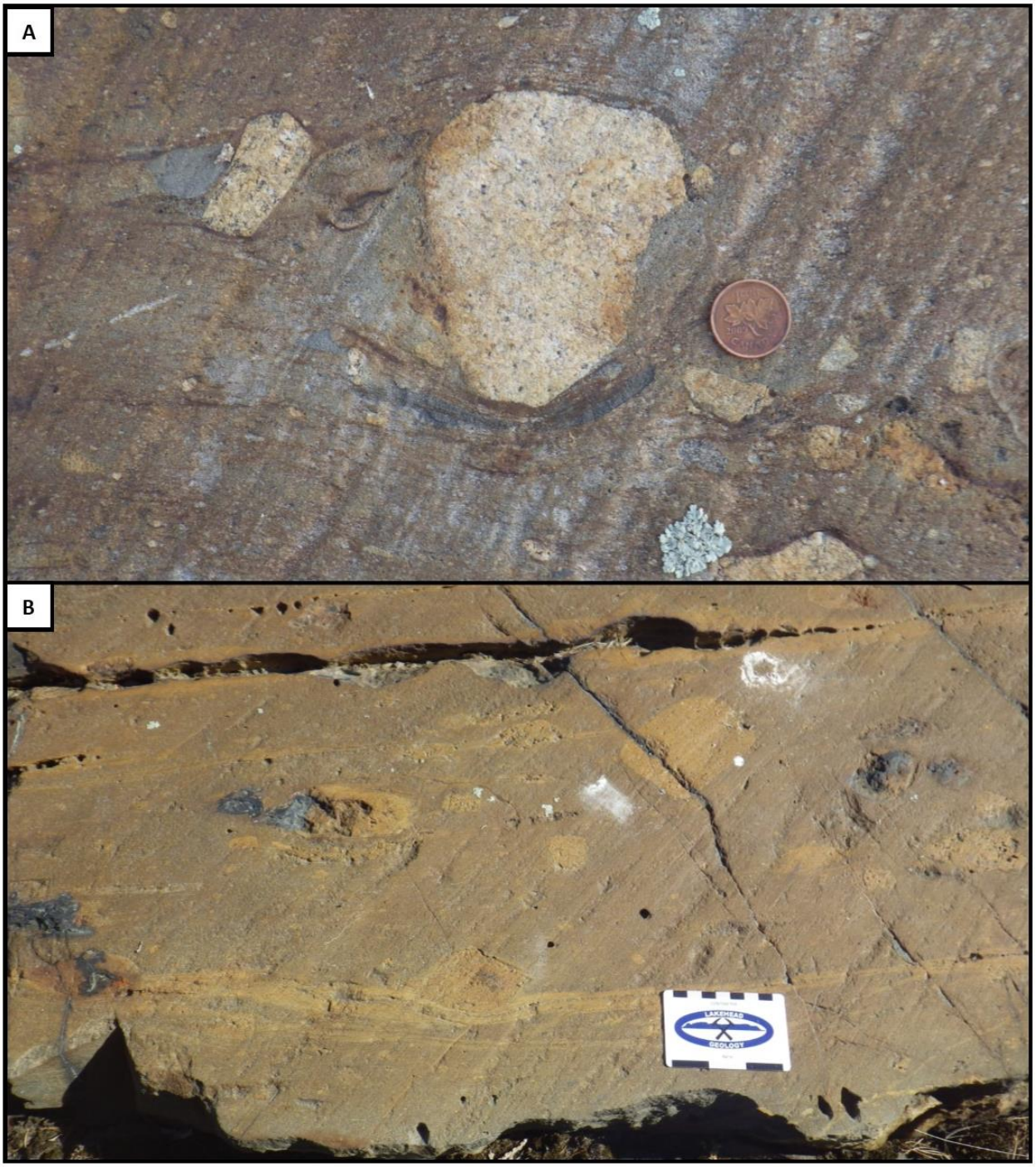

Figure 29: Outcrops of massive and weakly stratified diamictite in the McGregor Bay area. A: White granite clasts that displace the faint mm-thick underlying clay-rich laminae. The clasts are also draped with laminae and the clast to the left also appears to have undergone a small degree of clockwise rotation. The clast on the left is lying on a sand shadow that formed behind the larger clast. B: Weakly stratified diamictite with a white granite clast visibly depressing the wispy sand laminae which it overlies.

The weakly stratified diamictite facies occurs predominantly along the north shore of Lake Huron in the areas of McGregor Bay and east of Birch Point. Stratification within these units is defined by the presence of wispy, discontinuous, and irregular fine-grained sand to clay layers and laminae (Figure 28A, B). Layer thickness is highly variable ranging from millimeter scale up to ~4cm and they have a sporadic and irregular distribution within the diamictite. The diamictite has a silt- and clay-rich matrix and is clast poor, with few clasts larger than pebble-sized, and only rare scattered clasts, of white granitic rock, up to cobble-size. Thickness of the weakly stratified diamictite facies is usually only a few meters and it may not be continuous laterally. This facies is associated with clasts that can displace laminae beneath them (Figure 29A, B) as well as clast-rich layers (Figure 30A, B). Weakly stratified diamictite is associated predominantly with silty massive diamictite and has a gradational contact with adjacent massive facies.

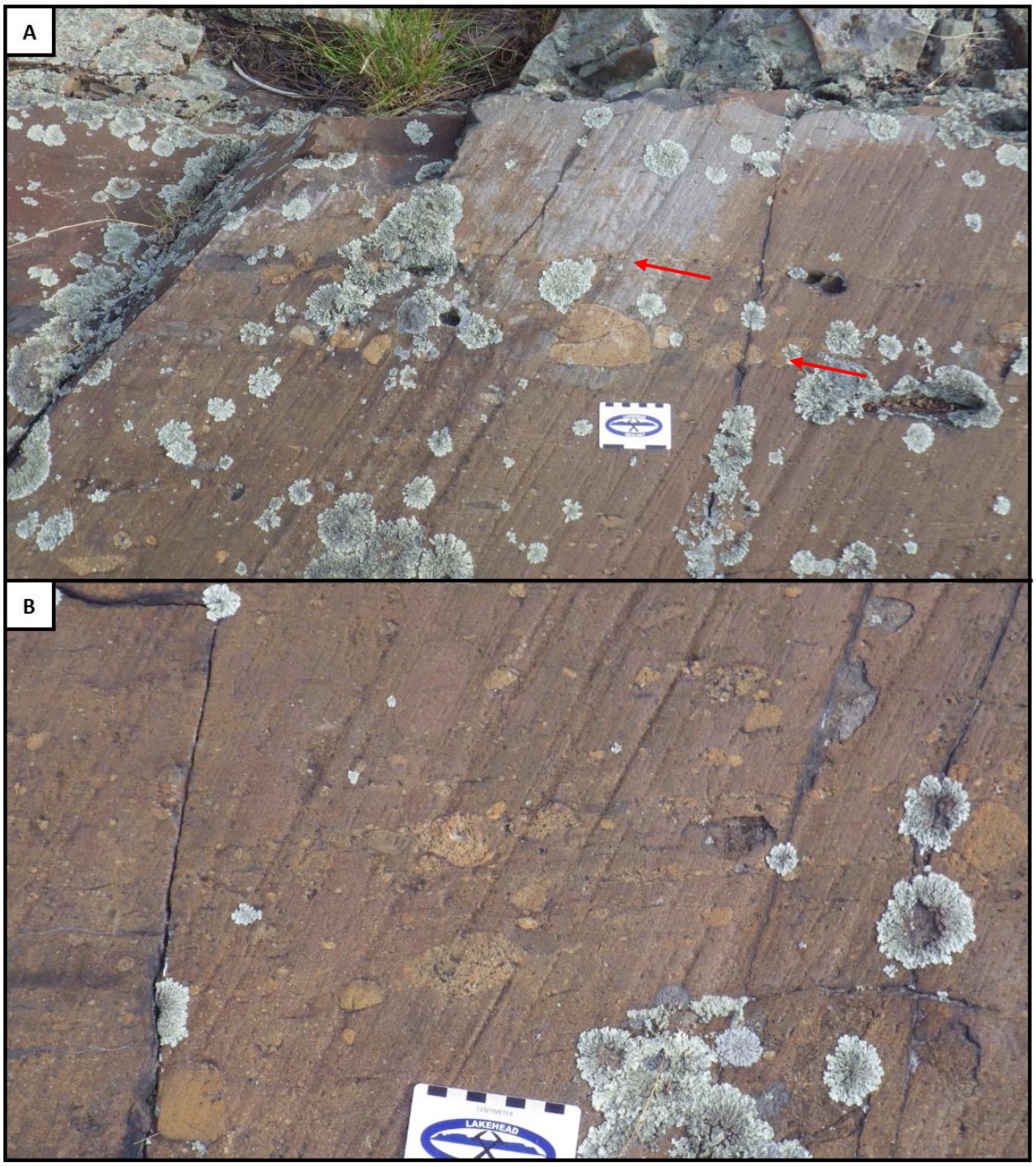

Figure 30: Weakly stratified diamictite outcropping east of Birch Point. A: Two clast-rich layers (red arrows) that occur within a massive to weakly stratified diamictite unit. These layers are fairly laterally continuous, are associated with thin mud wisps, and have clast lithologies that are similar to the surrounding diamictite. B: Less continuous and more irregular clast-rich layers within a massive to weakly stratified diamictite facies.

Diamictite units that appear to be massive in hand sample or outcrop may show internal stratification. Stratified diamictite is however a rare unit within the Bruce Formation but may be more common than previously considered due to the inability to discern stratification within hand samples in some cases. A stratified diamictite unit occurs near the base of the Bruce Formation in drill hole 150-1 (Figure 31A, B). Lamination occurs on the sub-millimetre scale, rarely up to one millimetre in thickness. Lamination is between a lighter grey and slightly more well sorted diamictite with thin dark clay-rich layers, and a poorly sorted brown silty diamictite with slightly more abundant fine-grained sand than the other two lithologies. The lamination ranges from parallel to wavy and contorted and in places is distorted around disaggregated clasts. Disaggregated clasts are of similar lithologies to the light grey and silty diamictite layers. There are also irregularly shaped patches and clasts of carbonate that similarly distort the laminae. These carbonate patches and clasts have a large range in size, from less than one millimetre to several millimetres in diameter.

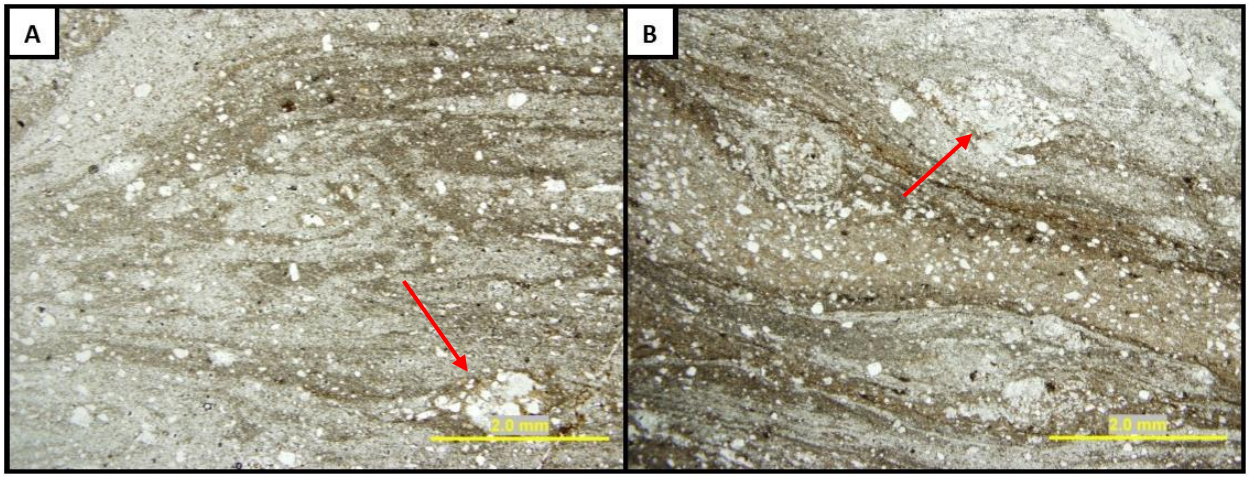

Figure 31: PPL images of stratified diamictite from drill hole 150-1. A: Contortion of laminae is a fairly common feature. Layering is between light grey more siliceous laminae and dark brown more clay-rich laminae. Fine- to medium-grained quartz sand is scattered throughout as well as clasts of grain aggregates (red arrow). B: Area of parallel lamination. A third laminae type also exists in this area, and is light brown with fine-grained sand in a clay-rich matrix. Irregular clasts of carbonate (red arrow) are rarely present along with the aggregate clasts. Laminae pinch and swell to accommodate clasts.

4.4 LITHOFACIES ASSOCIATION 4: SILTSTONE

A siltstone unit is present in many locations throughout the Quirke Lake and Iroquois Bay areas and ranges in thickness from 1-3m. This siltstone separates underlying diamictite from overlying carbonate-dominated facies of the Espanola Formation and has sharp to slightly gradational contacts with both the overlying and underlying units. In hand sample and outcrop this unit appears to be massive, however, a thin section taken from this unit in drill hole 150-1 reveals that the unit, at least in the Quirke Lake area, is composed of sub-millimetre scale lamination (Figure 32A). The lamination is defined by layers that have higher and lower concentrations of quartz grains. Lamination is parallel, but is slightly irregular in places. Rarely, lamination is disrupted and contorted (Figure 32B). Mineralogy of this siltstone unit is dominated by quartz and sheet silicates, largely sericite and chlorite. Accessory minerals include iron sulfides, biotite, potassium feldspar, and plagioclase.

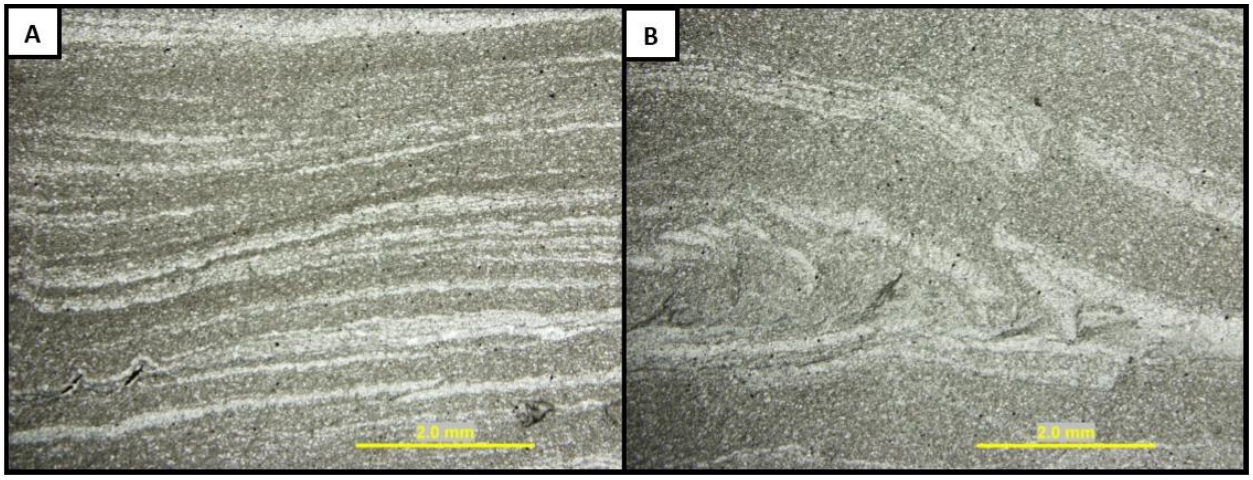

Figure 32: PPL thin section images of the siltstone unit that overlies the Bruce Formation. This sample is taken from drill hole 150-1. A: Parallel to slightly wavy mm-scale lamination formed by laminae that have a higher concentration of slightly coarser grained quartz and finer-grained and more clay-rich layers. B: Rarely, the laminae becomes contorted and deformed with visible displacement of the coarser-grained and more quartz-rich laminae probably caused by water escape.

4.5 LITHOFACIES ASSOCIATION 5: LAMINATED DROPSTONE DIAMICTITE

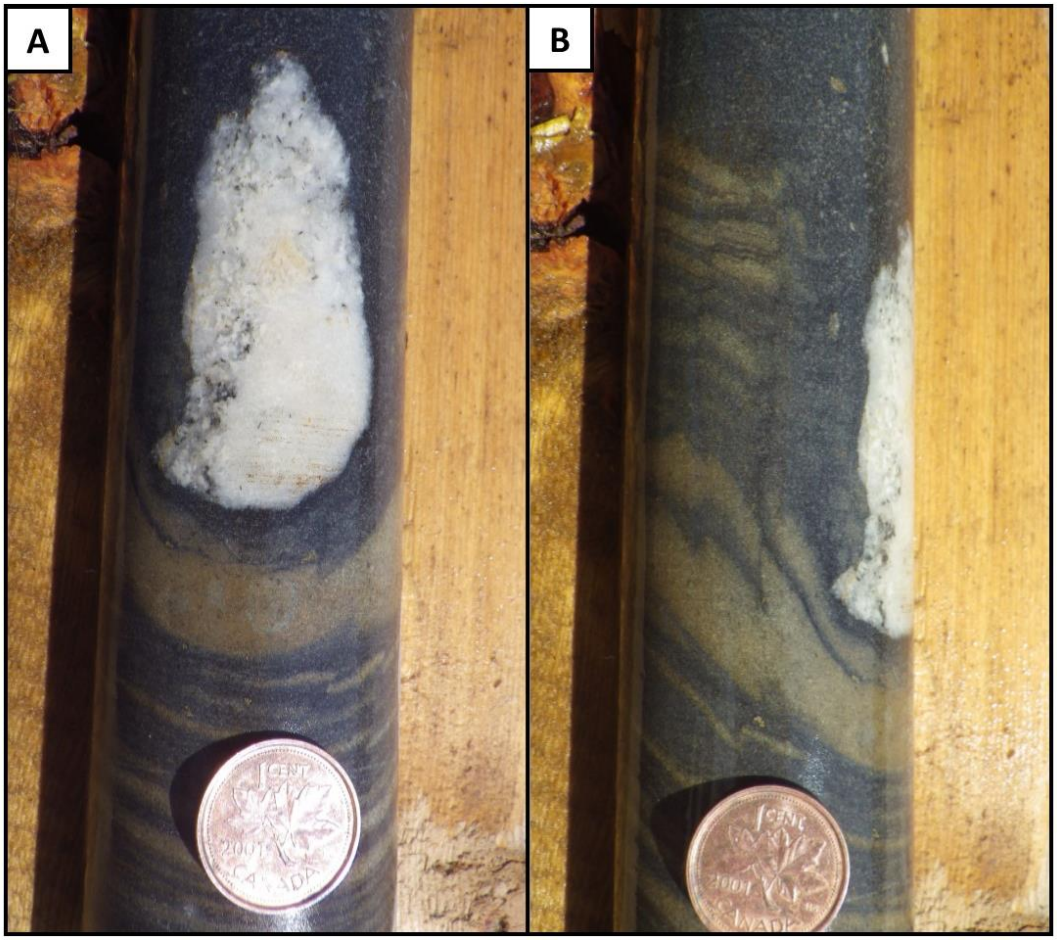

Figure 33: Laminated carbonate-rich diamictite facies in drill hole 150-2. A: White clast overlying laminated diamictite with some laminae being slightly fractured and offset. Brown layers have a carbonate matrix. B: A side view of the same clast shows the truncation and disruption of the laminae by the dropstone. Sediment overlying the laminated facies and associated with the dropstone is also noticeably coarser-grained and more poorly sorted.

The upper contact of the Bruce Formation in drill hole 150-2 has a transition that is different than the typical siltstone unit observed in the field and drill core. As it approaches the contact with the Espanola, the Bruce Formation is a siliceous grey colour and is composed mostly of fine- to medium-grained sand. This sandy matrix is interlayered in places, or contains patches, of darker areas that have a more clay-rich matrix. Aside from these rare clay-rich patches, the diamictite is massive. Clast composition is primarily white granite and clast size is

of pebbles to rare cobbles. Outsized clasts constitute approximately 20% of the unit. The upper contact is marked by a distinct decrease in the grainsize of the matrix and is overlain by a diamictite unit that only contains clasts in isolated areas. The majority of the unit is a dark coloured fine-grained sand and silt with laminations that are defined by brown weathering carbonate-rich layers that are parallel to contorted and range in thickness from 1-10cm (Figure 33A). These relatively well-sorted and finer-grained laminated areas are periodically contorted and disrupted by poorly-sorted, coarser-grained, and clast-bearing layers. Rarely, dropstones cut through the layering, indicating that the laminations within the sediment were forming contemporaneously with the deposition of the dropstones (Figure 33B). The carbonate-bearing and brown-weathering areas react with 5% HCL and contain carbonate as a cement component surrounding largely subrounded quartz grains and lesser potassium-feldspar and plagioclase (Figure 34A). Adjacent carbonate-poor layers have a clay-rich matrix (Figure 34B). This laminated unit containing dropstones is approximately 3m thick and is again overlain sharply by typical Bruce diamictite with a matrix dominated by fine- to medium-grained sand. Clasts are largely pebble-sized, with the largest clast in this unit being 3cm, though working with drill-core limits the sample population.

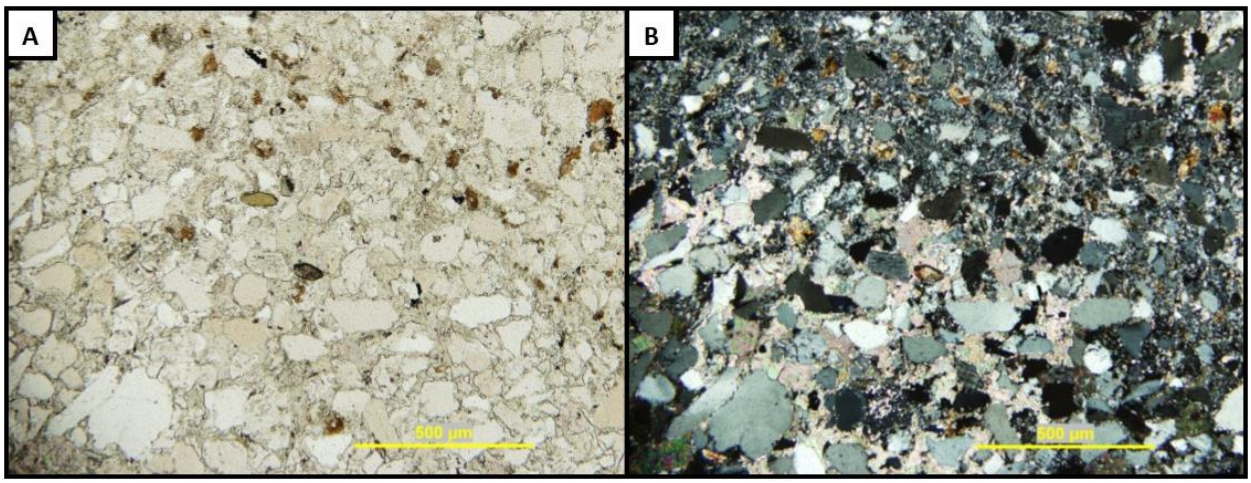

Figure 34: Thin section of the laminated carbonate-rich diamictite in drill hole 150-2. A: PPL image of the diamictite showing the predominance of fine- to medium-grained sand. Mineralogy is typical for the Bruce Formation, with a predominance of sand-sized quartz grains with lesser potassium feldspar and plagioclase. B: XPL image of the contact between a carbonate-rich laminae and carbonate-poor laminae. The carbonate component within the carbonate-rich laminae is present as a cement that surrounds the predominantly medium-grained sand. The layer that is carbonate-poor instead contains a much greater clay matrix component.

The clast-poor and carbonate-bearing laminated facies is interbedded with the unsorted and massive diamictite for approximately 12m, with variable thickness of the two units. Interbedding of these two lithologies is terminated by a conglomeratic unit that sharply overlies the uppermost carbonate-bearing dark sandstone and siltstone unit. This conglomeratic unit has a matrix of relatively well sorted, medium-grained sand and contains subround to well-rounded clasts of white granite and angular to subangular clasts of dark grey silty sandstone (Figure 35A). Larger dark grey clasts rarely contain coarse-grained sand to granule-sized white quartz grains within them and are similar in appearance to the underlying silty sand suggesting that the angular clasts were eroded from the underlying bed. Given that the underlying unit is preserved as clasts within the overlying coarser conglomeratic unit, the silty sandstones may have been either partially lithified or frozen before they were eroded by the overlying unit. This

unit is stained orange-red in places on the surface due to weathering of carbonate cement. The conglomeratic unit is in turn overlain by a sequence of very well sorted sandstone units, some of which are cross stratified (Figure 35B, C). Cross stratification is defined in some units by more poorly sorted and green layers, or by 1mm thin black layers that may also separate sandstone beds. This sandstone sequence is then overlain in turn by a conglomeratic unit with a fine to medium grained sand matrix and granule to rare cobble sized clasts of mostly white granite (Figure 35D). The unit is punctuated by two well-sorted and clast-poor layers approximately 1cm thick each which are slightly irregular and sharp-sided. The upper contact of the Bruce Formation is then capped by the laterally extensive siltstone unit that separates it from the Espanola Formation. The siltstone unit gradually transitions into a carbonate-rich siltstone that is roughly layered over a zone of approximately 3m.

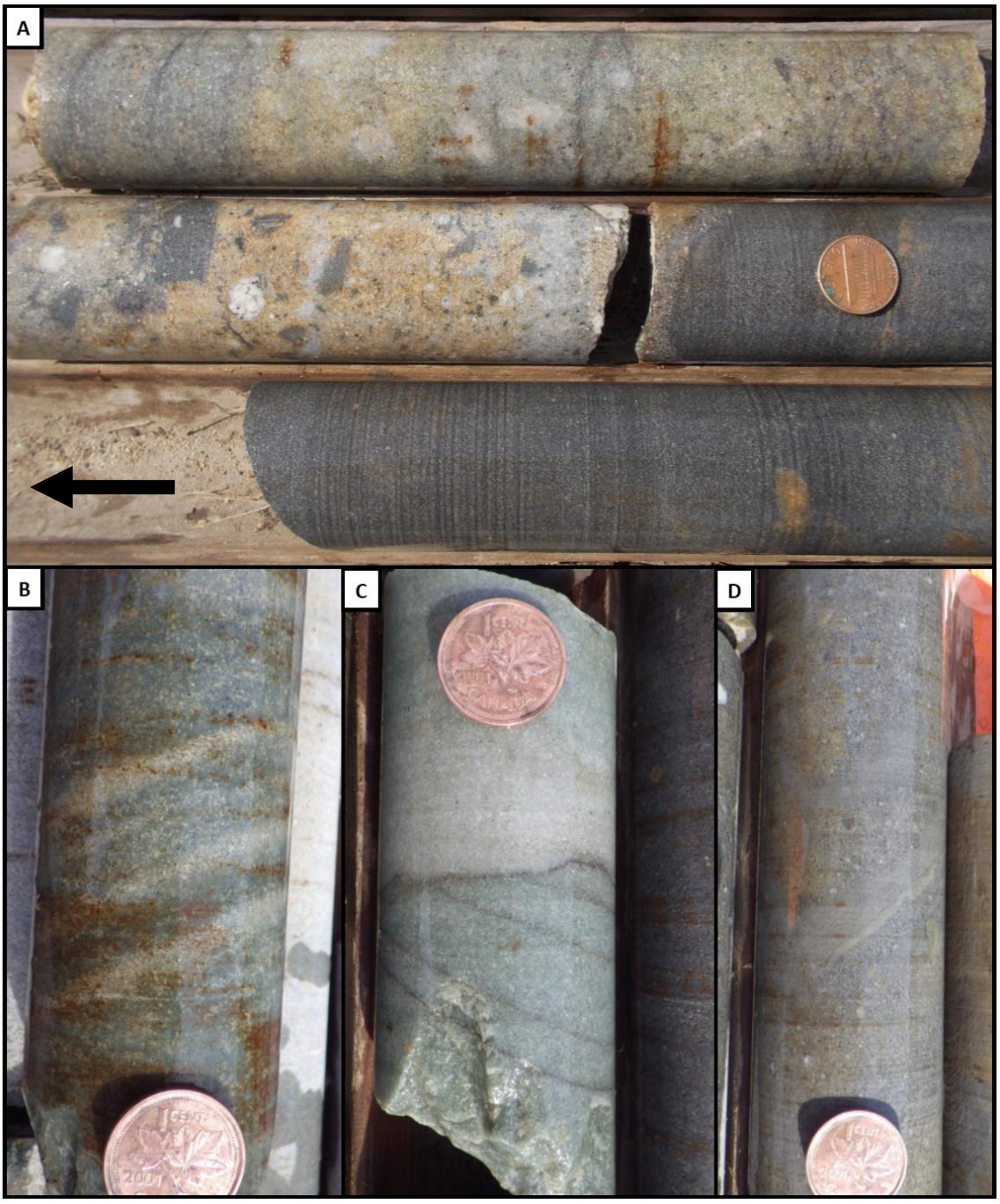

Figure 35: Upper Bruce Formation in drill hole 150-2. A: Sharp contact between massive fine-grained sandstone to siltstone unit with variable carbonate-cement and overlying conglomerate unit containing clasts of the underlying unit. Up direction is to the left. B: Cross stratified medium-grained sandstone overlying the conglomerate unit. C: Cross-stratified sandstone that is sharply overlain by a massive sandstone unit. Both units are of medium-grained sand. D: Conglomeratic unit that caps the transition zone of the Bruce Formation into the Espanola Formation. The intraformational conglomerate is highly siliceous and has 1-2cm thick clast poor layers that cross-cut it. Overlying the conglomerate is a siltstone unit that gradually increases upwards in carbonate content.

5 BRUCE FORMATION DISCUSSION

Early work on the Bruce Formation led to several hypotheses as to the depositional mechanism of the conglomerates that dominate the stratigraphy, including deposition by mud and debris flows as well as glacial activity (Collins, 1925; Pienaar, 1963; Robertson, 1964; Casshyap, 1969; Sims et al., 1981). Pienaar (1963) disputed a glaciogenic origin for the Bruce due to a lack of visible glacial features, while Sims et al. (1981) suggested submarine debris flows that were deposited as a result of an increase in slope due to faulting. However, a glacial mechanism has had the strongest support and become the most widely accepted interpretation based on its massive character and the predominance of extrabasinal clasts (Young, 1981; Hoffman, 2013). The extrabasinal clasts that constitute the coarse-grained fraction of the Bruce Formation are basement derived, suggesting that the sedimentary units underlying the overriding ice sheet were either unlithified at the time, or that ice was not grounded in the basin, or the ice sheet was grounded and non-erosive (Hoffman, 2013). As was discussed in the previous section, the underlying Mississagi Formation has been interpreted to have been deposited predominantly within a distal braided fluvial environment. Thus, in this section the depositional environment, particularly in regards to whether or not the Bruce ice-sheet was grounded, will be discussed in an effort to determine the depositional mechanisms of the Bruce Formation sediments.

While it is now generally accepted that the Bruce Formation conglomerates were deposited through glacial activity, the mechanisms of their deposition is still much more uncertain and hypotheses are broadly divided into deposits of a terrestrial origin (Casshyap, 1969; Parvianinen, 1973), marine origin (Frarey and Roscoe, 1970; O'Hare, 2010), or both

(Young, 1981). Given the interpretation of the underlying Mississagi sandstone as a fluvial deposit, a grounded glacier does seem to be an appropriate interpretation, but the lack of striated clasts and surfaces makes it difficult to definitively make that conclusion. Furthermore, the presence of stratification and dropstones in some areas indicates that deposition in water must have occurred to some extent (Young, 1981). Determining a transportation agent for the Bruce diamictite is further complicated by secondary processes that may have altered the sediment via mechanisms of winnowing and water-sorting (Robertson, 1964). It has been emphasized that diamict genesis requires knowledge of lithofacies relationships and sequence context for accurate interpretation (Eyles et al., 1985). For example, work completed on the modern west Antarctic ice sheet found that lodgement tills and diamictons deposited by the ice sheet are almost identical, and thus no genetic connotation can be derived from lithofacies alone (Anderson et al., 1983). Therefore, in determining the depositional environment of the Bruce Formation it is critical to take into consideration the formations that bound it, as well as the relationships between the lithofacies associations.

5.1 LITHOFACIES ASSOCIATION 1: BOULDER-LAG

A localized clast-supported conglomerate occurs at the lower contact of the Bruce Formation in drill holes 150-1 and 150-2. Mineralogy of the clast-supported conglomerate lithofacies is similar to the massive diamictites that dominate the stratigraphy, but is unique for the low matrix component and a prevalence of brittle crushing and fracturing between the contacts of adjacent grains. The ubiquity of evidence for mechanical crushing of grains within this lithofacies association, which is not present within the other lithofacies, suggests that these sediments may have been directly abraded by the overriding ice sheet. Similar units occur at the lower contact of the Bruce Formation along Highway 108 north of Elliot Lake and also along the western shore of Little Chilbow Lake, which is located approximately 30km west-southwest of Elliot Lake, where a clast-rich basal layer overlies a stacked sequence of rippled sandstones (Robertson, 1964). Based on the evidence observed in this study, the most likely explanation for the formation of these clast-rich basal layers is via current winnowing of a coarse-grained periglacial unit. Boulder-lag deposits such as these are common features of shallow continental shelves in glacial environments and the associated rippled units in the Little Chilbow Lake area supports the interpretation of active wave and/or tidal reworking (cf. Eyles, 1988, 1994; Hambrey, 1994; López-Gamundí, 2016). Therefore, Lithofacies Association 1 may represent deposition during a brief grounded interval following ice override, as the majority of the remainder of the Bruce diamictites point to delamination of the ice sheet and subsequent deposition in a subaqueous environment, which will be discussed in the following sections. Overlying these clast-supported conglomerates are massive diamictite facies with no preferred

clast orientation indicating deposition in quiet water (Eyles, 1988; Hambrey, 1994). This contact may represent the transition from grounded to floating ice in this area.

5.2 LITHOFACIES ASSOCIATION 2: ICE SHELF RAIN-OUT

Lithofacies Association 2, including both the massive sandy and silty diamictites, constitutes the vast majority of the Bruce Formation stratigraphy. Clasts in these units are predominantly of white granite that are subround and the composition of the sand fraction is predominantly quartz and potassium feldspar, suggesting that the sediments of the Bruce Formation diamictites were all similarly liberated largely from felsic intrusive terrane. Only rare sand and silt injections or interbeds and cobble layers punctuate the massive facies and the sandy interbeds may be laminated, graded, or cross-stratified and typically have some degree of soft-sediment deformation when layering is present to highlight it.

Figure 36: Lower contact of the Bruce Formation at Little Chilbow Lake. Example of the sharp contact between underlying sandstones of the Mississagi Formation and the overlying diamictites of the Bruce Formation.

The massive nature of the diamictites and their great lateral extent strongly suggest that Lithofacies Association 2 represents a rain-out till that was deposited beneath a floating ice shelf. While the Bruce Formation can range up to 460m thick, it is typically no thicker than 60m in most places, which is a thickness that is much less than units that are associated with warm-based glaciers and suggests that the Bruce diamictites were sourced from a cold-based glacier with little sediment entrainment (Ginn, 1961; Parviainen, 1973; Card et al., 1977; Carlson et al., 1990; King et al., 1991; Benn and Evans, 2006; O'Hare, 2010). This further strengthens the interpretation of a rain-out till for the massive diamictite lithofacies association, as cold-based regimes are a necessity for the existence of an ice-shelf, and the relatively thin deposits of the Bruce Formation would be the result of low meltwater input and sediment supply beneath the floating ice (Anderson et al., 1983; Powell et al., 1996). The presence of a typically sharp contact between these facies and the underlying sandstones of the Mississagi Formation, as well as the uptake of unlithifed Mississagi sand into the base of the Bruce Formation strongly suggests that the Bruce ice sheet was grounded and erosive as it advanced into the Huronian basin (Figure 36). Given the interpretation of dry-based grounded ice, this could account for the lack of subglacial terrestrial deposits directly superseding ice advance, as a dry-based glacier would result in erosion and glaciotectonization without a depositional sedimentary record (Anderson et al., 1983; Visser, 1991). Following ice advance, a rapid decoupling from the bed could have occurred, perhaps through glacio-isostatic effects, with the newly developed ice shelf depositing diamictite via rain-out (cf. Visser, 1991). This would explain the sequence of a usually sharp and erosive contact at the base of the Bruce Formation, indicating a grounded ice front, but the general lack of associated subglacial deposits.

The interbeds of conglomerate, sandstone, and siltstone that may be graded, parallel laminated, or cross-stratified and punctuate the massive sandy and silty diamictites at random intervals are interpreted as representing subaqueous input into the environment via sub- or englacial streams. Alternatively, some of these interbeds may be the result of reworking by intermittent current activity. Dry-based glaciers in polar environments produce little meltwater, and as such the majority of sediment will be deposited in the vicinity of the grounding line (Eyles et al., 1985; Miller, 1996; Ashley and Smith, 2000). As delamination of the ice shelf occurred, rapid retreat of the grounded ice is inferred to have left behind this scarce evidence of subaqueous outwash. In this scenario, the unstable environment would result in rapid migration of glacial stream mouths and would lead to the sparse deposition of gravel, sand, and silt that is interbedded with the diamictite, but not allow for the full development of a grounding-line fan (Cheel and Rust, 1982; Powell, 1988, 1990). Gravel beds, which are typically more laterally extensive, are probably winnowed lags, and the cross-stratified, lens-shaped sandstone bodies would be deposited in the channels that bifurcate away from water-sediment exit points on the grounding line (Banerjee and McDonald, 1975; Rust and Romanelli, 1975; Nystuen, 1976; Powell, 1981). Rare graded sand beds are the result of downslope resedimentation and redistribution through mass movement, which is a common process that occurs in the grounding line zone (Powell, 1988; King et al., 1991; Salvi et al., 2006). Soft-sediment deformation and slumping of laminated and cross-stratified beds, as seen in the sandy interbeds of the massive diamictite facies, is most likely caused by instability as a result of rapid deposition, as slump structures are very common in glacial environments (Ashley,

1975; Strum and Matter, 1978; Le Blanc Smith and Eriksson, 1979; Visser et al., 1984; Smith and Ashley, 1985; Eyles and Lagoe, 1998; Nitsche et al., 2000; Winsemann et al., 2004).

5.3 LITHOFACIES ASSOCIATION 3: GLACIOMARINE DEPOSITS

The weakly stratified to stratified diamictite lithofacies association occurs predominantly along the north shore of Lake Huron, east of Birch Point, and south of Iroquois Bay and has a number of internal features including: silt and clay wisps, clast-rich layers, rare dropstones displacing lamination, and sand lenses. Silt and clay wisps are usually only 1-3mm in thickness and laterally discontinuous. Where stratification is better defined, the laminae thickness can be up to 4cm in places, but is similar in that the layering is highly discontinuous and irregular. Dropstones, usually of pebble- to cobble-sized white granite, occasionally displace laminae beneath them. While less common, fine- and medium-grained sand lenses, usually ~50cm in thickness, interbed with the weakly stratified diamictites. These lenses are massive and have sharp contacts that may be wispy. Clast-rich layers are rare, and only observed within a few meters of the contact with the underlying Mississagi sandstone at the outcrops east of Birch Point. These clast-rich layers are only one-clast thick and have a similar lithological composition as the diamictites adjacent to them.

The laminated to weakly laminated diamictite lithofacies association is interpreted to represent a glaciomarine environment and is suggested to be similar to the Upper Proterozoic Port Askiag Formation in Scotland. The Port Askiag Formation contains a massive diamictite lithofacies that was deposited in a quiet water environment, largely through deposition of fines

occurring predominantly through suspension, with intermittent deposition by ice rafting (Spencer, 1971; Eyles and Clark, 1985). In this environment, the stratified diamictites with sandstone stringers and discontinuous pebble bands formed through episodic traction currents (Eyles and Clark, 1985). In the laminated to weakly laminated lithofacies association of the Bruce Formation, dropstones displacing laminae and clast-rich layers are present within a few meters of each other, suggesting that both current activity and ice rainout were ongoing processes. The clast-rich layers are interpreted to have been formed through winnowing by currents and ice rainout is indicated by presence of dropstones disturbing lamination around them (Eyles and Clark, 1985; Eyles et al., 1985; Miall, 2000). While not observed in this study, iceberg dumping has been found in association with these facies in previously completed studies of the Bruce diamictite, and further strengthens the interpretation that ice rainout influenced the deposition of these sediments (O'Hare, 2010). Sandstone lenses and interbeds within diamictite, as is occasionally the case in the weakly stratified diamictites of the Bruce Formation, are also features that have been interpreted to represent intermittent traction current deposits (Mills, 1983; Eyles et al., 1985).

In outcrops east of Birch Point, the weakly stratified diamictite lithofacies association occurs directly above the Mississagi-Bruce contact, which indicates that at this location the Bruce ice sheet may not have been grounded at any point in time and that all diamictites were probably deposited in a glaciomarine environment. An alternative explanation would be that iceberg activity occurred in the area prior to ice sheet advance. The matrix of the Bruce Formation diamictite adjacent to the contact with the underlying Mississagi sandstones is very poorly sorted and contains abundant silt- and clay-sized material. These finer-grained, silty

diamictite units are parallel layered to parallel laminated and are overlain by the weakly laminated diamictite lithofacies with a low clast content. The intermittent current activity, indicated by the weak lamination, silt and sand interbeds, and pebble bands within the laminated sediments all suggest that the environment was a shelf facies association in proximity to the ice front (Miller, 1996).

5.4 LITHOFACIES ASSOCIATION 4: DEEP SHELF RAIN-OUT

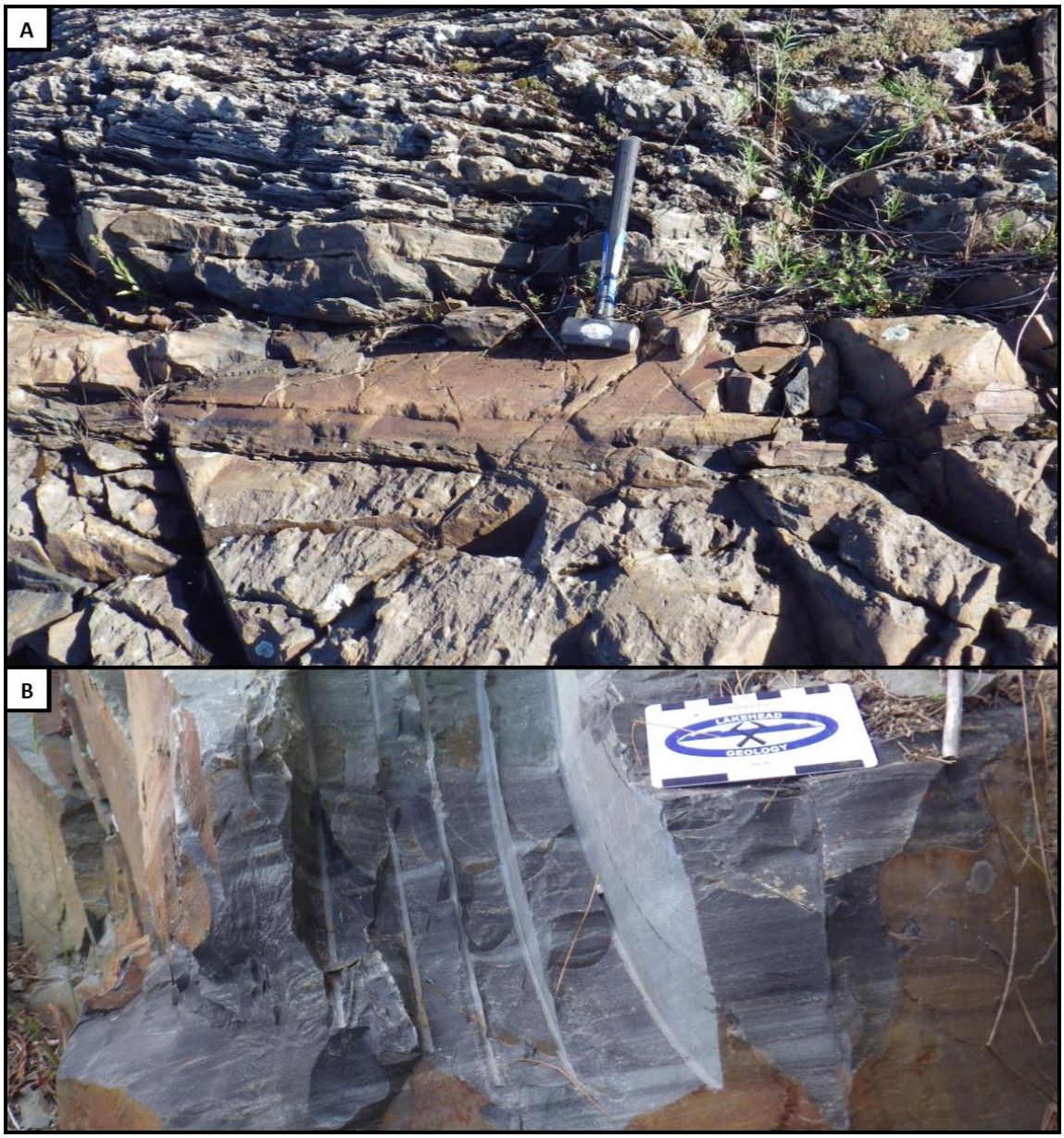

Figure 37: Siltstone unit that caps the Bruce Formation. A: The siltstone unit outcropping southeast of Iroquois Bay (hammer is on it). Thickness of the unit is at a minimum here and is only 0.5m thick on average. B: Siltstone unit outcropping along Highway 108 north of Elliot Lake. Parallel lamination is present throughout, with laminae being up to 1cm thick in places.

The ~1-3m thick siltstone unit that separates the Bruce Formation diamictites from the overlying Espanola Formation is exceptional for its pervasiveness and uniformity. The thickness of the unit appears to possibly thin towards the south, as an outcrop in the Iroquois Bay area

has a siltstone unit only ~0.5m thick overlying the diamictites (Figure 37A), but there is not strong enough evidence to support this interpretation and more observations would be required. The mineralogy of the unit is similar to the sediments of the diamictites and it is very finely parallel laminated on the sub-millimetre up to 1cm scale with laminations being between more and less quartz-rich lithologies (Figure 37B). Sorting of the matrix is very good, and despite the mineralogical variation between the laminae, the grainsize is consistently silt to clay-sized. The lower contact of Lithofacies Association 4 with the underlying diamictite is uniformly sharp and planar while the contact with the overlying laminated carbonates of the Espanola Formation is sharp to gradational. In drill hole 150-2, the siltstone unit gradually increases upwards in carbonate content before being overlain by an interlaminated to interbedded carbonate-siltstone unit.

The uniformity of the siltstone unit, including its areal extent and consistent grainsize leads to the hypothesis that this Lithofacies Association represents a rain-out siltstone deposit. In this scenario, rapid northward retreat of the ice-sheet at the end of the Bruce glacial event would result in an effective shutting-off of the sediment supply, meltwater-induced sea level rise to outstrip isostatic rebound, and result in only fine-grained material being carried to the deeper shelf (Miller, 1996). The stratified nature of the sediment and the interpretation of the underlying Lithofacies Associations being glaciomarine leads to the conclusion that the silts were deposited in a marine environment (Eyles et al., 1985). A lack of evidence for traction current activity supports the interpretation of a deeper water environment with deposition occurring exclusively through rain-out (cf. Eyles et al., 1985). Differences in mineralogy between alternating laminae indicates a variable input of terrigenous sediment transported by aeolian

processes and/or over- and interflow plumes. It is possible the finer-grained and more sheet silicate-rich layers may represent glacial outwash material that travelled as inter- and over-flows before being deposited through rain-out and the quartz-rich layers may exclusively represent wind-blown material sourced directly from the terrestrial environment by strong winds. Similar couplets of silt-mud and sand-mud laminae have been identified up to several kilometers from the grounding line of glaciers in Alaska (Mackiewicz et al., 1984). These sediments have been influenced by tidal currents but are similarly sourced from over- and interflow plumes (Mackiewicz et al., 1984; Cowan and Powell, 1990). The laminated sediments of the Alaskan deposits differ from those observed here because of the presence of ice-rafted debris in association with those deposits (Mackiewicz et al., 1984), but the process through which the lamination formed may be similar.

Many of the features of the siltstone is consistent with a loess deposit but has not been referred to here as such because of a general lack of carbonate cement, its marine environment, and because loess is typically dominated by angular to subangular quartz (Richthofen, 1882; Smalley and Vita-Finzi, 1968; Pettijohn, 1975; Pye, 1987; Tungsheng, 1988), but this forms only 30-50% of the unit here. Despite these differences, the siltstone is strongly similar to loess because of its grainsize; direct association with glacial activity, especially recent glacial recession; and because of its widespread occurrence (Smalley and Vita-Finzi, 1968; Pye, 1987; Tsoar and Pye, 1987; Smalley et al., 2000; Soreghan et al., 2000; Hamblin, 2016). These similarities support the hypothesis that rapid glacial retreat at the end of the Bruce glacial event was followed by a sediment starved environment and deposition of a laminated blanket of siltstone through intermittent rain-out of aeolian dust and inter- and over-flow plumes.

5.5 LITHOFACIES ASSOCIATION 5: GLACIOMARINE ICEBERG RAFTING

In one section of core from drill hole 150-2, the upper Bruce Formation contains a unit with dropstones that displace carbonate-rich laminated sediments which cause the layering to become highly contorted in places. The laminae have highly variable thickness, ranging from 1 millimeter up to several centimeters and alternate between matrix-rich layers and layers with a carbonate-rich cement. The presence of laminated sediments containing clasts of significantly larger size than the surrounding sediment suggests that the laminated carbonate-rich diamictite Lithofacies Association is a dropstone facies of glaciomarine origin. A dropstone facies is indicative of deposition in a body of water, wherein lamination is forming through continuous sedimentation and is punctuated by ice rainout dropping material into the underlying sediment and displacing the laminae (Miall, 2000). This interpretation is supported by the identification of another locally developed laminated dropstone facies in the Blind Falls area, which has been interpreted to represent deposition from floating ice into partially consolidated sediment (Robertson, 1964). Dropstone facies can form up to several thousand kilometers from an ice front as long as there is an abundance of icebergs to transport glacial debris, and given a lack of evidence for winnowing of sediments and bottom currents in the laminated carbonate-rich diamictite lithofacies association, this unit likely represents an intermediate to distal environment where direct glacial influence is limited (Boulton and Deynoux, 1981; Eyles et al., 1985; Miall, 2000).

The carbonate-rich layers within the diamictite unit suggest that carbonate precipitation was occurring contemporaneous with the siliciclastics and that it was being deposited with and within the surrounding sediment. This interpretation is supported by the disruption of the

carbonate-rich laminae by the dropstones, indicating that the carbonate had already formed when the iceberg rafted material was being deposited. The presence of carbonate-rich sediments interbedded with glaciogenic deposits in ancient formations such as the Bruce and Espanola Formations has been considered enigmatic because of the assumption that carbonate sediments are representative of warm environments at low latitudes (Anderson, 1983; Eyles et al., 1985; Miall, 2000). Furthermore, carbonates that are interbedded with siliciclastics can be of a detrital origin, deposited through processes such as sediment gravity flows (Eyles et al., 1985; Fairchild, 1993; Miall, 2000). Given that downslope resedimentation is a common process in glaciomarine continental margin environments, the idea that some carbonate sediments associated with glacial deposits may be detrital in origin should not be discounted (Marlowe, 1968; Frakes and Crowell, 1969; Boulton, 1972; Carlson and Molnia, 1977; Piper and Slatt, 1977; Lawson, 1981; Stow, 1981; Piper and Normark, 1982; Miall, 1983, 1985; Paul, 1983; Visser et al., 1984; Eyles et al., 1985). The origin of the carbonate fraction within the dropstone facies of the upper Bruce Formation is not yet understood, and geochemical analysis will be discussed later in this study along with samples taken from the Espanola Formation carbonates in an effort to narrow down possible depositional mechanisms.

The laminated dropstone lithofacies is sharply overlain by a conglomeratic unit that is in turn overlain by well-sorted sandstones. The presence of angular clasts of the underlying siltstone facies within the coarse conglomeratic unit above suggests that the siltstone was at least partially cohesive and was eroded by the overlying conglomerate. Cohesion of the siltstone clasts from the underlying unit may be caused by the presence of the early carbonate cementation. This conglomerate that sharply overlies the carbonate-rich siltstone is interpreted

to be a mass flow deposit that scoured into the underlying sediment. Sediment gravity flows are common in distal glaciomarine environments and thus would not be unexpected in association with the dropstone facies (e.g. Eyles et al., 1985; Hambrey, 1994; Allen et al., 2011). Overlying the mass flow deposit is then a sequence of sandstones that broadly coarsens upwards into pebble conglomerate. These sandstones are well-sorted and are cross-stratified in places and were possibly formed by reworking and sorting of sediments. Traction current activity in the glaciomarine environment serves to winnow the fine-grained component (cf. Eyles et al., 1985; Hambrey, 1994) and would result in an interval of well-sorted sand. The cross-stratified sandstone bodies overlying the conglomerate unit in drill hole E150-2 do not occur in any of the other drill holes, suggesting that environment of deposition was isolated, such as a subaqueous fan. The short interval of conglomerate that overlies the sands may again represent one or more mass flow deposits. This sequence is then overlain by laminated siltstone of the aeolian siltstone lithofacies, which represents a shift to predominantly rain-out depositional processes.

5.6 CONCLUSIONS

The Bruce Formation is a massive and areally extensive unit of diamictite that directly overlies a distal braided fluvial system. The contact between the underlying fluvial deposits and the overlying diamictite is usually separated only in places by a thin transition zone of very poorly sorted coarse-grained sand to gravel. This transition zone is massive in many cases, but can also show heterolithic lamination near the contact between medium-grained sandstone and very coarse-grained sandstone to conglomerate. Based on the interpretation of the upper Mississagi Formation being a distal braided fluvial to glaciodeltaic system, and the drastic increase in grainsize approaching the Bruce Formation with a typically sharp contact between the two, the Bruce glacial advance is interpreted to have been a cold-based ice sheet that was initially grounded in most of the basin. This interpretation is supported by the abundant evidence of glacial tectonism in the sands of the underlying Mississagi Formation. What little sedimentation was taking place during the height of the glacial period may have been as intermediate to distal glaciomarine processes. Polar conditions would have led to little to no subglacial deposition prior to rapid delamination of the ice sheet from the bed. Delamination of the ice, possibly due to ice-loading should be able to account for the observation that, prior to glacial advance, the continental margin was dominated by a high energy fluvial environment, while immediately following is a laterally extensive blanket of massive diamictite. The laterally continuous and uniform massive diamictite is then inferred to have been deposited largely through ice rainout. Break-up and disintegration of the ice shelf at the end of the Bruce glacial event led to rapid retreat and definitive evidence of iceberg activity as far north as the Elliot Lake area. Thickness of the Bruce Formation is highly variable (Ginn, 1961; Frarey and Roscoe,

1970; Card et al., 1977; Young, 1981), but there is a general thickening trend towards the south (Parvianinen, 1973; Young, 1981), which may be a reflection of accommodation space, influenced by regional block faulting or irregular temporal distribution of the grounding line. It has also been noted that there is an upwards trend in the Bruce Formation of increasing matrix material and decreasing clast size and abundance (Parvianinen, 1973). This trend fits well with the suggestion that the upper Bruce Formation represents retreat of an ice sheet and deposition in an increasingly more distal glaciomarine environment.

In summation, the Bruce Formation was deposited primarily in a glaciomarine environment, as is suggested by the thickness and wide extent of the formation and the unsorted nature of the deposits and the large range in grainsizes (Hambrey and Harland, 1981). This interpretation is strongly supported by the preferred preservation of glaciomarine deposits in ancient glacial environments, particularly on glaciated coastlines of subsiding shelves (Anderson, 1983; Andrews and Matsch, 1983; Eyles et al., 1985; Eyles, 1993). Furthermore, the inferred rapid retreat and decoupling of the Bruce ice sheet is the expected course of events on a glaciated continental shelf where proglacial isostatic depression combined with large-scale marine deglaciation results in a catastrophic submarine glacial retreat facies sequence being preserved in the rock record (Miller, 1996). The residual effects of ice-loading on the margin of the continent, along with sea-level rise, resulted in marine transgression and deposition of fine-grained laminated sediments overlying the diamictite (Cassyhap, 1969; Bennet et al., 1991). The laminated siltstone unit that directly overlies the diamictites in the Bruce Formation was deposited in a distal glaciomarine environment where glacial influence was non-direct and sedimentation occurred through rain-out processes. The contact with the overlying Espanola

Formation is then marked by a sharp to gradual transition into laminated carbonates and siltstones, of which the depositional setting will be discussed in the following sections.

6 ESPANOLA FORMATION

The Espanola Formation, the middle formation of the Quirke Lake Group, has been broadly defined as being composed of three major members and a local fourth member that is developed in some of the southernmost exposures (Collins, 1914; Quirke, 1917; Robertson, 1964; Young, 1973; Card et al., 1977; Bernstien and Young, 1990; Long, 2009). The three major members of the Espanola Formation are defined by their dominant lithologies, resulting in the subdivision of a lower limestone unit, a middle siltstone unit, and an upper heterolithic or dolostone member (Collins, 1914; Quirke, 1917; Robertson, 1964; Young, 1973; Card et al., 1977; Bernstien and Young, 1990; Lafontaine, 2013). A sandstone-rich member constitutes the local fourth member, and it is developed in outcrops south of Espanola where it overlies the middle siltstone member (Frarey and Roscoe, 1970). The Espanola Formation conformably overlies the Bruce Formation with a contact that has been described as commonly abrupt, and where gradational is marked by a transition from laminated siltstone, to calcareous siltstone, and finally into the lower limestone member (Robertson, 1964; Parviainen, 1973; Card et al., 1977; Long, 2009). The exception to this conformable contact is far to the north, in the Geneva Lake area where the Espanola Formation sits directly atop Archean granitic basement (Eggertson, 1975). Thickness of the formation is highly variable, with each individual member ranging anywhere from 15m to ~300m, but there is a general trend of a southward thickening to the entire formation due to an increase in the thickness of the siltstone member and the presence of the additional sandstone member (Meyn, 1970; Young, 1973; Eggertson, 1975; Card et al., 1977).

The Espanola Formation is unique within the Huronian stratigraphy because of its carbonate-content, which is ubiquitous throughout the formation but is highly variable in its proportion of the total rock composition (Frarey and Roscoe, 1970; Young, 1973; Bernstien and Young, 1990; Bekker et al., 2005). Proportions of carbonate in the Espanola Formation ranges anywhere from 10-90%, and analysis of rocks from the Sudbury-Espanola areas have determined that the lower limestone member has the highest concentration of carbonate minerals, averaging 30%, while the following three members have carbonate concentrations that range from 10-20% (Card et al., 1977; McLennan et al., 1978). The ratio of calcite to dolomite is also variable across all three members and both the limestone and dolostone members contain calcite as the dominant carbonate mineral while the siltstone member contains equal proportions of both calcite and dolomite (Card et al., 1977). A general trend has also been noted that farther to the north, in the Geneva Lake area, the gross composition of the Espanola Formation is more calcareous than along the north shore of Lake Huron (Eggertson, 1975).

6.1 LITHOFACIES ASSOCIATION 1: INTERLAMINATED CARBONATE AND SILTSTONE

The interlaminated carbonate and siltstone lithofacies association dominates the lower Espanola Formation in the Sault Ste. Marie- Elliot Lake and Espanola-Sudbury areas and consists predominantly of interlayered white carbonate and grey-green siltstone (Figure 38A). Layer thickness ranges from the mm-scale up to 2cm, and limestone layers are typically thicker than adjacent silt laminae; however, the proportion of limestone laminae to siltstone laminae is variable both regionally and stratigraphically, ranging from predominantly siltstone with minor carbonate laminae, to predominantly carbonate laminae with very thin (mm-scale) silt laminae. Laminations range from parallel to wavy to heavily contorted in places. Variable amounts of contortion are adjacent to and grade into one another, and layers of highest contortion are loosely correlated with areas of greatest carbonate concentration (Figure 38B). In the most extreme cases of deformation the lithofacies degrades into irregular carbonate clasts in a siliciclastic matrix (Figure 39A). Lamination can be very poorly defined in places, and in certain sections where carbonate is present in far greater concentration than siltstone, the siltstone laminae can be wispy and highly discontinuous (Figure 39B). These carbonate layers contain only minor amounts of siliciclastics and typically form pure mosaics of silt to fine-grained sand-sized calcite. Silt layers are more variable in composition and contain some scattered grains of fine-grained quartz sand in a silt- and clay-sized matrix. Less commonly, carbonate is interlayered with mm-scale dark brown clay-rich layers or with chert layers.

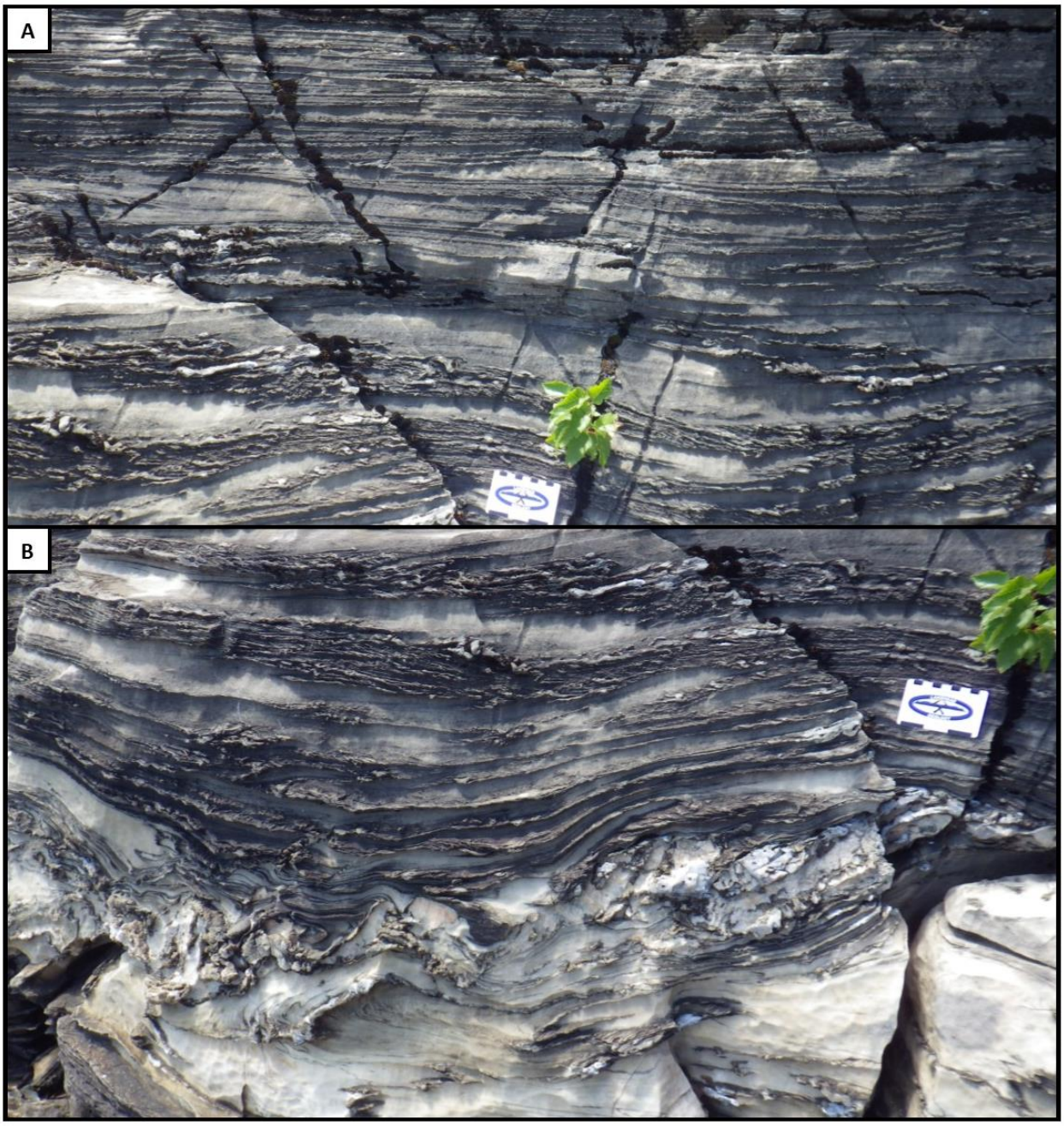

Figure 38: Laminated carbonate and siltstone lithofacies association outcropping along the western shore of Quirke Lake. A: Parallel laminated section of stratigraphy with the carbonate laminae being thicker on average than the darker and less eroded siltstone laminae. Lamination is cut by very low angle erosion surfaces. B: Mildly to highly contorted section of stratigraphy in the laminated carbonate and siltstone.

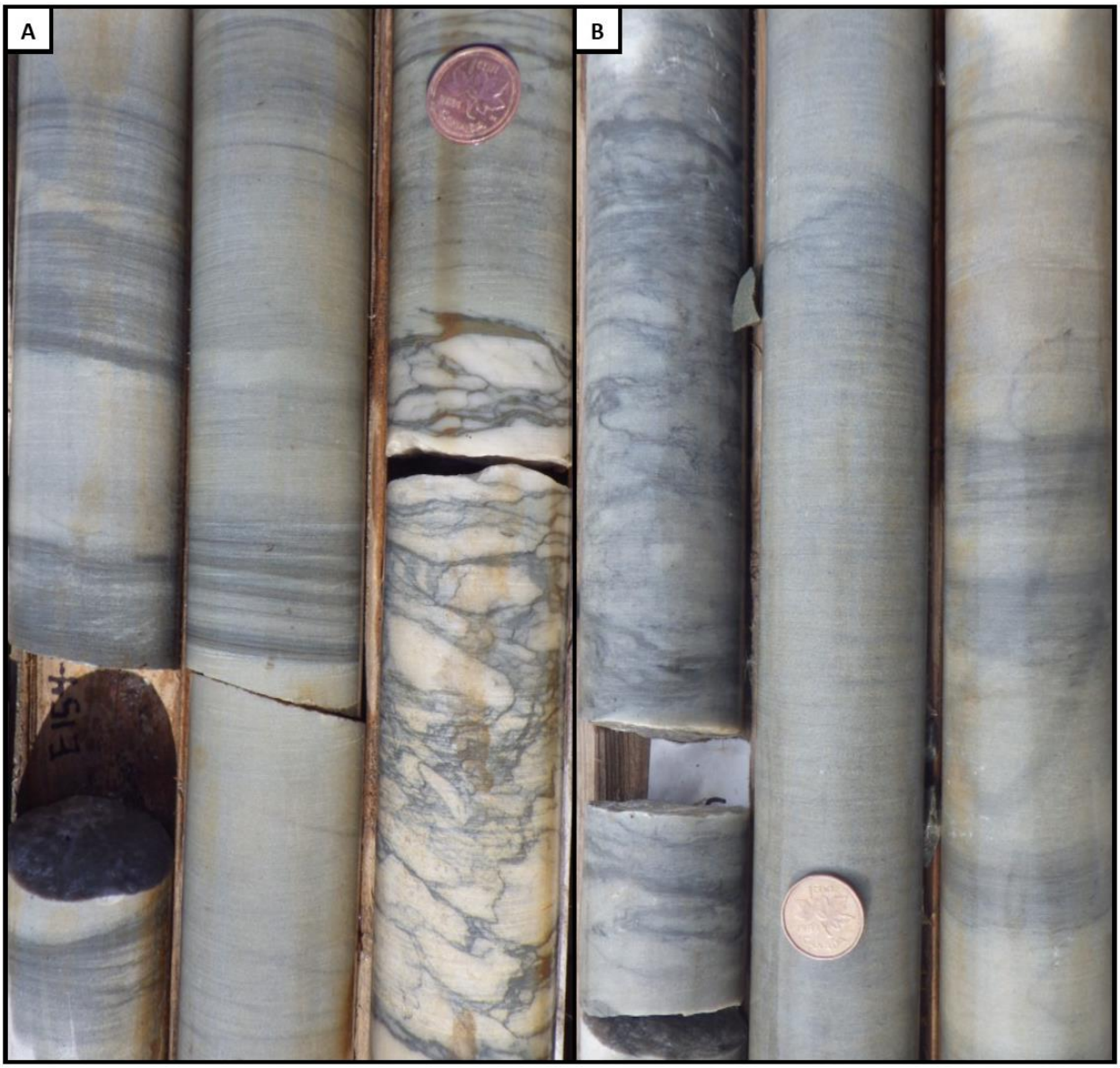

Figure 39: Common appearance of the laminated carbonate and siltstone lithofacies in drill core. A: A well laminated section of stratigraphy devolves into a slump breccia, with clasts of white carbonate surrounded by a clay- and silt-rich matrix. A 1-3mm thick brown irregular mud layer caps the slump breccia. B: Section of the laminated carbonate and siltstone unit where lamination is wispy to highly diffuse and the stratigraphy is dominated by the carbonate fraction.

Petrographic analysis of thin sections from the interlaminated to interbedded carbonate and siltstone lithofacies in the Quirke Lake area shows that, in the generation of this silt

laminae (Figure 40A, B), the lower contact is a slightly gradual upwards transition into a layer that has a higher silt to carbonate ratio. The upper contact however, is fairly sharp with the overlying silt-poor carbonate layer (Figure 40C). Furthermore, the overlying carbonate grains appear to sink into the underlying layer and distort it (Figure 40D). The carbonate grains are silt to fine sand-size and form a slightly inequigranular mosaic with very minor interstitial siliciclastics present, while the silt layers contain a mixture of mostly silt- and clay-sized particles with rare scattered quartz grains up to fine sand-size.

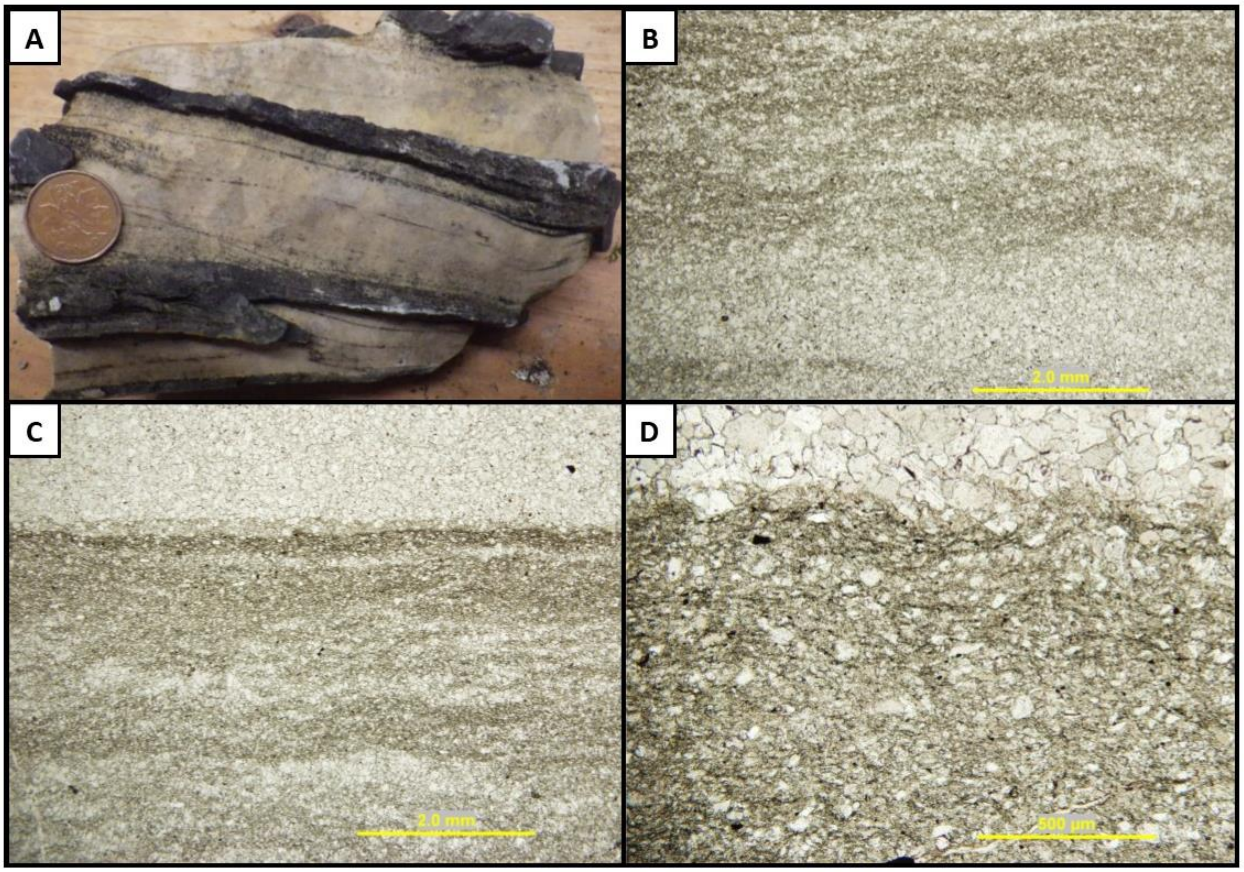

Figure 40: Sample of the laminated carbonate and siltstone lithofacies association from Quirke Lake. A: ~2cm thick white carbonate layers interbedded with ~1cm thick grey siltstone layers. The carbonate layers also have faint silt laminae less than 1mm thick within them. B: PPL image of the contact of a thin siltstone laminae in a carbonate layer. The lower contact is a slightly gradational upwards transition. C: PPL image of the sharp upper contact of the same silt laminae. D: Close-up of the upper contact. The overlying carbonate grains sink into the underlying grains and distort it.

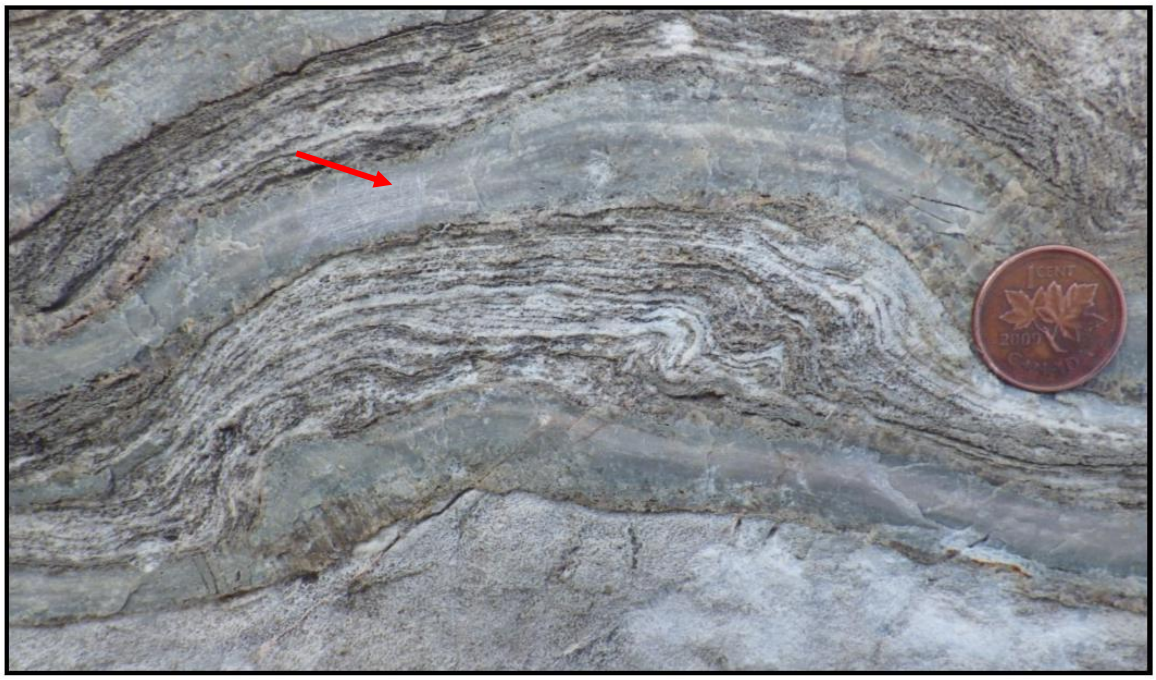

Figure 41: Laminated carbonate and siltstone lithofacies association outcropping along Highway 107 immediately north of Elliot Lake. Chert layers ~1cm thick on average are interbedded with the interlaminated carbonate and siltstone and are deformed in a similar fashion to the adjacent laminae. The chert layers (red arrow) have a faint mm-scale lamination to them, between greener and paler laminae.

The laminated carbonate and siltstone lithofacies association is best preserved in the northern exposures as well as in drill core due to the higher degree of metamorphism effecting the southern exposures of the formation. Towards the north shore of Lake Huron many outcrops of Espanola carbonates are black on the surface and units with higher carbonate content are typically best identified as layers that erode more readily, giving the surface of the outcrop a ribbed appearance. Furthermore, it is more common for the limestone member to have been eroded away towards the south, and often outcrops are submerged. However, where exposed the extreme western, eastern, and southern outcrop area of the lower limestone member appears to be remarkably similar to those observed farther to the north and in central exposures. On a fresh surface (and where metamorphism is not too extreme) limestone is a white colour and uniform in appearance and is interlayered with siltstone layers

that vary from the mm-scale up to several centimetres in thickness. Siltstone layers are also typically thinner than their associated limestone layers but thickness is also fairly variable. The siltstone layers have sharp to very slightly gradational contacts with the limestone layers.

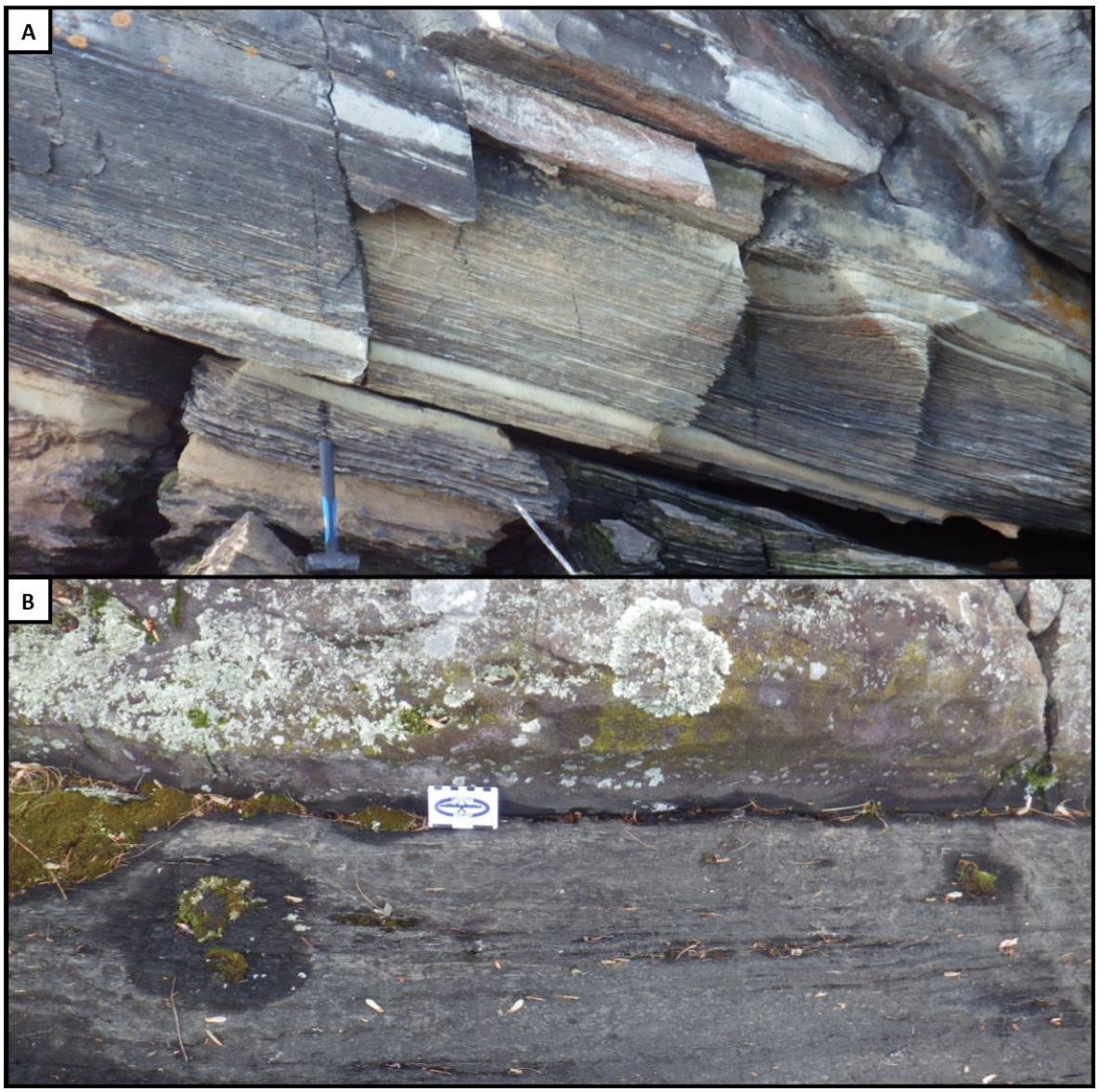

Figure 42: Contacts between the lower laminated carbonate and siltstone lithofacies association and the overlying siliciclastic-rich lithofacies associations. A: At Quirke Lake the contact between the underlying laminated carbonate and siltstone lithofacies association and the overlying parallel laminated siltstone beds is a slightly gradational change wherein the carbonate-rich beds decrease in thickness and abundance. B: Sharp and planar contact between the laminated carbonate and siltstone facies and the overlying laminated siltstone and sandstone facies in the Moose Bay area.

Chert layers were also observed within the laminated limestone and siltstone lithofacies association and these layers typically range from 5mm to 2cm in thickness and are commonly fractured. Chert layers may be massive but quite often internally contain fine, sub-millimetre- to millimetre-scale parallel lamination (Figure 41). Some chert layers contain millimetre-scale laminations of clay and silt as well. Chert layers in most instances are fractured and broken up, sometimes to the extent of forming brecciated layers within a micritic carbonate matrix. There are however, chert layers that are planar to wavy and relatively undeformed within similarly undeformed layered carbonate and siltstone units.

Changes in layer thickness of carbonate, siltstone, and chert are variable both laterally and upwards in stratigraphy but there is a general trend of a loss of carbonate approaching the contact with the overlying siltstone member. The upper contact of the laminated carbonate and siltstone lithofacies associations with the overlying siliciclastic-dominated lithofacies associations is usually a gradational change through which limestone layers become less common until siltstone and calcareous siltstone is the dominant lithology (Figure 42A). Where the contact between the laminated limestone and siltstone and overlying siliciclastic-dominated facies is sharp, the contact is similar but the change is abrupt and is distinctly divided by a lithology with limestone laminae that is overlain by a parallel laminated siltstone to sandstone unit lacking carbonate laminae (Figure 42B). The exception to this transition of the lower parallel laminated carbonate and siltstone unit being overlain by the siltstone lithofacies association is in certain locations in the Elliot Lake area where intrusive breccias separate the two units.

The second most predominant lithofacies that is a consistent feature of the laminated carbonate and siltstone lithofacies association are massive carbonate layers that usually range from 2 to 10cm in average thickness and consist almost entirely of white fine- to medium-grained carbonate (Figure 43A). Rare thin silt laminae, 1-3mm thick, may be included within a massive carbonate bed but are uncommon and may be discontinuous. Contacts between the massive carbonate facies and adjacent facies are sharp and massive carbonate beds commonly occur within the interlaminated carbonate and siltstone facies. Faulting and soft-sediment slumping that commonly affects the laminated carbonate and siltstone lithofacies affects the massive carbonate layers similarly (Figure 43B). Massive carbonate beds are common throughout the laminated carbonate and siltstone lithofacies association but are best developed in road outcrops along Highway 108 north of Elliot Lake and in the Bruce Mines area.

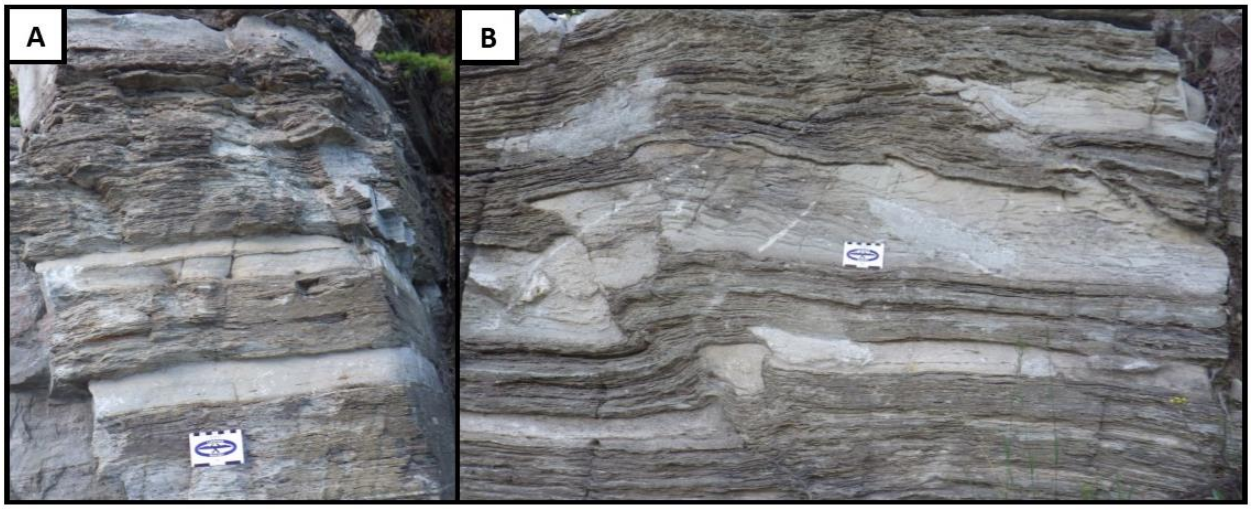

Figure 43: A: Interlaminated carbonate and siltstone lithofacies association that is punctuated by sharp-sided white massive carbonate beds. B: Faulted outcrop of interlaminated carbonate and siltstone lithofacies with massive carbonate interbeds. Rare, faint, mm-scale silt and clay laminations occur within the otherwise massive carbonate interbeds.

6.2 LITHOFACIES ASSOCIATION 2: CARBONATE SLUMP BRECCIA

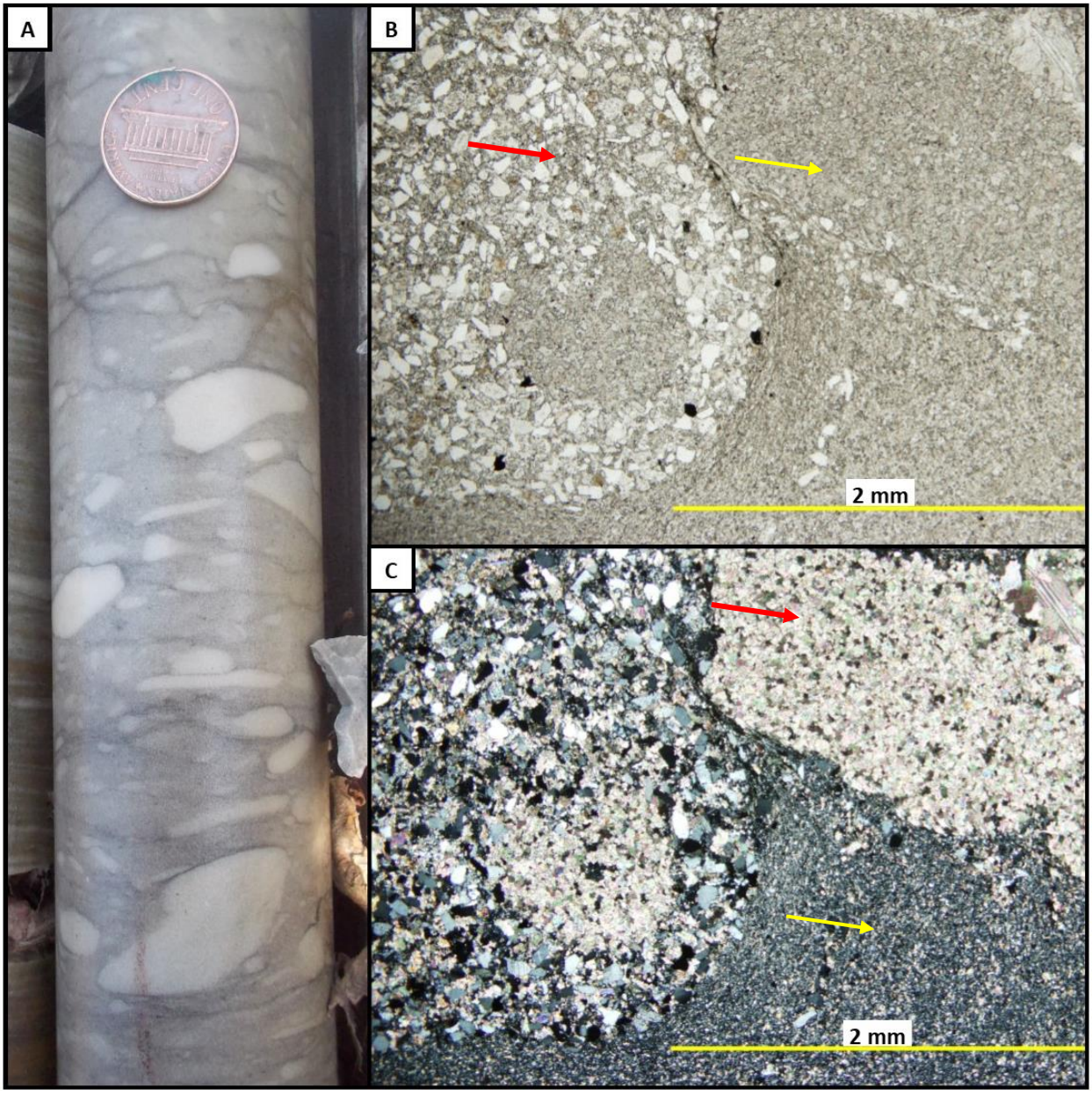

Figure 44: Carbonate slump breccia unit present in drill hole 150-2. A: Sub-rounded and elongate clasts of white carbonate surrounded by a siliciclastic-dominated matrix of silt to fine-grained sand. B: Petrographic image in PPL of the slump breccia. The sand-rich fraction (red arrow) and the finer-grained fraction (yellow arrow) are separated by sharp contacts. C: In XPL the three distinct facies within the slump breccia are distinguishable. The finer-grained fraction is separated into a carbonate facies (red arrow) and a siliciclastic facies (yellow arrow).

A carbonate slump breccia is present in the lower to middle stratigraphy within the Espanola Formation in drill hole 150-2 and consists of subangular and subrounded to elongate clasts of white carbonate in a grey siliciclastic-dominated matrix (Figure 44A). This is vertically gradational with contorted to parallel laminated units. The breccia ranges from clast supported to matrix supported, with matrix supported being more prevalent. White carbonate clasts are largely subrounded and elongate and vary widely in size from ~3mm to 1cm on average. Petrographic analysis of this facies reveals that the matrix of the slump breccia is composed of sediments of two distinct grainsizes; clay and poorly sorted fine-grained sand (Figure 44B, C). One is of a clay to silt unit dominated by sheet silicates, while the other is a coarser and poorly sorted fine-grained sand to siltstone dominated by angular to rounded quartz grains with lesser potassium feldspar and plagioclase. This slump breccia is vertically gradational with contorted interlaminated carbonate and siltstone and mudstone, which in turn transitions into parallel laminated carbonate and siltstone.

6.3 LITHOFACIES ASSOCIATION 3: SILICIFIED CARBONATE

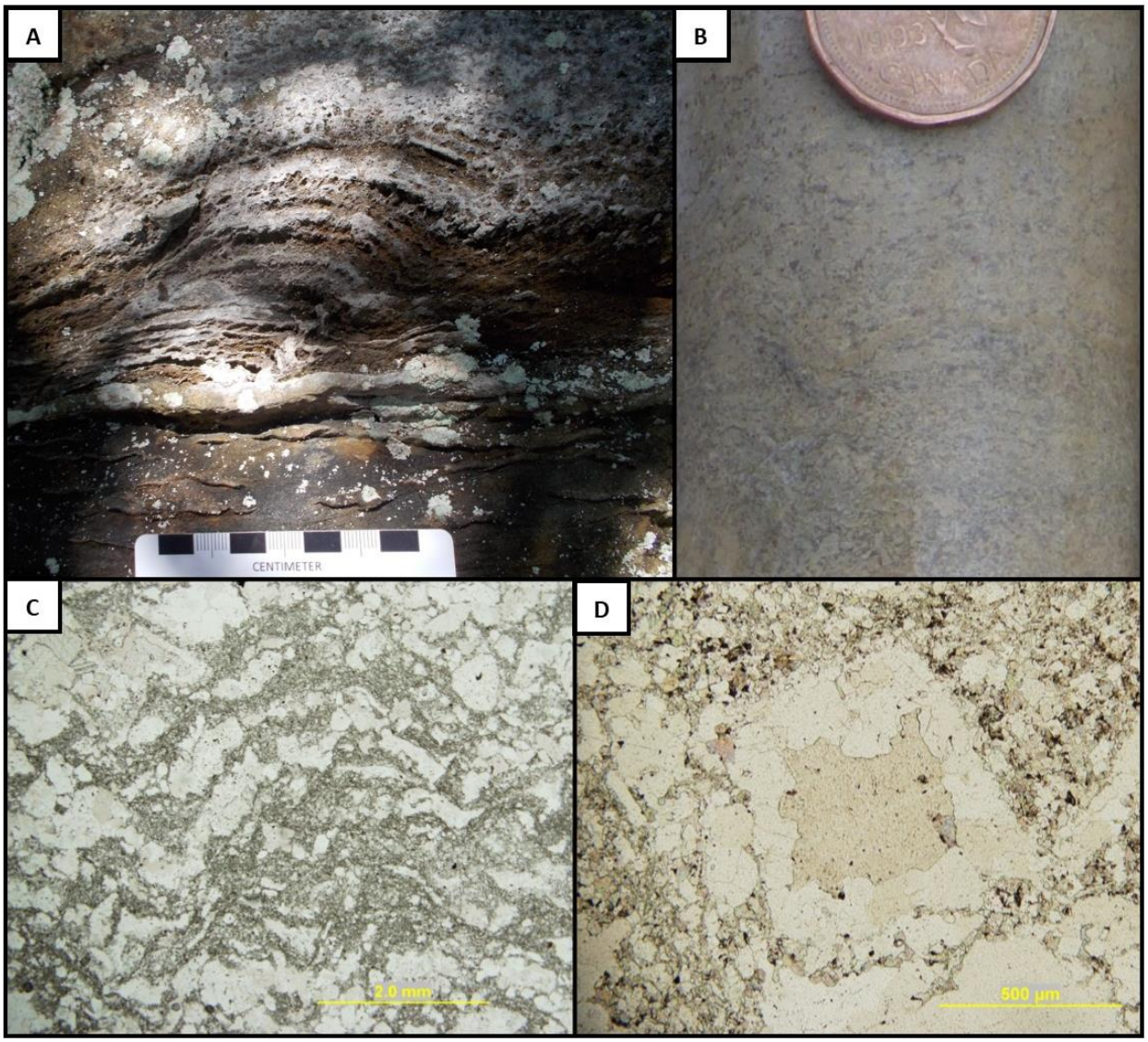

Figure 45: A: Silicified carbonate unit overlying a lenticular bedded unit at Quirke Lake. B: In drill core the silicified carbonate unit is speckled with clear quartz grains in a white matrix of finer-grained quartz and carbonate. C: PPL image of the silicified carbonate unit. Jagged and irregular lamination in a chevron pattern is between coarser carbonate grains with varying degrees of silicification and finer-grained carbonate and quartz. D: Carbonate crystal that is rimmed with quartz.

A layer of silicified carbonate is present in the lower middle stratigraphy of the Espanola Formation in the Quirke Lake area and is also present in the drill core. This unit has sharp

contacts with the units that overlie and underlie it. Along the western shore of Quirke Lake the silicified carbonate unit overlies lenticular laminated mudstone with sand-rich silt, and underlies fine-grained sandstone (Figure 45A). In drill core, and on a cut surface, the coarser-grained quartz gives the unit a speckled appearance with medium-grained sand sized quartz scattered fairly uniformly throughout the facies (Figure 45B). The silicified carbonate is roughly laminated, with laminae being 5mm thick on average and alternating between coarser-grained silicified carbonate layers and finer-grained carbonate layers (Figure 45C). Laminae are wavy to jagged and usually laterally discontinuous. In thin section, coarser-grains that have not been fully replaced have silicified rims with relict carbonate centers (Figure 45D). The silicified carbonate lithofacies association is approximately 50cm thick and is overlain by fine-grained sandstone and siltstone.

6.4 LITHOFACIES ASSOCIATION 4: GRADED AND INTERBEDDED SILTSTONE AND SANDSTONE

The lowermost parallel laminated carbonate and siltstone lithofacies association is typically overlain by the graded and interbedded siltstone and sandstone lithofacies association, which is recognizable primarily by its sharp increase in siliciclastic fraction and coincident decrease in the carbonate fraction. This lithofacies association is common throughout the drill core and sporadically in outcrops in the Quirke Lake area and along the north shore of Lake Huron. Parallel laminated, massive, and graded siltstone and fine-grained sandstone are the three most common lithofacies, and parallel laminated to massive siltstone directly overlies the contact with the underlying, parallel laminated carbonate and siltstone

(Figure 46A). In some sections, this lithofacies association is dominated by normally graded beds that range in thickness from 1-3cm on average, and up to 5cm thick, which grade from fine- or rarely medium-grained sand to clay-rich silt (Figure 46B). Contacts between adjacent graded beds and other lithofacies are sharp and may be either flat, slightly irregular, or serrated. Rarely, the upper silty portion of a fining upwards unit may show fracturing perpendicular to the bed top. These fractures are typically narrow and may be filled with coarser sediment that is akin to the sand both above and below. Sand fractions of graded beds have a variable amount of carbonate cement and siltstone units within the graded and interbedded siltstone and sandstone lithofacies association are also sporadically calcareous.

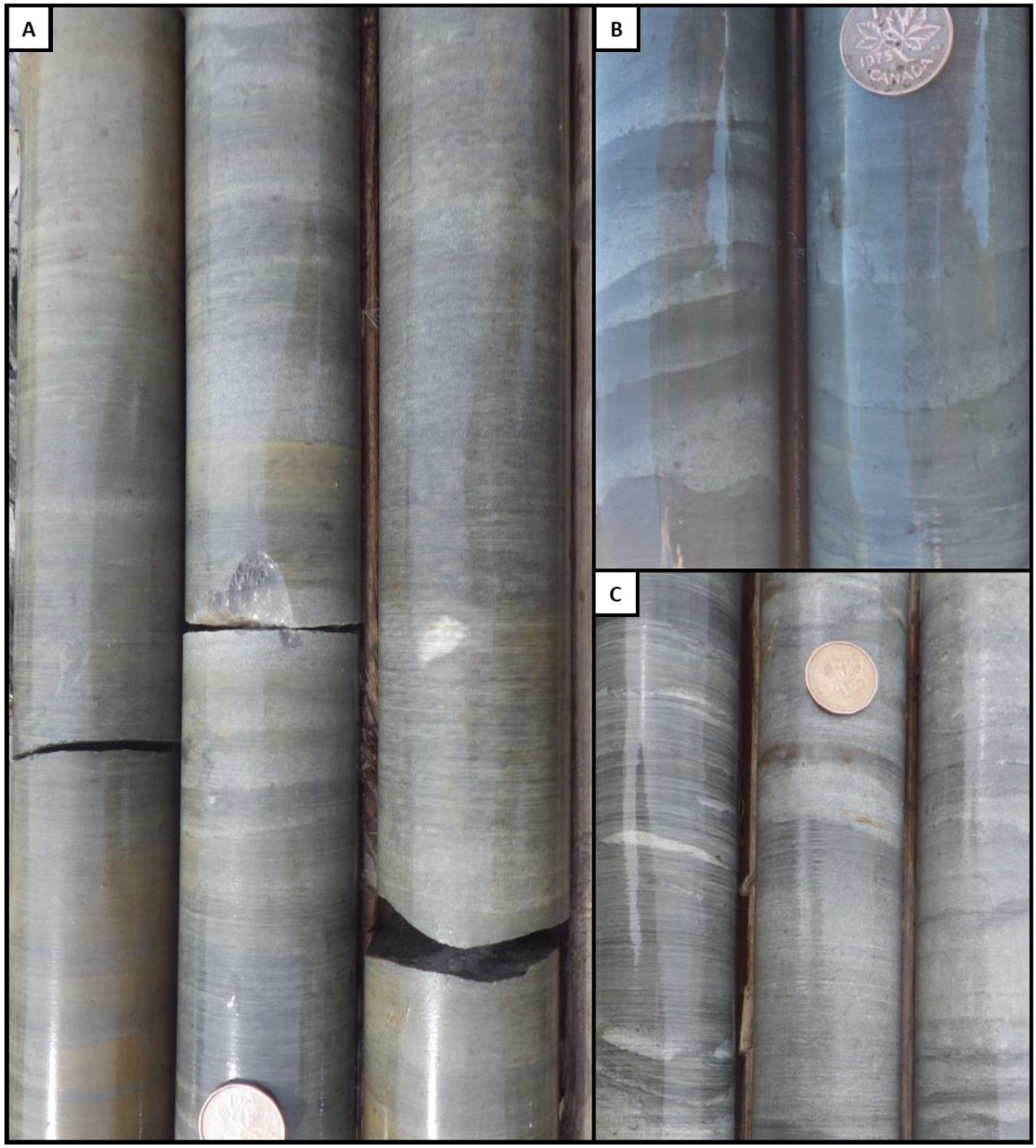

Figure 46: A: Common appearance of the graded and interbedded siltstone and sandstone lithofacies association in drill core. Graded beds, ~1cm thick on average, like those in the center of the image are prevalent in many places and are found in association with interbedded to massive siltstone and sandstone. B: Section of stratigraphy that is dominated by graded beds with sandy bases and silty tops. The contacts between adjacent beds are sharp and often irregular loaded surfaces. C: The left hand portion of the image contains a section of stratigraphy from the graded and interbedded siltstone and sandstone lithofacies association that is more silt dominated with visible irregular lenses of sandstone.

Wavy to lenticular bedding is also common throughout the lithofacies association and is identifiable by siltstone and sandstone being either interlaminated with one another, or with siltstone to mudstone surrounding lenses of sandstone up to 1-2cm thick (Figure 46C). The sandstone fraction of the wavy and lenticular laminated units is fine- to medium-grained sand and has a variable carbonate fraction that ranges from minimal to the predominant component. Wavy or lenticular bedded sections of stratigraphy can also be associated with slumped sections of stratigraphy. This transition is best preserved in drill core where wavy and lenticular bedded siltstone with sandstone transitions into a contorted 'mush' of siltstone with disseminated patches of sandstone.

Lamination in parallel laminated sections is on the mm-scale up to ~2cm and typically very planar, particularly adjacent to the contact with the underlying parallel laminated carbonate and siltstone lithofacies association and in the Iroquois Bay area. Massive units are more typically of fine-grained sandstone and have a variable range of thickness, from ~1cm up to several centimeters or decimeters and are typically interbedded with parallel laminated siltstone and sandstone or normally graded beds. Contortion and loading of parallel laminated sections in the siltstone and sandstone lithofacies association is a common feature and often occurs where fine-grained sand or silt overlies clay or clay-rich siltstone (Figure 47A). In the Iroquois Bay area parallel lamination is well exposed and lamination is visible between darker, siltier laminae and lighter more sand-rich laminae (Figure 47B).

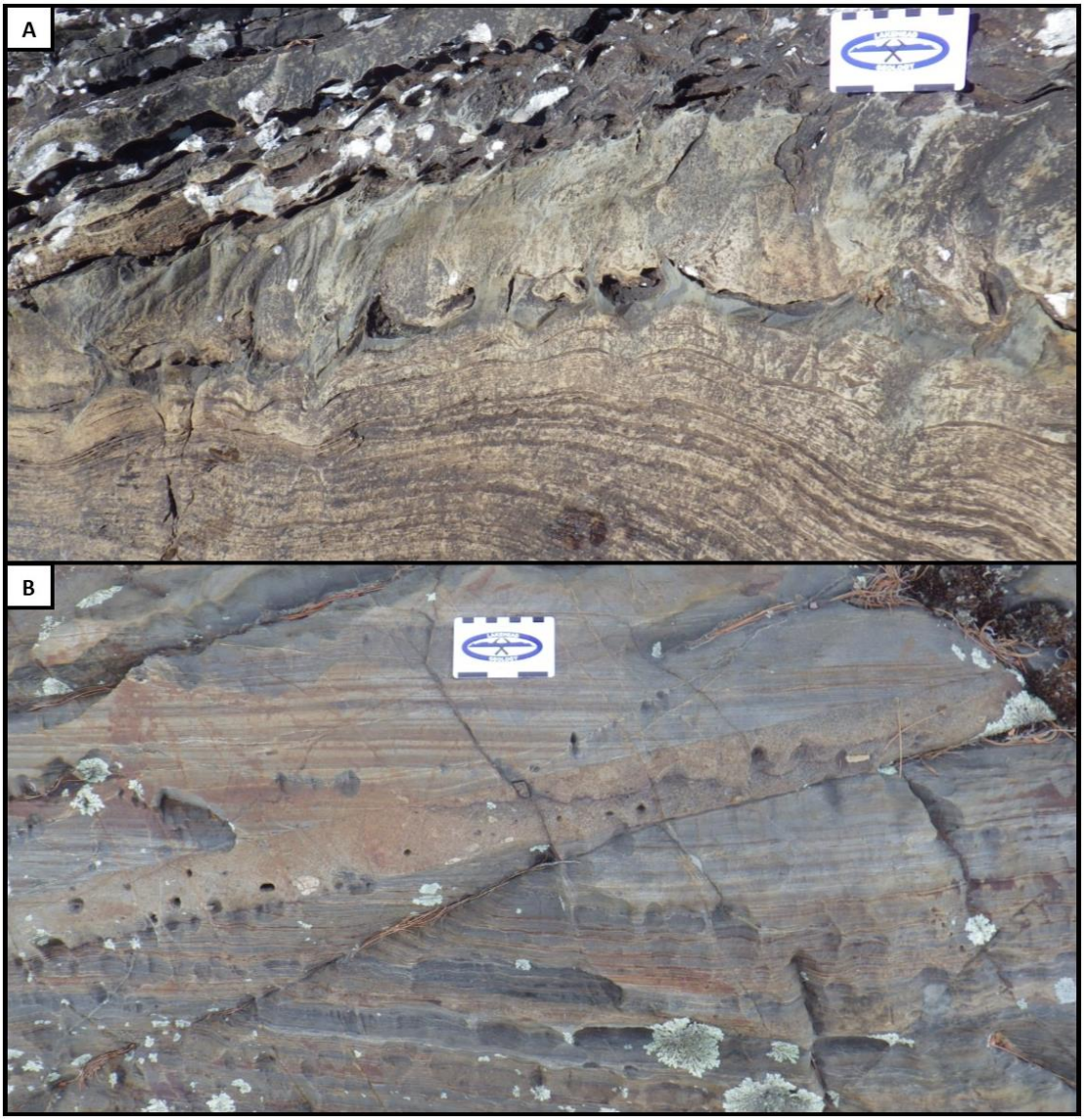

Figure 47: A: Parallel laminated to massive siltstone and sandstone outcropping at Quirke Lake. Underneath the scale card a finer-grained siltstone layer has become deformed by an overlying fine-grained sandstone unit loading into it. B: Parallel laminated siltstone and sandstone in the Iroquois Bay area, cross-cut by a conglomeratic dyke.

6.5 LITHOFACIES ASSOCIATION 5: HETEROLITHIC INTERBEDDED SILTSTONE

The middle and upper portions of the stratigraphy of the Espanola Formation in the Elliot Lake area contain sections that are unique for their high variability and rapid changes of

lithofacies. This lithofacies association is often in contact with the graded and interbedded siltstone and sandstone lithofacies association and the ferruginous carbonate interbeds lithofacies association but is distinguishable by the greater variation of lithologies and more chaotic stratigraphy, including a greater abundance of rip-up clasts and rip-up layers. Parallel lamination, ripple lamination, rip-up layers, massive beds, hummocky cross-stratification, and normally graded beds are the most common lithofacies present, and the lithologies are siltstone and calcareous siltstone, with variable carbonate, sandstone, and mudstone (Figure 48A, B). Parallel bedding between massive and normal graded beds typically ranges from 0.5-2cm thick, on average. These beds are largely siltstone and calcareous siltstone with lesser carbonate and sandstone. Contacts between beds are usually sharp and quite often irregular and erosive.

Soft-sediment deformation and dewatering structures are also common features of the interbedded siltstone facies. Dewatering and upwards injection of fluids and non-cohesive sediments results in siltstone beds that are highly fractured to the point of devolving into intraformational clast-rich layers. The siltstone clasts in these cases are cohesive, elongated, and angular. Soft-sediment deformation is common as sand and silt balls deforming finer-grained sediments beneath them and are often prevalent in horizons that are 2-3cm thick on average. They are usually associated with parallel and ripple laminated siltstone and sandstone (Figure 49A).

Figure 48: A: Typical appearance of the interbedded heterolithic siltstone lithofacies association in drill core. This lithofacies association is characterised primarily by the rapid facies changes that are well preserved in this section of stratigraphy. The units consist primarily of siltstone (red arrow) and lesser carbonate-rich siltstone to sandstone (yellow arrow) with layers being ~1cm thick on average. In places the finer-grained siltstone layers are fractured or broken up into clast-rich layers B: Outcrop expression of the same lithofacies at Quirke Lake. The typical stratigraphy is punctuated in the center of the outcrop by a ~10cm thick white parallel laminated carbonate unit.

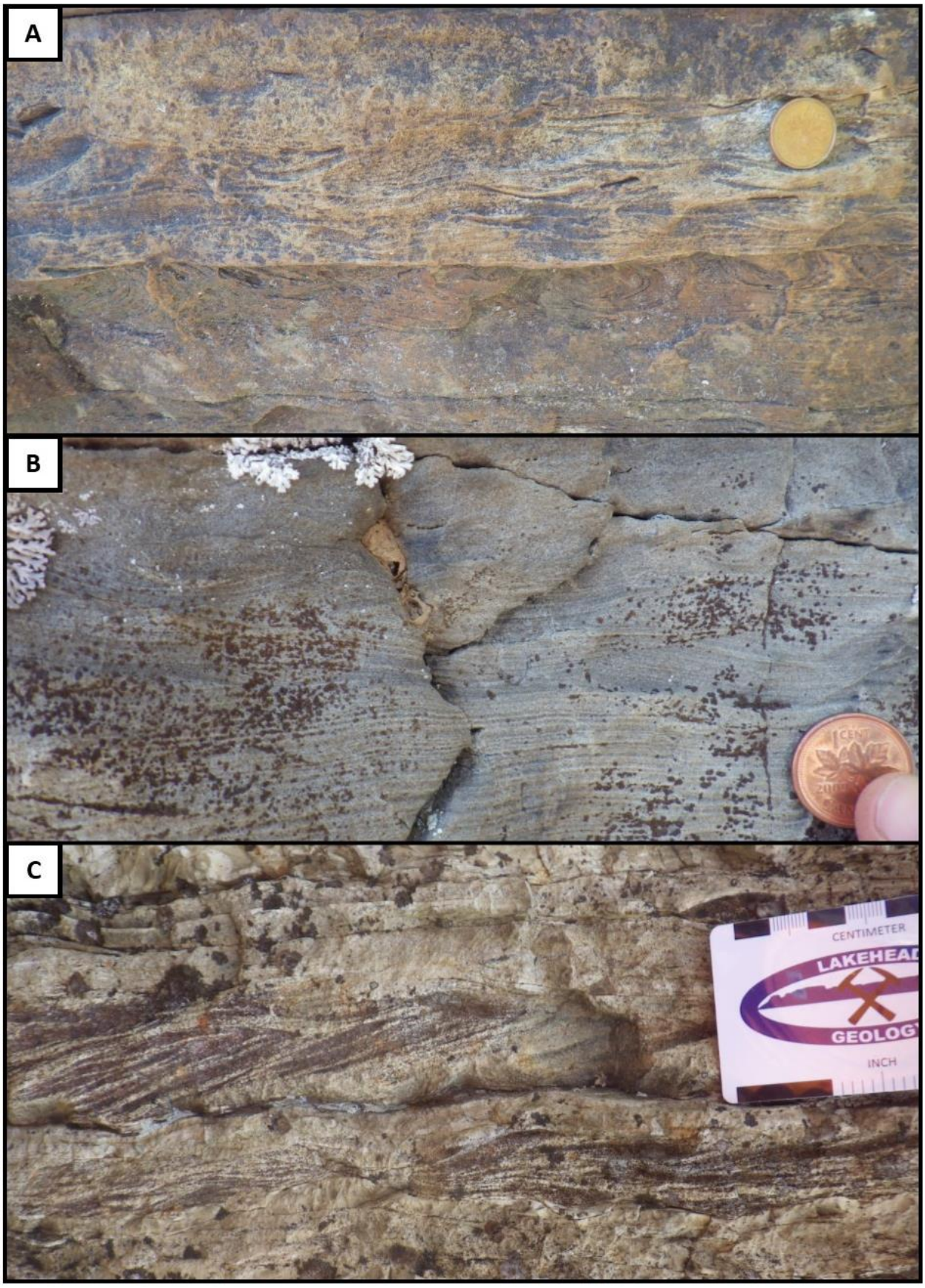
A
B
C
CENTIMETER
INCH

Figure 49: A: Mud-rich siltstone that is sharply overlain by a fine-grained sandstone to siltstone unit. The underlying finer-grained unit is parallel laminated with the uppermost 3cm being loaded wave ripple lamination. A sharp, slightly undulatory contact divides this unit from the overlying wave ripple laminated coarser unit. B: Parallel laminated fine sandstone that grades up into wave ripple lamination. C: Ripple laminated fine sandstone unit from the middle Espanola Formation in the Ten Mile Lake area. Ripple laminated beds are ~3-5cm thick on average. This section contains a wave ripple laminated layer that is sharply overlain by a unidirectional current ripple laminated layer. Ripple laminated layers in this image are adjacent to and separated by massive sandstone layers.

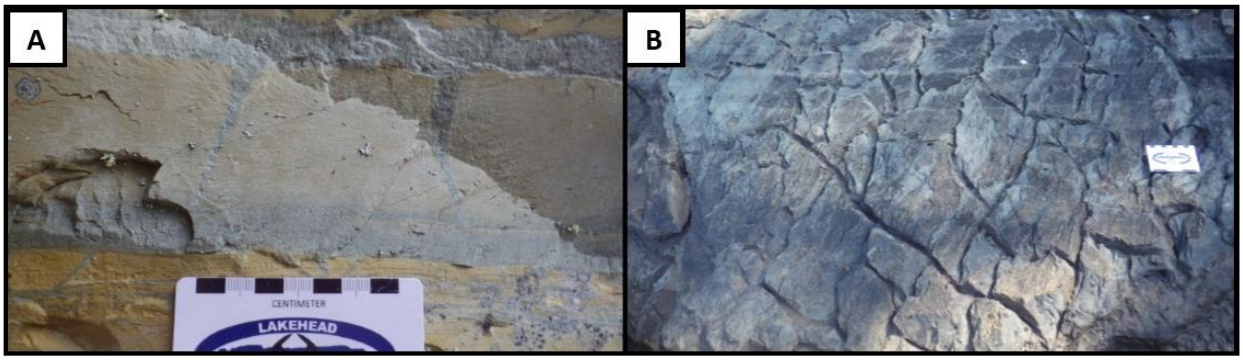

Figure 50: A: Side-view of desiccation cracks in a carbonate-rich siltstone horizon outcropping at Quirke Lake. The cracks taper downwards and are filled in with the coarser material from the overlying layer. B: Surficial expression of a desiccation-cracked siltstone unit at Quirke Lake.

Ripple laminated siltstone to fine-grained sandstone is very common in the Elliot Lake and Espanola areas. Ripple laminated units are typically 1-2cm thick, rarely up to 5cm thick, and are most commonly found in association with parallel laminated, graded, and massive siltstone and sandstone (Figure 49B). Both wave ripple and current ripple lamination are present in siltstone and fine-grained sandstone with wave ripples being more common. Wave ripples and current ripples can occur in close proximity to one another (Figure 49C). In the Quirke Lake area, and in drill core, desiccation features are rarely present in siltstone units and are visible both in cross-section and plan view (Figure 50A, B). Hummocky cross-stratification is also a fairly common feature in silt-rich, fine-grained sandstone facies of the interbedded heterolithic siltstone lithofacies association. These units are typically 2-5cm thick on average and are

interbedded most commonly with massive, parallel, or ripple laminated fine-grained sandstone (Figure 51A, B).

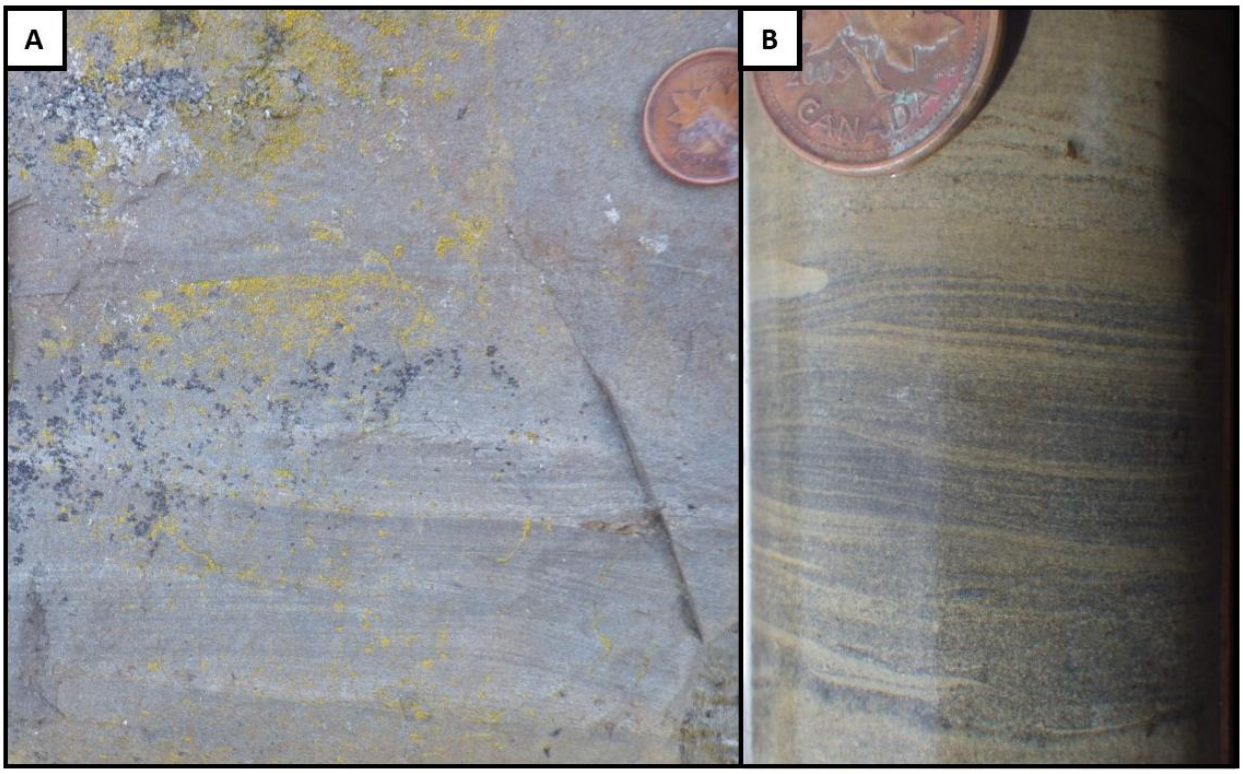

Figure 51: A: Hummocky cross-stratified fine-grained sandstone to siltstone outcropping at Panache Lake. The hummocky cross-stratified facies is slightly gradational into an overlying massive sandstone unit. B: Approximately 1cm thick hummocky cross-stratified fine-grained sandstone to siltstone unit near the upper contact of the Espanola Formation in drill hole E150-1. The hummocky cross-stratified unit is in contact with more well sorted fine-grained sandstone units.

Normally graded beds are also present in the interbedded heterolithic siltstone lithofacies association and are typically 2-5cm thick with a progression of grainsizes from medium- to fine-grained sand to siltstone with a variable clay fraction (Figure 52). In places, the lowermost sandstone area shows small scale cross-stratification. Graded beds typically occur in sets of less than three before a change in lithofacies occurs and were not observed forming

many packages of multiple sets as in the graded and interbedded siltstone and sandstone lithofacies association, but are otherwise similar.

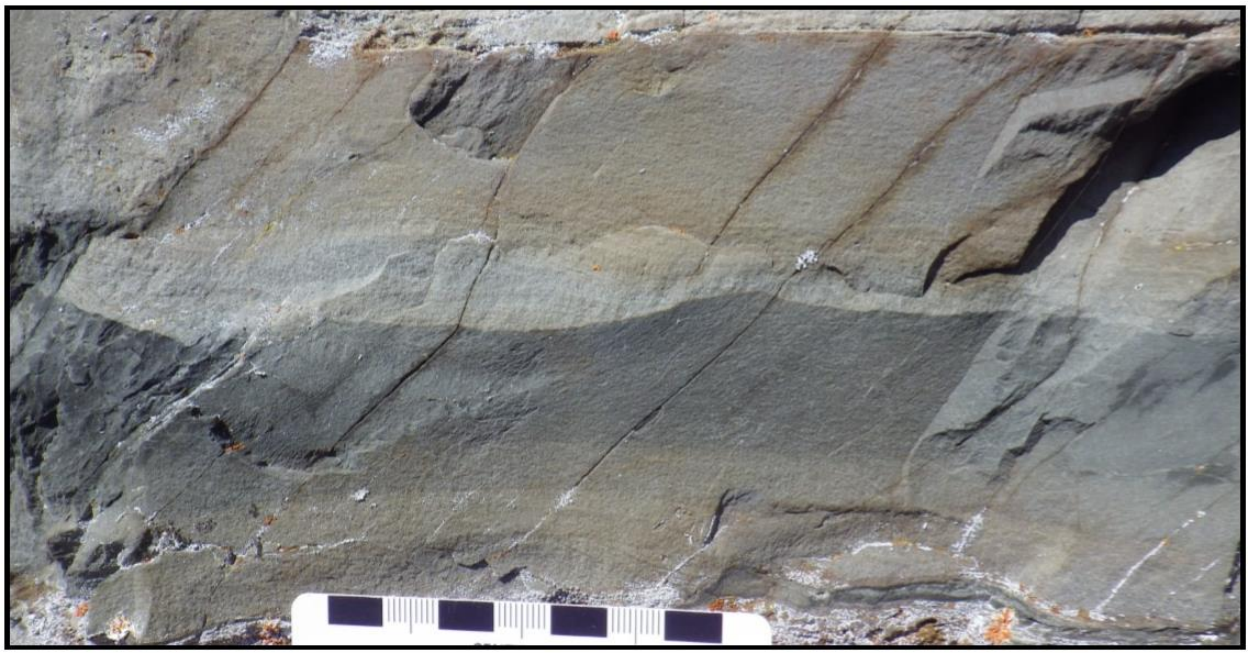

Figure 52: Two ~5cm thick normally graded beds in the interbedded siltstone lithofacies association. Contacts between the beds and the overlying and underlying units is sharp and irregular.

Near Wells Island the Espanola Formation contains some similar features to the interbedded heterolithic siltstone lithofacies association, but stratigraphic position is not constrained due to a lack of outcropping contacts with the Bruce Formation or Serpent Formation. Massive sandstone interbeds and parallel laminated siltstones and sandstones are both common at this location; in addition, graded beds, hummocky cross-stratification, and rippled units are also common. Extreme soft sediment deformation, in the presence of sand balls within fine-grained massive to weakly laminated mudstone to siltstone is also fairly common in close association with parallel laminated beds, ripple lamination, and hummocky cross-stratification (Figure 53A). At this location ripple lamination is an uncommon facies and is

present as wave ripple lamination directly overlying parallel lamination of fine-grained sandstone (Figure 53B).

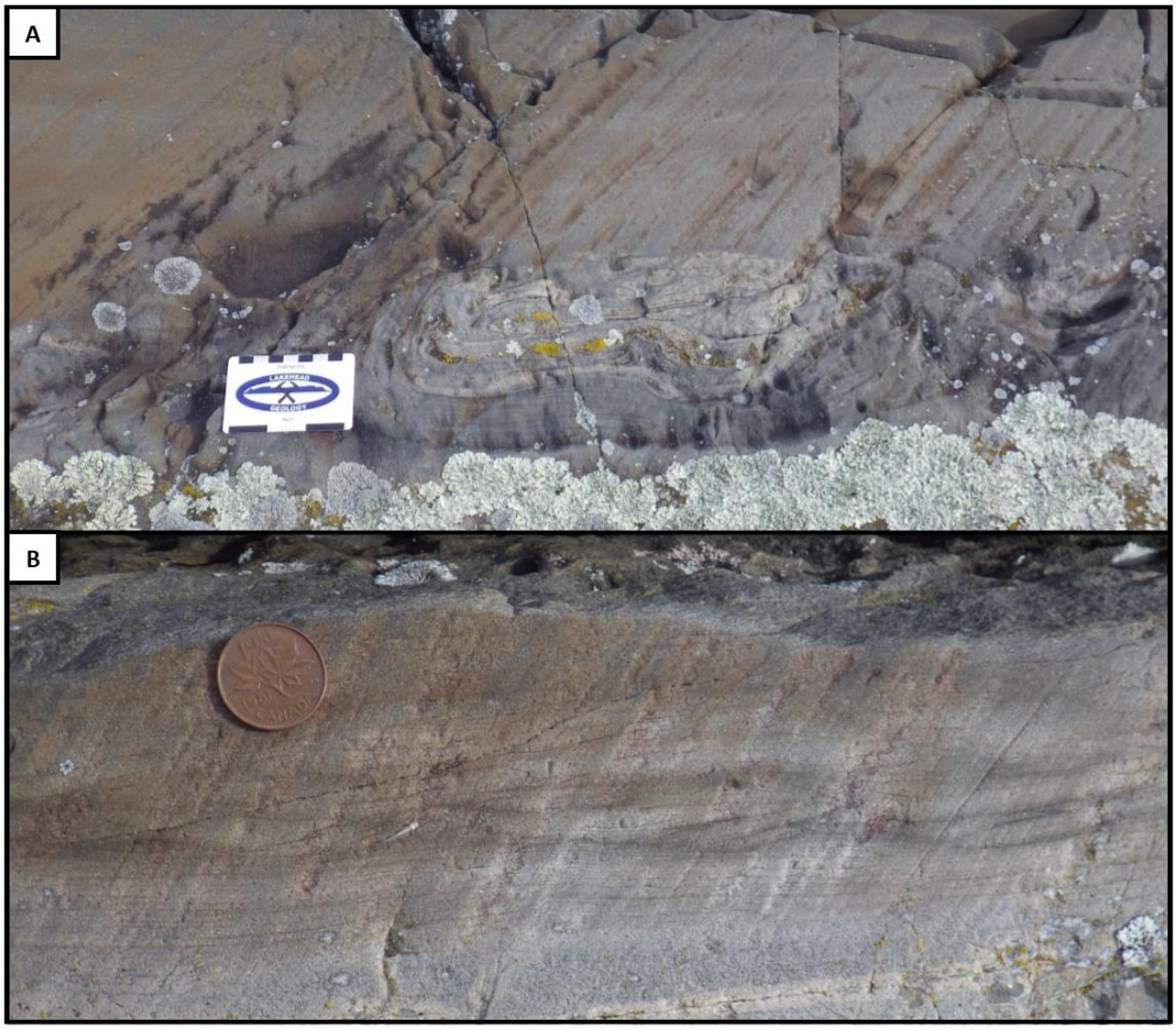

Figure 53: A: Medium-grained sand balls loaded into and deforming the underlying clay-rich siltstone unit. The sand that the balls loaded from is not preserved. B: Wave ripple lamination that is underlain by mm-scale parallel lamination.

6.6 LITHOFACIES ASSOCIATION 6: FERRUGINOUS CARBONATE INTERBEDS

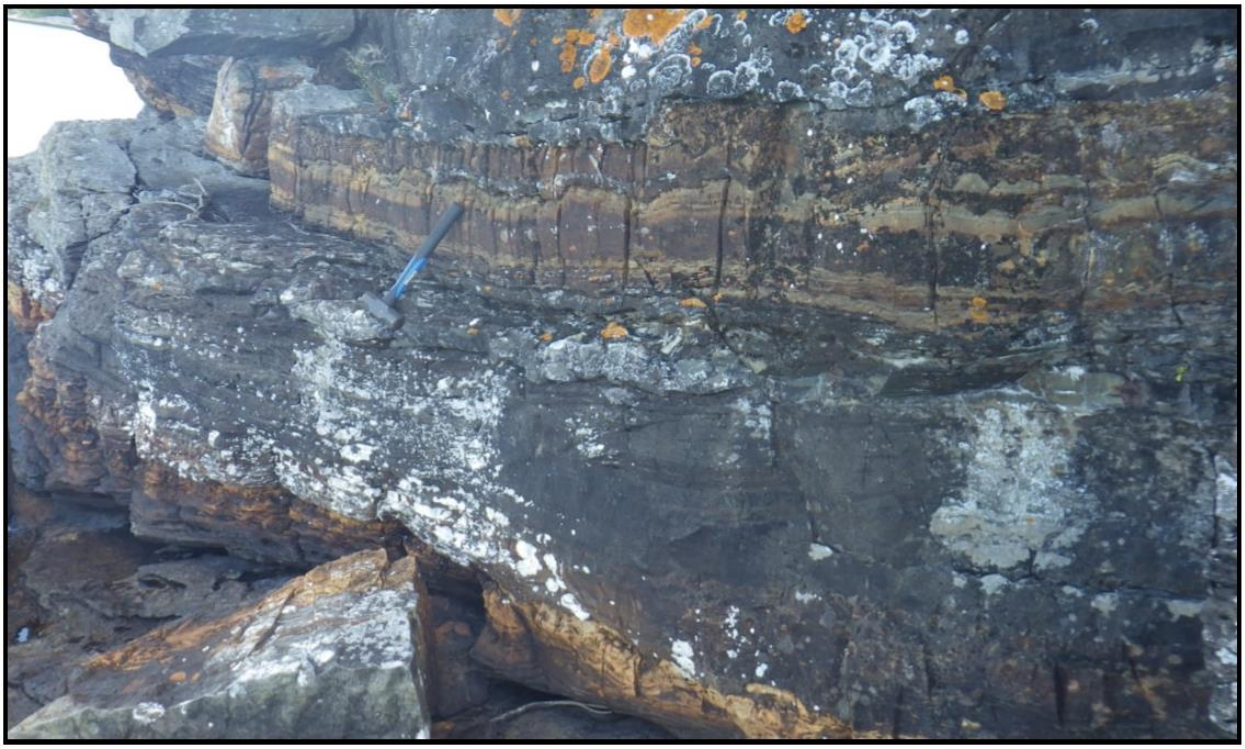

Figure 54: Ferruginous carbonate units, ~50cm thick on average, interbedded with siltstone and sandstone units at Quirke Lake.

The ferruginous carbonate interbeds lithofacies association is identifiable by the presence of rusty orange to red weathering ferruginous carbonate units up to ~50cm thick that are found interbedded with the heterolithic interbedded siltstone lithofacies association (Figure 54). Siliciclastic beds may contain any structures that are observed in the interbedded heterolithic siltstone lithofacies association including; massive, parallel laminated, hummocky cross-stratified, ripple laminated, or graded. Fine-grained sandstone and siltstone are the most prevalent siliciclastic components with mudstone occurring as an accessory. Rare chert layers that are similar in appearance to those present in the interlaminated carbonate and siltstone lithofacies association are also present as commonly fractured layers within the ferruginous

carbonate interbeds (Figure 55A). Elongated chert clasts can also be diffusely scattered in massive to finely laminated ferruginous carbonate beds (Figure 55B). Along with the ferruginous carbonate interbeds that punctuate the siliciclastic-dominated beds, white-weathering carbonate beds are also rarely associated with this lithofacies association and are most typically found directly underlying ferruginous carbonate interbeds. White-weathering carbonate interbeds are parallel to ripple laminated and are usually only 2-3 cm thick but may be up to 10cm thick (Figure 56A). Contortion of these units is very common, and in places these beds form rip-up layers with bent, deformed, and elongated carbonate pebbles (Figure 56B).

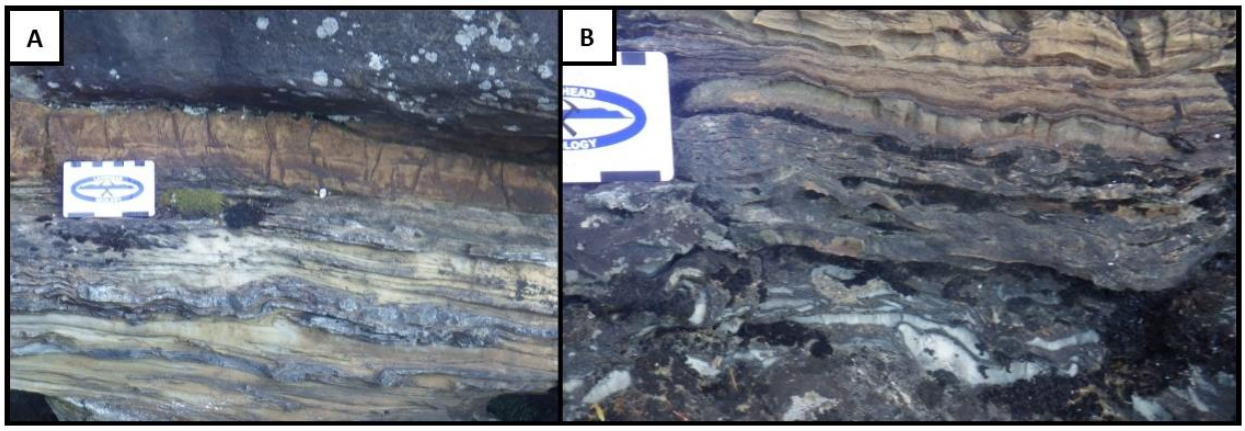

Figure 55: A: Unit of parallel laminated white weathering carbonate with chert laminae overlain by rusty red ferruginous carbonate. The carbonate beds are sharply overlain by a massive fine-grained sandstone unit. B: Contorted and broken-up layer of white weathering carbonate in siltstone underlying a ferruginous carbonate interbed.

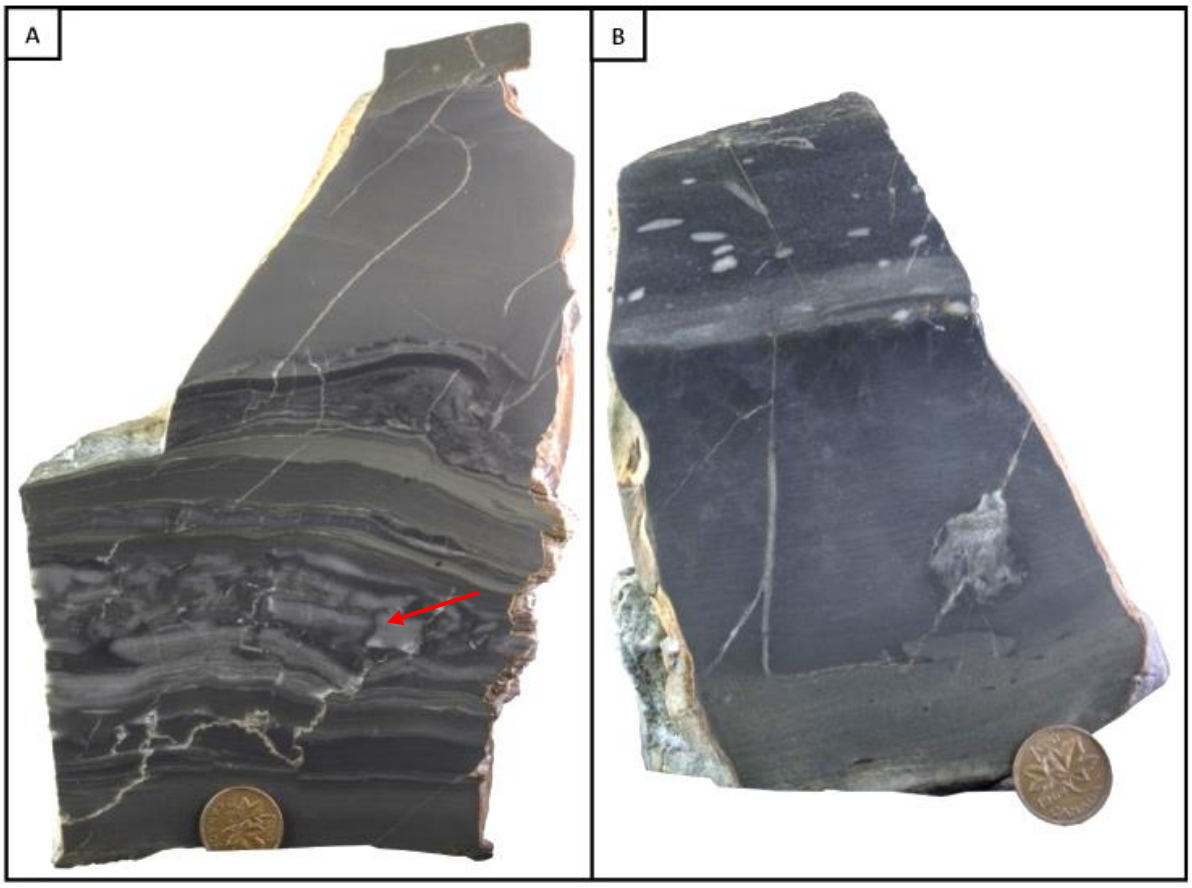

Figure 56: Polished slabs of ferrginuous carbonate interbeds from the Quirke Lake area. A: Polished slab of a ferruginous carbonate interbed with siltstone layers and a unit containing fractured chert clasts (red arrow). B: The middle section of this slab is of very finely (mm-scale) laminated micritic ferruginous carbonate. The top of the slab is marked by a carbonate-rich silt unit that is slightly coarser-grained and contains roughly flat-lying elongated clasts of chert that range in length from ~2-8mm.

Ferruginous carbonate interbeds may be parallel laminated, ripple laminated, hummocky cross-stratified, or intraformational conglomerates and typically contain two or more of these facies within a single interbed. Much like the associated siliciclastic-dominated lithofacies associations, ferruginous carbonate units are internally composed of rapid facies changes and sharp, often erosive contacts between adjacent facies. Within the ferruginous carbonate beds are layers and interbeds of siltstone up to ~1-3cm thick that are commonly parallel laminated (Figure 57A, B). Ripple lamination of the ferruginous carbonate is mostly

associated with massive, parallel laminated, conglomeratic, or heavily contorted facies. Ripple laminated beds are typically 2-4cm thick and are underlain by parallel laminated units. Wave ripple lamination is the most abundant type of ripple lamination within the carbonate units and occurs in layers ~1-5cm thick (Figure 58A). Petrographic analysis of wave ripple laminated ferruginous carbonate shows that the lamination within this facies alternate between micritic carbonate and siliciclastic-rich micritic carbonate laminae (Figure 58B). Hummocky cross-stratification usually occurs in beds up to ~5cm thick and is similar to hummocky cross-stratified units in the interbedded heterolithic siltstone lithofacies association with the exception of the host lithologies being predominantly micritic carbonate as opposed to siliciclastics.

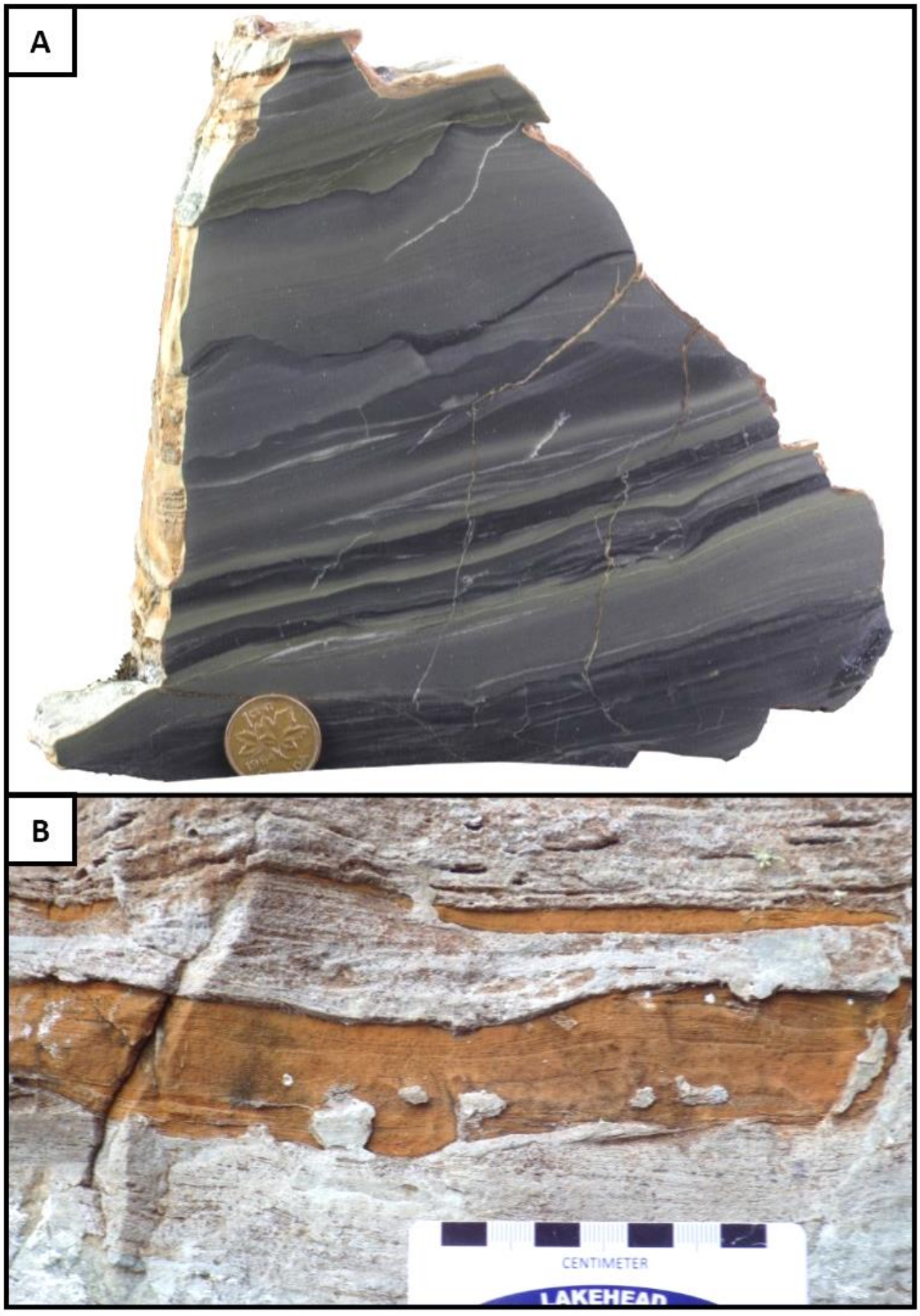
A
B
CENTIMETER
LAKEHEAD

Figure 57: A: Polished slab of a sample collected from the upper Espanola Formation at Quirke Lake. The sample is dominated by parallel to wavy laminated siltstone and dolostone with rare ripple lamination. Siltstone units and more silt-rich dolostone units are identifiable in hand sample by a green colour and slightly more resistive tendency to weathering. The upper half of the sample contains two dolostone beds that are finely laminated and have highly erosive and irregular contacts. The uppermost irregular dolostone bed is sharply overlain by a siltstone unit that grades upwards into another section of laminated siltstone and dolostone facies. B: Outcrop exposure showing the laminated siltstone and dolostone facies in the field. White dusted sections are the silt-rich beds while dolostone beds are rusty red in colour on a weathered surface.

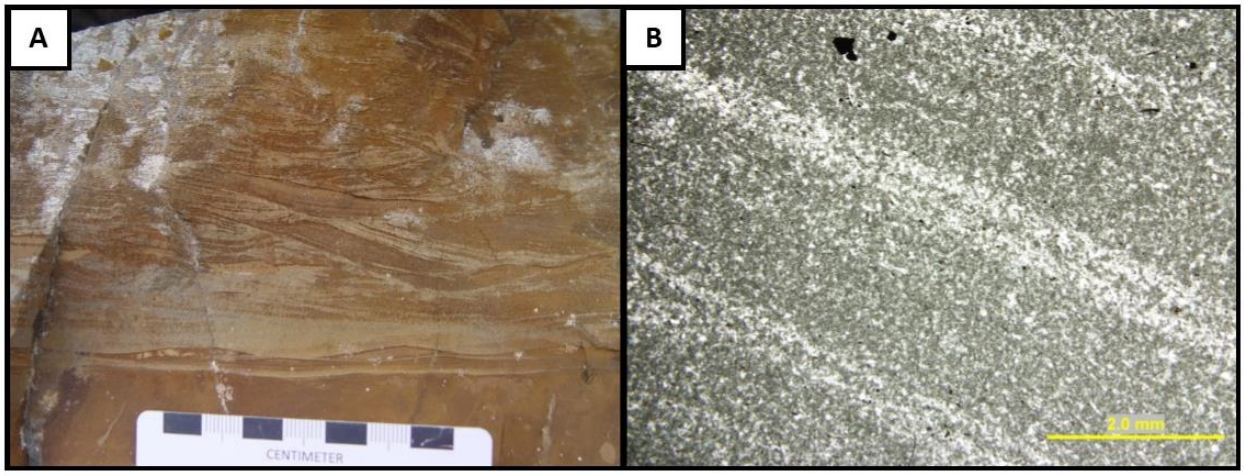

Figure 58: A: Outcrop of wave ripple lamination in a rusty red ferruginous carbonate unit. B: Petrographic analysis of the ripple laminated carbonate facies shows that lamination is formed by micritic carbonate and siliciclastic-rich layers.

The intraformational conglomerate lithofacies is a common unit observed in the ferruginous carbonate interbeds lithofacies association within the Elliot Lake area. These units are typically ~5-15cm thick and generally have a high clast content and are almost always clast supported. In outcrop, clasts consist of rusty-orange carbonate within a darker brown-grey siliciclastic-rich matrix (Figure 59A). Orientation of clasts can be subparallel to chaotic and disoriented and clast size is highly variable as well, with mm-scale clasts being found within the same units as clasts up to 15cm in size. Elongate and round to subround is the most common shape and angularity of clasts and many are bent (Figure 59B). Many intraformational

conglomerate units are discrete and are bounded above and below by grey-green siltstone to fine-grained sandstone beds. Contacts with underlying siltstone are commonly slightly irregular, suggesting that the intraformational conglomerate beds may have somewhat erosive contacts with units below. The upper contacts are usually less irregular and faint lamination may be observed in the overlying siltstone. Intraformational conglomerate units are not always discrete units, and may be located at the base, interstitially, or at the top of massive to parallel and ripple laminated, rusty-weathering, ferruginous carbonate beds (Figure 60).

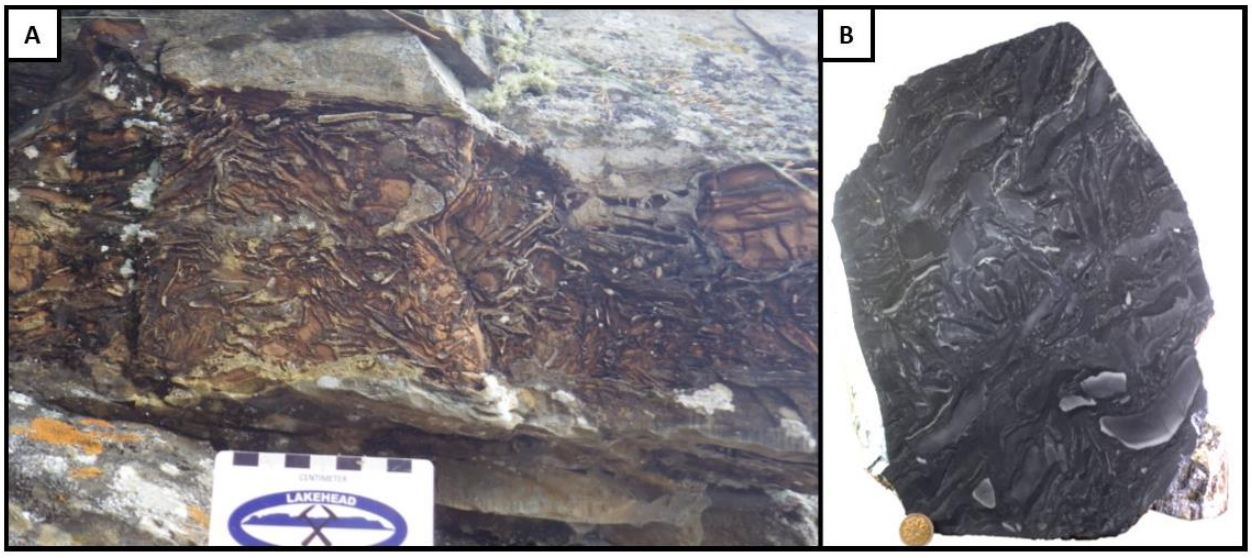

Figure 59: A: Intraformational conglomerate unit consisting of typically elongated clasts of ferruginous carbonate in a silt-rich matrix. Clast content is high and clast size is variable, ranging from mm-scale up to ~15cm long. The intraformational conglomerate is over- and underlain by siltstone to fine-grained sandstone units with sharp and slightly irregular to probably erosive contacts. B: Slab of an intraformational conglomerate unit. Many of the micritic carbonate clasts are bent to some extent suggesting that they may have been soft and ductile during resedimentation.

Figure 60: Ferruginous carbonate interbed overlying a siltstone unit at Quirke Lake. A flat pebble layer of irregular thickness separates the two units. Further up in the unit, near the top of the image, elongated clasts of less erosive chert occur sporadically throughout a ~5cm thick interval.

Petrographic analysis of the intraformational conglomerate shows micritic clasts of varying sizes within a siliciclastic-rich matrix with a high quartz content (Figure 61A). The clasts are round to subround and many are fractured with quartz infilling the fractures. Fractures are not necessarily isolated to discrete clasts and may cut through matrix and clast alike. Some clasts also have a rim of quartz cement that borders them, and a thin black layer may separate these quartz rims from the surrounding matrix (Figure 61B). Rarely, quartz grains may show elongation that suggests that precipitation of the quartz may have been contemporaneous with fracturing. Furthermore some displacement has been observed along fractures, up to 500µm,

and suggests that the quartz-filled fractures in the clasts were formed after deposition of the sediments.

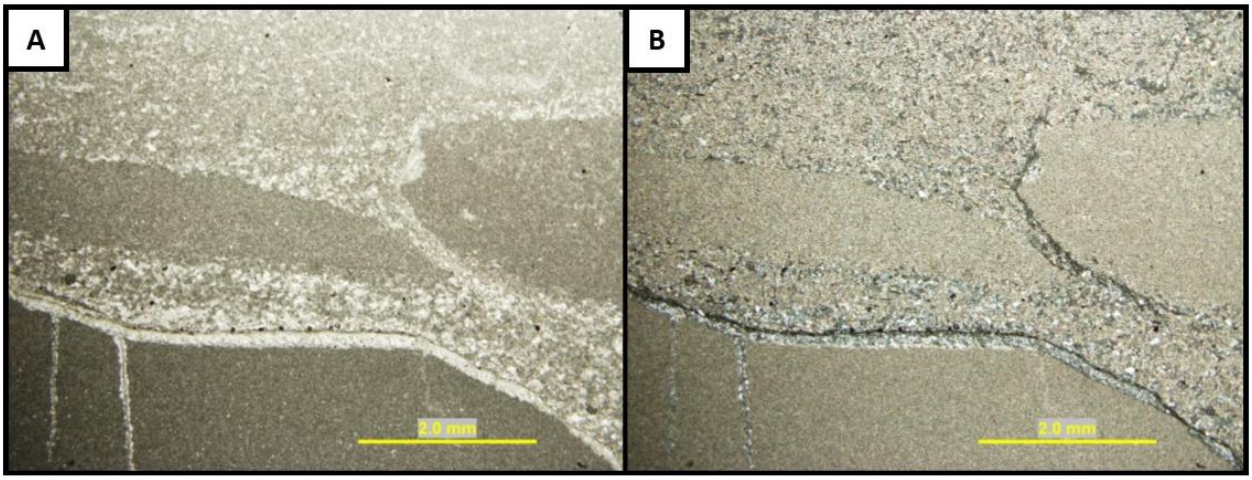

Figure 61: Petrographic images of a sample taken from an intraformational conglomerate unit. A: PPL image including micritic carbonate clasts that are typically elongated and surrounded by a more poorly sorted matrix. The bottom portion of the image is of a ferruginous carbonate layer that is visibly akin to the clasts in the intraformational conglomerate unit overlying it. A band of quartz separates the ferruginous carbonate layer from the overlying unit. B: XPL image showing the matrix of the intraformational conglomerate unit as being a mixture of micritic carbonate with silt-sized siliciclastics scattered uniformly throughout.

6.7 LITHOFACIES ASSOCIATION 7: CROSS-STRATIFIED AND PARALLEL LAYERED SANDSTONE

Along the north shore of Lake Huron, in the vicinities of Aird Island, Wells Island, and Iroquois Bay the middle to upper Espanola Formation is dominated by fine- to medium-grained cross-stratified sandstones and parallel layered fine-grained sandstone and siltstone. Ripple lamination, hummocky cross-stratification, massive sandstone beds and lenses, and graded beds are all minor lithofacies that occur within the sandstone-dominated lithofacies association of the middle to upper Espanola Formation in the southern outcrops. This lithofacies association is gradational into the overlying Serpent Formation along the north shore of Lake

Huron with the contact between the two being generally considered to take place following the last interbed of carbonate-rich sandy siltstone.

Trough cross-stratified sandstone is the most common facies approaching the Serpent Formation in the Iroquois Bay and Aird Island areas and usually consists of sets of medium-scale (30-60cm thick) beds composed of medium-grained sandstone. Wedge-shaped massive sandstone beds of well-sorted medium-grained sand are intermittently emplaced between beds, and sets are usually separated by parallel laminated silty-sandstones (Figure 62A). Bundled sets of small-scale (<30cm) trough cross-stratification occur in the upper parts of the Espanola Formation in the vicinity of Aird Island and are interbedded with planar cross-stratified and parallel laminated layers.

Packages of sharp-sided parallel layers is the second most common lithofacies within the cross-stratified and parallel laminated sandstone lithofacies association, and it is usually composed of fine-grained sandstone to siltstone. Parallel layers within this lithofacies association are very similar in appearance to the parallel laminated facies within the graded and interbedded siltstone and sandstone lithofacies association. Individual laminae thickness is ~5mm to 1cm on average and are commonly very parallel and straight. Soft-sediment deformed wavy to contorted laminae occasionally disrupts the bedding. Parallel layered units are most often in contact with trough cross-stratified sandstone beds and are usually finer-grained and more poorly sorted than the cross-stratified beds.

Planar cross-stratification is a common facies within the cross-stratified and parallel laminated sandstone lithofacies and is generally found in association with parallel laminated

sandstones and siltstones. These units are small- to medium-scale and are of fine- to medium-grained sand (Figure 62B). The grainsize of the planar cross-stratified sandstones is commonly finer-grained and slightly more poorly sorted than the trough cross-stratified sandstone units with which they are associated.

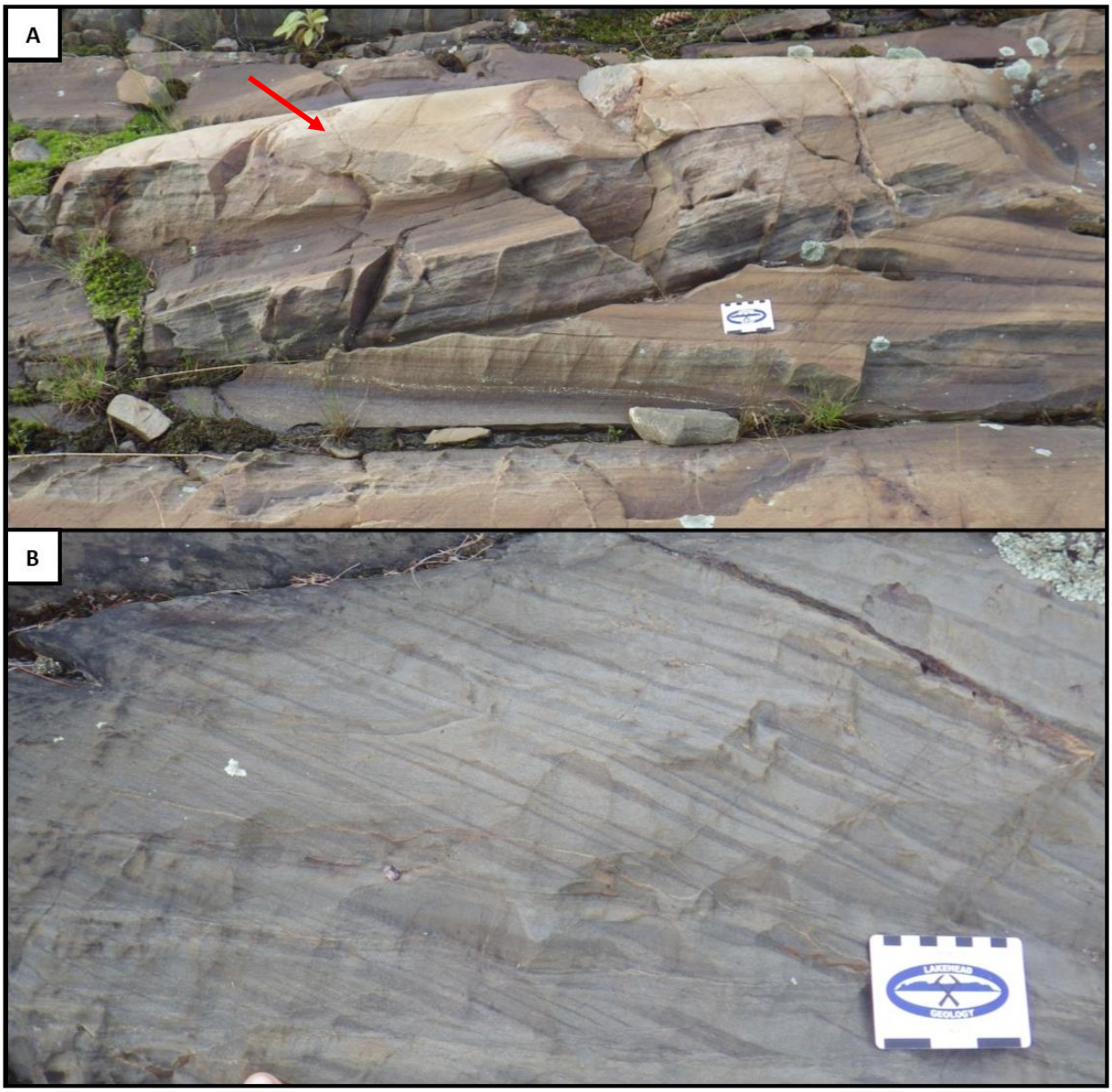

Figure 62: A: Cross-stratified sandstones of the local cross-stratified and parallel laminated sandstone lithofacies association. Medium-scale trough cross-stratified units are separated here by a wedge-shaped, coarser-grained, and well-sorted sandstone plug that infills the space between them (red arrow). B: Planar cross-stratified sandstones of the local cross-stratified and parallel laminated sandstone lithofacies association outcropping in the Iroquois Bay area.

Massive sandstones are rare and are often found in association with parallel laminated silty sandstones or cross-stratified sandstones. Thickness of massive sandstone units is typically 15-20cm, and they are commonly laterally discontinuous and/or wedge-shaped. Massive sandstones are typically of well-sorted medium-grained sand and are most often coarser and better sorted than the units with which they are associated.

Normally graded beds and ripple lamination within the cross-stratified and parallel laminated sandstone lithofacies association are a rare facies and outcrop in the vicinity of Iroquois Bay and Aird Island. Both graded beds and ripple laminated units are 2-3cm thick on average and have sharp to irregular contacts with adjacent beds. Graded beds usually occur in sets of less than three beds with sharp planar contacts. They are similar in appearance to those occurring within the interbedded siltstone lithofacies association. The change in grainsize is from medium- to fine-grained sand at the base to silt and clay at the top.

6.8 LITHOFACIES ASSOCIATION 8: INTRUSIVE BRECCIA

Intrusive breccias are a common feature in the Espanola Formation in the Quirke Lake and Ten Mile Lake areas and in drill core. Thickness of the intrusive breccias is highly variable and cross-cuts the stratigraphy of the drill core up to several 10’s of meters in thickness in some places. Clast content of the intrusive breccias is dominated by angular to slightly rounded clasts of predominantly siltstone composition. Clasts of carbonate, ferruginous carbonate, carbonate-rich siltstone, and sandstone are present in varying amounts as well, and the clast composition can be generally summarized as a melange of clasts derived from the Espanola Formation. Clast

size is overall highly variable and ranges from the mm-scale up to several centimetres but average clast size falls somewhere in the range of 3-5cm (Figure 63A). The matrix which surrounds the clasts is typically composed of silt with lesser sand, carbonate, and clay. Contacts between the breccias and the stratigraphy into which they intrude are sharp and irregular and are more easily delineated in outcrop than in drill core (Figure 63B). Aside from very obviously intrusive contacts between breccia units and the stratigraphy of the Espanola Formation, intrusive breccias are distinguishable from the common slump breccias and intraformational conglomerates by the more variable clast composition and the presence of clasts that are altogether exotic to certain sections of stratigraphy.

Figure 63: A: Intrusive breccia in drill hole 105-2. Clast size is highly variable, ranging from 1mm up to several cm, and clasts are randomly oriented throughout. B: Outcrop of the Interbedded ferruginous carbonate and siltstone lithofacies association that has become intruded by a breccia.

7 ESPANOLA FORMATION DISCUSSION

Depositional environment interpretations for the Espanola Formation are based on a traditional three to four member stratigraphic division. Overall the sequence stratigraphy of the Formation has been interpreted to represent a shoreline migration, involving a transgression followed by a subsequent regression during the Bruce glacial recession (Robertson, 1964, 1968; Parvianien, 1973; Young, 1973, 1990). The lower limestone member is largely suggested to have been deposited in a subtidal environment under relatively low energy conditions based on the fine parallel laminations that are predominant throughout (Young, 1973; Eggertson, 1975; Bernstien and Young, 1990). Fine laminations within this member indicate a quiet environment, and the predominance of carbonate with lesser siltstone and shale partings suggests that clastic input was minimal (Young, 1973; Eggertson, 1975). The source of these laminations has been interpreted to be seasonal in origin, or through influxes of sediment via storm-derived currents or turbidity currents (Robertson, 1964; Bernstien and Young, 1990).

The overlying Siltstone Member is also interpreted to have been deposited in deeper waters, deeper even than in the underlying Limestone Member and has been suggested to be largely similar to the underlying Limestone Member and differing merely in the carbonate content (Collins, 1925; Young, 1973; Eggertson, 1975; Bernstien and Young, 1990). Deposition of the sediments in the Siltstone Member is similarly suggested to have been through turbidity currents or storm-derived currents (Young, 1973; Bernstien and Young, 1990). The upper Heterolithic and Dolostone Members are generally accepted to represent a higher energy environment due the presence of features that indicate tidal and storm processes (Bernstien and Young, 1990). Previously, the Heterolithic Member was referred to as the Sandstone

Member, and was suggested to represent facies deposited by a distal meandering river, but more recent investigations have favoured a tide- and storm-dominated nearshore environment (Card, 1969; Young, 1973; Bernstien and Young, 1990). Cross-bedding, ripple lamination, scoured surfaces, and heterolithic lamination amongst other features that have been recognized from the Heterolithic Member have all been used to identify the environment as being similar to other ancient shallow-marine sequences (Robertson, 1964; Eggertson, 1975; Anderton, 1976; Johnson, 1978; Walker, 1984; Bernstien and Young, 1990).

Many studies of the depositional environment of the Espanola Formation have been limited to only certain areas of exposure, such as the central north shore of Lake Huron, or the Elliot Lake area (e.g. Bernstien and Young, 1990; Al-Hashim, 2016). This approach, while providing excellent detail of facies in specific locations, does not fully allow for interpretations of lateral variability. Throughout this study, two main geographical areas were studied; the Sault-Ste. Marie-Elliot Lake and Espanola-Sudbury areas. General observations of these two regions leads to the conclusion that the lower laminated carbonate and siltstone lithofacies association is the most laterally extensive and ubiquitous lithofacies throughout the depositional basin. The overlying siliciclastic-dominated lithofacies associations are more sporadic and variable in their presence, and some lithofacies may be absent in one area or another.

7.1 LITHOFACIES ASSOCIATION 1: DISTAL/OFFSHORE SHELF

The laminated carbonate and siltstone lithofacies association in this study is largely equivalent to the Limestone or Bruce Limestone Members that have been interpreted in other studies. This lithofacies association is dominated by parallel laminated white-weathering carbonate layers with less abundant grey-green siltstone layers. Accessory lithologies include chert or claystone interlayered with the carbonate. The lower stratigraphy of the Espanola Formation is dominated in the Sault Ste. Marie-Elliot Lake and Espanola-Sudbury areas by the interlaminated carbonate and siltstone facies with secondary contributions by the massive carbonate, and carbonate slump breccia facies. This lithofacies association is underlain by the 1-3m thick, very fine-grained sandstone to siltstone layer that is aerially extensive throughout the Formation and was described in the Bruce Formation discussion and interpreted to represent a suspension deposit akin to loess. If the siltstone unit that marks the contact of the Bruce diamictite from the overlying carbonate-bearing deposits of the Espanola Formation is accepted to be rain-out of fine sediments in a body of water, then this suggests that the overlying interlaminated carbonate and siltstone member was deposited in a similar or transitional environment. Several pieces of evidence from the lower stratigraphy strongly support this conclusion including; the laterally continuity and extent of the laminated carbonate and siltstone lithofacies association, the predominance of parallel lamination, and the prevalent soft sedimentary deformation in the form of contortion and loading of laminae. All of these features, along with the contact with the underlying siltstone lithofacies, suggests that deposition of the interlaminated carbonate and siltstone lithofacies association took place in a distal/offshore shelf environment with apparent abundant soft-sediment deformation.

The strongest evidence of a quiet-water environment dominated by suspension rain-out is the overall lack of any features suggesting influence of traction currents or erosional features upon the lower portion of the stratigraphic sequence (cf. Allen, 1982; Buatois and Mangano, 1994; Talling et al., 2012; Clerc et al., 2013; Bussert, 2014). This observation holds true for the majority of outcrops observed in both the northern and southern study areas. The ubiquity of parallel lamination (albeit, in various states of contortion) indicates that the most common process involved in their deposition was suspension settling (cf. Orton and Reading, 1993). Given that the source of the siliciclastic sediment in the laminae and layers would be terrestrial and probably transported during higher energy events, the carbonate fraction is more likely to represent the background sedimentation, through precipitation from the water mass. This hypothesis is supported by petrographic findings that preserve evidence of carbonate grains deforming a silt-rich layer below them in a manner that suggests the carbonate settled out from suspension (Figure 40D). The lower contact of the same laminae is more gradational and transitions from carbonate to silt-sized siliciclastics. These contacts may represent the settling out of individual buoyant plumes carrying siliciclastics sourced from fluvial input. Silt may also be delivered as wind-blown loess and be deposited through rainout. The thicker silt layers may represent major wind-storm events while the minor silt fraction mixed in with the carbonate layers would be deposited during normal wind conditions. This interpretation is attractive because it fits well with the interpretation of the underlying siltstone unit being wind-blown loess. It seems unlikely that the transportation of loess would abruptly discontinue in an offshore marine shelf environment, and this would suggest that the interlaminated carbonate

and siltstone lithofacies association is a result of the ongoing processes of carbonate precipitation and aeolian transportation.

Contortion of the interlaminated carbonate and siltstone facies is variable and gradually transitions in laterally extensive beds from parallel lamination, to contorted laminae, and back into parallel laminated facies. The prevalence of contortion and slumping in the laminated carbonate and siltstone lithofacies suggests that mechanisms of soft-sediment failure and mass movement were common. All of these features suggest deposition in an environment that was unstable (Bussert, 2014). This may have been the result of a combination of topographic relief produced during deglaciation, fluctuating sedimentation rates, and instability caused by isostatic adjustments following retreat of the Bruce ice sheet.

The second most common lithofacies that is observed with the interlaminated carbonate and siltstone lithofacies is the massive carbonate lithofacies. This lithofacies occurs periodically and is abundant within the stratigraphy in the Elliot Lake and the Bruce Mines area. Massive carbonate units have sharp upper and lower contacts, are laterally extensive, and irregularly punctuate the interlaminated carbonate and siltstone facies with which it is associated. Rarely, mm-thick parallel to wispy mud or silt laminae may occur within massive carbonate beds. Given the interpretation of the siliciclastics being terrestrially-sourced sediments and the carbonate fraction representing precipitates from the water mass, these units could either represent periods of low siliciclastic input, or periods of rapid carbonate precipitation.

It is important to note that other studies of the Espanola Formation stratigraphy have interpreted the Limestone Member to represent deposits of a shallow-water environment (LaFontaine, 2012; Al-Hashim, 2016). These interpretations are based on sedimentological evidence from the Ten Mile Lake area and the areas east and north of Elliot Lake, where the presence of flat-pebble conglomerates, cross-stratification, and ripple lamination indicate storm and/or wave influence upon the sediments. The interbedding of these structures with the ubiquitous parallel lamination of the laminated carbonate and siltstone lithofacies association suggests that the northcentral-most exposures of the Espanola Formation in the areas north of Elliot Lake may have been deposited closer to the shoreline of the depositional basin and may represent lateral equivalents of the deeper shelf sediments.

7.2 LITHOFACIES ASSOCIATION 2: SLUMP BRECCIA

The slump breccia preserved in drill hole E150-2 consists of a lithofacies of silt- and micrite-sized carbonate and siliciclastics and a fine- to medium-grained sandstone fraction that has abundant subround to round quartz grains throughout. The presence of the slump breccia facies that is associated with the interlaminated carbonate and siltstone lithofacies association is indicative of an unstable slope. In thin section the siliciclastic matrix component of the carbonate breccia consists of silty-clay, and distinctly coarser and more poorly sorted fine-grained sand. The presence of the finer mud deposits with the coarser, sand-sized sediments may have allowed for greater slope instability and contributed to conditions favourable for mass movement. Furthermore, the inconsistency of the fine- to medium-grained sand fraction

within and associated with the finer-grained units is anomalous. Its derivation from a shallower shelf environment to a deeper environment through gravity-driven processes would account for this anomaly. In prodelta slope environments, such as that of the modern day Mississippi Delta, mass movement is a common process and results in abundant resedimentation of coarser material from the delta front in the distal offshore (Coleman, 1981). Following the deposition of the carbonate slump lithofacies association, quiet water conditions returned with deposition of finely parallel laminated carbonate and silt. One other valuable piece of information that can be garnered from the carbonate slump unit is that the carbonate remained cohesive during transportation, indicating that the carbonate units were cemented early in the depositional timeline.

7.3 LITHOFACIES ASSOCIATION 3: HARDGROUND?

The silicified carbonate lithofacies association is a localized lithofacies that outcrops in the Quirke Lake area and is also present in drill core. This unit is sharp sided, typically occurs in the lower middle stratigraphy and is bounded by siliciclastic-dominated units. One possible explanation for the silicified carbonate horizon is through a period of low sedimentation. If there was a break in the deposition of siliciclastics and only carbonate was being precipitated at very slow rates, then perhaps early silicification of this horizon may have occurred. Fluctuations in the water mass may have resulted in a period of slow precipitation of carbonate, with intermittent silicification, causing the quartz to surround and replace carbonate grains. This unit may represent some sort of quasi-hardground, which are surfaces formed by early marine

cementation during periods of low sedimentation (Shinn, 1969; Purser, 1969; Kennedy and Garrison, 1975; Schlager and James, 1978; Bromley and Allouc, 1992; Savrda, 1995; Obrochta et al., 2003; Roberts and Boyd, 2004; McLaughlin et al., 2008; Christ et al., 2015).

7.4 LITHOFACIES ASSOCATION 4: PRODELTA

A common lithofacies association in the middle to upper middle stratigraphy of the Espanola Formation in the Elliot Lake area is the graded and interbedded siltstone and sandstone. This lithofacies association contains continuous interbedding of graded beds, massive beds, and parallel laminated siltstone and sandstone. It is predominately located directly above the interlaminated carbonate and siltstone lithofacies association with a sharp to gradational contact, and near the contact is similar in appearance with the underlying facies with the exception of an overall loss in carbonate layers and laminae and a shift to a siliciclastics-dominated facies. The graded and interbedded sandstone and siltstone lithofacies association most likely represents a prodelta environment. The predominance of siliciclastics over carbonates in the graded and interbedded siltstone and sandstone lithofacies association in comparison to the underlying interlaminated carbonate and siltstone lithofacies association suggests that clastic input increased, perhaps due to the transition from an outer shelf to prodelta environment.

The two most common facies types, parallel laminated sediments and graded beds, are interpreted to represent deposits formed by the two major processes operating in these environments; background sedimentation via suspension settling and gravity-driven mass flow

deposition. Parallel lamination is the result of variable input of suspension-settled sediments that are sourced from rivers. This material is carried in buoyant plumes before being deposited distally away from the source (Orton and Reading, 1993). Graded beds, which are very common throughout the lithofacies association and can occur in stacked successions of units ~1-3cm thick, are interpreted to be deposits generated by sediment gravity flows (Young, 1973, Bernstien and Young, 1990). These are sediment-laden traction currents that are sharp based, as is the case with those present in the Espanola Formation. Furthermore, the bases of these units are often irregular boundaries, emphasizing their erosive nature and indicating that the currents were in contact with the bottom as opposed to rainout of sediment from plumes.

Another common feature throughout the graded and interbedded siltstone and sandstone lithofacies association are massive units or units that have wispy and highly contorted lamination. Faulting of beds and laminae is also present. These features are all suggested to represent products of slumping and mass movement. Processes of deformation and mass movement through soft-sediment failure are very common in prodelta environments and sometimes sediments within the prodelta environment are dominated by material that was deposited on the delta front and relocated through mass movement processes (Coleman et al., 1983; Lindsay et al., 1984; Coleman, 1988).

7.5 LITHOFACIES ASSOCIATION 5 AND 6: WAVE- AND STORM-INFLUENCED SUBTIDAL TO INTERTIDAL ENVIORNMENT

The interbedded siltstone lithofacies association of the middle to upper Espanola Formation dominates this portion of the stratigraphy in the Elliot Lake area and Espanola area. This lithofacies association is interbedded with the ferruginous carbonate interbed lithofacies association and broadly speaking, these two lithofacies associations together constitute what is referred to in previous studies as the Dolostone Member, which is generally accepted to have been deposited in a nearshore environment (Young, 1973; Eggertson, 1975; LaFontaine, 2012). Furthermore, a great deal of sedimentary features throughout this unit suggest that periodic subaerial exposure occurred, that the environment was rapidly changing between high and low energy conditions, and that storm and wave activity was ongoing. Evidence for these processes is abundant in the form of ripple lamination, hummocky cross-stratification, upper flow regime parallel lamination, rain-out parallel lamination, and desiccation features. The entirety of the lithofacies association often alternates between layers of variably carbonate-rich siltstones and sandstones, silty carbonates, and mudstone.

Ripple lamination within the interbedded siltstone lithofacies association is typically symmetrical, with lesser asymmetrical ripples. Both types of ripple lamination can be developed in fine-grained sandstone, siltstone, or carbonate-rich siltstone, and are associated predominantly with parallel lamination and hummocky cross-stratification. The presence of these types of lamination within close stratigraphic proximity with one another suggests that the depositional environment was largely subtidal. The presence of both symmetrical and asymmetrical ripple lamination, as well as hummocky cross-stratification and parallel

lamination suggest that the environment was transitional to shoreface and upper shoreface. Within the shoreface environment, symmetrical ripples will form in the deeper, lower shoreface, while asymmetrical ripples will form in the shoaling wave zone of the upper shoreface environment (Clifton, 1976; Komar, 1976; Bourgeois and Leithold, 1984). Hummocky cross-stratified units and parallel laminated units formed through rainout are more commonly present within the adjacent offshore-transition zone, where storm-generated hummocky cross-stratified units punctuate parallel laminated fair-weather sediments (Komar, 1976; Bourgeois and Leithold, 1984).

The presence of desiccation cracks in siltstone and carbonate-rich siltstone units within the interbedded siltstone lithofacies association has been observed in the Quirke Lake area both in cross section and on the surface of a bedding plane. These features display a typical v-shaped cross-sectional morphology, with cracks being infilled with material from the overlying sediment. On bedding surfaces the desiccation cracks are arranged in a typical polygonal pattern. Desiccation cracks in the Quirke Lake area indicate that the interbedded siltstone lithofacies was also transitional into an intertidal zone. Another feature that is commonly used along with desiccation features to identify the intertidal zone is fenestrae, or infilled pore spaces commonly developed by degradation and degassing of microbialite. Fenestrae have been identified in the Elliot Lake and surrounding areas within the upper Espanola Formation in previous studies, which supports the argument that the upper facies were partially deposited in an intertidal environment in the northern and central parts of the depositional basin (Bekker et al., 2005; Al-Hashim, 2016).

The ferruginous carbonate interbedded lithofacies association is dominated by ripple, parallel, and hummocky cross-laminated carbonate units as well as abundant intraformational conglomerates. Silty layers and laminae are also present in fairly high abundance in some beds and are typically 0.5-1cm thick and parallel to rarely ripple laminated. Ferruginous carbonate interbeds always have sharp contacts with adjacent lithofacies, and they are found interbedded predominantly with the interbedded siltstone lithofacies association. The ferruginous carbonate lithofacies association is present throughout the Elliot Lake area and central northern exposures and was also observed as far south as the Loon Lake area immediately south of Espanola. The presence of abundant hummocky cross-lamination and intraformational conglomerates in this lithofacies can be used as diagnostic features to suggest that the depositional environment of the ferruginous carbonate interbeds is likely a shoreface to offshore transitional zone. Firstly, hummocky cross-stratification is well-known to be a structure that is diagnostic of storm influence in the zone between fair weather and storm wave base (Leckie and Walker, 1982; Plint, 2010; Bayet-Goll et al., 2014). These environments are characterised by alternating high and low energy conditions, which in this instance is observed as hummocky cross-stratified beds and rain-out parallel laminated beds, respectively (Komar, 1976; Bourgeois and Leithold, 1984). The dominance of hummocky cross-stratification within ferruginous carbonate interbeds associated with parallel and ripple laminated siltstone and micritic carbonate suggests that the primary depositional process was low energy deposition from suspension during fair-weather conditions. Periodic storm events resulted in the deposition of higher-energy hummocky cross-stratified units interbedded with the parallel laminated units. Wave ripple lamination commonly occurs in lateral and stratigraphic association with both hummocky cross-

stratification and upper flow regime parallel lamination and likely represents deposition in the adjacent lower shoreface. In particular, wave ripples overlying hummocky cross-stratification is likely the result of reworking of the tops of the beds as the geostrophic flow dies out. In the lower shoreface zone, fair-weather waves begin to make contact with the bottom, resulting in the formation of symmetrical ripples that pass landward into asymmetrical ripples (Komar, 1976; Bourgeois and Leithold, 1984).

Some intraformational conglomerate units are similar in appearance and are suggested to be akin to flat-pebble conglomerates because of the elongated and rounded to sub-rounded nature of the micritic clasts. Flat-pebble conglomerate beds in ancient sequences, like the ones observed in the ferruginous carbonate interbedded lithofacies association, are interpreted to have been largely deposited below fair weather wave base in the subtidal environment (Kazmierczak and Goldring, 1978; Markello and Read, 1982; Sepkoski, 1982; Demicco, 1983; Wilson, 1985; Grotzinger, 1986; Lee and Kim, 1992; Mount and Kidder, 1993). The flat-pebble conglomerates present within the Espanola Formation are similar in appearance to carbonate flat-pebble conglomerates described from the Snowy Range Formation in Wyoming and Montana, which have been associated with shallow water strata with facies that are similar to those observed in the Espanola Formation (Myrow et al., 2004). In the Snowy Range Formation, several processes are interpreted to have created flat-pebble conglomerate beds, including mass movement of laminated shoreface-derived carbonates and storm and/or wave reworking and winnowing in beach and shoreface environments. These variations in origin explains the diversity of individual flat-pebble conglomerates in terms of thickness, orientation of clasts, clast content, and associated facies (Myrow et al., 2004). Given the common association of

hummocky cross-stratification, parallel lamination, and ripple lamination with flat-pebble conglomerates in the upper Espanola Formation, the majority of the units may have been deposited from the shoreface to the transitional-offshore zone through failure and downslope resedimentation.

7.6 LITHOFACIES ASSOCIATION 7: FLUVIODELTAIC SANDSTONES

The locally distributed cross-stratified and parallel laminated sandstone lithofacies association was best observed in this study along the north shore of Lake Huron in the Iroquois Bay and Moose Point areas. This lithofacies association is distinct from the remainder of the Espanola Formation because of the overall coarser grainsize (medium-grained sandstone), low carbonate content, and abundance of trough cross-stratification. Cross-stratified units are most commonly associated with parallel laminated and massive sandstones. This lithofacies association, along with the transitional cross-stratified sandstones with calcareous interbeds lithofacies association, which will be discussed with the Serpent Formation sedimentology, constitutes the gradational contact between the underlying Espanola Formation and overlying Serpent Formation. The division between these two lithofacies associations is based on the greater abundance of medium-scale, trough and planar cross-stratified sandstones and the greater thickness of continuous rain-out parallel layered units within the cross-stratified and parallel laminated lithofacies association. These features suggest a stronger fluvial influence in these sections of stratigraphy and indicate that the predominant environment of deposition for these facies was fluviodeltaic. Sets of more well-sorted, cross-bedded sandstones represent

distributary channels and/or distributary mouth bars while parallel layered successions represent interdistributary areas. Distributary channels within the delta plain environment are similar to typical alluvial channels, of which cross-bedded sandstones are the most abundant facies (Ramos et al., 1986). Parallel laminated sections, which typically separate sets of cross-bedded sandstones are interpreted to represent overbank or interdistributary deposits. More well-sorted and coarser-grained sandstone beds that typically have a lenticular form and are found associated with both cross-stratified and parallel laminated sediments likely represent higher-energy flood deposits.

These interpretations are supported by previous studies of the sandstone/heterolithic members of the Espanola Formation, of which the cross-stratified and parallel laminated sandstone lithofacies association constitutes a part (Young, 1973; Bernstien and Young, 1990). These sediments were first interpreted to represent a probable distal fluvial environment, which was then re-examined and suggested to have been formed under more wave-, tide-, and storm-influence in the nearshore environment (Young, 1973; Bernstien and Young, 1990). This re-evaluation is broadly valid because of the presence of heterolithic sand-mud facies and mudstone units that represent fluctuating energy conditions under tidal influence in a shallow marine or tidally-influenced braid channel environment (Anderton 1976; Johnson 1978; Weimer et al., 1982; Walker 1984). However, certain sections of stratigraphy are lacking in these features, and thus, by dividing up the heterolithic/sandstone Member into two lithofacies associations, the division can be made between predominantly fluvial processes and predominantly wave/tidal processes in the nearshore-marine environment.

7.7 LITHOFACIES ASSOCIATION 8: INTRUSIVE BRECCIAS

The Espanola Formation stratigraphy contains abundant post depositional injection structures, particularly in the Quirke Lake area and in the drill core, which have been observed in other studies and have been well documented (Eisbacher, 1970; Eggertson, 1975; Young, 1972; Young, 1981). Both intrusive breccias and clastic dykes are features that are common within the Espanola Formation and are present within both the dolostone and siltstone members (Young, 1972). In this study intrusive breccias were observed in the Quirke Lake area, Ten Mile Lake area and in the drill core. Clastic dykes which cross-cut the stratigraphy of the Espanola Formation were most commonly observed along the north shore of Lake Huron, but were also sporadically encountered further to the northeast and in the drill core as well. The clastic dykes, also referred to as discordant sandstone masses, have been suggested to have been formed as a result of a downward injection of sediments, which was caused by sub-permafrost instabilities and channeled by normal faults (Eisbacher, 1970). Another interpretation states that the dykes formed via upward injections from the Bruce Formation that were possibly due to high pore water pressures as a result of loading (Young, 1972). The presence of lithologies in breccias and dykes sourced from stratigraphy that can either overlie or underlie them, suggests that lithology cannot be used to determine where they came from. What can be confirmed about the source of the breccias and dykes, is that they likely represent evidence for short-lived and severe mass movements (Eggertson, 1975). Whatever the driving mechanism was for their emplacement, their ubiquity and the abundance of evidence for slumping in the Espanola Formation, confirms that mass movement had a large contribution to the stratigraphy.

8 ESPANOLA FORMATION – GEOCHEMISTRY

Geochemical analysis on the Espanola Formation has been receiving greater interest recently in light of suggestions that it may represent a Paleoproterozoic cap carbonate deposit (Bekker et al., 2001, 2005; Hoffman, 2013). This hypothesis is based most strongly upon its stratigraphic setting atop a glacial diamictite, a characteristic negative $\delta^{13}C$ signature, and its direct association with a significant increase in atmospheric oxygen through correlation with timing of the disappearance of the MIF-S signal (Bekker et al., 2005; Hoffman, 2013). There are however, some differences between the Espanola Formation and the Neoproterozoic cap carbonates, including that there is a high amount of siliciclastics within the Espanola Formation and that only the upper part is dolomitic (Young, 2013b). In comparison, the later Neoproterozoic cap carbonates are dominantly dolomitic and believed to have been deposited rapidly during glacial retreat and before deposition of siliciclastics (Hoffman et al., 1998; Hoffman, 2011; Young, 2013b). There are also specific sedimentary structures such as giant wave ripples and sheet cracks that are observed in Neoproterozoic deposits but are absent within the Espanola Formation stratigraphy (Corsetti and Kaufman, 2003; Bekker et al., 2005). Furthermore, the Espanola Formation cap carbonate, being the only cap carbonate preserved within the three glacial cycles of the Huronian Supergroup, is at odds with the ubiquity and uniformity of the Neoproterozoic cap carbonates (Young, 2013b, 2014). Thus, the origins of the Espanola Formation are enigmatic due to some strong similarities between it and the Neoproterozoic cap carbonates, including carbon isotopic compositions and stratigraphic setting, but the differences between the two are also cause for debate regarding how similar they are in terms of their genetic origins. Through geochemical and isotopic analysis of the

carbonate fraction in the Espanola Formation, this study hopes to build upon previously collected data and observations to further evaluate and investigate the similarities and differences between the Espanola Formation cap carbonate and the later Neoproterozoic cap carbonates.

8.1 MINERALOGY OF THE CARBONATE FRACTION

Previous examinations of the carbonate fraction of the Espanola Formation have disclosed that content of carbonate minerals ranges from 10-30% on average (Card et al., 1977). The composition of the carbonate fraction is variable, with most units containing predominantly calcite, but dolomite being dominant in some facies (Young, 1973; Card et al., 1977). In this study, samples collected from the Espanola Formation that were analyzed using the partial digestion method show that the carbonate fraction of the Formation is dominated by calcite (Figure 64). The majority of the samples have relatively pure calcite compositions, while some show a minor amount of Fe and Mn within them. There is also a small subset of samples that range from between the compositions of calcite and dolomite and also contain variable amounts of Fe and Mn. These samples therefore contain a mixture of calcite and dolomite grains within them. Lastly, there is a cluster of samples that fall close within the range of pure dolostone, but the incorporation of some Fe and Mn pulls the samples away, in the direction of the ankerite field. These results are consistent with previously described carbonate mineral compositions of the Espanola Formation (Young, 1973; Card et al., 1977).

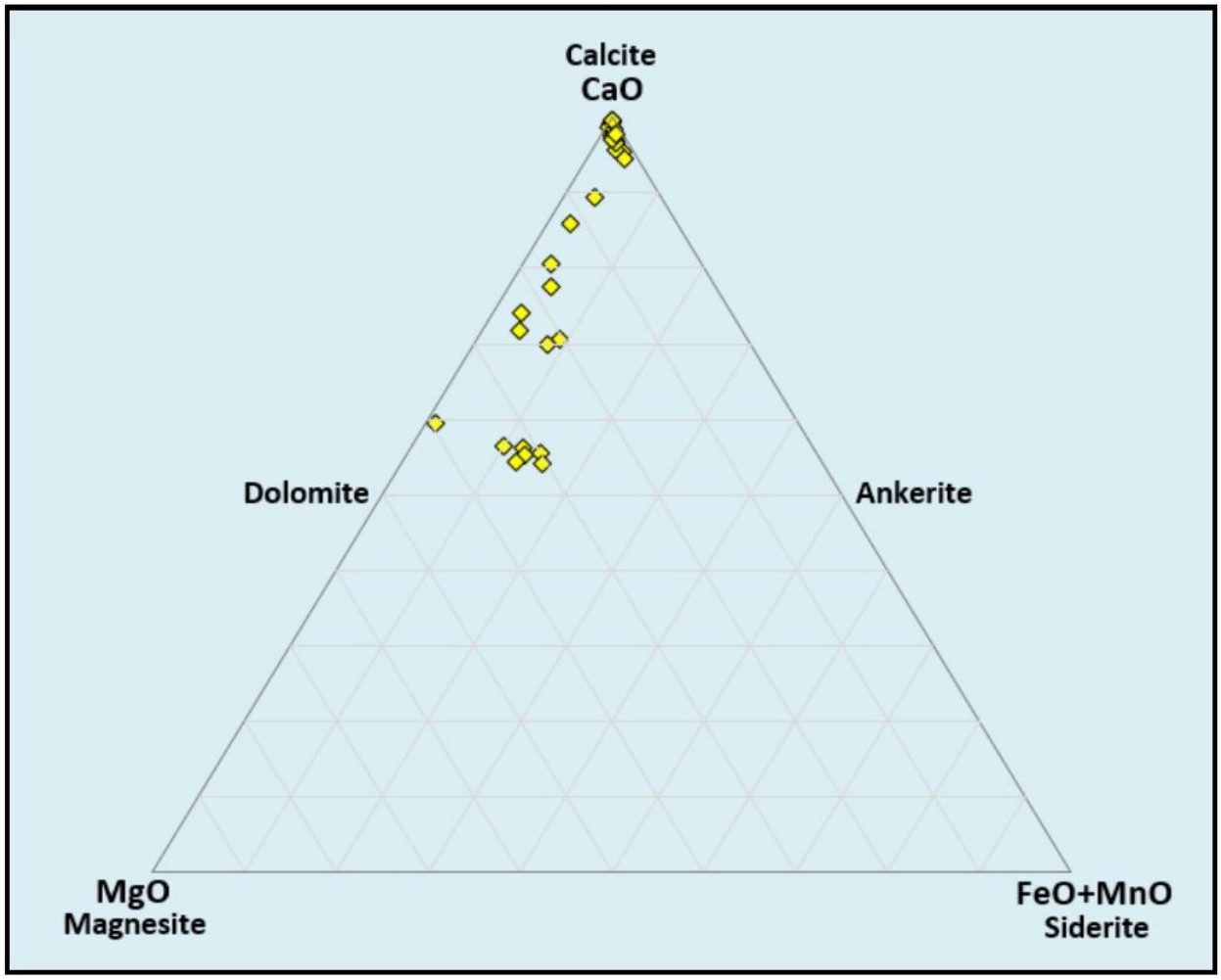

Figure 64: A composite ternary diagram (weight %) that includes all of the carbonate samples of the Espanola Formation utilized in this study.

8.2 REE PATTERNS OF THE ESPANOLA FORMATION CARBONATES

Partial digestions were completed on carbonate samples collected from the Espanola Formation in an effort to isolate the REE pattern preserved within the carbonate from the high siliciclastic component within many samples. Numerous studies have suggested that carbonates precipitated from a body of water will preserve information about the chemistry of water in which they formed (cf. references in Fralick and Riding, 2015). This information may be preserved within the REE concentrations, as these elements largely behave in a similar manner,

with some exceptions, and undergo little alteration in their relative abundances during sedimentary process (McLennan et al., 1980, 1983, 2003; McLennan, 1989). Therefore, it is the exceptional behaviour of certain elements under given conditions that allows for the analysis and interpretation of the depositional environment with regards to the chemistry of the water in which the precipitates were forming.

8.2.1 Y/Ho FRACTIONATION

Terrigenous materials have a constant chondritic Y/Ho weight ratio of ~28, but seawater values have ranged from ~44-74 in the past, suggesting that there must be a fractionation process that influences the ratio (Nagarajan et al., 2011). Thus, the ratio of Y to Ho is used in the study of carbonate minerals to interpret the degree of fractionation between these two elements within a water mass, which in turn can provide information about the environment in which the precipitates formed. Environmental interpretations based on the Y/Ho ratio of a precipitate are made possible by the behavioural differences between Y and Ho in the subaqueous setting (Kawabe et al., 1991), differences that result in an enrichment of Y compared to Ho in seawater (Nozaki et al., 1997). Several mechanisms for the fractionation of Y and Ho have been suggested, such as weathering processes and differing solution complexation and solubilities of phosphates (Bau et al., 1995; Nozaki et al., 1997). The most probable reason for the observed fractionation trends is due to a deviation in completive reactions and scavenging of Y compared to Ho and other REE (Nozaki et al., 1997). While Y and Ho have similar ionic radii, Y behaves differently from Ho in solution because of the thermochemical effects of the presence or absence of 4 f electrons (Kawabe et al., 1991; Nozaki et al., 1997).

Scavenging by particulate matter and fractionation of Y and Ho occurs predominantly in the ocean, as a study completed by Nozaki et al. (1997), indicates that fractionation occurring in estuarine systems and rivers is not sufficient to explain the seawater Y/Ho ratio. Modern seawater has an average Y/Ho weight ratio of ~54, while ancient seawater ratios have fluctuated between values of 44 to 74 (Nagarajan et al., 2011).

Espanola Formation carbonates have Y/Ho weight ratios with an average superchondritic value of ~35 (Figure 65). There is however, a large range and variability of Y/Ho ratios, with values being anywhere from ~20-50 (Figure 66). Y/Ho associated with low Y (ppm) tend to have values that cluster around 20-30, while an increase in total Y (ppm) is associated with higher and more variable Y/Ho values.

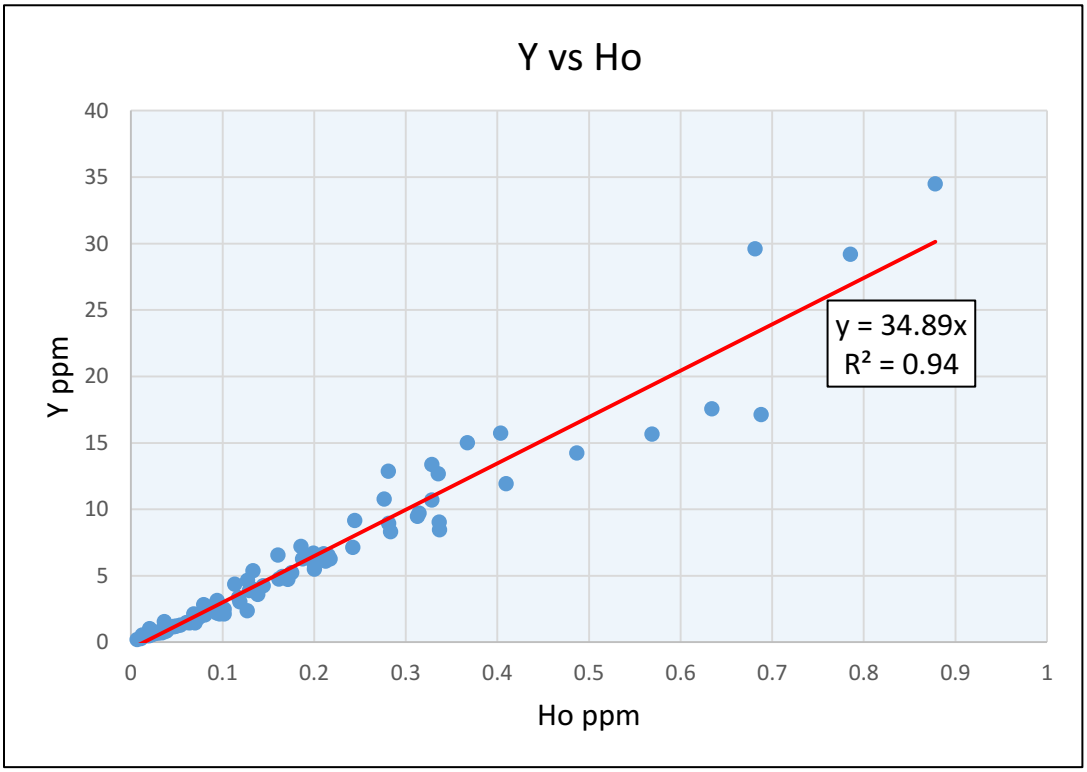

Figure 65: Plotting a trendline on a cumulative graph of all Y/Ho values produces an average ratio of ~35.

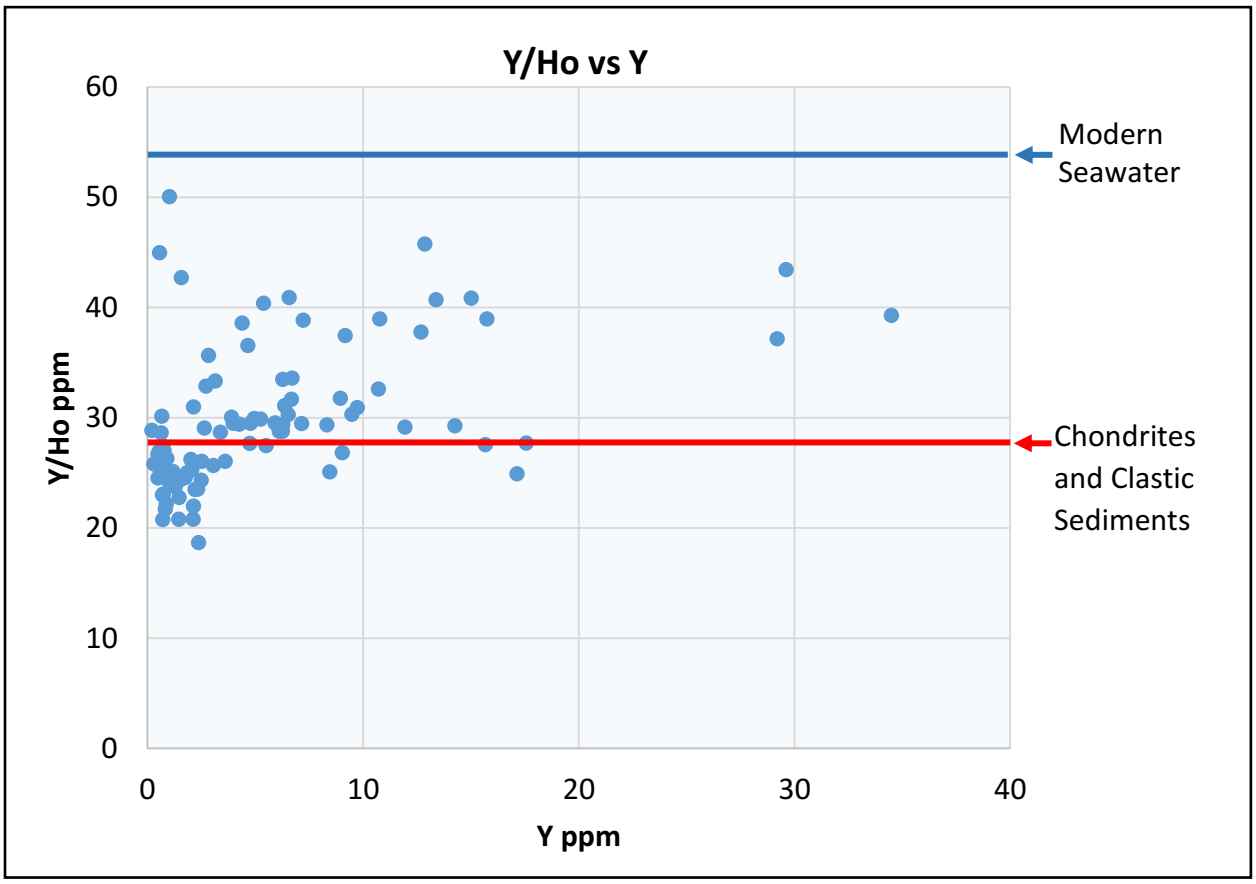

Figure 66: Y/Ho ratios of the Espanola carbonates show a wide spread in values that cluster around and below chondritic values as well as scattered between chondrite and modern seawater. It is worth noting that the samples with extremely low Y concentrations (<5 ppm) also tend to have low Y/Ho ratios, which suggests that these values may not be as accurate as samples with higher Y concentrations. Average Y/Ho of chondrite and seawater from Bau and Dulski (1994).

8.2.2 REE PATTERNS

Samples collected from the interlaminated carbonate and siltstone lithofacies association and the ferruginous carbonate interbeds lithofacies association from the Quirke Lake area show some differences in REE patterns between the two (Figure 67). The interlaminated carbonate and siltstone lithofacies association has a slight positive slope for the light REEs, while the heavy REEs have a negative slope. Furthermore, light REEs are relatively

enriched in comparison to heavy REEs. The middle REE forms the apex between the positive slope of the light REEs and the negative slope of the heavy REEs, giving the pattern a 'hat-shaped' appearance. The ferruginous carbonate interbeds lithofacies association also displays a vaguely 'hat-shaped' appearance, but the light REEs are depleted relative to the heavy REEs and the middle REEs have a more well defined apex due to the presence of a slightly positive Eu anomaly. Samples taken from white weathering carbonate units directly underlying rusty red weathering ferruginous carbonate interbeds show patterns similar in appearance to their associated unit, but also display more prominent light REE depletions.

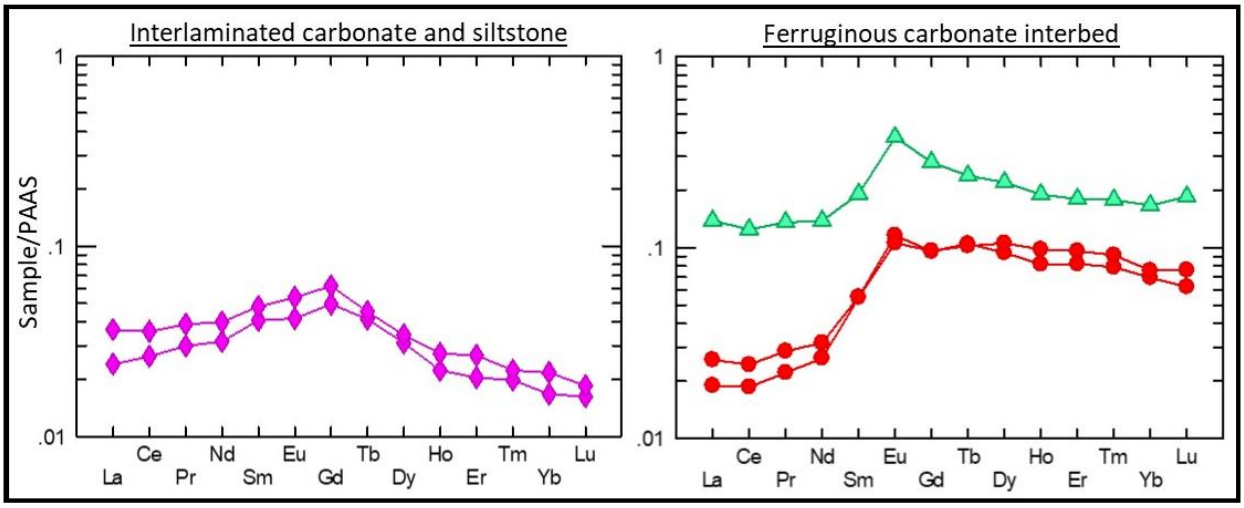

Figure 67: REE plots of samples collected from the Quirke Lake area. On the left are samples from the interlaminated carbonate and siltstone lithofacies association. On the right are samples from the ferruginuous carbonate interbed lithofacies association. The red samples are collected from a white weathering carbonate layer below a ferriginous carbonate interbed. The green sample is from a rusty red weathering ferruginous carbonate interbed.

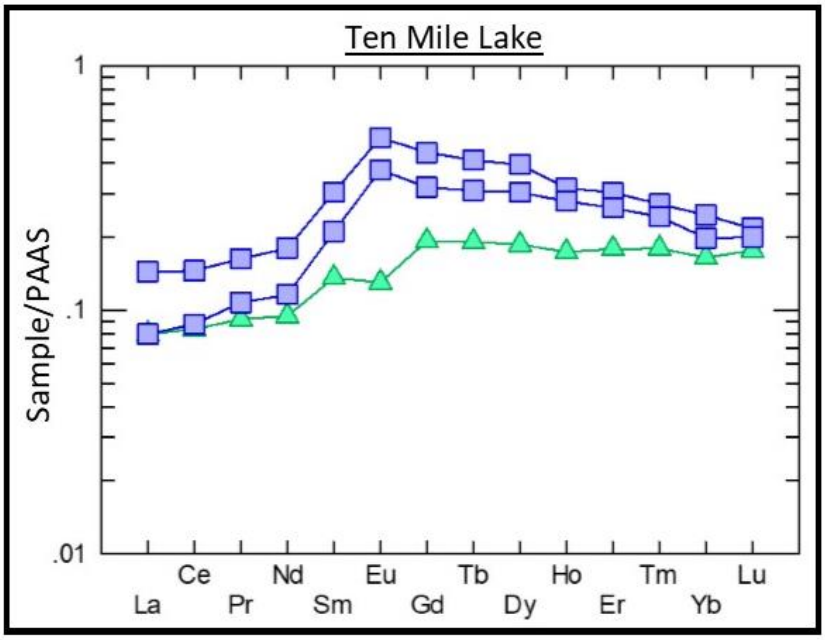

Figure 68: REE patterns of samples collected from the Ten Mile Lake area. Blue samples are from carbonates of the ferruginous carbonate interbeds lithofacies association of the Espanola Formation while the green sample is from the interlaminated carbonate and siltstone lithofacies association.

Samples collected from the Ten Mile Lake area show REE patterns typical for the upper stratigraphy of the Espanola Formation (Figure 68). The upper ferruginous carbonate interbed samples are depleted in light REE relative to the heavy REE and have a 'hat-like' appearance due to the relatively more abundant middle REE. The interlaminated carbonate and siltstone lithofacies association also has light REE depletion relative to heavy REE, but lacks the 'hat-shaped' pattern seen in the upper member. Instead, the middle REE have a positive slope and the heavy REE have a flat pattern. There is a slight negative Eu anomaly in the lower member carbonate.

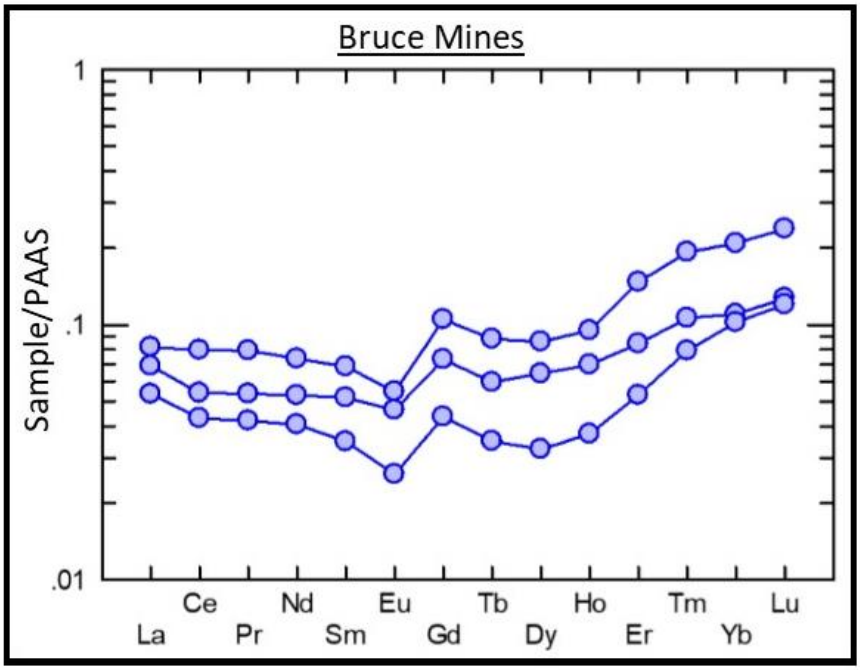

Figure 69: Samples collected from the interlaminated carbonate and siltstone lithofacies association in the Bruce Mines area.

Samples collected from the interlaminated carbonate and siltstone lithofacies association in the Bruce Mines area show REE patterns that have similar Eu depletions to the sample from the same lithofacies association in the Ten Mile Lake locale (Figure 69). The samples have fairly flat to slightly negatively sloped light REE and consistent negative Eu-anomalies that may be a continuation of the curving downward trend of the light REE. Heavy REE have a positive slope.

Samples collected from the interlaminated carbonate and siltstone lithofacies association of the Espanola Formation in drill hole 144, directly above the contact with the Bruce Formation, show a progressive change in REE patterns moving up stratigraphy, from a flat and shale-like pattern, to the 'hat-like' pattern that is common in the Espanola carbonates (Figure 70). Heavy REE is rarely enriched relative to light REE.

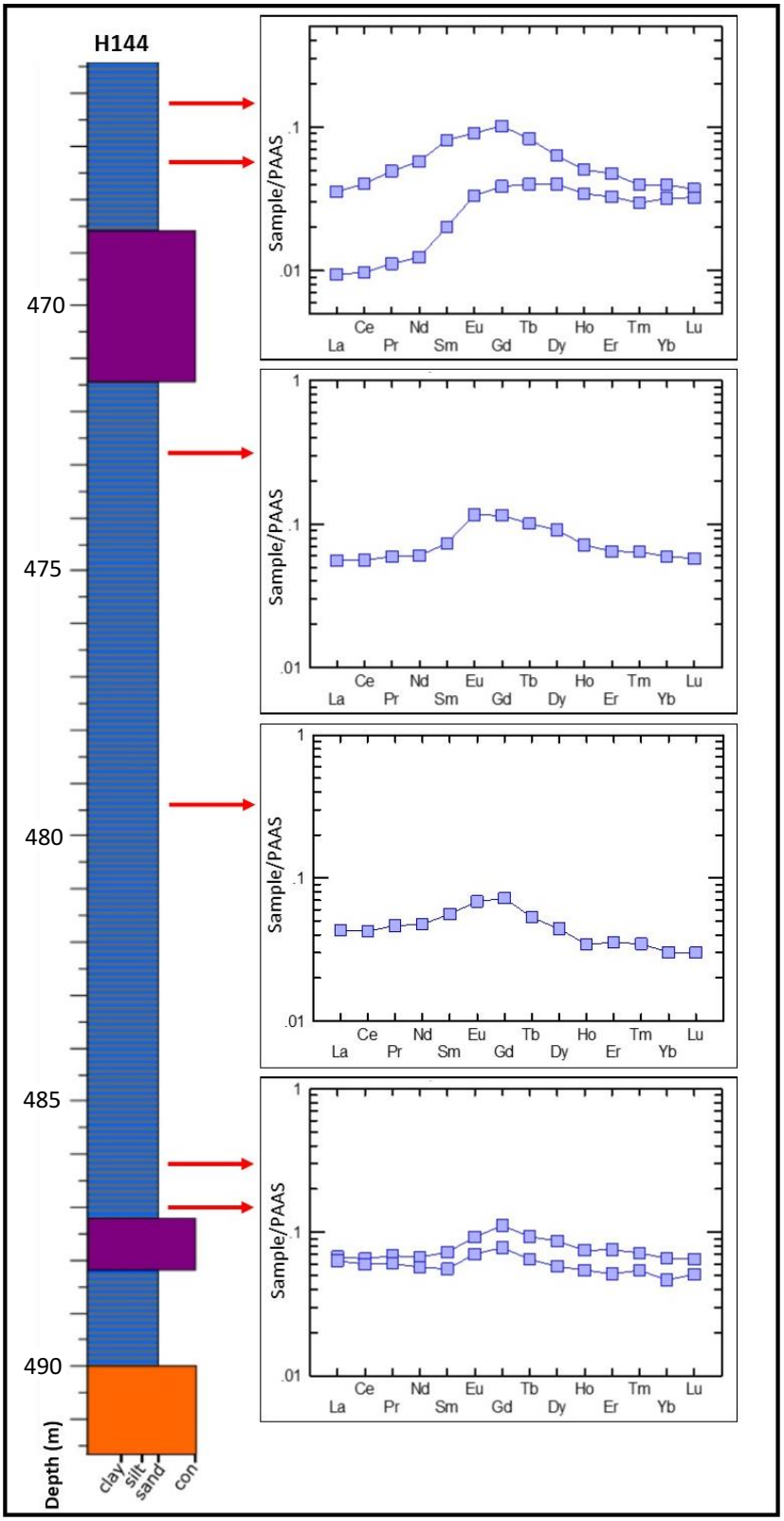

Figure 70: REE patterns of carbonate samples from the interlaminated carbonate and siltstone lithofacies association in drill hole 144-1.

8.3 STABLE ISTOPES

Along with REE analysis, $\delta^{13}C$ and $\delta^{18}O$ isotopic analysis was also completed on samples collected from the Espanola Formation carbonates. Stable isotopic studies of carbonates is a popular method used as a proxy to determine the isotopic composition of the water mass from which the precipitates formed. This is possible because isotopes will behave differently, both chemically and physically, due to their differing masses, and result in a fractionation during environmental processes (Hoefs, 2009; Walther, 2009). Thus, there will be a deviation from the typical relative isotope abundance as a result of a physical, biological, or chemical process, and the deviation from the normal isotopic composition can then be used to infer the processes which may have been active (Brownlow, 1979; Hoefs, 2009; Walther, 2009). Two of the most commonly used stable isotopes in studies of carbonate minerals, and those that were used in this study, are the carbon and oxygen isotopic systems (Anderson and Arthur, 1983; Al-Hashim, 2016). The standards used in this study, and the most ubiquitous standard used for comparison of isotopic composition of carbonates is the Vienna Pee Dee Belemnite (V-PDB); (Coplen, 2011).

Oxygen isotope fractionation between carbonate and water is dependent primarily upon temperature. A strong temperature control, coupled with the high amount of oxygen within fluids, results in oxygen being highly susceptible to being reset by meteoric or hydrothermal waters. In limestones, this results in the $\delta^{18}O$ commonly being reset, while the $\delta^{13}C$ will still retain the near original values of the precursor carbonate phase (Veizer, 2003).

The carbon cycle in the ocean is governed by input through igneous activity and the weathering of carbon-bearing rocks, and by output through formation of $CaCO_3$ or through

photosynthesis and burial of organic carbon (Bachan and Kump, 2015). Through an equilibrium between these processes, carbonate rocks have had $\delta^{13}C$ of around 0‰ PDB at least as far back as 3.5 Ga ago (Schidlowski et al., 1983; Hayes et al., 1992; Veizer, 2003; Bachan and Kump, 2015). Two periods within the Precambrian punctuate the status quo of this relatively constant 0‰ PDB signature of $\delta^{13}C$, with positive and negative excursions in the Paleoproterozoic and Neoproterozoic, respectively, and are associated with the glaciations that occurred during these times (Veizer, 2003). The anomalously negative PDB signature of $\delta^{13}C$ in the Neoproterozoic in particular, is observed within cap carbonates, which are carbonate successions directly overlying glacial sediments.

8.3.1 ESPANOLA FORMATION STABLE ISOTOPES

A cross-plot of all $\delta^{13}C_{carb}$ and $\delta^{18}O$ data shows that the majority of the Espanola Formation has $\delta^{13}C$ values that range from -4‰ to -1.5‰ (Figure 71). There is more variability in the range of $\delta^{18}O$ values, with values typically within the range of -20‰ to -13‰. There is a subset of samples that have both anomalously more negative $\delta^{13}C$ and $\delta^{18}O$ values, with $\delta^{13}C$ as low as -11‰ and $\delta^{18}O$ within the range of -20‰ to -22‰. This subset of more negative $\delta^{13}C$ and $\delta^{18}O$ values are associated with the laminated carbonate dropstone lithofacies association that occurs within the upper Bruce Formation in drill hole E150-2, directly below the contact with the Espanola Formation.

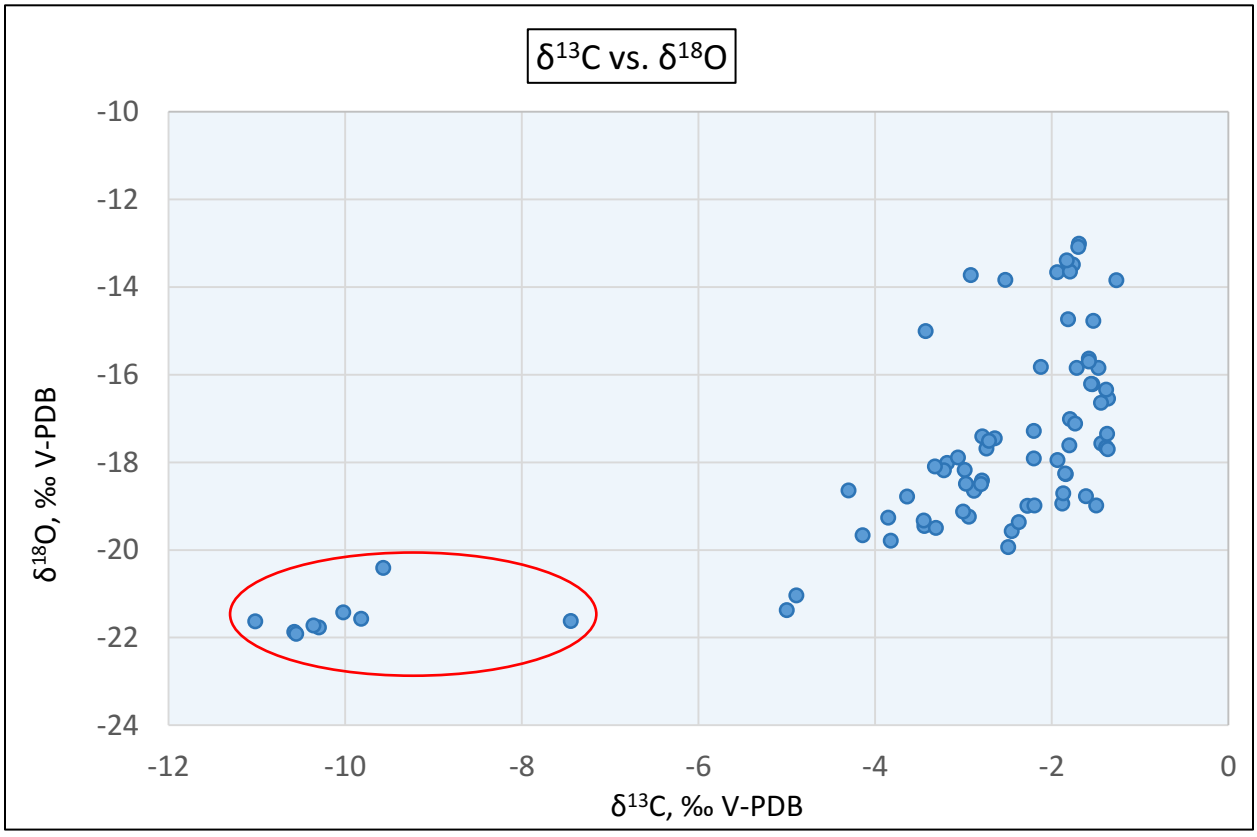

Figure 71: Cross-plot of $\delta^{13}C_{carb}$ and $\delta^{18}O$. The anomalously low $\delta^{13}C$ and $\delta^{18}O$ values that are contained within the red oval are samples from the laminated dropstone lithofacies association in drill hole E150-2.

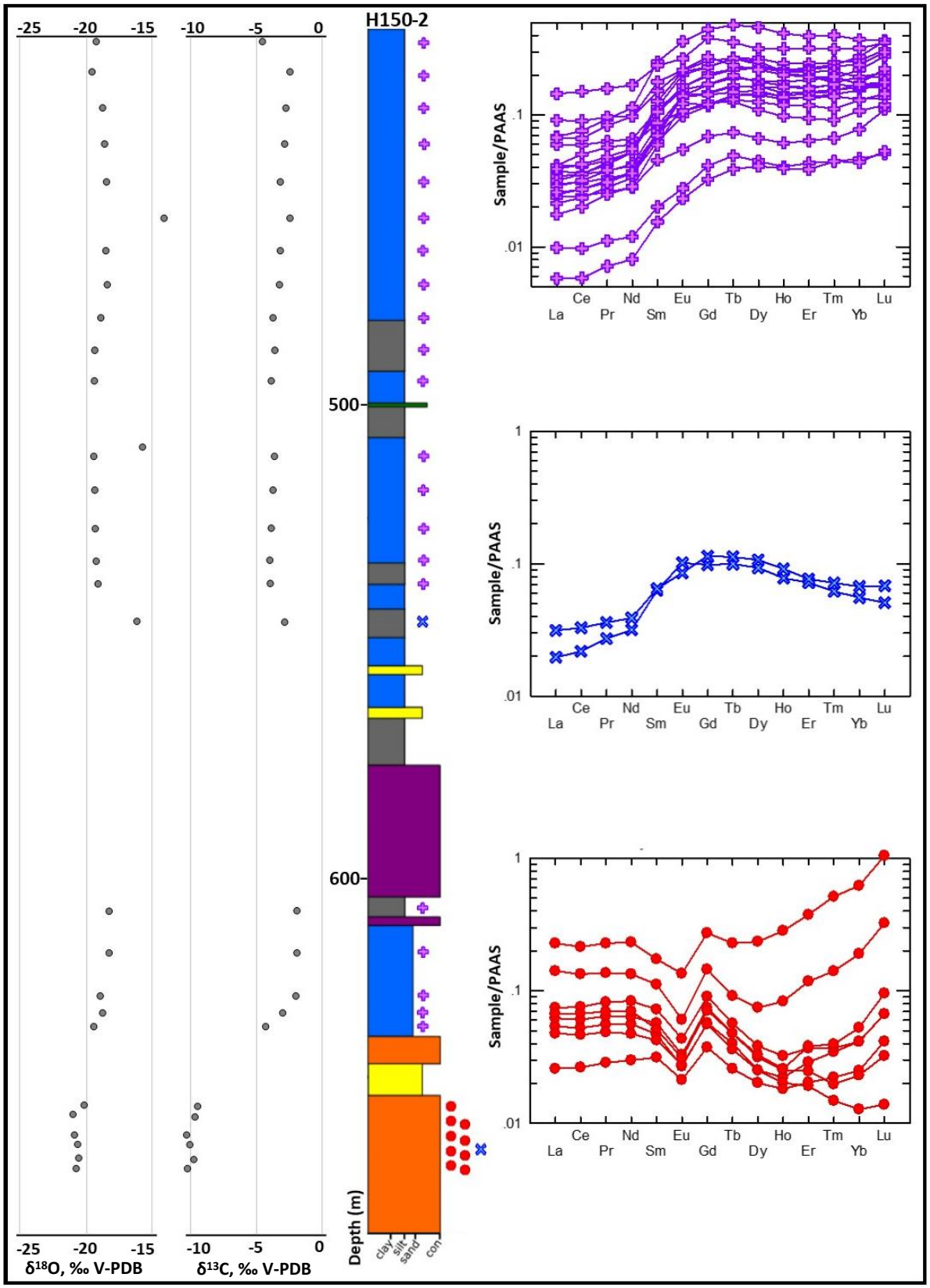

Figure 72: A simplified stratigraphic section for drill hole E150-2. $\delta^{13}C_{carb}$ and $\delta^{18}O$ isotopic data are plotted in accordance with their position on the stratigraphic column to visualize trends.

High density (~5m interval) sampling of drill hole E150-2 yielded several interesting results in terms of $\delta^{13}C_{carb}$ values and REE patterns. Firstly, this drill hole produced two important and strong patterns within the $\delta^{13}C_{carb}$ values (Figure 72). At the upper contact of the Bruce Formation, samples analysed from the laminated dropstone lithofacies association, which is unique to this location, record a highly negative signal in the $\delta^{13}C$ values. These values average at approximately -10‰ and record the most extreme negative isotopic anomaly observed from any of the Espanola Formation carbonate samples. Furthermore, these extremely negative $\delta^{13}C$ values are associated with REE patterns that are different than the remainder of the samples collected from drill hole E150-2 (Figure 72). These REE patterns are characterized by flat light REE, consistent negative Eu anomalies, and heavy REE that range from negatively to positively sloped. While not as strongly anomalously negative as the $\delta^{13}C$ values, the $\delta^{18}O$ values from the laminated dropstone lithofacies association are also more negative than the remainder of the samples, with values being in the range of ~20-21‰.

The second pattern derived from the $\delta^{13}C$ values records an upward increase in $\delta^{13}C$ values and was observed through consecutive samples from the middle and upper members. The upwards trend is a gradual and consistent increase in $\delta^{13}C$ from approximately -4‰ to -2.5‰ moving up stratigraphy (Figure 72). The associated $\delta^{18}O$ values typically fall within the range of -20‰ to -18‰ (with the exception of two outliers) but do not show a systematic upwards trend such as is observed with the $\delta^{13}C$ values. REE patterns from the upper stratigraphy have, for the most part, very consistent features. They have relatively depleted light REE and take on the 'hat-shaped' appearance that is common for samples of the middle and upper stratigraphy. Heavy REE are typically flat but may be slightly positively-sloped. Two

outlier samples, one of which is located within the laminated dropstone lithofacies association, have similar ‘hat-shaped’ REE patterns but are different in that they have slightly negatively-sloped heavy REE.

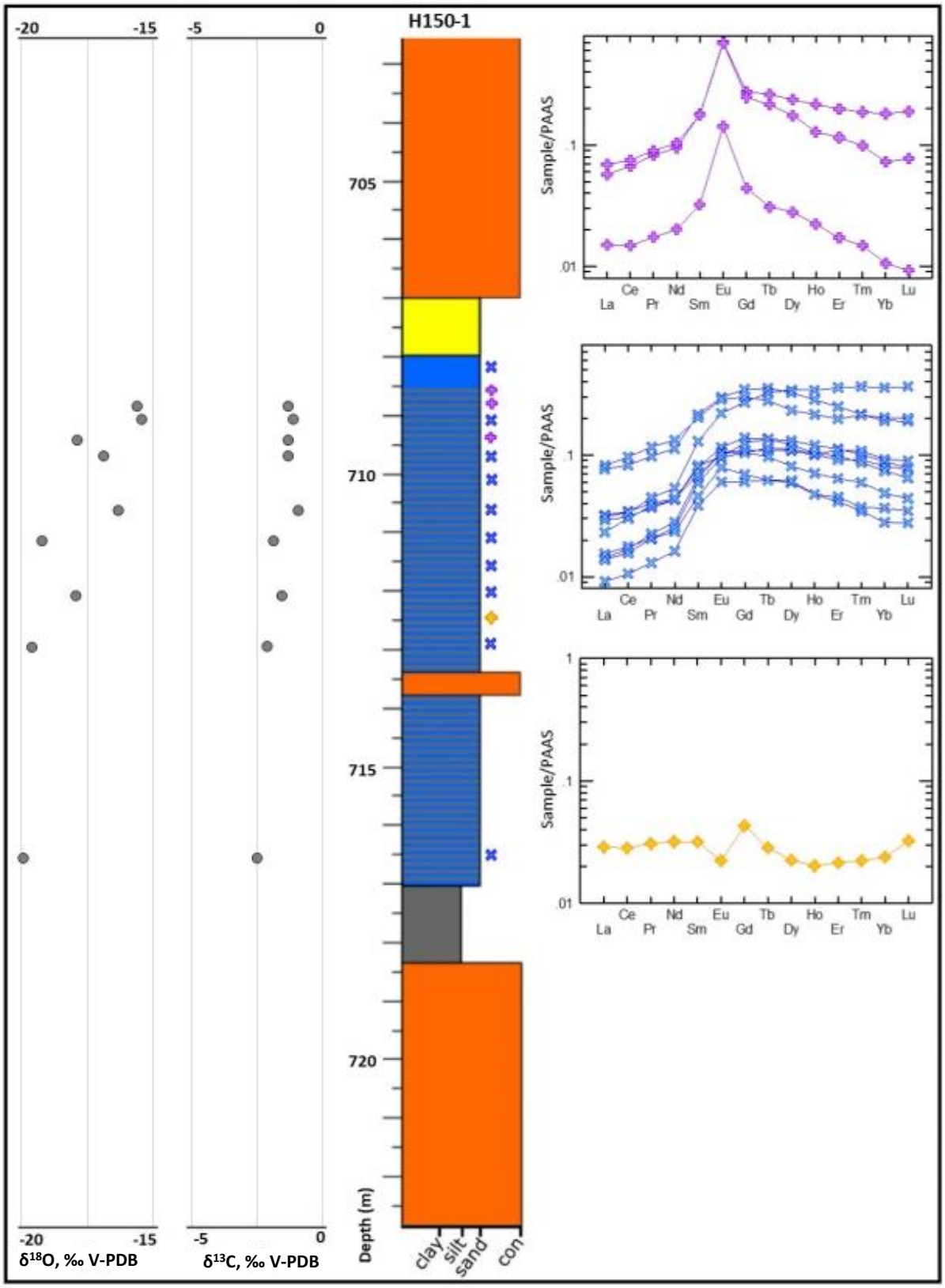

Figure 73: Isotopic data and REE patterns for the interlaminated carbonate and siltstone lithofacies association directly above the contact with the Bruce Formation in drill hole E150-1.

Systematic sampling of drill hole E150-1 near the contact with the Bruce Formation shows $\delta^{13}C_{carb}$ values ranging from approximately -5‰ to -2‰ and becoming heavier upwards within the interlaminated carbonate and siltstone lithofacies association (Figure 73). The majority of the samples show REE patterns that are similar in appearance to those of the upper and middle stratigraphy in both drill holes E150-2 and 144-1. These samples have a 'hat-shaped' appearance with depleted light REE, middle REE enrichment, and a flat to negatively-sloped heavy REE pattern. One outlier sample displays a REE pattern that is similar to the unique pattern observed in the laminated dropstone lithofacies association of drill hole E150-2. This pattern is distinct for its flat light REE and negative Eu-anomaly. There is a small subset of data points between 708.5m and 709.5m depth that have different REE patterns from any other samples collected from the Espanola Formation. These samples have uniquely strong positive Eu-anomalies, even relative to the positive anomalies observed in some of the samples from the ferruginous carbonate interbeds in the Ten Mile Lake and Quirke Lake areas. The patterns also have positively-sloped light REE and moderate negatively-sloped heavy REE. What is particularly interesting about these anomalous REE patterns is that this ~1m thick horizon occurs in the same stratigraphic position and is found in the same samples and adjacent samples as a Ba-enriched horizon (Figure 74). The association of the high Ba horizon and the REE patterns with strongly positive Eu-anomalies suggests that there is a connection between the two (Figure 75).

8.4 BA-ENRICHMENT – DRILL HOLE E150-1

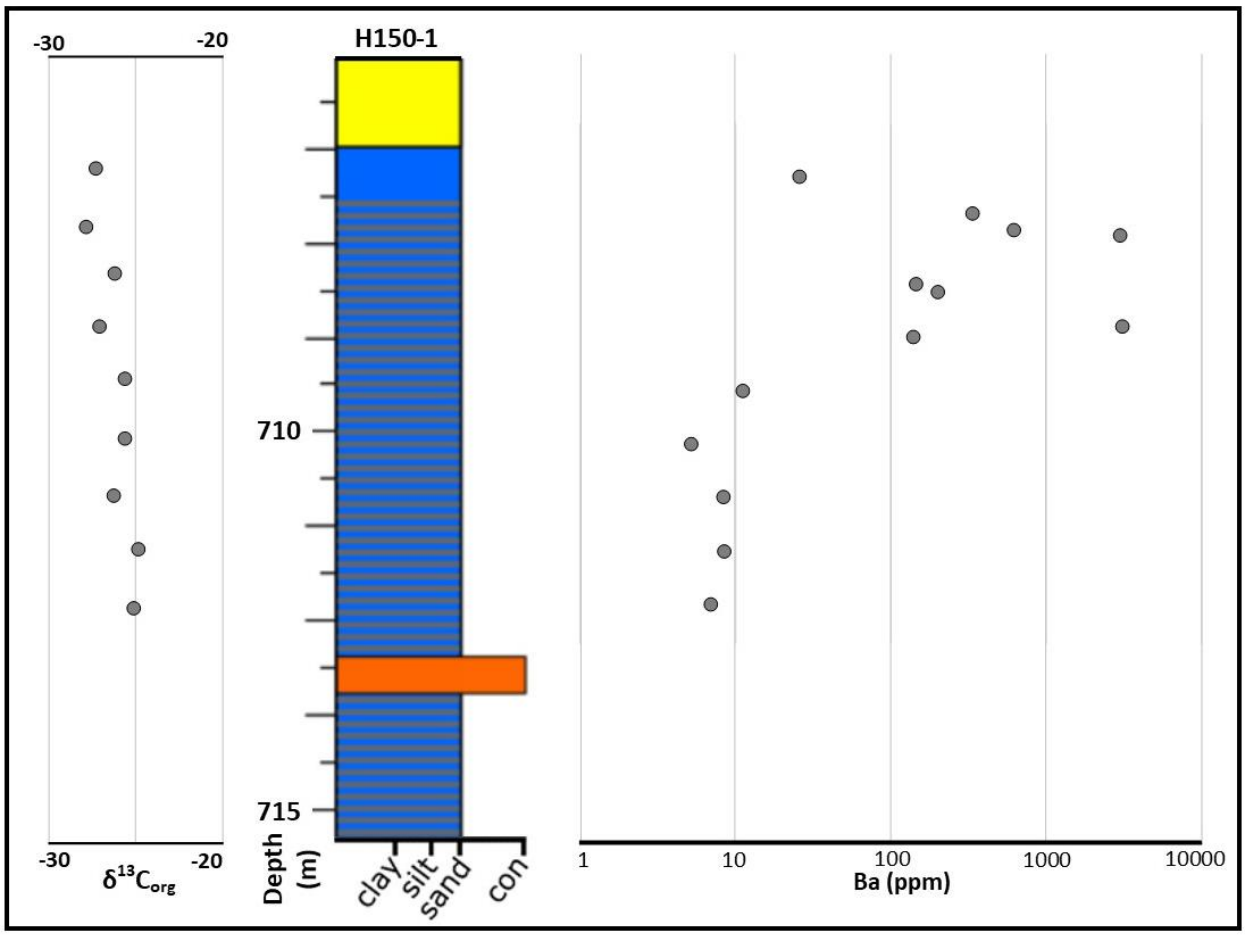

Figure 74: Ba (ppm) values and $\delta^{13}C_{org}$, ‰ PDB values of the interlaminated carbonate and siltstone lithofacies association directly above the contact (within ~10m) with the Bruce Formation in drill hole 150-1.

Drill hole E150-1 has a horizon located between approximately 5-10m above the contact with the Bruce diamictites within the interlaminated carbonate and siltstone lithofacies association that has anomalously high Ba concentrations (Figure 74). Partial digestion values fall typically within a range of ~10ppm but increase over an interval of approximately 2m to values that range up to ~3600ppm. This Ba-rich horizon is also associated with the three samples that have anomalous REE patterns with strong positive Eu-anomalies. Organic $\delta^{13}C$ values from the

same set of samples show a slight decreasing trend in values from approximately -25‰ to -27.5‰.

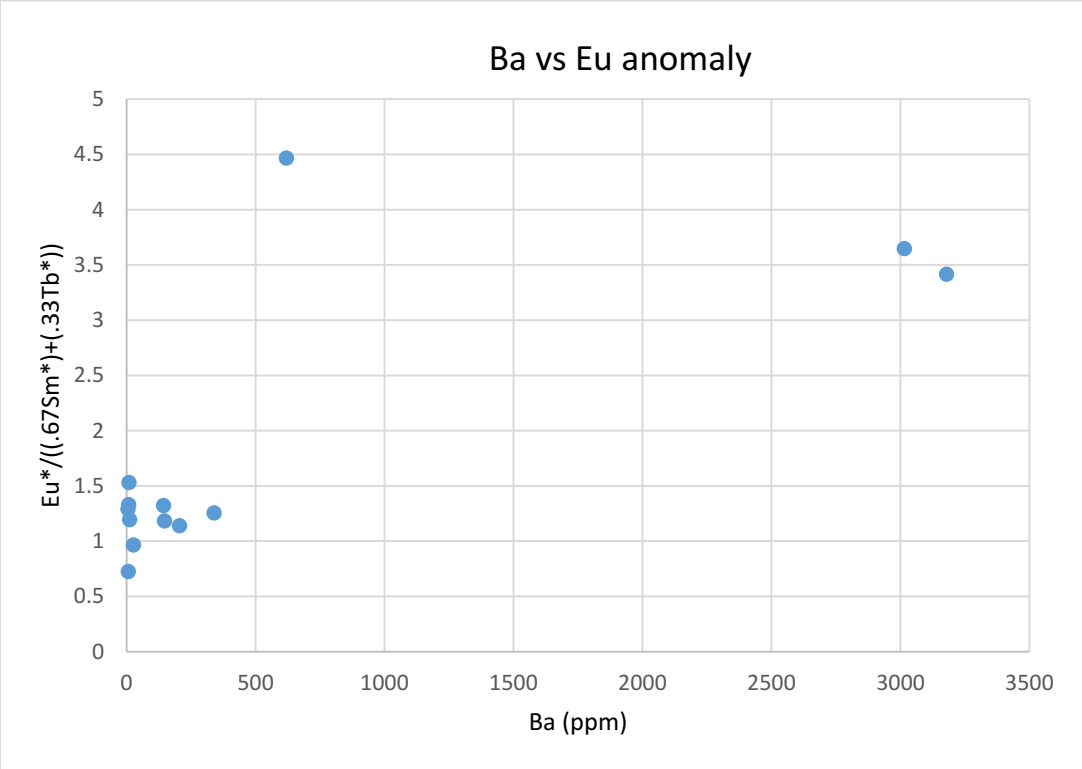

Figure 75: A plot of Ba (ppm) vs Eu anomaly (calculated as Eu*/((.67Sm*)+(.33Tb*))) shows that there is a correlation between positive Eu anomaly and high Ba concentrations.

9 GEOCHEMISTRY DISCUSSION

9.1 REE PATTERNS

Geochemical analysis of the Espanola Formation carbonates in this study focused on REE analysis of partial digestions to isolate the signature of the carbonate fraction. Partial digestions of carbonate-bearing samples of the Espanola Formation allow for identification of the REE patterns of the carbonate fraction of the samples that may otherwise be concealed by the high amount of siliciclastics in many of the samples. As has been previously discussed, REE are useful indicators of provenance because they do not undergo appreciable fractionation during sedimentation processes (McLennan, 1989). Furthermore, they have a low residence time in seawater and have similar partition coefficients during incorporation into precipitates, making these minerals useful in determining the chemistry of the water mass from which they participated (Wright et al., 1987; Nothdurft et al., 2004; Bau and Alexander, 2006).

One strong and consistent pattern observed from the carbonate samples collected from the middle and upper stratigraphy of the Espanola Formation is that they have a 'hat-like' appearance. The middle REE may develop a hump-shaped pattern, moving from a positive slope into a negative slope or may only preserve a positive slope that flattens approaching the heavy REE. Heavy REE are typically, but not exclusively, enriched relative to the light REE. Light REE may sometimes show a slight positive slope, while the heavy REE may show a slight negative slope, or very rarely, a slight positive slope as well.

Ce anomalies were not present in any of the samples analysed. Negative Eu anomalies are ubiquitous in the laminated dropstone lithofacies association sampled in drill hole E150-2, but absent in all other samples with the exception of those taken from the interlaminated

carbonate and siltstone lithofacies association in the Bruce Mines area, Ten Mile Lake area, and one sample from drill hole E150-1. The laminated dropstone facies displays a REE pattern that is unique and consistent, with a flat light REE pattern, a negative Eu anomaly, and a variable heavy REE pattern that ranges from negative to positively sloped. Samples collected from the interlaminated carbonate and siltstone lithofacies association in the Bruce mines area were very similar but had a positive heavy REE slope in all three samples.

The presence of several distinct REE patterns recorded within the Espanola Formation carbonate samples suggests that there may have been influence from two or more unique water masses from which the precipitates were sourced. One signature is recognizable for a marked negative Eu anomaly, relatively flat light REE, and variable heavy REE that ranges from a weak negative to positive slope. The upper and middle stratigraphy of the Espanola Formation has fairly consistent REE signatures that have a somewhat 'hat-shaped' pattern. These samples are recognizable for their middle REE-enrichment, depletion in light REE, and variable concentrations of heavy REE.

9.1.1 REE PATTERNS INTERPRETATION

One fairly consistent signature present within the majority of the REE patterns generated from the middle and upper stratigraphy of the Espanola Formation carbonates is a depletion in the light REE relative to PAAS. Light REE depletion is a feature that has also been noted from some Neoproterozoic cap carbonates and is suggested to be characteristic of precipitation from marine waters (Zhang and Nozaki, 1996; Font et al., 2006; Huang et al., 2011;

Meyer et al., 2012). Similarly, samples collected from another possible Paleoproterozoic cap carbonate in the Sausar Group in India by Mohanty et al. (2015) also had enrichment of heavy REE relative to light REE and was interpreted to indicate a marine origin for the carbonates. Generally speaking, a depletion of light REE relative to heavy REE is a common feature of well-mixed seawater (Elderfield and Greaves, 1982; Derry and Jacobsen, 1990; Piepgras and Jacobsen, 1992; Bertram and Elderfield, 1993; Alibo and Nozaki, 1999; Bolhar et al., 2003) and is the result of light REE being more susceptible to absorption reactions, resulting in their removal from solution (Cantrell and Byrne, 1987; Byrne and Kim, 1990; Sholkovitz et al., 1994). Young (2013a) previously suggested that a dolomite-rich sample collected from the Espanola Formation had strong light REE depletion because of hydrothermal influence, but this is a feature that is distinctive of seawater in general, and is not just indicative of direct hydrothermal influence. Thus, the predominance of a light REE depletion in the carbonates of the middle and upper stratigraphy of the Espanola Formation may suggest that there is a stronger seawater influence on their geochemistry than the carbonates in the lower stratigraphy.

Some other features that were used by Young (2013a) to suggest that the Espanola Formation carbonates preserve evidence of hydrothermal activity is the enrichment of Fe and Mn and the presence of positive Eu anomalies. Suggested evidence of hydrothermal activity in the Espanola Formation carbonates was then used by Young (2013a) to interpret that the carbonates were deposited in a restricted rift basin. Both an enrichment of Fe and Mn and mild to strong positive Eu anomalies are present within some Neoproterozoic cap carbonates as well (cf. Huang et al., 2011; Meyer et al., 2012; Verdel et al., 2018). Aside from the high-Ba horizon

with strongly positive Eu anomalies, mild positive Eu anomalies are present in the Espanola Formation carbonate samples collected from the ferruginous carbonate interbeds in the upper stratigraphy at Ten Mile Lake and Quirke Lake, but are very rarely present within samples of the upper and middle stratigraphy of drill holes E150-1 and E150-2. These positive Eu anomalies are similar in magnitude to those identified by Meyer et al. (2012) from the Scout Mountain Member in Idaho, which is a Sturtian cap carbonate. Positive Eu anomalies and high Fe and Mn concentrations observed from Neoproterozoic cap carbonates has also been suggested to be representative of hydrothermal input (Huang et al., 2011; Meyer et al., 2012). An alternative explanation suggested for the positive Eu anomalies observed in some of the Ediacaran cap carbonates is through increased weathering of detrital feldspars that would occur in the greenhouse conditions during the interglacial (Verdel et al., 2018). The other possible Paleoproterozoic cap carbonate in the Sausar Group in India was also noted to have high Fe and Mn but negative Eu anomalies (Mohanty et al., 2015; Sarangi et al., 2017). High Fe and Mn in carbonates of Paleoproterozoic age cannot be used as evidence for a restricted rift setting as it has been noted that anoxic and Fe-rich conditions largely prevailed in open water settings, including continental shelves, as late as the Mesoproterozoic (Planavsky et al., 2011). Given that the majority of the Espanola Formation carbonates have either a mild or no positive Eu anomaly, it seems highly unlikely that hydrothermal activity had a strong influence on the geochemical composition of most of the carbonate fraction.

There are also strong similarities in many of the REE patterns from the middle and upper Espanola Formation carbonates to those collected by Meyer et al. (2012, see Figure 7) from the Scout Mountain Member in Idaho, including the presence of a mild to moderate middle REE

enrichment which imparts a ‘hat-shaped’ appearance to the patterns. This pattern is believed to be derived from either preferential adsorption of light REE on Mn-oxides and heavy REE on Fe-oxides or dissolution of phosphate minerals (Byrne et al., 1996; Rasmussen et al., 1998; Hannigan and Sholkovitz, 2001; Haley et al., 2004; Surya Prakash et al., 2012; Soyol-Erdene and Huh, 2013; Kang et al., 2014). Middle REE enrichment in some dolomite samples from the Ediacaran Doushantuo cap carbonate in China was suggested by Zhao et al. (2018) to be derived from the release of middle REE from Fe-Mn oxides during diagenesis. The middle REE enrichment in the Scout Mountain Member was not discussed by Meyer et al. (2012), but they did interpret their signatures to be the result of a mixture of well-mixed seawater (light REE depletion) and oxygen-poor deep basin marine waters (Eu anomaly).

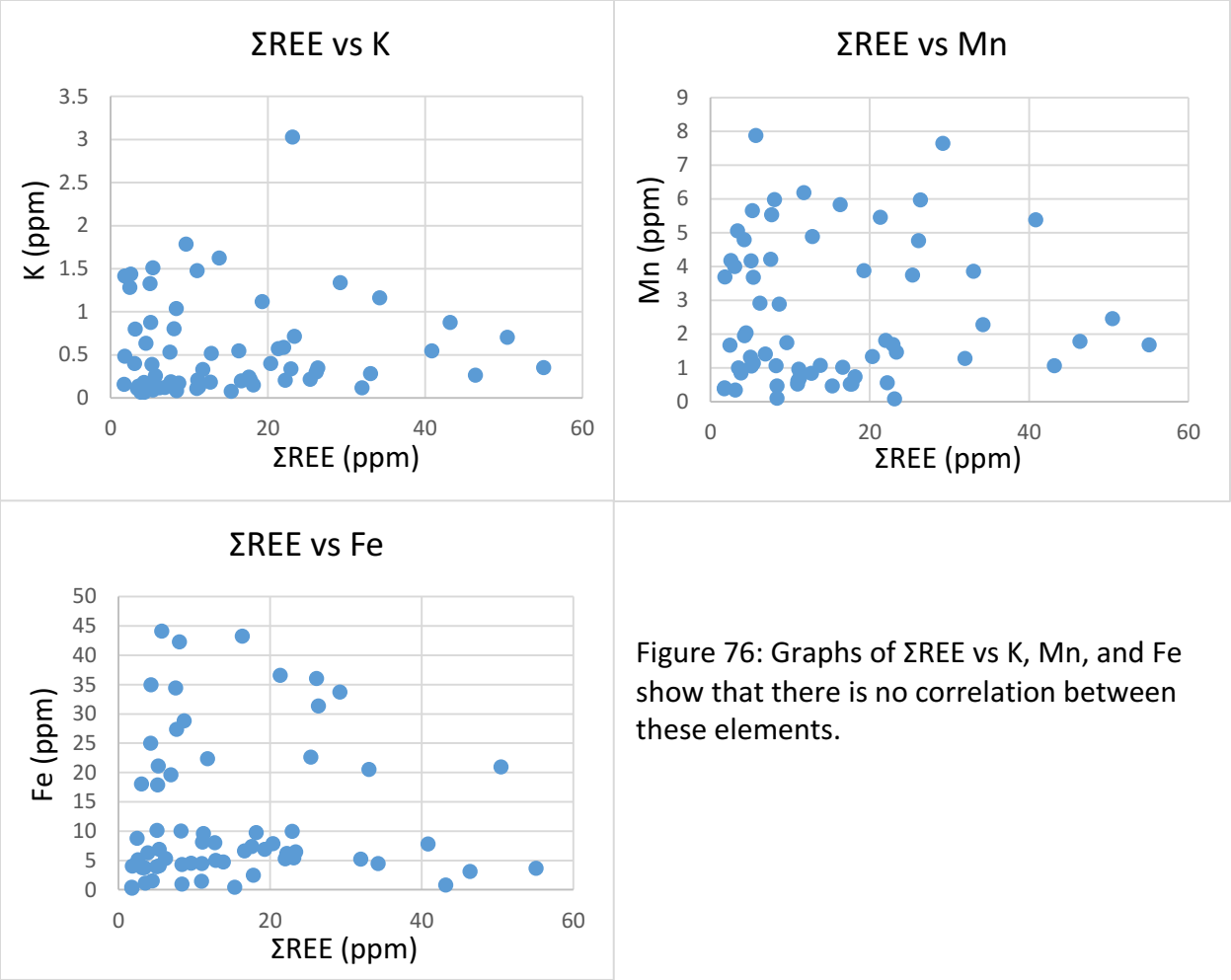

Figure 76: Graphs of ΣREE vs K, Mn, and Fe show that there is no correlation between these elements.

A lack of association between the Fe, Mn, and P values and ΣREE in the Espanola Formation samples indicates that the middle REE enrichment signature of the carbonate fraction may be derived independently from direct influence by these factors (Figure 76). It is unknown what the direct cause of the middle REE enrichment is in the Espanola Formation carbonate samples, but one possible explanation is that it may be the result of varying input from riverine sources. REE analyses derived from riverine precipitates are noted to have highly variable patterns and can display light, middle, or heavy REE enrichments (e.g. Elderfield and Greaves, 1982; Elderfield et al., 1990; Laybourne and Johannesson, 2008). Furthermore, the influence of phosphate dissolution on middle REE cannot always be quantified, as there is not

always a strong correlation between the two when analysing river sediments (Hannigan and Sholkovitz, 2001). Therefore, it may be the fluctuating input of riverine water with a middle REE enrichment, coupled with marine waters with light REE depletion, a common state of both ancient and modern seawater that influenced the REE patterns of the majority of the Espanola Formation carbonates. A recent study completed on REE distribution in the modern northeast Atlantic by Crocket et al. (2018) found that greater interaction with continental margin sediments and terrigenous inputs led to higher light REE and middle REE concentrations in seawater. Marine sediments and pore waters on continental margins have elevated light and middle REE relative to seawater (Abbott et al., 2015) and REE patterns produced by Crocket et al. (2018, see Figure 9B) for potential REE sources to seawater from organic matter, volcanic ash, and pore waters are very similar to some patterns from carbonates of the Espanola Formation, including the middle REE enrichment and rare mild positive Eu anomalies. However, it is not necessary to attribute the positive Eu anomalies to this process as anoxic seawater conditions will impart a hydrothermally-derived positive Eu anomaly to the ocean (Planavsky et al., 2010). Therefore the geochemistry of the middle and upper Espanola Formation carbonates is suggested to represent a combination of influence by seawater and riverine input on a continental margin environment. The light REE depletion, heavy REE enrichment, positive Eu anomalies, and Fe and Mn enrichment are suggested to be features reflective of the seawater signature. This signature is then modified to varying degrees by riverine influx and interaction with continental shelf sediments that have enrichment in light REE and middle REE. The addition of these two signatures results in a less drastic depletion in light REE and a varying enrichment of middle REE that can impart a ‘hat-shaped’ pattern.

Another piece of evidence that can be used to interpret the degree of interaction between marine and meteoric waters is the Y/Ho of the carbonate samples. The Y/Ho of the Espanola Formation carbonates are highly varied and fall within a broad range from ~20-50, with an average value of ~34. Modern seawater has a positive Y anomaly that falls within the range of 40-80 in open marine environments and within 33-40 in more nearshore or restricted environments (De Baar et al., 1985a, 1985b; Nozaki and Zhang, 1995; Bau et al., 1997). The Y/Ho is also strongly dependent upon phosphate mineral solubility, salinity, and fractionation through chemical and biological processes, with freshwater carbonates recording lower Y/Ho than their marine counterparts (Liu and Byrne, 1997; Hill et al., 2000; Webb and Kamber, 2000; Shields and Webb, 2004; Johannesson et al., 2006; Lawrence et al., 2006). The average Y/Ho value of ~34, and large variations from this average in the Espanola Formation carbonate samples may therefore be indicative of probable high, but varying, input of river and freshwater influence. This would result in values falling between high Y/Ho of typical seawater and freshwater influenced more by terrigenous material with chondritic ratios. Furthermore, freshwater influence would not only be reflective of fluvial input, but of the large addition of meltwater during recession of the glacier.

One last feature of REE pattern analysis used in carbonates is Ce anomalies as a proxy for oxidation conditions (Schroder and Grotzinger, 2007; Meyer et al., 2012; Bodin et al., 2013). Ce is unique amongst the REE because it has both a +3 and +4 oxidation state, making it the only redox sensitive REE aside from Eu. Under oxic conditions, fractionation of Ce occurs when Ce^{3+} becomes partially oxidized to Ce^{4+} by coming into contact with the surface of Mn oxides and oxyhydroxides, or by precipitating directly as cerianite (CeO_2) (German and Elderfield,

1990; German et al., 1991). When oxidized to the +4 state, Ce becomes unable to engage in solid-solution reactions and the remaining water mass becomes depleted in Ce, relative to the other REE (German and Elderfield, 1990). The overall lack of any Ce anomaly throughout the entirety of the samples from the Espanola Formation carbonates indicates that the waters from which the carbonates precipitated were not in contact with significant oxygen (McLennan et al., 1979).

Generally speaking, negative Eu anomalies are present in the laminated dropstone lithofacies association and in some locations in the interlaminated carbonate and siltstone lithofacies association occurring in the lower stratigraphy of the Espanola Formation. A Eu depletion, relative to chondrite, has been previously noted from the lower stratigraphy of the Espanola Formation by Al-Hashim (2016) and has been hypothesized to be derived from a depletion in the upper crust that developed by the Paleoproterozoic (Nance and Taylor, 1976, 1977; McLennan et al., 1979). The ability of Eu^{2+} to substitute for Sr^{2+} in plagioclase results in a retention of Eu^{2+} relative to other REE during partial melting of the lower continental crust, and a subsequent Eu depletion in upper crustal rocks (Jakes and Taylor, 1974; McLennan, 1989; McLennan et al., 1993). Therefore, weathering of granodioritic upper continental crust provides a negative Eu anomaly to post-Archean shales (Jakes and Taylor, 1974; Nance and Taylor, 1976; McLennan et al., 1983; McLennan et al., 1990). It has also been noted that the carbonate fraction in the Espanola Formation has similar REE patterns to the associated terrigenous material in some cases (McLennan et al., 1979).

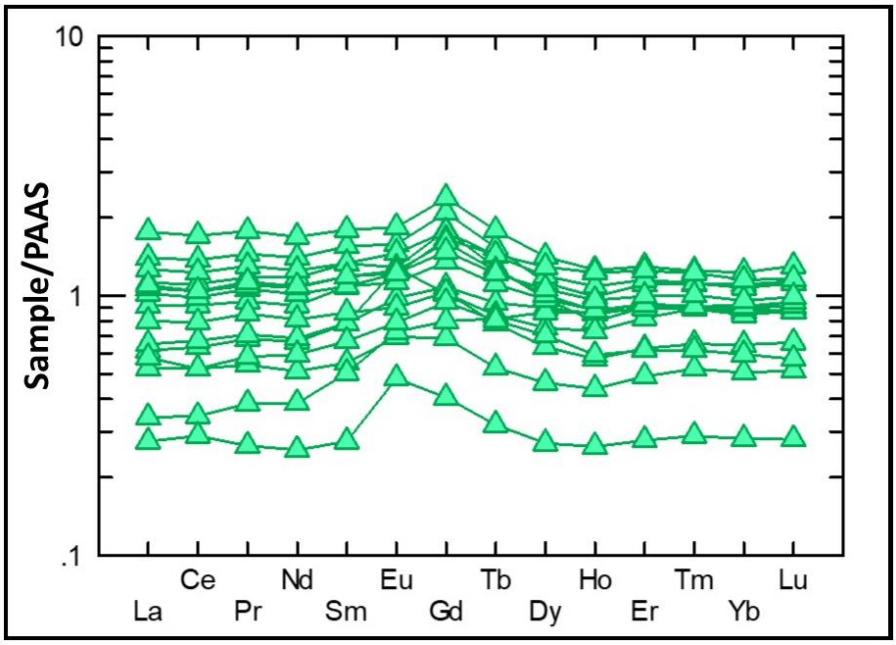

Figure 77: Whole rock REE patterns for samples from the laminated dropstone facies show no negative Eu anomalies. Some samples have positive Eu anomalies.

However, this interpretation for the source of the negative Eu anomalies in the Espanola Formation carbonates does not work as the Y/Ho values range from approximately 24 to 38, suggesting that there was variable influence by riverine input during deposition of those units, as well as the fact that the whole rock REE (reflective of the terrigenous component) patterns do not record a negative Eu anomaly (Figure 77). Thus, it is suggested that remobilization by highly reducing diagenetic fluids is the cause for the negative Eu anomaly in samples from the laminated dropstone facies and the lower stratigraphy of the Espanola Formation. The process of diagenetic remobilization of Eu occurs when Eu^{3+} comes into contact with highly reducing fluids and becomes reduced to soluble Eu^{2+} (MacRae et al., 1992; Sawlowicz, 2013). This process could account for the removal and remobilization of Eu and a resulting depletion relative to the other REE. The mechanism for producing the highly reducing fluids is suggested to be through methane seepage, an idea that has already been proposed to have influenced deposition of

some Neoproterozoic cap carbonates (cf. Kennedy et al., 2001; Wang et al., 2008). Furthermore, not only would methane seepage influence dissolved REE in sub-surface sediments and bottom waters, it would also directly drive the precipitation of authigenic carbonates in those environments and could be a strong driving mechanism for precipitation of the carbonate fraction of some of the Espanola Formation (Aloisi et al., 2002; Bayon et al., 2013; Lemaitre et al., 2014).

An interesting byproduct of methane seepage is enrichment of Mn and Fe in bottom waters overlying active sites, due to sediment re-suspension (Charlou et al., 2004; Bayon et al., 2011; Lemaitre et al., 2014). This could provide an alternative explanation for some of the high Fe and Mn observed in the carbonates of the lower Espanola Formation. Furthermore, as was previously mentioned, the other possible Paleoproterozoic cap carbonate in the Sausar Group in India, which has been suggested to be correlative with the Espanola Formation, similarly records negative Eu anomalies and enrichment of Fe and Mn in some sections (Mohanty et al., 2015; Sarangi et al., 2017).

9.2 HIGH BA HORIZON

An isolated occurrence of strong positive Eu anomalies is present within the interlaminated carbonate and siltstone lithofacies association in drill hole E150-1, approximately 8-10m above the contact with the Bruce Formation diamictites. These samples are also associated with high Ba concentrations. Typically, strong positive Eu anomalies can be used to infer influence by hydrothermal fluids (Bau and Dulski, 1996; Meyer et al., 2012).

Another possible reason for the occurrence of the Eu anomalies is through analytical interference with barium oxides (Jarvis et al., 1989). Furthermore, what is interesting about the localized occurrence of high-Ba values in this drill hole is that barite horizons are found in association with some Neoproterozoic cap carbonates (Hoffman and Schrag, 2002; Jiang et al., 2003; Shields et al., 2007). Barite horizons in Neoproterozoic cap carbonate successions occur at the contact between underlying dolomitic and overlying calcitic units, which suggests that they mark a shift from a sulfate-poor to sulfate-rich marine environment, due to the known inhibiting effect of sulfate ions on the precipitation of dolomite (Baker and Kaster, 1981; Shields, 2005; Shields et al., 2007). Given the lack of a strong divide in carbonate mineralogy of the Espanola Formation and a general opposite trend, from more calcite-dominated to more dolomite-dominated moving up stratigraphy, this interpretation is not as convincing of an explanation for the genesis of the barite in drill hole E150-1, but it is noteworthy that it does occur in the calcite-dominated section. While the stratigraphic control on the Ba-rich horizon is not as clean cut in the Espanola Formation as in Neoproterozoic cap carbonates, nor as laterally extensive, it is interesting that it occurs within a few meters of the contact with the underlying Bruce diamictite, and roughly within or close to the same stratigraphic horizons which host negative Eu anomalies and lower $\delta^{13}C_{carb}$. This is possibly an important piece of information as these features have been hypothesized to be the result of methane seepage, and similarly, a Neoproterozoic cap carbonate in China preserves barite in association with $\delta^{13}C$ evidence of methane seepage (Jiang et al., 2003). The presence of a strong positive Eu anomaly in the Ba-rich horizon could therefore be used to propose that the Eu that was leached by highly reducing fluids may have been transported with Ba to a location that was sulfate-rich and deposited

along with the barite. This could provide an explanation for the sink of the lost Eu as well as a mechanism for the deposition of the barite. An alternative reason for the relationship between the high Ba and positive Eu-anomaly is that these fluids were hydrothermal in origin. The small and isolated occurrence of the Ba-rich horizon suggests that whatever the source of the fluids, the conditions that allowed for deposition of the barite were short-lived and isolated.

9.3 STABLE ISOTOPES

Isotopic analysis consisted predominantly of $\delta^{13}C_{carb}$ and $\delta^{18}O_{carb}$ collected from several outcrops in the areas around Elliot Lake, Bruce Mines, and abundantly from the drill core. A small subset of samples from drill hole E150-1 in the interlaminated carbonate and siltstone lithofacies association directly above the contact with the Bruce Formation diamictites was chosen for $\delta^{13}C_{org}$ data as well. Emphasis was placed on samples collected from the drill core in this study because of the good stratigraphic control for these samples. Stable isotopic analysis of the Espanola Formation has been previously completed for some of the drill holes and field outcrops of the Espanola Formation (Bekker et al., 2005; Al-Hashim, 2016). The presence of the trend in increasing $\delta^{13}C$ values from drill hole E150-2 and its close similarity in values between those collected here and those in Bekker et al. (2005), provide strong evidence that the values are precise and accurate. However, $\delta^{13}C$ and $\delta^{18}O$ data presented by Al-Hashim (2016) is much more variable with $\delta^{13}C$ showing high scatter between values of ~-11‰ to -1‰ and no systematic trends and is thus believed to be data that is not trustworthy for comparison purposes in this study. The results of this study bolster the previously collected datasets from Bekker et al. (2005) and have unveiled unique results and the possibility of some new

conclusions in regards to the Espanola Formation carbonates. Previously completed stable isotope analysis of the Espanola Formation have already uncovered several interesting pieces of information, including the presence of consistent negative $\delta^{13}C$ values, which is a feature that is also recognized from the Neoproterozoic cap carbonates (Veizer et al., 1992; Bekker et al., 2001; Bekker et al., 2005). Oxygen is also depleted in $\delta^{18}O$ from the Espanola Formation carbonates, which has been suggested to be the result of interaction with hot fluids (Bekker et al., 2005). A lack of correlation between $\delta^{13}C_{carb}$ and $\delta^{18}O$ is therefore used to suggest that the depleted $\delta^{13}C$ values observed within the Espanola carbonates are of a primary origin and reflective of anomalous water chemistry (Bekker et al., 2005).

Stable isotope analysis of the Espanola Formation carbonates revealed two interesting results. The first is the presence of a highly negative $\delta^{13}C_{carb}$ excursion at the top of the Bruce Formation in drill hole E150-2. Values collected from an unusual laminated dropstone facies are extremely low and fall in the range of ~-10‰ for $\delta^{13}C$. Associated $\delta^{18}O$ are also more negative than the values that are typical for the remainder of the samples, but the magnitude of the difference is not as stark as that of the $\delta^{13}C$ values. While anomalous $\delta^{13}C$ values are recognized from the Espanola Formation carbonates, the extreme negative $\delta^{13}C$ anomaly preserved within the laminated dropstone lithofacies association at the upper contact of the Bruce Formation in drill hole E150-2 suggests that the water mass which deposited these carbonates was unique. The presence of consistent and unique REE patterns with negative Eu anomalies in association with these low $\delta^{13}C$ values also supports this interpretation. These negative $\delta^{13}C$ values are close to the same values recorded from the Wonoka-Shuram anomaly, the most extreme negative carbon isotope anomaly associated with the Neoproterozoic glacial cycles (Halverson

et al., 2005). The Wonoka-Shuram anomaly records $\delta^{13}C_{carb}$ as low as ~-11‰ and has been noted to have a unique association with the rise of metazoan life (Halverson et al., 2005; Grotzinger et al., 2011). This provides an interesting comparison to the Bruce glacial event and the Espanola Formation, which are hypothesized to be directly correlated to global changes involving a rise in atmospheric oxygen through photosynthesizing bacteria (Sekine et al., 2011; Hoffman, 2013). Several hypotheses have been put forth to explain the Wonoka-Shuram anomaly, including; 'Snowball Earth' and CO_2 build-up (Hoffman et al., 1998), methane release (Kennedy et al., 2001), oxidation of dissolved organic matter (Rothman et al., 2003), weathering of fossil organic matter (Kaufman et al., 2007), and upwelling of ^{13}C-depleted deep oceanic waters (Williams and Schmidt, 2018). The similarities in values obtained from carbonates in the laminated dropstone lithofacies association in the upper Bruce Formation in drill hole E150-2 may suggest that similar processes to the driving mechanism for development of the extremely negative $\delta^{13}C$ Wonoka-Shuram anomaly were ongoing during its deposition. Lastly, it is interesting to note that the Paleoproterozoic Sausar Group in India which also preserves negative Eu anomalies has a peak negative excursion of -7.4‰ V-PDB (Mohanty et al., 2015) which is close to the range of some of the highly negative values collected from the laminated dropstone facies.

As was previously discussed, the negative Eu anomaly in the laminated dropstone facies and some samples from the interlaminated carbonate and siltstone facies was interpreted to be the result of remobilization by reducing fluids. Methane release can also be used to invoke the extreme negative $\delta^{13}C_{carb}$ signature from samples of the laminated dropstone facies. This process was already explained as producing diagenetic fluids, which are highly reducing, and in

reducing fluids Eu^{3+} becomes reduced to Eu^{2+}, even at low temperatures (Sawlowicz, 2013). Just as was discussed in terms of the negative Eu anomalies, methane seepage is interpreted to be the source of the highly negative $\delta^{13}C_{carb}$ signature and is a feature that is suggested to be the cause of the negative $\delta^{13}C_{carb}$ in Neoproterozoic cap carbonates (Kennedy et al., 2001; Jiang et al., 2003; Wang et al., 2008). One of the major complications to this hypothesis, just as in discussion of the Neoproterozoic cap carbonates, is the lack of an associated methane-derived $\delta^{13}C$ signature (e.g. Shields, 2005; Corsetti and Lorentz, 2006). However, there have been recent investigations of the Neoproterozoic Doushantuo cap carbonate that have identified unequivocal evidence for methane seeps in the form of negative $\delta^{13}C_{carb}$ values as low as -48‰ (Jiang et al., 2003; Wang et al., 2008). Unfortunately no definitive methane seep signature was identified in the Bruce or Espanola Formations, but alternative explanations that have been provided to explain the typical lack of these signatures in cap carbonates is that the methane seep signature will become diluted by ambient seawater during precipitation of carbonate and homogenization during diagenesis (Jiang et al., 2003, 2006a, 2006b).

One complication in comparing the Wonoka-Shuram Anomaly to the highly negative $\delta^{13}C_{carb}$ signature in the laminated dropstone facies of the Espanola Formation is that within the three Neoproterozoic units that record the Wonoka-Shuram anomaly, the carbonates are interpreted to have been deposited largely in shallow water facies (Corsetti and Kaufman, 2003; Jiang et al., 2007; Loyd et al., 2012). Likewise, the peak negative excursion of -7.4‰ in the Sausar Group is located in a rhythmically laminated carbonate unit that was interpreted as a shallow marine facies (Mohanty et al., 2014). This is at odds with the interpretation put forth here for the environment of the laminated dropstone facies, which would be in a deeper water

shelf environment, below storm wave base. That being said, interpretation of a shallow water facies is not critical to the comparisons made in this study, as methane seeps occur in all depths and a broad range of settings (Suess, 2014).

The second interesting result unveiled during sampling of drill hole E150-2 is a systematic upwards trend in increasing $\delta^{13}C_{carb}$ from ~-4‰ to -2.5‰. A similar pattern was produced by systematic sampling of drill hole E150-1 by Bekker et al. (2005), where a general upwards trend of increasing $\delta^{13}C$ occurs through the upper stratigraphy of the Espanola Formation. Both the occurrence of highly negative $\delta^{13}C$ at the base of cap carbonates, and the upwards increase in values of $\delta^{13}C$ through stratigraphy has also been reported from Sturtian glaciations, and is a typical feature of Neoproterozoic cap carbonates in general (Kennedy et al., 1998; Halverson et al., 2005, 2010). One interpretation of $\delta^{13}C$ patterns observed in the Umberatana Group in South Australia, is that the variation is facies influenced, with shallow water facies producing values ranging from –3.6‰ and –0.3‰, and deeper water facies ranging from –5.5‰ to –3.5‰ (Giddings and Wallace, 2009). This work has been supported by observations of other cap carbonates (de Alvarenga et al., 2004; Shen et al., 2005; Rieu et al., 2006; Kasemann et al., 2010).

The presence of an upwards trend of increasing $\delta^{13}C$ in the Espanola Formation provides an interesting correlation to Sturtian glacial events and cap carbonates, as well as further evidence to support the sedimentological interpretation of the middle and upper members representing a regressive systems tract with an upwards shallowing trend. Furthermore, Giddings and Wallace (2009) also found that the most negative values in the Neoproterozoic Umberatana Group cap carbonate occurred in the basinal facies, with values ranging from

-6.7‰ to -3.7‰. The presence of the most negative values of the Espanola Formation being within the laminated dropstone facies, a definitively deeper shelf environment of deposition, may further suggest that these sediments were possibly being deposited under deeper water conditions than the remainder of the middle and upper members of the formation which overlie it. The inferred mechanism for the depth-dependent factor on $\delta^{13}C$ in the Umberatana Group cap carbonate is suggested to be a result of stratification wherein organically-derived carbon accumulates in deep water before destratification, and upwelling of the $\delta^{13}C$-depleted waters occurs in the aftermath of the glacial event (Giddings and Wallace, 2009). In considering the Espanola Formation, this depth factor may be more difficult to invoke because of lower concentrations of organic matter. Perhaps an alternative explanation could be that the trend is a result of a decline in the influence of methane seepage with time.

Omitting the very negative data points from drill hole E150-2, the remainder of the Espanola carbonate samples have $\delta^{13}C$ that ranges from -3.43‰ to -1.27‰. These values are consistent and fall within the range of -4.0‰ to -0.8‰ from previously collected data from a different drill hole by Bekker et al. (2005), and are overall slightly more negative on average than data presented by Veizer et al. (1992), who analysed samples from the lower member of the Espanola Formation and produced values with a range of -1.3+/-0.7‰. Thus, a negative $\delta^{13}C$ signal for the carbonates of the Espanola Formation appears to be consistent across the lateral continuity of its exposure, as well as throughout its stratigraphy. A negative $\delta^{13}C$ signal has also been produced from samples analyzed from carbonate of the Snowy Pass Supergroup that overlie the second of three glacial horizons, which is believed to represent an equivalent carbonate-bearing formation to the Espanola (Bekker and Karhu, 1996; Bekker et al., 1999,

2001). The consistency in stratigraphy and carbon isotopic composition between these two formations suggests that the signal was not produced by a local environment, but instead may represent a seawater signal with global implications (Bekker et al., 2005). It has also been suggested by Al-Hashim (2016) that the $\delta^{13}C$ of the Espanola Formation is a local, rather than global signal because of spatial variability and lack of systematic stratigraphic trends (Al-Hashim, 2016). However, as has already been discussed, the accuracy of the values from which Al-Hashim (2016) has based the hypothesis of a local signal has been brought into question, as they are far different from those presented by Bekker et al. (2005) and those presented in this study. Furthermore, the identification of the stratigraphic trend of increasing $\delta^{13}C$ in both drill holes E150-2 and E150-1 made in this study further supports an argument that the $\delta^{13}C$ of the Espanola carbonates is a seawater signature with an overprint of a decaying meltwater signature.

A small subset of samples was chosen for $\delta^{13}C_{org}$ from the interlaminated carbonate and siltstone lithofacies association in drill hole E150-1 directly above the contact with the Bruce Formation. The values produced from close interval sampling over approximately 5m of core produced $\delta^{13}C_{org}$ values that ranged from ~-25‰ to -27.5‰ with an upwards decreasing trend over the 5m of stratigraphy. In general, total organic carbon concentrations (TOC) from the analysed samples were very low and ranged from 0.2-0.6%. The $\Delta\delta^{13}C$ between carbonate and organic carbon for the samples in the interlaminated carbonate and siltstone lithofacies association in drill hole E150-1 ranges from 22.8 to 24.5, which falls within the range of previously presented values (Bekker et al., 2005). While the dataset for this study is not large enough to draw any conclusions about the relationship between $\delta^{13}C_{org}$ and $\delta^{13}C_{carb}$ values,

there is a pattern of inverse correlation between the two data sets, with more negative $\delta^{13}C_{org}$ being associated with less negative $\delta^{13}C_{carb}$ values. Anti-correlation and decoupling between $\delta^{13}C_{org}$ and $\delta^{13}C_{carb}$ is a feature that has been recognized from Ediacaran successions and has been suggested to be the result of a larger oceanic organic carbon reservoir relative to the inorganic carbon reservoir, which would cause a lag effect during interaction between the two (Calver et al., 2000; Rothman et al., 2003; Fike et al., 2006; McFadden et al., 2008).

10 SERPENT FORMATION

The Serpent Formation is the third and final Formation of the Quirke Lake Group. It directly overlies the Espanola Formation in most outcrops, with the exception of some areas in the western Quirke Syncline where the Gowganda Formation directly overlies the Espanola and the Serpent Formation was either eroded or was not deposited. The Serpent Formation is an arenitic sequence with minor shale, siltstone, carbonate, and conglomerate that ranges in thickness from 250-350m but varies locally due to the aforementioned erosion by the overlying glacially deposited Gowganda Formation (Card et al., 1977; Fedo et al., 1997; Long, 2009). Where in contact with the underlying Espanola Formation, the contact is conformable and occurs over a gradational interval up to 120m in thickness in the Sudbury-Espanola area (Card et al., 1997). This gradational contact contains interbedded siltstone, silty limestone, and sandstone (Card et al., 1997).

North of the Sudbury Impact Crater and in the Geneva Lake area the lower Serpent Formation contains a lower conglomeratic unit that is distinguishable from the Bruce Formation by a light-coloured arkosic matrix and from the Gowganda Formation by a more limited clast array (Eggertson, 1975; Long, 2009). Previous studies of the Serpent Formation have used the presence of this conglomerate to propose the existence of two members in the area north of Sudbury (Long, 1976; Rousell and Long, 1998). The lower member is a massive and weakly stratified cobble and pebble conglomerate that is several meters to tens of meters thick and overlain by a second member that contains planar and trough cross-stratified sandstones along with pebble conglomerates (Long, 1976; Rousell and Long, 1998). To the northeast, in the Geneva Lake area, the stratigraphy is similar, with the lowermost Serpent Formation being

dominated by a basal cobble conglomerate that is overlain by cross-bedded sandstones with lenses of pebble conglomerates (Eggertson, 1975). The Serpent Formation in the Geneva Lake area is distinctly coarser-grained than in the north shore of Lake Huron area, which is a consistent observation with the interpretation that the source area for the Serpent sediments is in the areas north of Elliot Lake and the Cobalt Embayment (Eggertson, 1975; Long, 2009)

The Serpent Formation is particularly noteworthy for its unique mineralogy within the Huronian Supergroup stratigraphy. Serpent Formation sandstones have a high fraction of plagioclase, whereas there is very little to none within the feldspathic arenitic units of other Formations (Fedo et al., 1997b). The plagioclase is largely pure albite, leading to the suggestion that the mineralogy is secondary in origin and that the Serpent Formation underwent potassium and sodium metasomatism during post-depositional plutonism (Fedo et al., 1997b). Another suggestion that has been made for the unique presence of plagioclase in the Serpent Formation is that less intense paleoweathering conditions immediately prior to continental glaciation and deposition of the Gowganda Formation led to greater preservation of these minerals (Fedo et al., 1997a).

The Serpent Formation was best observed in this study along the north shore of Lake Huron in the vicinities of Aird Island and Iroquois Bay. Stratigraphic context in the sandstone-dominated Serpent Formation is good in this area much for the same reasons as the Mississagi Formation, including the high angle of bedding allowing for the mapping of continuous sections. The transitional zone between the Espanola Formation and the Serpent Formation has been included in this section because the contact is very diffuse and gradational into the overlying Serpent Formation stratigraphy.

10.1 LITHOFACIES ASSOCATION 1: TRANSITIONAL CROSS-STRATIFIED SANDSTONES WITH CALCAREROUS INTERBEDS

Figure 78: Set of small-scale bundled trough cross-stratification occurring in the uppermost stratigraphy of the transitional lithofacies association in the Aird Island area.

Figure 79: A carbonate-rich interbed (red arrow) shows strong recessive weathering in comparison to the silt-rich, fine-grained sandstone units that lie below and above.

The upper contact of the Espanola Formation with the Serpent Formation in the vicinities of Aird Island and Iroquois Bay is a transitional zone involving the gradual decrease and eventual loss of carbonate-rich siltstone interbeds within stratigraphy that is dominated by fine- to medium-grained cross-stratified and parallel laminated sandstone. Along with the presence of carbonate-rich interbeds, this lithofacies association is marked by the presence of abundant small- and medium-scale, cross-stratified, fine- and medium-grained sandstone units. Trough cross-stratification occurs most typically as bundled sets in the Aird Island vicinity adjacent to planar cross-stratified or parallel laminated sandstone (Figure 78). Individual troughs are shallow and broadly scour into underlying units. Planar cross-stratified units also similarly occur in sets that are small- to medium-scale and wedge-shaped. Paleocurrents collected from cross-stratified sets indicate a bimodal distribution.

Carbonate-rich siltstone and sandstone interbeds range greatly in thickness but are approximately 50cm on average. They are internally parallel laminated between finer-grained silt and carbonate-rich laminae, and coarser sandier laminae. These carbonate interbeds are continuous laterally and sharp sided. The carbonate-rich interbeds in the Aird Island and Iroquois Bay areas are recessively weathered (Figure 79).

Immediately east of Iroquois Bay, the Espanola Formation, transitioning into the Serpent Formation, is dominated by parallel lamination and parallel bedding, with normally graded beds and planar cross-stratification. Parallel laminated beds are usually fine-grained sand and are defined by laminations that have higher and lower amounts of silt and clay. Carbonate-rich beds are rare, typically only react with HCL when scratched, and are often identifiable by their appearance as being black and having a pitted surface that is recessively

weathered compared to adjacent units. The stratigraphy of the transitional zone in the Iroquois Bay area also has distinctly more evidence of soft sedimentary deformation and slumping than the Aird Island stratigraphy.

Massive, medium-grained sandstone beds, parallel laminated beds, and rare hummocky cross-stratified beds are also units that are present within the transitional lithofacies association. Massive beds are typically composed of medium-grained sandstone and most have sharp contacts with adjacent units. Within the massive units, muddy wisps or calcareous wisps can be abundant, and these areas may transition into parallel lamination. Small-scale trough cross-stratified sandstone units may also occasionally erosively scour into the tops of massive beds. Parallel lamination typically consists of fine- and medium-grained sand laminae and silt laminae. Contacts between laminae are sharp and only occasionally contorted by soft-sediment slumping.

10.2 LITHOFACIES ASSOCIATION 2: LARGE-SCALE PLANAR CROSS-STRATIFIED SANDSTONES

Figure 80: A: Finer-grained and more poorly sorted wavy laminated sandstone separating two well-sorted planar cross-stratified beds with sharp contacts. B: Close up of a large-scale planar cross stratified sandstone unit. The internal laminae are very parallel and mm-scale.

The middle section of the Serpent Formation stratigraphy in the Aird Island vicinity is dominated by large-scale, well sorted, medium-to coarse-grained, planar cross-stratified sandstones. These units are separated by units of parallel laminated and bedded more poorly-sorted sandstones with laminae that are dark, ~1-2mm thick on average and are silt- and clay-

rich (Figure 80A, B). Planar cross-stratified beds are typically low angle (<10˚) near their bases and gradually increase in slope upwards. Planar cross-stratified beds are up to 5m in height at the greatest but are typically in the range of 2-3m in height. Rare muddy layers may separate individual planar cross-stratified beds or denote reactivation surfaces within beds themselves. While planar cross-beds are most commonly separated by wavy to parallel laminated sections, cross-beds may overlie one another, with sharp contacts between the two. Petrographic analysis of large-scale cross-beds shows that these units are very well-sorted and are composed of sub-rounded grains of predominantly quartz, with lesser plagioclase and feldspar (Figure 81A). In the Aird Island vicinity, large-scale planar cross-beds have a strong bimodal paleocurrent distribution orientated northeast-southwest, which is the same prevailing current directions as the associated underlying transitional lithofacies association (Figure 82A).

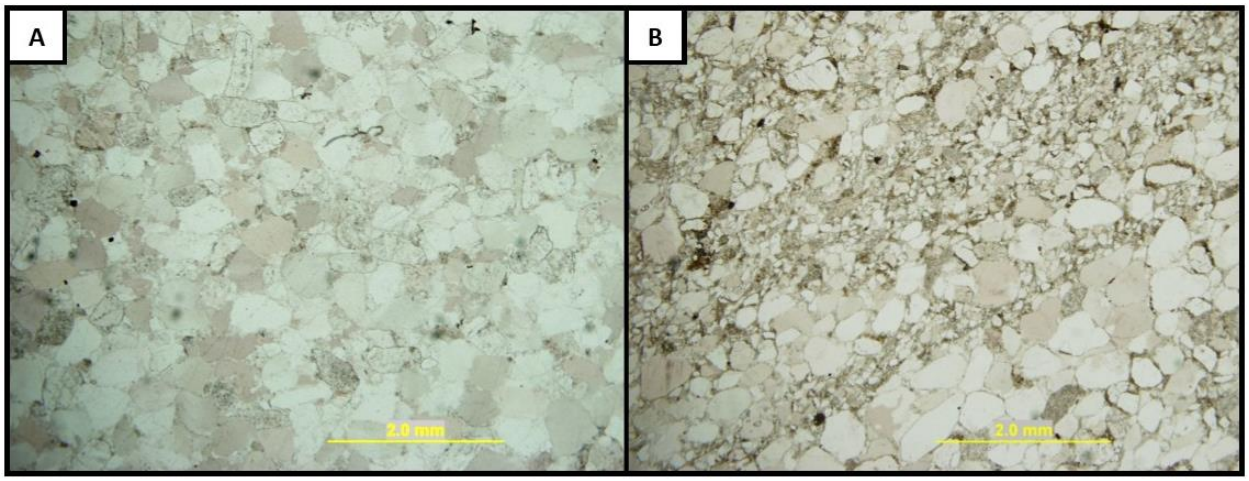

Figure 81: Samples of the Serpent Formation from the large-scale planar cross-stratified sandstones lithofacies association at Aird Island. A: PPL image of a sample taken from a large-scale planar cross-stratified bed. The sands are well-sorted and medium-grained and dominated by quartz with lesser plagioclase and potassium feldspar. B: PPL image of a sample taken from a wavy bedded sandstone unit that separates two planar cross-stratified beds. Well-sorted medium-grained sandstone is roughly interlaminated with poorly sorted fine-grained sandstone to siltstone.

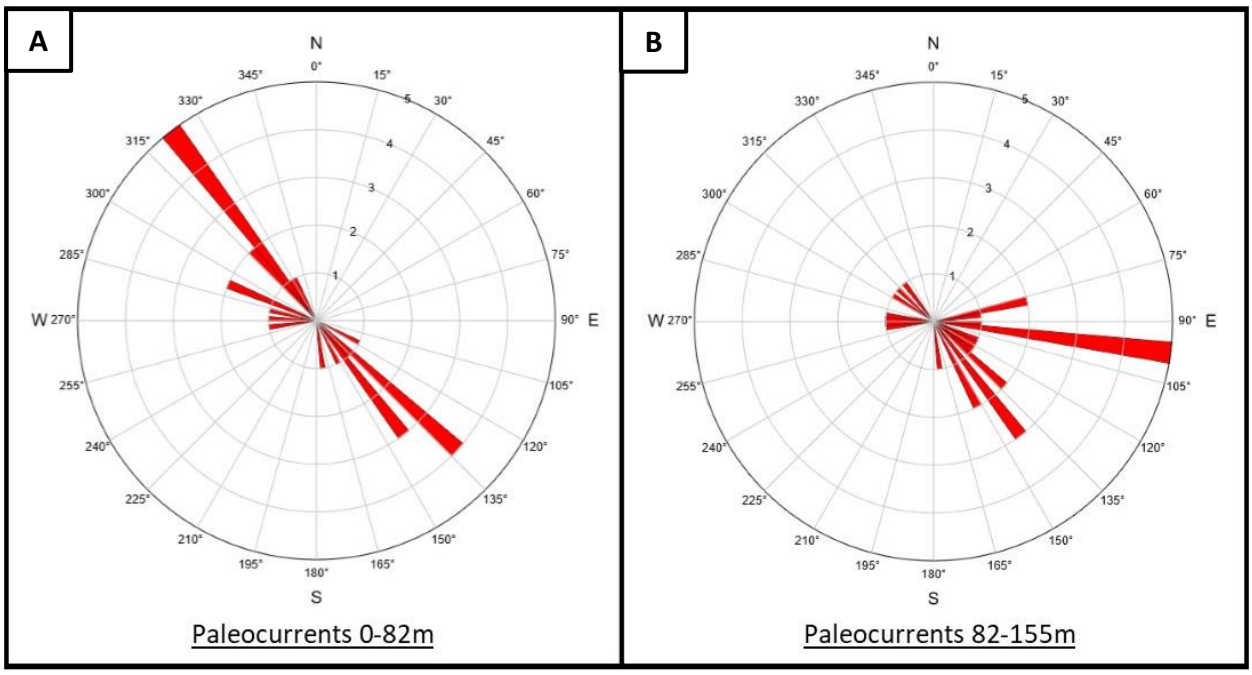

Figure 82: A continuous 155m stratigraphic section of the Serpent Formation in the vicinity of Aird Island has been divided into two rose diagrams with measurements from the first 82m and the following 73m, based on a strong differentiation between the two sections. A: Paleocurrents of the lowermost 82m of stratigraphy of the Serpent Formation in the Aird Island area show a strong northwest-southeast bidirectionality. B: Paleocurrents of the uppermost 73m of stratigraphy show a more strongly unidirectional current direction to the east, with a relic of the strong southeast and northwest currents.

Parallel lamination is the second most common lithofacies within the large-scale planar cross-stratified lithofacies association in the Aird Island area. These units are typically ~50cm thick and distinctly more poorly sorted than the associated planar cross-beds and have a high silt fraction (Figure 81B). Clay-rich silt laminae are commonly 1-4mm thick with poorly sorted medium-grained sand ~1-3cm thick separating them (Figure 83A). Laminae are fairly wavy in appearance, and the sand beds that are directly adjacent to them are commonly distinctly more poorly sorted. Sand beds internally contain faint and discontinuous mud and silt flasers ~1mm thick within them. Contacts between the parallel laminated lithofacies and more well-sorted sandstone units are most often sharp, but occasionally there is a slight gradation from more poorly-sorted sands into well-sorted sands (Figure 83B).

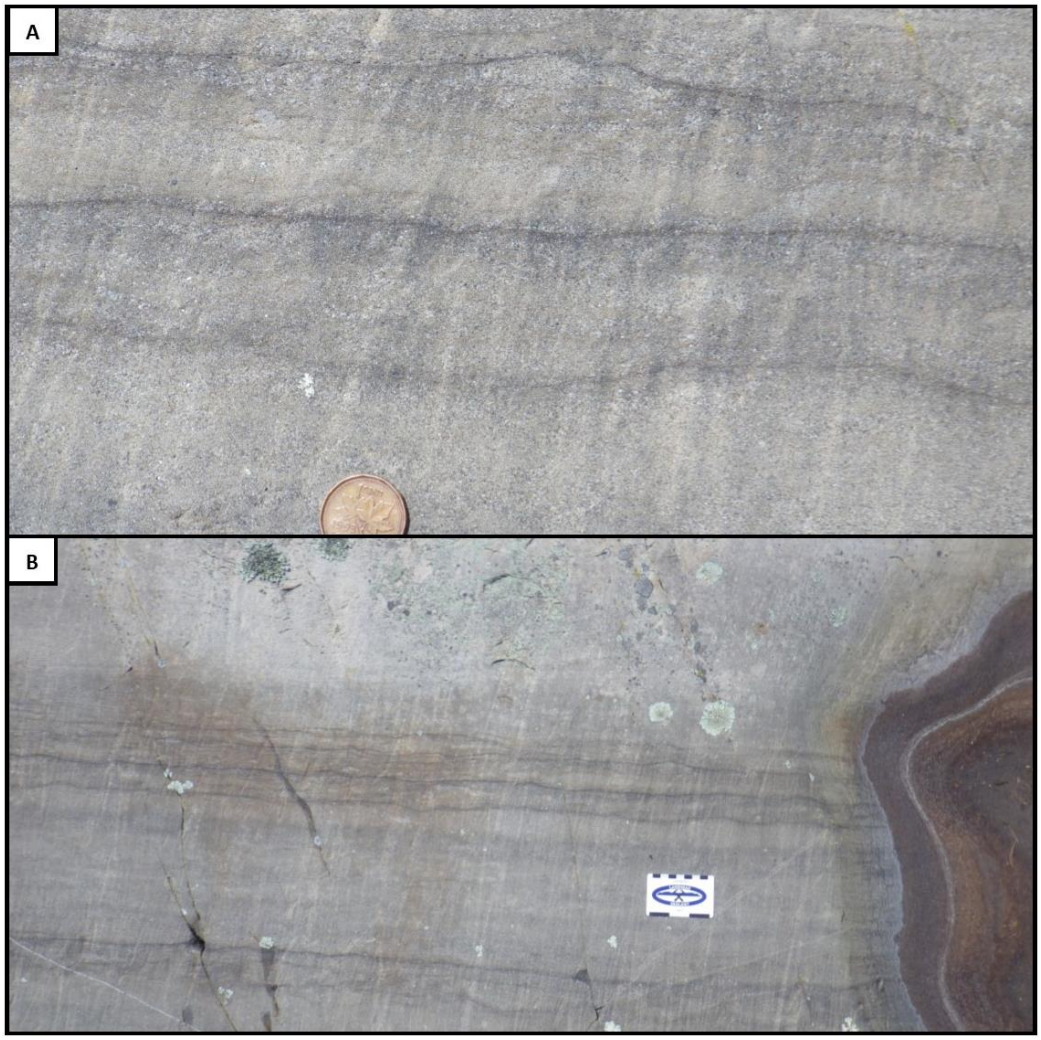

Figure 83: A: Close-up of a wavy-laminated unit from the large-scale planar cross-stratified sandstone. Clay- and silt-rich tops are approximately 2-3mm thick on average and overlie poorly sorted medium- to coarse-grained sand. B: A slightly more gradational contact between an underlying wavy laminated unit and an overlying well-sorted sandstone bed.

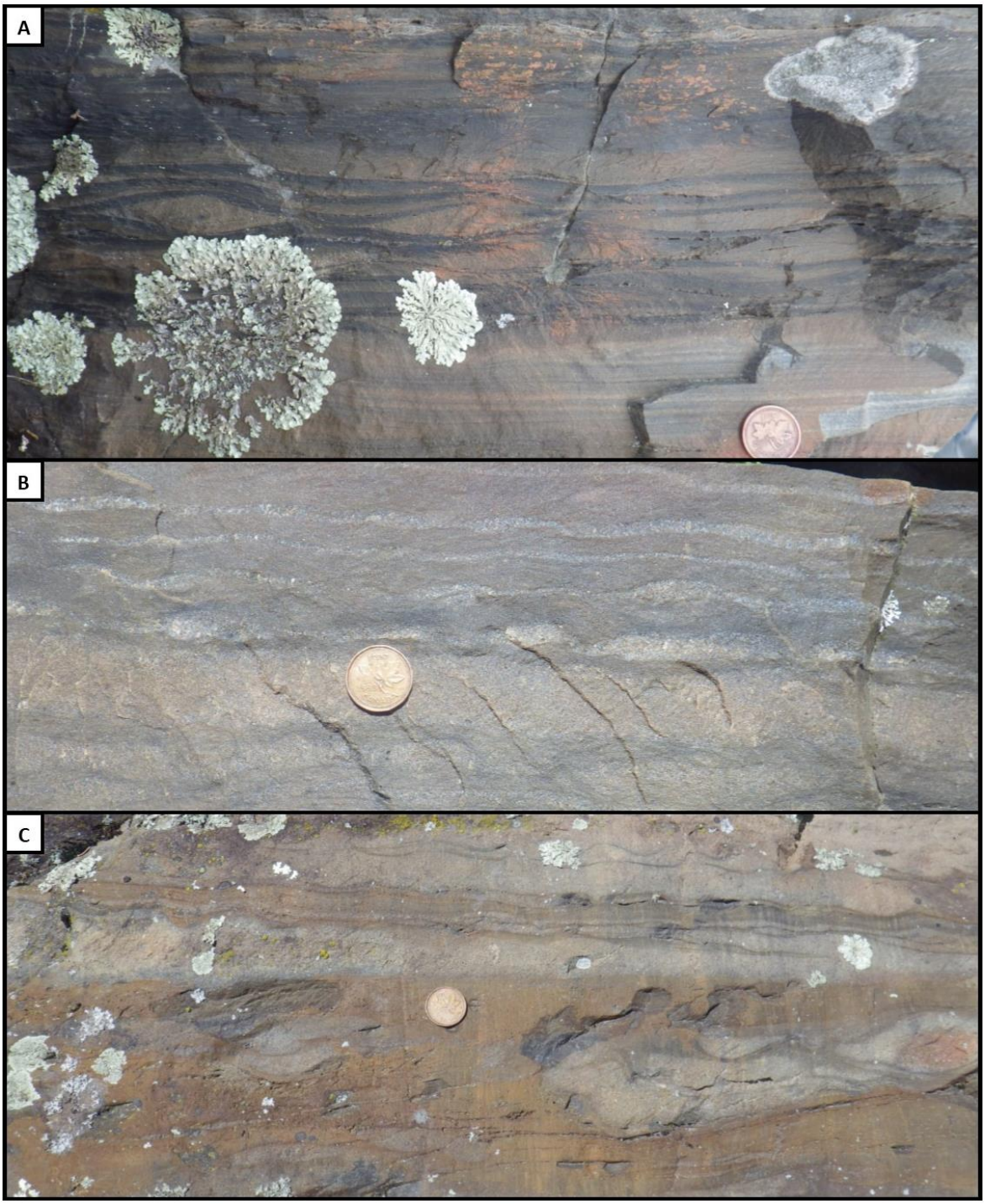

Figure 84: A: Parallel, wavy, and lenticular bedded sandstone and mudstone, with laterally continuous graded beds, from the Serpent Formation outcropping near Iroquois Bay. B: Wavy to slightly lenticular bedding that is punctuated by a 1cm thick sand layer under the coin. C: The lower half of this image shows a mud-rich horizon that contains sand balls that have loaded down into the underlying finer-grained sediment. Overlying this unit is a sand-rich unit with a 2cm thick area in the middle that is wavy to lenticular bedded with a lower contact that interfingers with the underlying sandstone. The sandstone at the top is flaser bedded.

Wavy and lenticular bedding is also present within this lithofacies association in both the Aird Island and Iroquois Bay vicinities and is found in association typically with massive sandstone and parallel laminated to layered more silt-rich sandstone (Figure 84A, B). Grainsizes in wavy bedding is of coarse- to medium-grained sand layers and silt and clay-rich layers. These units range in thickness from a few centimeters up to 30-100cm in places but change between lenticular and wavy bedding within the larger packages. Soft-sediment deformation, in the presence of sand balls deforming muddy units beneath them, are a fairly regular occurrence within these units (Figure 84C). Small scale ripple lamination is visible within medium-grained sandstone units that can be overlain by muddy laminae and lenticular bedding.

10.3 LITHOFACIES ASSOCIATION 3: INTERBEDDED PARALLEL LAYERED SANDSTONES

The large-scale planar cross-stratified lithofacies association in the Aird Island vicinity is capped by a sequence of interbedded parallel layered sandstones that are internally massive or parallel laminated (Figure 85A). A similar sequence of beds occurs in the vicinity of Iroquois Bay, much lower down in the stratigraphy, near the contact with the Espanola Formation (Figure 85B). At Aird Island the sands range in grainsize from medium-grained to rarely coarse-grained and are very poorly sorted with a large clay and silt fraction. Parallel lamination is the most common facies within units and individual beds themselves have sharp and planar contacts with adjacent beds. The contact with the underlying large-scale planar cross-stratified sandstone lithofacies association at Aird Island is sharp and erosive, with the lowermost planar bed overlying a cross-stratified unit. Directly overlying the interbedded parallel layered

sandstones lithofacies association in this locale is the trough-cross stratified sandstones with mud rip-ups lithofacies association.

In the Iroquois Bay area the interbedded parallel layered sandstones lithofacies association is slightly finer-grained, with units being predominantly of fine- to medium-grained sand. Packages of 4-10cm thick mm-scale parallel laminated beds of mud and silt occur throughout the sandstone beds. More well-sorted cross-beds also occur occasionally within the stratigraphy as small-scale planar and trough cross-stratification. Contacts between units is sharp and the average thickness of planar bedded and cross-bedded sandstone units ranges from 17-42cm. At Iroquois Bay the interbedded parallel layered sandstones lithofacies association is in contact with units of well-sorted planar and trough cross-stratified sandstones that range from small to large-scale and are separated by parallel laminated silt packages up to ~1m in thickness.

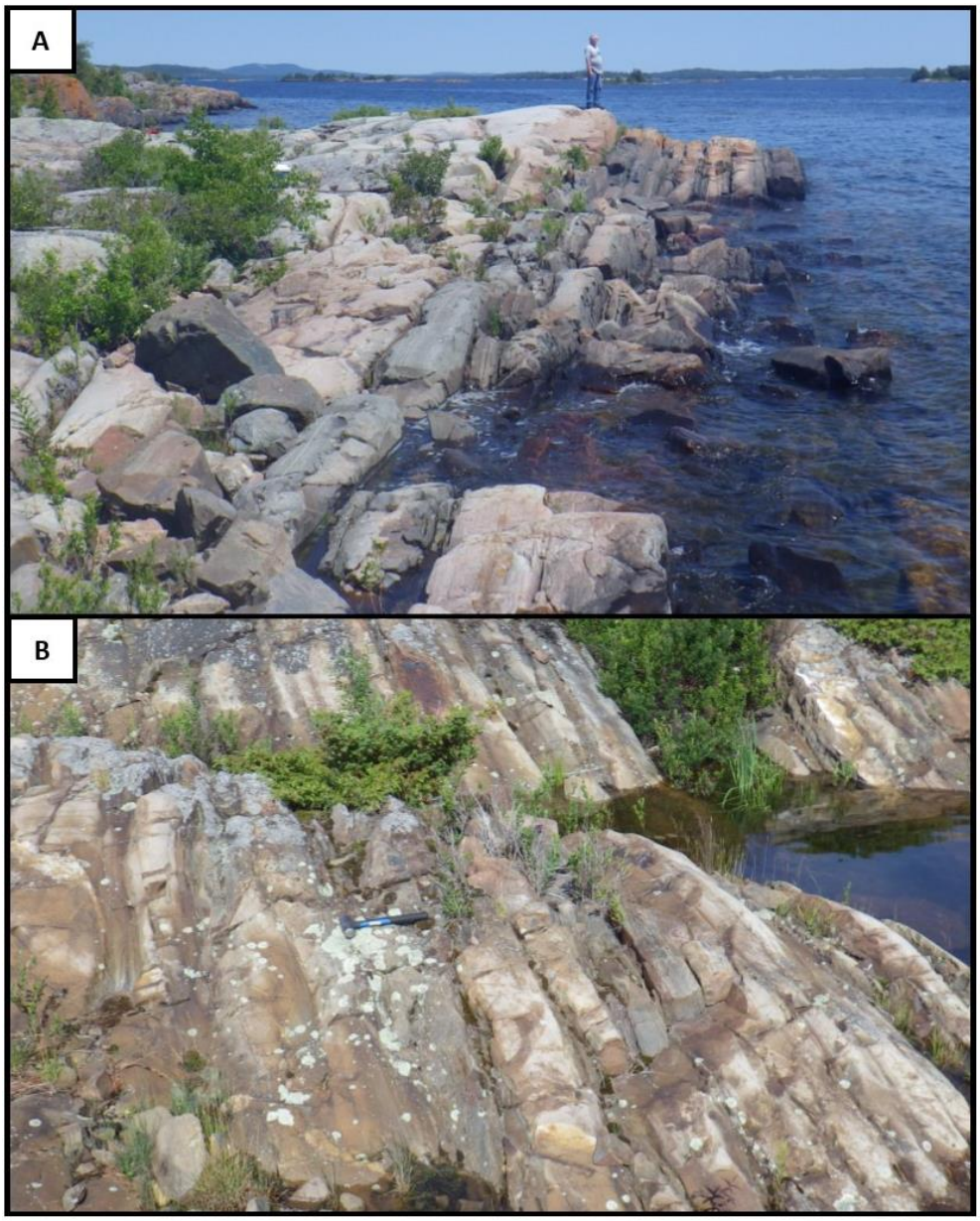

Figure 85: A: The top of the large-scale planar cross-stratified sandstone lithofacies association at Arid Island is capped by a sequence of planar beds that are internally massive or parallel laminated. These units are distinctly more poorly sorted and finer-grained than the planar cross-stratified sandstone units that directly underlie them. B: In the Iroquois Bay area a similar sequence of planar beds occurs within a section of cross-stratified sandstones with silt-rich sandstone interbeds.

10.4 LITHOFACIES ASSOCATION 4: TROUGH CROSS-STRATIFIED SANDSTONES WITH MUD RIP-UPS

Overlying the large-scale planar cross-stratified lithofacies association is the trough cross-stratified lithofacies association that is also distinguishable by the presence of abundant mud-rip ups throughout the stratigraphy at Aird Island (Figure 86A). Trough cross-stratified units are medium- to large-scale and occur in fairly continuous sets. They consist of well-sorted medium-grained to coarse-grained sandstone with the exception of the bases in many instances, which can contain abundant mud rip-ups and associated mud- and silt-rich wisps (Figure 86B). Trough cross-beds often occur in sets, with troughs broadly scouring into underlying beds. Cross-beds may be draped by clay-rich layers up to 15cm thick in places.

Medium- to large-scale planar cross-stratified units are also fairly common in the trough-cross stratified lithofacies association and typically consist of well-sorted medium-grained sand as well. Planar cross-beds have sharp contacts with adjacent units and typically occur as solitary beds, or small sets of 2-3 beds, and are most common adjacent to trough cross-stratified units. Clay-rich layers are also associated with planar cross-beds as well as rare mud rip-ups at the base of units. Paleocurrents of both planar and trough cross-stratified sandstones have a more unidirectional distribution than the underlying lithofacies (Figure 82B).

Mud rip-ups are often elongated, dark brown, and can be eroded out leaving holes in some places. They are commonly found at the base of cross-stratified beds, but can be associated with rare parallel laminated or massive sandstone units that rarely occur within the trough cross-stratified lithofacies association. Massive sandstones are often medium-grained sand, while parallel laminated units are fine-grained sand to mud-rich silt laminae. Mud rip-ups

in these units, as in the case of the cross-stratified beds, are found most commonly at the bases or tops of units and are associated with mud laminae and wisps.

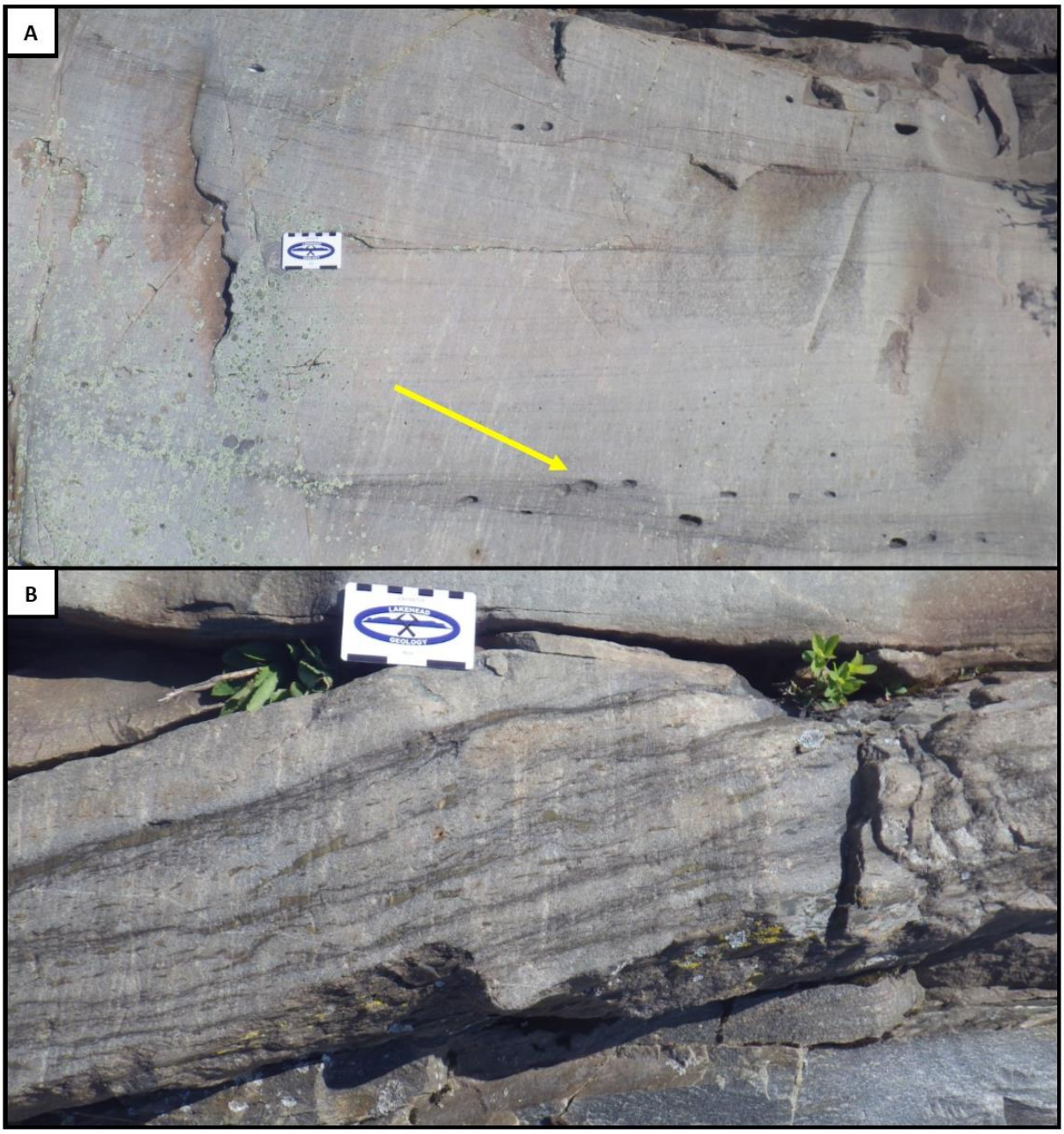

Figure 86: A: Sequence of well-sorted medium- to coarse-grained trough cross-stratified beds outcropping at Aird Island. The yellow arrow points to a clast-rich layer at the base of a trough. The clasts are elongated and have been eroded away. B: Trough cross-stratified bed that has heterolithic bedding with abundant mud wisps, layers, and rip-ups. Clasts are highly irregular in shape and generally oriented with the laminae.

11 SERPENT FORMATION DISCUSSION

The Serpent Formation gradationally and conformably overlies the Espanola Formation throughout the Huronian basin and has been interpreted to have been deposited in a large range of hypothesized depositional environments, including; continental fluvial, aeolian, and fluvial-deltaic to shallow marine (Frarey and Roscoe, 1970; Casshyap, 1971; Card et al., 1973; Robertson, 1973; Young, 1973; Long, 1976). Overall, the Serpent Formation is dominated by planar and trough cross-stratified beds, with planar cross-stratified units being larger on average, and typically over 1m in thickness (McKee and Weir, 1953; Long, 1976). A shallow marine environment for the Serpent Formation is inferred based on associated carbonate in some of the sandstones of the upper units (Pettijohn, 1970) and interlayering with carbonate beds in its basal sections. Opposing hypotheses to this interpretation suggest that the carbonates may have been deposited in lacustrine environments or inland sabkas (Long, 1976). However, much of the discussion involving the depositional environment of the Serpent Formation sandstones is in relation to the large-scale planar cross-stratified units. Proponents of a predominantly fluvial environment with associated aeolian influences point to desiccation features in associated mudstone units and diffuse and unimodal paleocurrent distributions (Long, 1976). The results of this study, which focused mostly on the sedimentology of the lower Serpent Formation in the north shore of Lake Huron area, leads to the conclusion that the depositional environment of the Serpent Formation sandstones in the southern exposures probably represent a broad transition from a shallow marine to fluvial environment. This interpretation is supported by the upper stratigraphy of the Espanola Formation representing a nearshore shallow marine environment.

11.1 LITHOFACIES ASSOCIATION 1: TIDE- AND STORM-INFLUENCED NEARSHORE ENVIRONMENT

The transitional cross-stratified sandstones with calcareous interbeds lithofacies association is dominated by medium- to fine-grained cross-bedded sandstones that are intermittently punctuated by parallel laminated sandstones, siltstones, and carbonate-rich siltstones with lesser massive sandstone units. Cross-stratified units are predominantly of medium-scale trough and planar cross-stratification occurring in bundled sets. In the vicinity of Aird Island these cross-stratified sets have northwest-southeast bidirectional paleocurrents. This lithofacies association is akin to the upper Heterolithic Member of the Espanola Formation that has been described in previous studies and represents a gradual transition zone that separates the underlying Espanola Formation from the overlying Serpent Formation. This transition zone is interpreted to represent a nearshore environment experiencing tide- and storm-influence.

As has been previously discussed in regards to the Espanola Formation stratigraphy, hummocky cross-stratification is a diagnostic facies that is formed by storm influence and is only preserved in the nearshore environment between storm- and fairweather-wave bases (Leckie and Walker, 1982; Plint, 2010; Bayet-Goll et al., 2014). Tidal influence upon these sediments is preserved in the wedge-shaped planar cross-stratified sets and strong bidirectional paleocurrents. The predominance of trough- and planar-cross stratification within the transitional cross-stratified sandstones with calcareous interbeds lithofacies association, along with lesser hummocky cross-stratification are features indicative of storm activity in an open water and shallow marine setting (Aigner, 1985; Duke et al., 1991; Long and Yip, 2009).

11.2 LITHOFACIES ASSOCIATION 2: LARGE-SCALE PLANAR CROSS-STRATIFICATION

The large-scale planar cross-stratified lithofacies association is the primary lithofacies association observed in the middle Serpent Formation stratigraphy along the north shore of Lake Huron and is dominated by a repetitive sequence of large-scale cross-beds that are adjacent to one another or separated by planar laminated, more poorly sorted sandstone units. Large-scale planar cross-stratification has been documented as the dominant structure of the Serpent Formation and has been suggested to have formed via migration of bedforms with straight to undulose leading edges (Long, 1976). Several possible depositional settings for these structures have been suggested, including aeolian, shallow marine shelf, and fluvial (Long, 1976). An aeolian environment is rejected based on the lack of associated gravel lag surfaces and ventifacts, as well as the lack of small-scale avalanche features on foresets, which is a feature that is commonly suggested to be formed through deposition by wind (Glennie, 1970; Reineck and Singh, 1973; Gradzinsky and Jerzkiewicz, 1974; Long, 1976). A fluvial environment has been suggested based on the abundance of planar cross-stratification, desiccation features, mud clasts, and lack of associated structures that would be expected in a nearshore and tidally-influenced environment (Long, 1976). However, the results of this study indicate that mud clasts are associated with the overlying trough cross-stratified lithofacies association and that wavy and lenticular bedding are found in association with the large-scale planar cross-stratified beds. These features, along with strong bimodal paleocurrents, have been used here to suggest that the large-scale planar cross-stratified lithofacies association was deposited in a nearshore tidally-influenced environment.

The lower tidal-dominated nearshore environment is dominated by solitary beds of large-scale, planar cross-stratified, medium- to coarse-grained sandstones that are separated by intervals of medium-grained sandstones with wavy to parallel laminae of silt- and clay-rich wispy layers. Occasionally, beds of planar cross-stratification may be separated by tidal bedded units, which commonly include varying thicknesses of wavy and lenticular bedding. Thicker ripple lamination and flaser lamination are also rarely associated with these units, and the tidal bedding may be separated by massive medium-grained sand layers usually 1-2cm thick that are sharp-sided. Where in contact with the underlying local fourth member of the Espanola Formation, the tidal dominated lithofacies association has abundant evidence of soft sediment deformation and loading with cleaner, medium-grained sandstones disrupting underlying medium to fine grained sandstones with a higher silt content.

The domination of this lithofacies association by large-scale, low-angle planar cross-stratified sandstones, occurring in solitary beds, and separated by tidal bedding or wavy laminated poorly sorted sandstones suggests a tidally-dominated nearshore environment of deposition. This interpretation is supported also by the strongly bimodal northwest-southeast paleocurrent directions of beds within this stratigraphic section. Bimodality of paleocurrent directions for this lithofacies association and the underlying transitional lithofacies association in the vicinity of Aird Island is a strong indicator of a shallow marine environment as 180˚ variations in paleocurrents is a common feature resulting from current reversals under tidal influence (Allen, 1963; Hofman, 1966; Hrabar et al., 1971; Banks, 1973; Young and Jefferson, 1975). The low angle planar cross-stratified beds may represent the migration of large scale sandwaves along a tidal shelf, with the more poorly sorted wavy laminated beds between them

representing interbar areas. These sandwaves are produced via large flow-transverse bedforms (Ashley, 1990) that range in thickness from 0.5-10m and are very common structures in ancient subtidal sandstone sequences (cf. Richards, 1986; Kreisa et al., 1986; Surlyk and Noe-Nygaard, 1991). A decrease in the angle of foresets in the down current direction, as is commonly preserved in the large-scale planar cross-beds, is a common feature of tidal sandwaves on tide-dominated shelves (McCave, 1971; Walker, 1984; Bose et al., 1997; Nemeth et al., 2007).

The occasional presence of wavy and lenticular bedding in the large-scale planar cross-stratified lithofacies association also provides strong evidence for a shallow marine depositional environment. Interlayering of sand and mud to form wavy and lenticular lamination is common in nearshore environments and is the result of fluctuations in flow velocities, with mud representing deposition during slack water conditions (Reineck and Wunderlich, 1968; Reineck and Singh, 1980; Weimer et al., 1982; Dalrymple, 2010). The presence of lenticular and wavy bedded units may herald migration of sand sheets and form on the downcurrent side of sand bars (Fichter and Poche, 2001).

11.3 LITHOFACIES ASSOCIATION 3: INTERBEDDED PARALLEL LAYERED SANDSTONES

A minor lithofacies association located in the Aird Island vicinity and Iroquois Bay area is recognizable by a predominance of interbedded parallel layered sandstones. In the Aird Island vicinity, this lithofacies association specifically separates the large-scale planar cross-stratification lithofacies association from the overlying trough cross-stratified sandstone with mud rip-ups lithofacies association. These parallel layered sandstone beds are typically

internally parallel laminated to massive and in the Iroquois Bay area are occasionally punctuated by cross-stratified units. Given the superimposition of this lithofacies association upon the underlying tidally-influenced shallow marine sediments of the transitional and large-scale planar cross-stratified lithofacies associations, these parallel layered units suggest a transitional environment into the depositional environment of the overlying trough cross-stratified sandstones with mud rip-ups. The shift to finer-grained sediments within this lithofacies association, and the loss of large-scale planar cross-stratified beds suggests that the parallel layered sandstones are the result of changes to lower energy conditions and tidal influence.

This lithofacies association may represent a shift in predominant tidal transport paths, possibly due partially to delta outbuilding which heralds deposition of the trough cross-stratified sandstones with mud rip-ups lithofacies association that overlies it in the vicinity of Aird Island. The fringe zones of major tidal current transport paths are areas of low tidal and wavy activity and experience deposition of finer-grained sediments, which could attest to the overall decrease in grainsize observed in this lithofacies association in comparison with the underlying large-scale planar cross-stratified lithofacies association (Stride, 1963; McCave, 1971, 1972).

11.4 LITHOFACIES ASSOCIATION 4: TROUGH CROSS-STRATIFIED SANDSTONES WITH MUD RIP-UPS

The trough cross-stratified sandstone with mud rip-ups lithofacies association is well exposed along the north shore of Lake Huron in the vicinity of Aird Island. This lithofacies association overlies the large-scale planar cross-stratified lithofacies association and is characterised by a shift to a predominance of large and medium-scale trough cross-stratification with abundant mud-rip ups and wisps. Furthermore, this lithofacies association in the vicinity of Aird Island is also marked by a distinct shift from strong bimodal paleocurrents to unidirectional paleocurrents with a relic of the southeast current influence. The shift to more unidirectional from bimodal paleocurrents likely indicates a transition from a predominantly tidally-influenced environment to predominantly fluvially-influenced (cf. Shackleton, 1962; Ore, 1964; Klein, 1967; Mrakovich and Coogan, 1974; High and Picard, 1974). The sedimentological structures, including the predominance of medium- and large-scale trough cross-stratified units, and the abundance of mud rip-ups, likely sourced from upstream areas experiencing bank collapse or emergent conditions, support this interpretation. Sandstone-channel facies are dominated by cross-bedding, and particularly, trough cross-beds are common units in distributary channels and distributary mouth bars dominated by medium-grained sands (Dalrymple and Choi, 2007) and are the most common units in the trough cross-stratified sandstone with mud rip-ups lithofacies association. Under tidal influence, the sand in distributary mouth bars would be spread out offshore and provide the sediment for the tidal sand bars that dominated in the underlying large-scale, planar cross-stratified lithofacies association. The distributary mouth bars would therefore be similar to offshore tidal sands that

have been described from modern tidally influenced deltas (e.g. Coleman, 1969; Fisher et al., 1969; Coleman and Wright, 1975). Furthermore, in a tidal-influenced braid delta, tidal influence would carry up the channel landward and result in nearshore portions of the channels having a bidirectional influence as well. Abundant mud wisps and mud partings between individual cross-beds and between laminae in cross-beds, indicate large fluctuations in flow velocities and points to some remaining tidal-influence in what was likely a fluvial-deltaic environment (Dalrymple and Choi, 2007). Total fluvial dominance of sediments in channels would only prevail further inland (Dalrymple and Choi, 2007). The abundant intraformational mud flakes in the cross-stratified beds are probably derived from erosion of floodplain sediments during channel migration (Ramos et al., 1986).

12 DISCUSSION

The Bruce glacial event is the second of three glacial cycles preserved within the Paleoproterozoic Huronian Supergroup and is unique for its overlying cap carbonate, the Espanola Formation. Given the connotation of Neoproterozoic cap carbonates being the result of global icehouse conditions, there is speculation around the genetic origins of the Espanola Formation carbonate and its possible similarity to the later Neoproterozoic glacial cycles. This study involves a summation of the sedimentology and stratigraphy of the Bruce glacial cycle to constrain changes in the depositional environment, from the advance to the retreat, of the Bruce ice shelf. Geochemical analysis of the Espanola Formation carbonates supplements this investigation by providing information about the water chemistry from which they precipitated and allows for further discussion of the depositional mechanisms.

12.1 TECTONIC SETTING OF THE BRUCE GLACIAL CYCLE

One complication in discussing the implications of the Espanola Formation carbonates is uncertainty regarding the tectonic and depositional setting. Discussions of the tectonic setting are divided between those that favour the early rift-drift transition, at the base of the Matinenda Formation, which would imply a post-rift open shelf environment, and those that argue that the Espanola Formation carbonates were deposited in an isolated rift basin prior to the rift-drift transition. Conclusively defining the timing of the rift-drift transition is critical to determining whether or not the Espanola Formation is a cap carbonate reflective of global icehouse conditions, or of an isolated depositional environment. As was discussed in the

introduction, proponents of the earlier rift-drift transition point to a transition to predominantly southward-directed fluvial transportation at the base of the Matinenda Formation, which is believed to indicate a shift from an active rift arm to lithospheric cooling induced subsidence (Card et al., 1972; Fralick and Miall, 1989; Bennet et al., 1991; Hoffman, 2013). A later rift-drift transition is argued based on the evidence for marine influence and greater lateral extent of the Gowganda Formation, which oversteps the Flack Lake Fault that confines the northern extent of the underlying Hough and Quirke Lake Groups (Frarey and Roscoe, 1971; Young and Nesbitt, 1985; Young et al., 2001; Young, 2014). The later rift-drift transition, situated at the base of the Gowganda Formation, infers that the Espanola Formation was deposited in a restricted rift basin (Young, 2013a). This hypothesis addresses the lack of cap carbonates outside of the Espanola Formation and its correlatives in the Snowy Pass Supergroup in Wyoming (Young, 2014), but unfortunately seems to be at odds with the evidence of a Huronian-age cap carbonate in India (Mohanty et al., 2014) and the sedimentological evidence. The results of this study support the earlier rift-drift transition, based on derivation of sediments from the north with roughly southward-directed paleocurrents plus a strong tidal influence in the marine environment, and it is proposed here that synsedimentary faulting in the Quirke Lake Group is not the result of active rifting, but rather is a response to ice, water, and sediment loading on the margin of the Superior craton causing reactivation along pre-existing basement faults.

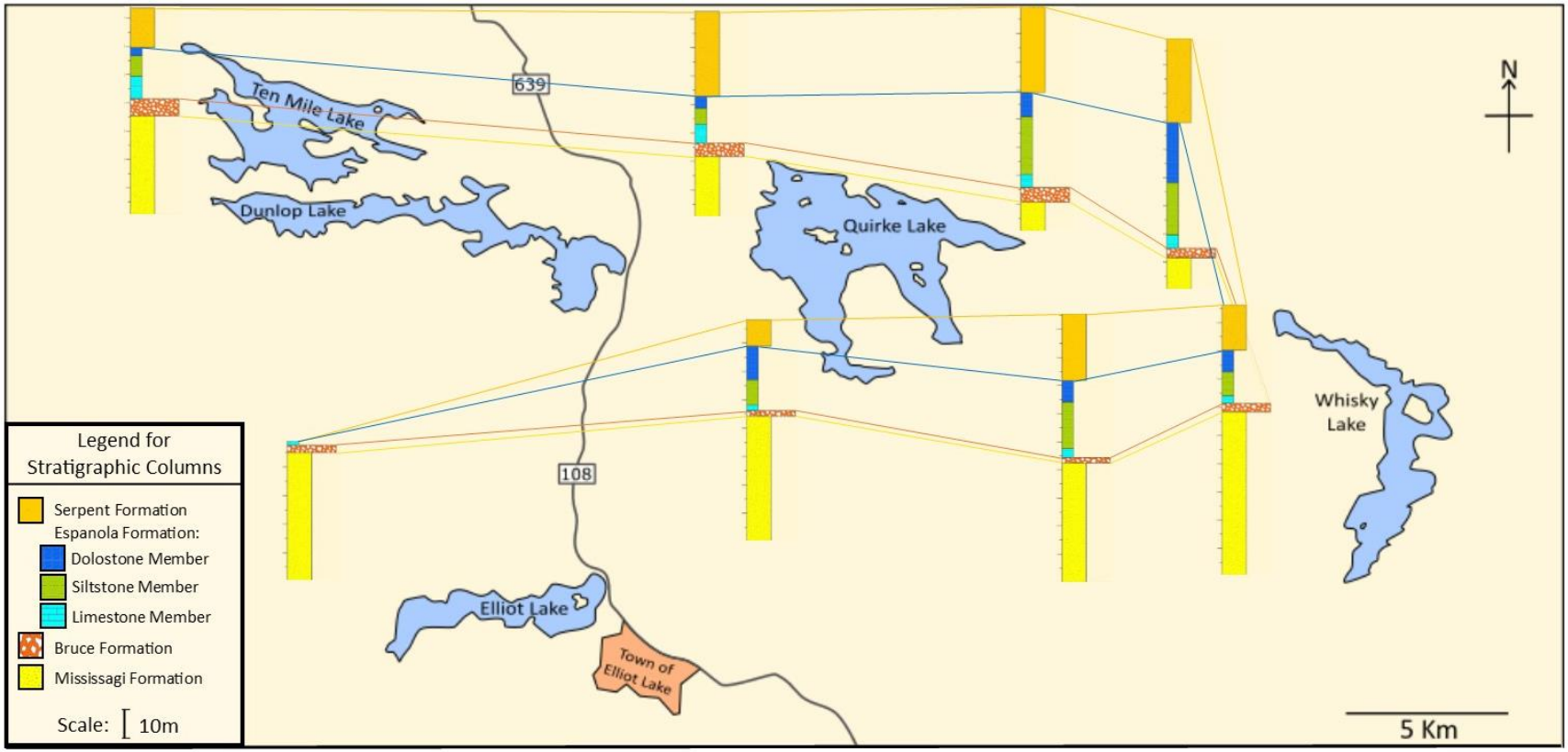

Figure 87: Fence diagram of the Bruce glacial cycle formations (Mississagi, Bruce, Espanola, and Serpent Formations) in the Elliot Lake area. The Serpent Formation has been eroded away to the west of Elliot Lake and the Gowganda Formation directly overlies the Espanola Formation in this area. Thickness of all formations in the Bruce glacial cycle is variable, with the Missisagi Formation thickening to the south, the Bruce Formation thining to the south, and the Espanola Formation and Serpent Formations having irregular thicknesses. Stratigraphic sections generated from Robertson (1957a); (1957b); (1958a); (1958b); (1959a); (1959b); (1963a); (1963b).

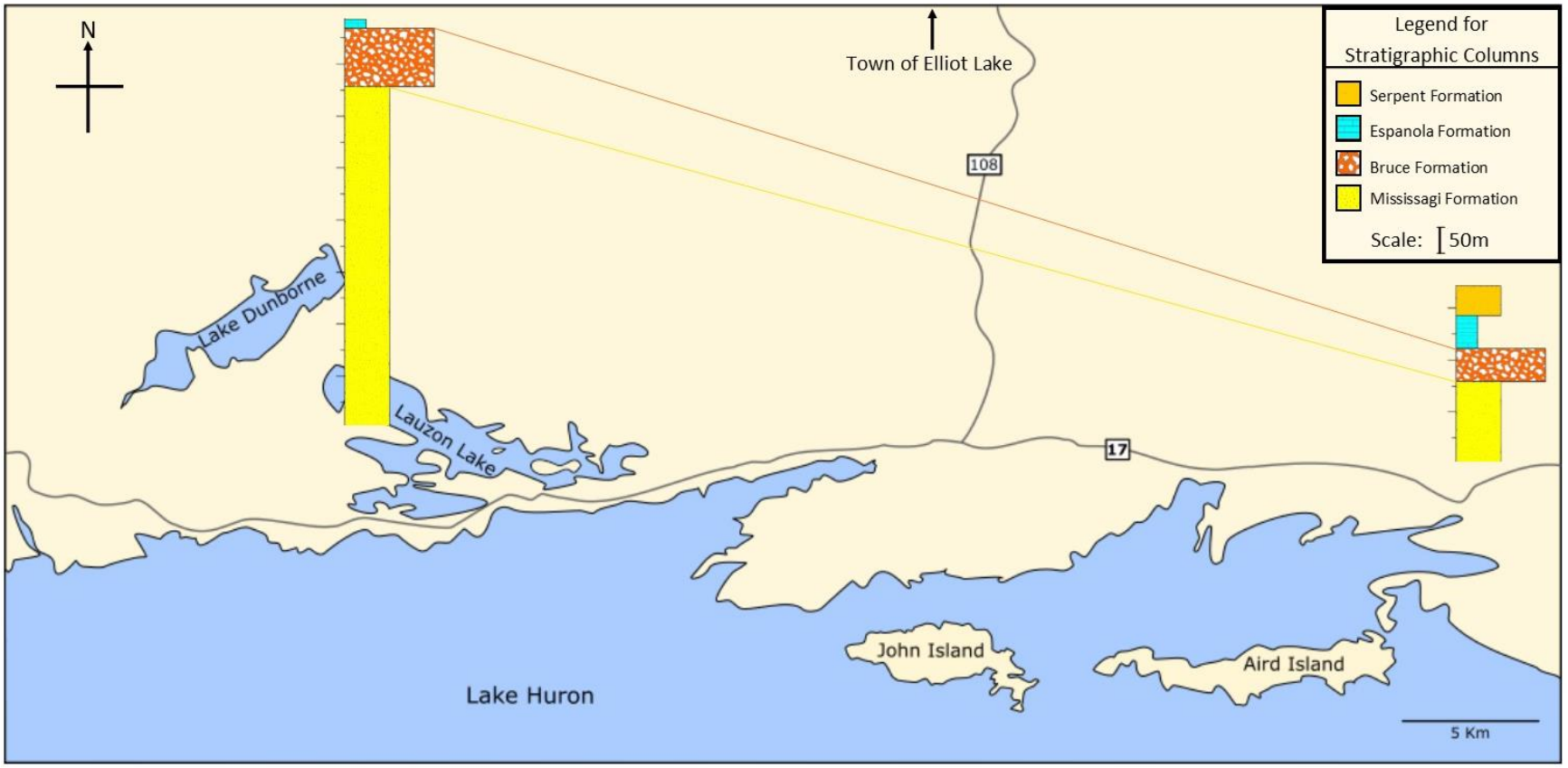

Figure 88: Fence diagram of the Bruce glacial cycle formations (Mississagi, Bruce, Espanola, and Serpent Formations) along the north shore of Lake Huron between Dunborne Lake and Aird Island. In the Lauzon Lake and Dunborne Lake areas the Serpent Formation has been eroded away and the Espanola Formation is directly overlain by the Gowganada Formation. The Mississagi Formation decreases dramatically in thickness from the Dunborne Lake area eastwards towards the Aird Island area. Stratigraphic sections generated from Robertson and Abraham (1960); Robertson (1965).

The Huronian Supergroup is a siliciclastic-dominated succession that is similar in thickness and stratigraphy to classic descriptions of post-rift successions. Typical post-rift basins overlie thinned continental crust with basins, plateaus, and embayments that contain 8-13km of sediments, which is consistent with what is observed from the stratigraphy of the Huronian Supergroup starting from the basal Matinenda Formation, which overlies the synrift volcanics (Bond et al., 2005) and sediments of the rift-fill Livingston Creek Formation. The post-rift siliciclastic successions are preserved through thermal and load-driven subsidence, which also results in onlap of the sedimentary prism landward with variations occurring as a result of sea-level changes (Bond et al., 1995). Furthermore, as has already been suggested, in active rift valleys regional drainage is directed away from the valley axis (Hoffman, 2013). If the Bruce Formation was indeed deposited by an ice sheet that initiated as a mountain glacier situated on an uplifted shoulder of a rift basin (Young, 2014), then it seems highly improbable that the Bruce glacial diamictites would contain a large abundance of sediment derived from granites sourced from the north (Casshyap, 1969), as this would involve moving sediment southward against the paleoslope of an uplifted rift arm.

In the case of the Huronian Supergroup, glacial loading and isostatic rebound would be the driving factors in preserving superimposed transgressive and regressive systems tracts in the sedimentary prism. The resulting stratigraphy is variable, and the Bruce glacial cycle preserved within the Mississagi, Bruce, Espanola, and Serpent Formations records lateral variability in the thicknesses of formations, as well as areas of non-deposition or erosion (Figure 87, 88). Isostatic loading in response to glacial activity may have also had an effect on fault movement. Reactivation of pre-existing basement faults as a result of ice advance has been a

documented phenomenon in the Emme Delta of northwest Germany, and further slippage may have been generated by subsequent glacial retreat and sea level rise due to loading by sediment and water (Brandes et al., 2011). An overlying body of water may have also created a high pore pressure and facilitated slip along faults (Brandes et al., 2011). All of these are important considerations when defining a rift-drift transition time for the Huronian Supergroup, as contemporaneous faulting and seismic activity affecting the lowermost three Groups of the Huronian does not necessitate that the area was actively rifting during their deposition. In particular, the Espanola Formation contains a number of syndepositional deformation features including contorted bedding, slump structures, load features, and water and sediment escape structures (Long, 2004; Young et al., 2001; Al-Hashim, 2016). Syn-depositional faults, breccias, and clastic dykes that formed contemporaneously during deposition of Espanola sediments have been suggested as representing tectonic reactivation during the rift-drift transition (e.g. Eisbacher, 1970; Young, 1972; Al-Hashim, 2016). While these features may be suggestive of activity along normal faults during deposition of the Espanola and the lower Huronian, claiming them as evidence for rift-related seismic activity during this time is erroneous, as a number of other causes could account for movement along these faults. If it is largely accepted that the Bruce Formation represents a glacial event, then isostatic readjustment, sediment loading or loading by a post-glacial marine incursion are all viable alternatives to explain fault movement aside from other explanations that have already been provided including lithospheric flexure during passive margin subsidence or far-field effects of other tectonic activity occurring on the Superior craton (Hoffman, 2013). Another very common feature of passive margin stratigraphy that has not been discussed yet is the common presence of growth faults in these settings

(Sheridan, 1981; Winker and Edwards, 1983). Growth faults are normal listric faults that can penetrate to depths of 10km, be active for long periods of time, and have a large influence on the local topography and depositional patterns (Bond et al., 1995). Therefore, passive margin sedimentary architecture will be influenced by synsedimentary faulting driven by subsidence related tectonic activity, along with isostatic readjustments due to glacial and marine advance-retreat cycles. These likely had a strong influence on the Huronian stratigraphy.

12.2 BRUCE GLACIAL CYCLE SUMMARY

Evidence for initiation of the Bruce glacial event is preserved within the upper Mississagi Formation, a sandstone Formation that is dominated by large- and medium-scale cross-stratified beds. The majority of the upper Mississagi Formation is interpreted to have been deposited in a distal braided fluvial environment, based primarily on the repetitive nature of planar and trough cross-stratification with no evidence for cyclicity (Long, 1976; cf., Pretious and Blench, 1951; Neill, 1969; Allen and Collinson, 1974). A fluvial nature is also supported by the presence of unimodal paleocurrent distributions and a lack of tidal structures or extensive mudstone units that are associated with marine environments (Parvianinen, 1973; Long, 1976, 1978). It is well known that Precambrian river systems were dominantly braided, due to the absence of microbial and macrofaunal binding (Schumm, 1968; Cotter, 1978; Eriksson et al., 1998). This would also explain the lack of cyclicity and floodplain facies as these braided fluvial systems would experience high avulsion rates. The upper Mississagi braid plain may have been similar to the late Neoproterozoic-early Cambrian Backbone Ranges and Vampire Formation braid plain deposits in northwestern Canada where river channels were recognized to reach widths of up to several kilometers (MacNaughton et al., 1997). Similarly, in the absence of vegetative binding, braid plains would reach potentially enormous sizes (Fedo and Prave, 1991; McCormick and Grotzinger, 1993), and where in contact with the shoreline, would also be characterised by rapidly shifting stream mouths (MacNaughton et al., 1997). Advancement of the Bruce ice sheet into the Huronian basin is heralded in many places by a distinct decrease in the sorting of sediments, and typically, an increase in grainsize. Furthermore, an increase in the presence of clay partings and heterolithic laminated cross-beds in many places suggests a shift

to a submergent braid-delta environment in the uppermost Mississagi Formation. Again, the lack of any logical hierarchy of bedforms is likely due to the extremely mobile nature of the fluvial channels, resulting in little else but channel and mouth bar sediments being preserved.

The contact between the sandstones of the upper Mississagi Formation and the diamictites of the Bruce Formation is most commonly sharp to slightly gradational and typically involves uptake and erosion of sands from the upper Mississagi Formation into the basal Bruce Formation. Erosion, and the presence of glaciotectonic features in the upper Mississagi Formation, indicates that the Bruce Formation was likely grounded on the unconsolidated sands in many parts of the Huronian basin at the time of advancement. However, rapid delamination of the Bruce ice sheet is suggested by the predominance of subaqueous and glaciomarine sediments in the Bruce Formation. The predominant facies types are massive diamictite with lesser laminated to weakly laminated diamictite in the Birch Point and Iroquois Bay areas. These sediments are interpreted to have been deposited subaqueously, beneath a floating ice shelf and in the glaciomarine environment. Sediments beneath floating ice shelves of dry-based glaciers are predominantly derived from melting of the shelf above (which is a slow process) and results in massive diamictites such as those preserved in the Bruce Formation (Carey and Ahmad, 1961). The majority of the Bruce Formation being deposited subaqueously indicates that delamination of the Bruce ice sheet occurred fairly rapidly following ice advance into the basin. The suggested method of delamination is by isostatic adjustment of the basement floor by ice loading, which is a response that has been noted in other glacial sequences (Muszynski and Birchfield, 1987; Visser, 1991). It is important to consider that the Superior craton was only the approximate size of modern day Antarctica, much smaller than

North America, and thus would have likely undergone rapid denudation because of its small size during the Bruce ice sheet advance. Likewise, the sharp contact between the Bruce Formation diamictites and the overlying carbonate-bearing sediments of the Espanola Formation suggests that retreat of the Bruce ice sheet was catastrophic.

A 0.5-3m thick laminated siltstone unit separating the Bruce and Espanola Formations is interpreted to represent a rain-out deposit formed after the rapid retreat of the Bruce ice sheet. The probable mechanism for mobilization and transportation of most of the silt is by aeolian processes. Another feature of pre-vegetated continental margin deposits is enhanced aeolian activity (Dalrymple et al., 1985). A predominance of silt-rich offshore facies and loess units has been observed from other pre-vegetative assemblages and is believed to be a result of this enhanced aeolian activity (MacNaughton et al., 1997). The Espanola Formation, into the lower Serpent Formation, is interpreted to represent a broadly shallowing upwards sequence, from a distal shelf to nearshore shelf environment. Sediments of the lower Espanola Formation are dominated by variably contorted parallel lamination and graded beds, while the upper sediments are in addition dominated by ripple lamination, hummocky cross-stratification, cross-bedding, and intraformational conglomerates. This overall trend indicates a shift from quiet, deeper water deposition primarily through rain-out and mass movement, to a shallower and higher-energy nearshore environment experiencing fluctuating influence by wave- tide- and storm-activity. The gradual regressive sequence preserved in the Espanola Formation is continued upwards through the Serpent Formation, with evidence of a nearshore environment in the lower stratigraphy in the form of hummocky cross-stratification and tidal bedding

deposited by storm and tidal activity, respectively. This is transitional upwards into a fluvially-influenced deltaic environment with abundant mud rip-ups in trough cross-stratified beds.

The tectonic setting of the Bruce glacial event was likely similar to the modern day east coast of North America, a passive margin sequence that is punctuated by transgressions and regressions brought about by glacial cycles. The Scotian Shelf, located just off the eastern coast of Canada, is a continental margin environment that experienced glacial ice cover several times during the middle to late Quaternary (Mosher et al., 1989; Stea et al., 1998). Sedimentation on the adjacent slope was dominated by ice-rafted detritus and glaciomarine muds (Hill, 1984; Mosher et al., 1994). While the outer shelf is dominated by laterally continuous till units, the inability to observe them directly means that there is still ambiguity regarding whether or not they were deposited by grounded ice or by ice-contact debris flows (Stravers and Powell, 1997; Gipp, 2000). Several variations between the two, including the predominance of extensive braid plains in Huronian times, results in somewhat different stratigraphies, but sea-level rise and fall during ice advance and retreat still had a strong influence on both. Furthermore, it has been suggested here that the relatively small Superior craton would have experienced more extreme denudation, and thus an ice shelf would have developed over most of the Huronian Basin.

12.3 SOURCE OF THE CARBONATE FRACTION

There is also speculation regarding the depositional environment of the Espanola Formation, with suggestions including both marine and lacustrine settings. The results of this study indicate that the Espanola Formation was deposited largely in an offshore to nearshore

marine environment, but with varying and sometimes considerable influence by freshwater input. Previously interpreted isotopic data and mineralogical analysis of the lower carbonate units has been used to suggest a lacustrine environment of deposition (Veizer et al., 1992). A marine origin is favoured however, based on the ability to correlate the Espanola Formation to the carbonate units in the Snowy Pass Supergroup, the transgressive nature of the stratigraphy, evidence for tidal influence, and the large size of the basin (Bekker et al., 2005). The results of this study support the interpretation of a marine setting for the Espanola Formation carbonates, but also support the idea that there was strong influence by meteoric waters (Veizer et al., 1992).

In conjunction with uncertainty regarding the depositional setting of the Espanola Formation, several theories have been proposed for the origin of the carbonate fraction. The presence of a carbonate formation overlying the Bruce glacial event, but not above the Huronian glacial events that precede and follow it, indicates that the environment at the end of the Bruce glacial was unique in some way. Theories as to the origin of the carbonate can be divided into three general categories, as outlined by Eggertson (1975). Firstly, carbonate precipitation may have been organically facilitated. Several studies of the Espanola Formation have outlined the presence of probable to possible microbial structures, including stratiform stromatolites, as well as crustose and small columnar stromatolites (Long, 1976; Hofmann et al., 1980; Long, 1998, 2009; Bekker et al., 2005; Al-Hashim, 2016). The presence of biologically produced structures, mostly observed in the upper parts of the formation suggest that some of the carbonate may have an organically derived origin (Veizer et al., 1992). Another source for carbonate that has been suggested is brine concentration through freezing of salt water

(Young, 1973). However, given that the carbonates largely lack evidence of coincident glacial activity and were deposited during glacial retreat, it seems unlikely that this process would have generated most of the carbonates present within the Espanola. There is also a lack of associated evaporitic minerals that would precipitate through this process alongside carbonate, although metamorphic scapolite has been described, even as abundant, from several units in the Espanola Formation and has been suggested to be metamorphic after evaporitic minerals (Eggertson, 1975; Young, 1985; Young, 2013a; Al-Hashim, 2016).

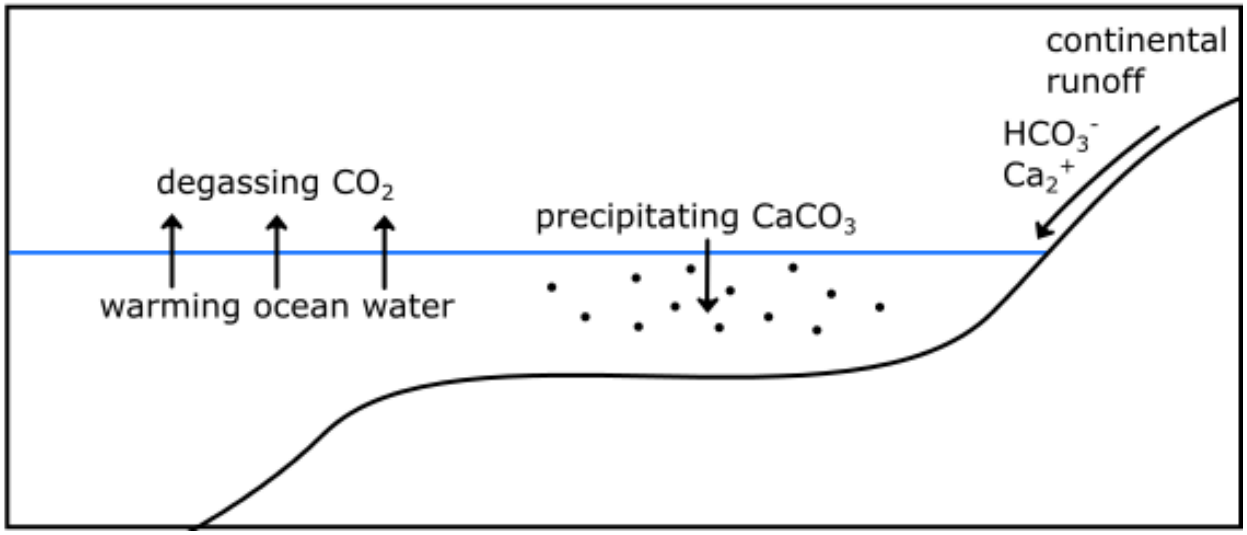

Figure 89: Schematic diagram outlining one hypothesis describing the driving mechanisms behind the precipitation of the carbonate fraction in cap carbonates. A combination of changes in CO_2 fugacity in warming ocean water coupled with input of high alkalinity continental runoff influences the precipitation of carbonate minerals. Modified from Shields, 2013.

There are a number of other inorganic mechanisms that could have influenced the precipitation of the carbonate fraction in the Espanola Formation. One possible mechanism that has been suggested in previous studies of the Espanola Formation is through a combination of releasing of CO_2 from warming seawaters increasing weathering rates and high

inputs of glacial meltwaters carrying cations, which would increase alkalinity and drive precipitation (Figure 89) (Smalley, 1971; Parviainen, 1973; Eggertson, 1975; Bekker et al., 2005). Increased weathering in high atmospheric CO_2 conditions following glaciation would result in highly alkaline continental runoff (Hoffman, 2011), and this freshwater input probably had considerable influence on the deposition of the Espanola Formation carbonates. The Y/Ho ratios and REE patterns that are hypothesized to show influence by riverine waters in this study would seem to support the hypothesis that much of the Espanola Formation carbonates were partially controlled by continental runoff, including input of a considerable amount of glacial meltwater. An alternative explanation for precipitation of some of the carbonate fraction, which was suggested in this study, and has been proposed as a factor for Neoproterozoic cap carbonates, is precipitation of carbonates driven by methane release by gas hydrate destabilization (Kennedy et al., 2001; Jiang et al., 2003; Wang et al., 2008). This process could have had some influence on the laminated dropstone facies in particular, with the extremely negative $\delta^{13}C_{carb}$ values being associated with this unit.

It is also worth mentioning that resedimentation may have had a large impact on the final distribution and setting of the carbonate fraction in the Espanola Formation. Petrographic characteristics of certain carbonate-rich units show aggregates of well-rounded carbonate grains that fall within the same sediment size as associated siliciclastic units, as well as grading of carbonate laminae and beds (Young, 1973; Bernstein, 1985; Bernstein and Young, 1990; Al-Hashim, 2016). There is also abundant evidence throughout the stratigraphy of the Espanola Formation for processes of soft-sediment deformation including slumping and mass movement that probably redistributed much of the carbonate fraction to deeper or more distal shelf

environments. It is possible that resedimentation processes may have been so predominant as to have influenced most of the carbonate fraction in the units along the north shore of Lake Huron (Bernstein and Young, 1990). This hypothesis seems plausible as there is a high degree of slumping particularly in this area. Mass movement and resedimentation processes have been suggested to be the result of what was likely high rates of carbonate accumulation, particularly at the beginning of deposition of the Espanola, and that as deposition slowed, a more typical ramp-like morphology took hold with conditions favourable for dolomitization of the upper stratigraphy (Bekker et al., 2005).

12.4 COMPARISON TO NEOPROTEROZOIC CAP CARBONATES

One of the major goals that this study set out to accomplish was to investigate the Espanola Formation and especially the geochemistry and isotopic composition of the carbonate fraction to compare and contrast with the younger and better studied Neoproterozoic cap carbonates. This is important in light of recent investigations that have argued the possibility of the Espanola Formation as representing a cap carbonate that was deposited under similar conditions to the later Neoproterozoic cap carbonates (Bekker et al., 2005; Hoffman, 2013). Furthermore, the very recent exploration of another possible Paleoproterozoic cap carbonate in India, which has been argued to be correlative with the Espanola Formation (Mohanty et al., 2015; Sarangi et al., 2017), starts to raise more possibilities about the implications of the Bruce glacial cycle and a Paleoproterozoic ‘Snowball Earth’ event. Laterally continuous carbonate units that overlie Cryogenian glacial deposits are referred to as ‘cap carbonates’ and are known

to be associated with flooding as a result of ice-melt (Kennedy, 1996; Bertrand-Safarti et al., 1997; Hoffman et al., 2007), but their exact mechanism of precipitation is still in debate. Comparison of the Espanola Formation to Neoproterozoic cap carbonates is further convoluted by the fact that there are lithological and isotopic differences between even Sturtian and Marinoan cap carbonates that complicates the idea of a uniform theory to explain their mechanism of deposition (Kennedy et al., 1998; Halverson and Shields, 2011). This study added to previously completed geochemical and isotopic investigations of the Espanola Formation with the result of uncovering some new features of the carbonates that support the hypothesis that they may have been precipitated under similar conditions to some of the Neoproterozoic cap carbonates. In this discussion some of the previous comparisons made between the Espanola Formation and Neoproterozoic cap carbonates will be considered in light of the new data collected in this study.

Bekker et al. (2005) suggested that the Espanola Formation represents a 'cap carbonate' akin in some ways to Neoproterozoic cap carbonates because of their similar tectonic settings, their largely subtidal deposition, and depletion in $\delta^{13}C$. One inconsistency that Bekker et al. (2005) outlined was a lack of stratigraphic or facies-related trends in the $\delta^{13}C$ values, whereas Neoproterozoic cap carbonates record $\delta^{13}C$ trends with time and basin position (cf. Kennedy et al., 1996; Hoffman et al., 1998; Halverson et al., 2002). However, in light of an upwards increasing trend of $\delta^{13}C$ observed in drill hole E150-2 in this study, a comparison was made with the data collected from drill hole E150-1 by Bekker et al. (2005). Similar values are noted between the two drill holes, suggesting that the same pattern is present in both. A trend of broadly increasing $\delta^{13}C_{carb}$ values from ~-4‰ to -2.5‰ preserved within drill hole E150-2 is

startlingly similar to the values previously collected from drill hole E150-1 by Bekker et al. (2005) and suggests that there is stratigraphic control on $\delta^{13}C$ of the middle and upper stratigraphy of the Espanola Formation. This trend of increasing $\delta^{13}C$ in the Espanola Formation stratigraphy falls within a similar pattern to what is observed in a Neoproterozoic cap carbonate from South Australia (Giddings and Wallace, 2009) and is suggested to be the result of a broadly shallowing upwards sequence based on the observation that shallow-water carbonates are $\delta^{13}C$ enriched relative to their deep-water counterparts (cf. James et al., 2001; Hoffman et al., 2007; Jiang et al., 2007). This interpretation fits well with what is recognizable from the sedimentology of the Espanola Formation. One possible explanation for this trend is that it is a reflection of upwelling of lower $\delta^{13}C$ deep water having a stronger influence on the middle and lower stratigraphy, and with the gradual shallowing and migration of the shoreline causing a decrease in this influence with time. This process is observed in modern systems (cf. Grotzinger and Knoll, 1995) and has been suggested as a possible mechanism for the systematic trend of lower $\delta^{13}C$ in deeper water carbonates of the cap carbonate in the Windemere Supergroup in northwestern Canada (James et al., 2001). Lower amounts of organic matter associated with the Paleoproterozoic Espanola Formation may suggest that this process is inadequate to explain the trend in this instance. A possible alternative explanation could be that the trend is a result of a gradual decrease in the amount of influence of meltwater with time.

Another discrepancy between Neoproterozoic cap carbonates and the Espanola Formation is the lack of a basal cap dolostone unit in the Espanola Formation. These are thin basal transgressive tracts of cap carbonate sequences commonly associated with Neoproterozoic cap carbonates (Hoffman and Schrag, 2002). Within cap dolostones are a

distinctive suite of sedimentary and biogenic structures such as giant wave ripples (Allen and Hoffman, 2005), sheet-crack cements, roll-up structures, and tube-like stromatolites (cf. Hoffman and Schrag, 2002; Corsetti and Kaufman, 2003). Bekker et al. (2005) suggested that some of the structures unique to the Neoproterozoic cap carbonates may be due to higher rates of inorganic precipitation as a result of supersaturation of carbonate alkalinity and that oceanic carbonate saturation may have been lower in the Paleoproterozoic glacial events. This explanation would fit well with the observation that several of the sedimentary structures such as sheet cracks and roll-up structures are present on Archean carbonate platforms and have been attributed to high carbonate alkalinities (Simonson et al., 1993; Sumner and Grotzinger, 2000). The unusual giant wave ripples are believed to be reflective of high storm intensity due to greater surface temperature gradients following deglaciation (Emanuel, 1987; Hoffman and Schrag, 2002). An alternative explanation for the lack of a cap dolostone unit in the Espanola Formation suggests that it can be largely attributed to a depth and depositional environment factor. The unique sedimentary structures associated with cap dolostones, including sorted peloids, low-angle cross-bedding, stromatolites, and wave ripples indicate that cap dolostones formed above wave base (Hoffman, 2011). Given the interpretation of the lower Espanola Formation being deposited predominantly in a deeper shelf environment, it does not seem unusual that a cap dolostone is not preserved at the base of the Formation.

One last discrepancy between Neoproterozoic cap carbonates and the Espanola Formation that was outlined by Young (2013a) is the incorporation of larger amounts of siliciclastics within the Espanola Formation, which adds considerable thickness to the stratigraphy. Young (2013a) considered this to be an important distinction between the

Espanola Formation and the Neoproterozoic cap carbonates because of the interpretation that Neoproterozoic cap carbonates formed rapidly and coincidentally with post-glacial sea-level rise, prior to the introduction of siliciclastics (Hoffman et al., 1998; Hoffman, 2011). The greater incorporation of siliciclastics in the Espanola Formation, and apparent delay in carbonate precipitation, can likely be explained by the same interpretations put forth by Bekker et al. (2005) to explain the lack of specific sedimentary structures; i.e. an overall lower oceanic carbonate saturation. Analysis of the chemical index of alteration from mature siliciclastics of the Huronian Supergroup and the laterally correlative Snowy Pass Supergroup indicate extreme weathering (Houston et al., 1981; Nesbitt and Young, 1982; Bekker, 1998). Relatively lower carbonate saturation conditions following the Bruce glacial event would indicate that precipitation of the carbonate fraction in the Espanola Formation may have been more dependent upon continent-derived alkalinity than its Neoproterozoic counterparts. Furthermore, carbonate accumulation would also be dependent upon an intricate balance between the introduction of alkalinity to seawater by high weathering rates and the subsequent oceanic drop in pH and rise in carbonate compensation depth (Bekker et al., 2005).

13 CONCLUSIONS

The Bruce glacial event represents the second of three glacial cycles preserved in the Paleoproterozoic Huronian Supergroup, a ~12km thick sequence of mostly sedimentary rocks that lies along the southern margin of the Superior Province. What makes the Bruce glacial cycle unique apart from the overlying and underlying cycles is the presence of a cap carbonate unit, the Espanola Formation, directly overlying glacial sediments of the Bruce Formation. Cap carbonate units are ubiquitous in Neoproterozoic glacial successions where they likewise occur directly overlying glacial sediments and have long been recognized as being associated with deglaciation (cf. Kennedy, 1996; Hoffman et al., 1997). The exclusive presence of these cap carbonates in association with glacial events in the Paleoproterozoic indicates that they are the result of unique environmental conditions (cf. Kennedy, 1996; Hoffman et al., 1998; Kennedy et al., 2001; Shields, 2005). In light of recent investigations that propose (Bekker et al., 2005) or deny (Young, 2013a) the possibility of the Espanola Formation being a cap carbonate resulting from a possible Paleoproterozoic 'Snowball Earth' event, the sedimentological, geochemical and isotopic composition of the Bruce glacial cycle was analyzed in this investigation.

The sedimentological evidence suggests that the Bruce glacial event took place on a passive margin and was immediately preceded by a braided fluvial to fluviodeltaic environment. These sediments are preserved within the upper Mississagi Formation, which is dominated by planar and trough cross-stratified sandstones and massive units that generally increase in grainsize and decrease in sorting prior to ice override. The typically sharp contact between the sandstones of the Mississagi Formation and the diamictites of the Bruce Formation indicates that the Bruce ice sheet was likely largely grounded as it entered the basin. This interpretation

is supported by an erosional uptake of Mississagi sand into the base of the Bruce Formation in several places. After entering the basin as a grounded ice sheet, rapid delamination and development of a floating ice shelf occurred, leading to the majority of the Bruce Formation sediments being deposited in a subaqueous setting. Facies of the Bruce Formation are overwhelmingly laterally extensive massive diamictites with lesser weakly laminated to laminated diamictites deposited beneath the floating ice. Following rapid retreat of the Bruce ice sheet, a laterally continuous siltstone unit separating the overlying carbonate facies of the Espanola Formation from the underlying glacial sediments of the Bruce Formation is interpreted here to be a wind-blown silt unit deposited in an offshore environment. Overlying the siltstone unit, the Espanola Formation stratigraphy records a gradual transition from a deeper, offshore environment, to a shallow, nearshore setting. The lower stratigraphy is dominated by deposits of rain-out such as the laminated carbonate and siltstone facies. Resedimentation and mass movement contort and slump these facies and form turbidity current deposits. The middle to upper stratigraphy of the Espanola Formation gradually record a shallowing upwards with a shift to a predominance of cross-stratification, ripple lamination, hummocky cross-lamination, and intraformational conglomerate beds. These units were deposited in a nearshore environment experiencing varying influence by tide, storm, and wave activity.

The geochemical and isotopic evidence of the Espanola Formation is largely consistent with the sedimentological interpretation and also provides new evidence to support the idea that the Espanola Formation carbonates were deposited through similar processes and in similar conditions to some of the Neoproterozoic cap carbonates. Aside from the consistent

negative $\delta^{13}C_{carb}$ that is both a feature of the Espanola Formation and the Neoproterozoic cap carbonates (cf. Bekker et al., 2005), two other similar features were identified in this study. The first is an extreme negative $\delta^{13}C_{carb}$ excursion in the laminated dropstone facies that is on the same order of magnitude as the Wonoka-Shuram anomaly (Halverson et al., 2005). This facies also contains consistent negative Eu anomalies. These geochemical features have been suggested to be the result of highly reducing fluids derived from methane seepage promoted during deglacial warming.

The second interesting result is an upwards trend in $\delta^{13}C_{carb}$ in the middle and upper stratigraphy of the Espanola Formation in drill hole E150-2. Values gradually shift from ~-4‰ to -2.5‰ over approximately 110m. This is a trend that has been observed in a Cryogenian cap carbonate in South Australia and is interpreted to be the result of an upwards shallowing (Giddings and Wallace, 2009). An upwards shallowing trend is consistent with the sedimentological interpretation of the Espanola Formation and suggests that depth may have also been a factor in the upwards increasing trend of $\delta^{13}C_{carb}$ values.

REE pattern analysis of the carbonate fraction also uncovered two distinct patterns. The first is recognizable by the presence of a negative Eu anomaly and is present within all samples from the laminated dropstone facies, as well as from several samples of the interlaminated carbonate and siltstone lithofacies association. Reducing fluids containing very light methane carbon causing remobilization of reduced Eu^{+2} is suggested to be the cause of the negative Eu anomaly in these units. The second pattern has a middle REE-enrichment that produces a 'hat-shaped' appearance. These patterns are dominant throughout the remainder of the Espanola Formation stratigraphy and are representative of a seawater signature with varying amounts of

freshwater influence. The last interesting result of the geochemical analysis of the Espanola Formation is the discovery of a unique Ba-rich horizon present approximately 10m above the contact with the Bruce Formation in drill hole E150-1. This horizon is associated with strong positive Eu anomalies and may represent a short-lived introduction of offshore, hydrothermally-dominated fluids.

The new geochemical and isotopic evidence presented in this study suggests that there are more similarities between the Espanola Formation and Neoproterozoic cap carbonates than previously thought. Some parallels were also disclosed between the Espanola Formation and the Sausar Group in India; another possible Paleoproterozoic cap carbonate (Mohanty et al., 2014; Sarangi et al., 2017). These new connections made between Neoproterozoic and Paleoproterozoic cap carbonates indicate that similar processes and conditions may have influenced their deposition.

The uppermost Espanola Formation sediments gradually transition into the lower Serpent Formation via an overall decrease and subsequent loss of carbonate-rich interbeds. Carbonate-rich interbeds occur in packages alongside trough cross-stratification, ripple lamination, parallel lamination, and hummocky cross-stratification. Deposition of the lower Serpent Formation was in a nearshore to fluvial environment with evidence for tidal influence. The Serpent Formation sediments conclude the isostatic rebound cycle following retreat of the Bruce ice sheet.

14 REFERENCES

Aalto, K.R., 1981. The Late Precambrian Toby Formation of British Columbia, Idaho, and Washington. In, Hambrey, M.J., and Harland, W.B., eds., Pre-Pleistocene tillites. I.G.C.P. Project 38, Cambridge University Press, 731-735.

Abbott, A. N., Haley, B. A., McManus, J., Reimers, C. E., 2015. The sedimentary flux of dissolved rare earth elements to the ocean. Geochimica et Cosmochimica Acta 154, 186–200.

Aigner, T., 1985. Storm depositional systems. Dynamic Stratigraphy in Modern and Ancient Shallow-marine Sequences. Lecture Notes in Earth Science 3. Springer- Verlag, Berlin, 174p.

Alibo, D. S., Nozaki, Y., 1999. Rare earth elements in seawater: particle association, shale-normalization, and Ce oxidation. Geochimica et Cosmochimica Acta 63, 363–372.

Al-Hashim, Mansour H., 2016. Sedimentology and geochemistry of the mixed carbonate-siliciclastic Espanola Formation, Paleoproterozoic Huronian Supergroup, Bruce Mines-Elliot Lake Area, Ontario, Canada. Western University, Department of Geology, 287p.

Allen, J.R.L., 1963. Asymmetrical ripple marks and the origin of waterlaid cosets of cross-strata. Liverpool Manchr. The Journal of Geology 3, 187-236.

Allen, J.R.L., 1982. Sedimentary structures, their character and physical basis; I, Amsterdam, Netherlands, Elsevier Science Publishing Co., Amsterdam, 611p.

Allen, J.R.L., Banks, N.L., 1972. An interpretation and analysis of recumbent folded deformed cross-bedding. Sedimentology 19, 257-283.

Allen, J.R.L., Collinson, J.D., 1974. The superimposition and classification of dunes formed by unidirectional aqueous flows. Sedimentary Geology 12, 169-178.

Allen, P.A., Allen, J.R., 2005. Basin analysis; principles and applications. Second edition. Blackwell Publishing Ltd. Oxford, United Kingdom, 549p.

Allen, P.A., Hoffman, P.F., 2005. Extreme winds and waves in the aftermath of a Neoproterozoic glaciation. Nature 433, 123-127.

Allen, P.A., Etienne, J.L., 2008. Sedimentary challenge to Snowball Earth. Nature Geoscience 1, 817-825.

Allen, P.A., Leather, J., Brasier, M.D., Riew, R., Mccarron, M., Le Guerroué, E., Etienne, J.L., Cossi, A., 2011. The Abu Mahara Group (Ghubrah and Fiq formations), Jabal Akhdar, Oman. In: Arnaud, E., Halverson, G.P., Shields-Zhou, G. (Eds.), The Geological Record of Neoproterozoic Glaciations. Geological Society, London, Memoirs 36, 251–262.

Aloisi, G., Bouloubassi, I., Heijs, S.K., Pancost, R.D., Pierre, C., Damste, J.S.S., Gottschal, J.C., Forney, L.J., Rouchy, J.M., 2002. CH_4-consuming microorganisms and the formation of carbonate crusts at cold seeps. Earth and Planetary Science Letters 203, 195–203.

Anderson, J.B., 1983. Ancient glacial-marine deposits: their spatial and temporal distribution. In: Anderson, J.B., Molnia, B.F. (Eds.), Glacial-Marine Sedimentation. Plenum Press, New York, 3-92.

Anderson, J.B., Brake, C. Domack, E., Myers, N., Wright, R., 1983. Development of a polar glacial-marine sedimentation model from Antarctic Quaternary deposits and glaciological information. In: Molnia B.F. (Ed), Glacial-Marine Sedimentation. Springer, Boston, MA, 233-264.

Anderson, T.F., Arthur, M.A., 1983. Stable isotopes of oxygen and carbon and their application to sedimentological and palaeoenvironmental problems. In: Arthur, M.A. Anderson, T.F. Kaplan, I.R. Veizer, J., Land, L.S., (Eds.), Stable Isotopes in Sedimentary Geochemistry. Society of Economic Palaeontologists and Mineralogists Short Course 10, Dallas, 1–151.

Anderton, R., 1976. Tidal shelf sedimentation: an example from the Scottish Dalradian. Sedimentology 23, 427-458.

Anderton, R., 1982. Dalradian deposition and the late Precambrian-Cambrian history of the N Atlantic region; a review of the early evolution of the Iapetus Ocean. Journal of the Geological Society of London 139, 421-431.

Andrews, J.T., Matsch, C.L., 1983. Glacial Marine Sediments and Sedimentation: an Annotated Bibliography. Geoabstracts, Norwich.

Ashley, G.M., 1975. Rhythmic sedimentation in glacial Lake Hitchcock, Massachusetts-Connecticut, *in* Jopling, A.V., McDonald, B.C. (eds.), Glaciofluvial and Glaciolacustrine Sedimentation: Society of Economic Paleontologists and Mineralogists Special Publication 23, 304-320.

Ashley, G.M., 1990. Classification of large-scale subaqueous bedforms: a new look at an old problem. Journal of Sedimentary Petrology 60, 160-172.

Ashley, G.M., Smith, N.D., 2000. Marine sedimentation at a calving glacier margin. Geological Society of America Bulletin 112 (5), 657-667.

Awramik, S.M., and Vanyo, J.P., 1986. Heliotropism in modern stromatolites. Science 231 (4743), 1279-1281.

Bachan, A., Kump, L.R., 2015. The rise of oxygen and siderite oxidation during the Lomagundi Event. PNAS 112 (21), 6562-6567.

Banerjee, I., McDonald, B. C., 1975. Nature of esker sedimentation. In: A. V. Jopling and B. C. McDonald (Editors), Glaciofluvial and Glaciolacustrine Sedimentation. Society of Economic Palaeontologists and Mineralogists Special Publication 23, 132-154.

Banks, N.L., 1973. Tide-dominated off-shore sedimentation, Lower Cambrian, north Norway. Sedimentology 20, 213-228.

Bates, M.P, and Halls, H.C., 1990. Regional variation in paleomagnetic polarity of the Matachewan dyke swarm related to the Kapuskasing Structural Zone, Ontario. Canadian Journal of Earth Science 27, 200-211.

Bau, M., Dulski, P., 1996. Distribution of yttrium and rare-earth elements in the Penge and Kuruman iron-formations, Transvaal Supergroup, South Africa. Precambrian Research 79, 37–55.

Bau, M., Dulski, P., Möller, P., 1995. Yttrium and holmium is South Pacific seawater: vertical distribution and possible fractionation mechanisms. Chem Erde 55, 1-15.

Bau, M., Möller, P., Dulski, P., 1997. Yttriumand lanthanides in easternMediterranean sea-water and their fractionation during redox-cycling. Marine Chemistry 56, 123–131.

Bayet-Goll, A., De Carvalho, C.N., Moussavi-Harami, R., Mahboubi, A., Nasiri, Y., 2014. Depositional environments and ichnology of the deep-marine succession of the Amiran Formation (upper Maastrichtian-Paleocene), Lurestan Province, Zagros Fold- Thrust Belt, Iran. Palaeogeography Palaeoclimatology Palaeoecology 401, 13–42.

Bayon, G., Birot, D., Ruffine, L., Caprais, J.C., Ponzevera, E., Bollinger, C., Donval, J.P., Charlou, J.L., Voisset, M., Grimaud, S., 2011. Evidence for intense REE scavenging at cold seeps from the Niger Delta margin. Earth and Planetary Science Letters 312, 443–452.

Bayon, G., Dupré, S., Ponzevera, E., Etoubleau, J., Chéron, S., Pierre, C., Mascle, J., Boetius, A., de Lange, G., 2013. Formation of carbonate chimneys in the Mediterranean Sea linked to deep-water oxygen depletion. Nature Geoscience 6, 755–760.

Bekker, A., 1998. Chemostratigraphy and climatostratigraphy of the Paleoproterozoic Snowy Pass Supergroup, Wyoming and its application for correlation with other sequences in North America. M.Sc. thesis, University of Minnesota, Duluth, 104p.

Bekker, A., and Karhu, J. A., 1996. Study of carbon isotope ratios in carbonates of the Early Proterozoic Snowy Pass Supergroup, WY and its application for correlation with the Chocolay Group, MI and Huronian Supergroup, ON [abstract]: Institute on Lake Superior Geology, 42nd Annual Meeting, Cable, Wisconsin, 1996, Proceedings 42 (1), 4–5.

Bekker, A., Eriksson, K. A., Kaufman, A. J., Karhu, J. A., and Beukes, N. J., 1999, Paleoproterozoic record of biogeochemical events and ice ages: Geological Society of America, Annual Meeting, Abstracts with Programs 31 (7), A-487.

Bekker, A., Kaufman, A.J., Karhu, J.A., Beukes, N.J., Swart, Q.D., Coetzee, L.L., Eriksson, K.A., 2001. Chemostratigraphy of the Paleoproterozoic Duitschland Formation, South Africa: implications for coupled climate change and carbon cycling. American Journal of Science 301, 261–285.

Bekker, A., Kaufman, A.J., Karhu, J.A., Eriksson, K.A., 2005. Evidence for Paleoproterozoic cap carbonates in North America. Precambrian Research 137, 167–206.

Benn, D.I., Evans, D.J.A., 2006. Glaciers and Glaciation. Hodder Education, London, Arnold. 802p.

Bennett, G., 1982. Geology of the Two Horse Lake Area, District of Algoma. Ontario Geological Survey, Geological Report 210, 63p.

Bennett, G., 2006. The Huronian Supergroup between Sault Ste Marie and Elliot Lake. Field Trip Guidebook. Institute on Lake Superior Geology 52, 1–65.

Bennett, G., Sawiuk, M., 1979. Jarvis Lake-Garden River area, southern part, District of Algoma. Ontario Geological Survey, Preliminary Map P.2241, scale 1:15,840.

Bennett, G., Dressler, B.O., Robertson, J.A., 1991. The Huronian Supergroup. In: Geology of Ontario. Ontario Geological Survey, pp. 549–591, Special Volume 4, Part 1.

Bernstein, L., 1985. Stratigraphy and sedimentology of the Espanola Formation (Huronian) in the Whitefish Falls area, Ontario. M.Sc Thesis, University of Western Ontario, London.

Bernstein, L., Young, G.M., 1990. Depositional environments of the Early Proterozoic Espanola Formation, Ontario, Canada. Canadian Journal of Earth Science 27, 539–551.

Bertram, C. J., Elderfield, H., 1993. The geochemical balance of the rare-earth elements and neodymium isotopes in the oceans. Geochimica et Cosmochimica Acta 57, 1957–1986.

Bertrand-Sarfati, J., Flicoteaux, R., Moussine-Pouchkine, A., Aït Kaci Ahmed, A., 1997. Lower Cambrian apatitic stromatolites and phospharenites related to the glacio-eustatic cratonic rebound (Sahara, Algeria). Journal of Sedimentary Research 67, 957–974.

Bodin, S., Godet, A., Westermann, S., Föllmi, K.B., 2013. Secular change in northwestern Tethyan water-mass oxygenation during the late Hauterivian–early Aptian. Earth and Planetary Science Letters 374, 121–131.

Bolhar, R., Van Kranendonk, M.J., Webb, G.E., Kamber, B.S., 2003. Geological and trace element evidence for a marine sedimentary environment of deposition and biogenicity of 3.45 Ga stromatolitic carbonates in the Pilbara Craton, and support for a reducing Archaean ocean. Geobiology 1 (2), 91-108.

Bond, G.C., Kominz, M.A., and Sheridan, R.E., 1995. Continental terraces and rises, in Busby, C.J., and Ingersoll, R.V., eds., Tectonics of sedimentary basins. Oxford, Blackwell Science, 149–178.

Boulton, G. S., 1972. Modern Arctic glaciers as depositional models for former ice sheets. Journal of the Geological Society of London 128, 361-393.

Boulton, G.S., and Deynoux, M., 1981. Sedimentation in glacial environments and the identification of tills and tillites in ancient sedimentary sequences. Precambrian Research 15, 397-422.

Brandes, C., Polom, U., Winsemann, J., 2011. Reactivation of basement faults: interplay of ice-sheet advance, glacial lake formation and sediment loading. Basin Research 23, 53-64.

Bromley, R.G., Allouc, J., 1992. Trace fossils in bathyal hardgrounds, Mediterranean Sea. Ichnos 2, 43–54.

Brownlow, A.H., 1979. Geochemistry. First edition. Prentice-Hall, Englewood Cliffs, NJ. 498p.

Buatois, L.A., Mangano, M.G., 1994. Lithofacies and depositional processes from a Carboniferous lake, Sierra de Narvaez, Northwest Argentina. Sedimentary Geology 93, 25-49.

Bussert, R., 2014. Depositional environments during the Late Palaeozoic ice age (LPIA) in northern Ethiopia, NE Africa. Journal of African Earth Science 99, 386–407.

Byrne, R. H., Kim, K. H., 1990. Rare-earth element scavenging in seawater. Geochimica et Cosmochimica Acta 54, 2645–2656.

Cantrell, K. J., Byrne, R. H., 1987. Rare-earth element complexation by carbonate and oxalate ions. Geochimica et Cosmochimica Acta 51, 597-605.

Card, K.D., 1978. Geology of the Sudbury-Manitoulin area, districts of Sudbury and Manitoulin. Ontario Geological Survey, Report 166, 238p.

Card K.D., Lumbers, S.B., 1977. Sudbury-Cobalt sheet, Ontario. Ontario Geological Survey, Map 2361, scale 1:253,400.

Card, K.D., Church, W.R., Franklin, J.M., Frarey, M.J., Robertson, J.A., West, G.F., Young, G.M., 1972. The Southern Province. In: Price, R.A., Douglas, R.J.W. (Eds.), Variations in Tectonic Styles in Canada: Geological Association of Canada, Special Paper 11, St. John's, NF, 335–380.

Card, K.D., Innes, D.G., Debicki, R.L., 1977. Stratigraphy, sedimentology, and petrology of the Huronian Supergroup in the Sudbury-Espanola area. Ontario Division of Mines, Geoscience Study 16, 99p.

Carey, S.W., Ahmad, N., 1961. Glacial marine sedimentation. Geology of the Arctic 2, 865-894.

Carlson, P. R. and Molnia, B. F., 1977. Submarine faults and slides on the continental shelf, northern Gulf of Alaska. Marine Geotechnology 2, 275-290.

Carlson, P.R., Bruns, T.R., Fisher, M.A., 1990. Development of slope valleys in the glacimarine environment of a complex subduction zone, northern Gulf of Alaska. In: Dowdeswell, J.A., Scourse, J.D. (eds.), Glacimarine Environments, Processes and Sediments. Geological Society Special Publication 53, 139-153.

Casshyap, S.M., 1967. On the classification of argillaceous sandstone, the Annals of the Geol. Dept. Aligarh Muslim Univ., Aligarh (India), vol. III.

Casshyap, S.M., 1969. Petrology of the Bruce and Gowganda Formations and its bearing on the evolution of Huronian sedimentation in the Espanola-Willisville area, Ontario, Canada. Palaeogeography Palaeoclimatology Palaeoecology 6, 5-36.

Casshyap, S.M., 1971. Petrology and sedimentation of Huronian arenites south of Espanola, Ontario. Canadian Journal of Earth Science 8, 20-49.

Catling, D.C., Claire, M.W., 2005. How Earth's atmosphere evolved to an oxic state: a status report. Earth and Planetary Science Letters 237, 1–20.

Chandler, W.R., 1969. Geology of the Huronian rocks, Harrow Township area, Ontario, unpublished Ph.D. thesis, University of Western Ontario, London, Ontario, 327p.

Charlou, J.L., Donval, J.P., Fouquet, Y., Ondréas, H., Knoery, J., Cochonat, P., Levache, D., Poirier, Y., Jean-Baptiste, P., Fourre, E., Chazallon, B., Party, Z.L.S., 2004. Physical and chemical characterization of gas hydrates and associated methane plumes in the Congo–Angola Basin. Chemical Geology 205, 405–425.

Cheel, R. J. and Rust, B. R., 1982. Coarse-grained facies of glaciomarine deposits near Ottawa, Canada. In: R. Davidson-Arnott, W. Nickling and B. D. Fahey (Editors), Research in Glacial, Glacio-Fluvial and Glacio-Lacustrine Systems. Geo-Books, Norwich, 279--295.

Christ, N., Immenhauser, A., Wood, R.A., Darwich, K., Niedermayr, A., 2015. Petrography and environmental controls on the formation of Phanerozoic marine carbonate hardgrounds. Earth-Science Reviews 151, 176–226.

Clerc, S., Buoncristiani, J., Guiraud, M., Vennin, E., Desaubliaux, G., Portier, E., 2013. Subglacial to proglacial depositional environments in an Ordovician glacial tunnel valley, Alnif, Morocco. Palaeogeography Palaeoclimatology Palaeoecology 370, 127-144.

Collins, W.H., 1925. North Shore of Lake Huron. Geological Survey of Canada Memoirs 143.

Collinson, J.D., 1970. Bedforms of the Tana River, Norway. Geografiska Annaler 52A, 31-56.

Coleman, J.M., 1969. Brahmaputra River; channel processes and sedimentation. Sedimentary Geology 3, 129-239.

Coleman, J.M., Wright, L.D., 1975. Modern river deltas: variability of processes and sand bodies. In: Broussard, M.L. (Ed), Deltas, Models for Exploration. Houston Geol. Soc., Houston, Texas, 99-149.

Coplen, T.B., 2011. Guidelines and recommended terms for expression of stable-isotope ratio and gas-ratio measurement results. Rapid Communications in Mass Spectrometry 25, 2538-2560.

Corfu, F., Andrews, A.J., 1986. A U–Pb age for mineralized Nipissing diabase, Gowganda, Ontario. Canadian Journal of Earth Sciences 23, 107–109.

Corsetti, F.A., 2015. Life during Neoproterozoic Snowball Earth. Geology 43 (6), 559-560.

Corsetti, F.A., Kaufman, A.J., 2003. Stratigraphic investigations of carbon isotope anomalies and Neoproterozoic ice ages in Death valley, California. Geological Society of America Bulletin 115, 916–932.

Corsetti, F.A., Lorentz, N.J., 2006. On Neoproterozoic cap carbonates as chronostratigraphic markers. In: Xiao, S., and Kaufman, A.J. (Eds.), Neoproterozoic geobiology and paleobiology. Dordrecht, Springer, 273–294.

Cotter, E., 1978. The evolution of fluvial style, with special reference to the central Appalachian Paleozoic. In: Miall, A.D. (Ed.), Fluvial Sedimentology. Canadian Society of Petroleum Geologists Memoir 5, 361-383.

Cowan, E.A., Powell, R.D., 1990. Suspended sediment transport and deposition of cyclically interlaminated sediment in a temperate glacial fjord, Alaska, USA. In: Dowdeswell, J.A., Scourse, J.D. (Eds.), Glacimarine Environments: Proccesses and Sediments. Geological Society Special Publication, 75-89.

Crocket, K.C., Hill, E., Abell, R.E., Johnson, C., Gary, S.F., Brand, T., Hathorne, E.C., 2018. Rare earth element distribution in the NE Atlantic: evidence for benthic sources, longevity of the seawater signal, and biogeochemical cycling. Frontiers in Marine Science 5 (147) 1-22.

Dalrymple, R.W., 2010. Tidal depositional systems. In: James, N.P., Dalrymple, R.W. (Eds.), Facies Models 4. Geological Association of Canada, Newfoundland, Canada, 201-231.

Dalrymple, R.W., and Choi, K., 2007. Morphologic and facies trends through the fluvial-marine transition in tide-dominated depositional systems: A schematic framework for environmental and sequence-stratigraphic interpretation. Earth-Science Reviews 81, 135-174.

Dalrymple, R.W., Narbonne, G.M., Smith, L., 1985. Eolian action and the distribution of Cambrian shales in North America. Geology 13, 607-610.

de Alvarenga, C.J.S., Santos, R. V., Dantas, E.L., 2004. C-O-Sr isotopic stratigraphy of cap carbonates overlying Marinoan-age glacial diamictites in the Paraguay Belt, Brazil. Precambrian Research 131, 1–21.

De Baar, H.J., Brewer, P.G., Bacon, M.P., 1985a. Anomalies in rare earth distributions in sea-water: Gd and Tb. Geochimica et Cosmochimica Acta 49, 1961–1969.

De Baar, H.J.W., Bacon, M.P., Brewer, P.G., Bruland, K.W., 1985b. Rare earth elements in the Pacific and Atlantic Oceans. Geochimica et Cosmochimica Acta 49, 1943–1959.

Debicki, R.L., 1990. Stratigraph, paleoenvironment and economic potential of the Huronian Supergroup in the southern Cobalt Embayment. Ontario Geological Survey, Miscellaneous Paper 148, 154p.

Demicco, R.V., 1983. Wavy and lenticular-bedded carbonate ribbon rocks of the Upper Cambrian Conococheague Limestone, Central Appalachians. Journal of Sedimentary Petrology 53, 1121–1132.

Derry, L.A., Jacobsen, S.B., 1990. The chemical evolution of Precambrian seawater −evidence from REEs in banded iron formations. Geochimica et Cosmochimica Acta 54 (11), 2965−2977.

Duke, W.L., Prave, A.R., 1991. Storm- and tide- influenced prograding shoreline sequences in the Middle Devonian Mahantango Formation, Pennsylvania. In: Smith, D.G., Reinson, G.E., Zaitlin, B.A., Rahmani, R.A. (Eds.), Clastic tidal sedimentology. Canadian Society of Petroleum Geologists Memoir 16, 349–370.

Eggertson, E B., 1975. The Espanola Formation; a Proterozoic carbonate north of Lake Huron, Ontario. Thesis, 97p.

Eisbacher, G.H., 1970. Contemporaneous faulting and clastic intrusions in the Quirke Lake Group, Elliot Lake, Onatrio. Canadian Journal of Earth Sciences 7, 215-225.

Eisbacher, G.H., 1981. Sedimentary tectonics and glacial record in the Windermere Supergroup, MacKenzie Mountains, northwestern Canada. Geological Survey of Canada, 40p.

Elderfield, H., Greaves, M. J., 1982. The rare-earth elements in sea-water. Nature 296, 214–219.

Emanuel, K.A., 1987. The dependence of hurricane intensity on climate. Nature 326, 483–485.

Eriksson, P.G., Condie, K.C., Tirsgaard, H., Mueller, W.U., Altermann, W., Miall, A.D., Aspler, L.B., Catuneanu, O., Chiarenzelli, J.R., 1998. Precambrian clastic sedimentation systems. Sedimentary Geology 120, 5-53.

Evans, D.A.D., 2003. A fundamental Precambrian-Phanerozoic shift in earth's glacial style? Tectonophysics 375, 353-385.

Evans, D.A.D., Raub, T.D., 2011. Neoproteroic glacial palaeolatitudes: a global update. In: Arnaud, E., Halverson, G.P., Shields-Zhou, G. (Eds.), The Geological Record of Neoproterozoic Glaciations. Memoir, 36. Geological Society, London, 93–112.

Eyles, C.H., 1988. Amodel for the formation of striated boulder pavements in glaciomarine sediments: an example from the Yakataga Formation, Alaska. Journal of Sedimentary Petrology 58, 62–71.

Eyles, C.H., 1994. Intertidal boulder pavements in the northeastern Gulf of Alaska and their geological significance. Sedimentary Geology 88, 161–173.

Eyles, C.H., Lagoe, M.B., 1998. Slump-generated megachannels in the Pliocene-Pleistocene glaciomarine Yakataga Formation, Gulf of Mexico, Geological Society of America Bulletin 110, 395-408.

Eyles, C.H., Eyles, N., Miall, A.D., 1985. Models of glaciomarine sedimentation and their application to the interpretation of ancient glacial sequences. Palaeogeography, Palaeoclimatology, Palaeoecology 51, 15-84.

Eyles, N., 1993. Earth's glacial record and its tectonic setting. Earth Science Reviews 35, 1-248.

Eyles, N., Clark, B.M., 1985. Gravity-induced soft-sediment deformation in glaciomarine sequences of the Upper Proterozoic Port Askaig Formation, Scotland. Sedimentology, 32, 789-814.

Eyles, N., Januszczak, N., 2004. 'Zipper-rift': a tectonic model for Neoproterozoic glaciations during the breakup of Rodinia after 750 Ma. Earth Science Reviews 65, 1-73.

Fairchild, I.J., 1991. Origins of carbonate in Neoproterozoic stromatolites and the identification 1539 of modern analogues. Precambrian Research 53, 281-299.

Farquhar, J., Huiming, Bao, Thiemens, M., 2000. Atmospheric influence of Earth's earliest sulfur cycle. Science 289, 756–758.

Fedo, C.M., Prave, A.R., 1991. Extensive Cambrian braidplain sedimentation: insights from the southwestern U.S.A. Cordillera. In: Cooper, J.D., Stevens, C.H. (Eds.), Paleozoic Paleogeography of the Western United States – II. Pacific Section SEPM 67, 227-235.

Fedo, C.M., Young, G.M., Nesbitt, H.W., 1997a. Paleoclimatic control on the composition of the Paleoproterozoic Serpent Formation, Huronian Supergroup, Canada: a greenhouse to icehouse transition. Precambrian Research 86, 201–223.

Fedo, C.M., Young, G.M., Nesbitt, H.W., Hanchar, J.M., 1997b. Potassic and sodic metasomatism in the Southern Province of the Canadian Shield: evidence from the Paleoproterozoic Serpent Formation, Huronian Supergroup, Canada. Precambrian Research 84, 17-36.

Fichter, L.S., Poche, D.J., 2001. Ancient Environments and the Interpretation of Geologic History. Macmillan Publishing Company, 310p.

Fisher, W.L., Brown, L.F., Scott, A.J., McGowan, J.H., 1969. Delta systems in the exploration for oil and gas. Bureau of Economic Geology, Univ. Texas, Austin, 78p.

Folk, R.L., 1968. Petrology of sedimentary rocks. Hemphill's, Austin, Texas, 170p.

Font, E., Nédélec, A., Trindade, R.I.F., Macouin, M., Charrière, A. 2006. Chemostratigraphy of the Neoproterozoic Mirassol d'Oeste cap dolostones (Mato Grosso, Brazil): an alternative model for Marinoan cap dolostone formation. Earth and Planetary Science Letters 250, 89–103.

Frakes, L. A. and Crowell, J. C., 1969. Late Paleozoic glaciation, I. South America. Geological Society of America Bulletin 80, 1007-1042.

Fralick, P.W., 1985. Early Proterozoic basin development on a cratonic margin: the lower Huronian Supergroup of central Ontario. Ph.D. Thesis, University of Toronto, Toronto, Ont. 466p.

Fralick, P.W., Miall, A.D., 1989. Sedimentology of the Lower Huronian Supergroup (Early Proterozoic), Elliot Lake area, Ontario, Canada. Sedimentary Geology 63, 127–153.

Fralick, P., Riding, R., 2015. Steep Rock Lake: Sedimentology and geochemistry of an Archean carbonate platform. Earth-Science Reviews 151, 132–175.

Fralick, P., Davis, D.W., Kissin, S.A., 2002. The age of the Gunflint Formation, Ontario, Canada; single zircon U-Pb age determinations from reworked volcanic ash. Canadian Journal of Earth Science 39 (7), 1085-1091.

Frarey, M.J., 1977. Geology of the Huronian belt between Sault Ste. Marie and Blind River, Ontario. Geological Survey of Canada, Memoir 383, 87p.

Frarey, M.J., Roscoe, S.M., 1971. The Huronian Supergroup north of Lake Huron. In: Symposium on Basins and Geosynclines of the Canadian Shield. Geological Survey of Canada, Paper 70-40, 143–158.

German, C.R., Elderfield, H., 1990. Application of the Ce anomaly as a paleoredox indicator: the ground rules. Paleoceanography 5, 823.

German, C.R., Holliday, B.P., Elderfield, H., 1991. Redox cycling of rare earth elements in the suboxic zone of the Black Sea. Geochimica et Cosmochimica Acta 55, 3553–3558.

Giddings, J.A., Wallace, M.W., 2009. Sedimentology and C-isotope geochemistry of the "Sturtian" cap carbonate, South Australia. Sedimentary Geology 216, 1–14.

Ginn, R.M., 1961. Geology of Porter Township. Ontario Geological Survey Report, 36p.

Gipp, M.R., 2000. Lift-off moraines: markers of last ice-flow direction on the Scotian Shelf. Canadian Journal of Earth Sciences 37, 1723-1734.

Glennie, K.W., 1970. Desert sedimentary environments. Developments in sedimentology, 14. Elsevier, Amsterdam, Netherlands, 222p.

Goodbred, Jr., S.L. and Saito, Y., 2011. Tide-dominated Deltas. In: Davis, R. and Dalyrymple, R.W. (eds.), Principles of Tidal Sedimentology. Springer Press, New York, 129-149.

Gradzinsky, R., Jerkiewicz, T., 1974. Dinosaur and mammal bearing aeolian and associated deposits of the Upper Cretaceous in the Gobi Desert (Mongolia). Sedimentary Geology 12, 249-278.

Grotzinger, J.P., 1986. Evolution of Early Proterozoic passive- margin carbonate platform, Rocknest Formation, Wopmay Orogen, Northwest Territories. Canadian Journal of Sedimentary Petrology 56, 831– 847.

Grotzinger, J.P., Knoll, A. H., 1995. Anomalous carbonate precipitates: is the Precambrian the key to the Permian? Palaios 10: 578–596.

Grotzinger, J.P., Fike, D.A., Fischer, W.W., 2011. Enigmatic origin of the largest-known carbon isotope excursion in Earth's history. Nature Geoscience 4, 285-292.

Gugliotta M., Flint, S.S., Hodgson D.M., Veiga, G.D., 2015. Stratigraphic record of river-dominated crevasse subdeltas with tidal influence (Lajas Formation, Argentina). SEPM Journal of Sedimentary Research 85, 265-284.

Halverson, G. P., Shields, G., 2011. Chemostratigraphy and the Neoproterozoic glaciations. In: Arnaud, E., Halverson, G. P., Shields, G. (Eds.), The Geological Record of Neoproterozoic Glaciations. Geological Society, London, Memoirs 36, 51–66.

Halverson, G.P., Hoffman, P.F., Schrag, D.P., Kaufman, A.J., 2002. A major perturbation of the carbon cycle before the Ghaub glaciation (Neoproterozoic) in Namibia: Prelude to snowball Earth? Geochemistry, Geophysics, Geosystems 3 (6), June.

Halverson, G.P., Hoffman, P.F., Schrag, D.P., Maloof, A.C., Rice, A.H., 2005. Towards Neoproterozoic composite carbon-isotope record. Geological Society of America Bulletin 117, 1181–1207.

Halverson, G.P., Wade, B.P., Hurtgen, M.T., Barovich, K.M., 2010. Neoproterozoic chemostratigraphy. Precambrian Research 182, 337–350.

Hamblin, A.P., 2016. A Late Ordovician ancient loessite deposit in a glacially-influenced setting?: the Milton member of the Queenston Formation in southern Ontario, and synthesis of the background concepts behind a novel interpretation; Geological Survey of Canada, Open File 7860, 42p.

Hambrey, M. J., 1994. Glacial environments. University College London, London, 296p.

Hambrey, M. J., Harland, W. B. (eds.), 1981. Earth's Pre- Pleistocene Glacial Record. Cambridge University Press, Cambridge, 1004p.

Harland, W.B., 1964. Critical evidence for a great Infra-Cambrian ice age. Geologische Rundschau 54, 45-61.

Hayes, J.M., Des Marais, D.J., Lambert I.B., Strauss, H., and Summons, R.E., 1992. Proterozoic biogeochemistry, in Schopf, J.W. and Klein, C., eds., The Proterozoic biosphere: A Multidisciplinary Study, Cambridge University Press, 81-134.

Hendry, H.E., Stauffer, M.R., 1977. Penecontemporaneous folds in cross-bedding; inversion of facing criteria and mimicry of tectonic folds. Geological Society of America Bulletin 88, 809-812.

High, L.R., Picard, M.D., 1974. Reliability of cross-stratification types as paleocurrent indicators in fluvial rocks. Journal of Sedimentary Petrology 44, 158-168.

Hilburn, I.A., Joseph, L., Kirschvink, J.L., Tajikab, E., Tadab, R., Hamanob, Y., Yamamotob, S., 2005. A negative fold test on the Lorrain Formation of the Huronian Supergroup: uncertainty on the paleolatitude of the Paleoproterozoic Gowganda glaciation and implications for the great oxygenation event. Earth and Planetary Science Letters 232, 315–332.

Hill, I.G., Worden, R.H., Meighan, I.G., 2000. Yttrium: the immobility-mobility transition during basaltic weathering. Geology 28, 923–926.

Hill, P.R., 1984. Sedimentary facies of the Nova Scotian upper and middle continental slope, offshore Eastern Canada. Sedimentology 31, 293-309.

Hiscott, R.N., 1981. Stratigraphy and sedimentology of the late Proterozoic Rock Harbour Group, Flat Islands, Placentia Bay, Newfoundland Avalon Zone. Canadian Journal of Earth Sciences 18 (3), 495-508.

Hoefs, J., 2009. Stable isotope geochemistry. Sixth edition. Springer-Verlag Berlin Heidelberg, 285p.

Hoffman, P.F., 1989. Precambrian geology and tectonic history of North America. In: Bally, A.W., Palmer, A.R. (Eds.), The Geology of North America – An Overview. The Geological Society of America, 447–512.

Hoffman, P.F., 2011. Strange bedfellows: glacial diamictite and cap carbonate from the Marinoan (635 Ma) glaciations in Namibia. Sedimentology 58, 57-119.

Hoffman, P.F., 2013. The Great Oxidation and a Siderian snowball Earth: MIF-S based correlation of Paleoproterozoic glacial epochs. Chemical Geology 362, 143-156.

Hoffman, P.F., Li, Z., 2009. A palaeogeographic context for Neoproterozoic glaciation. Palaeogeography, Palaeoclimatology, Palaeoecology 277, 158–172.

Hoffman, P.F., Schrag, D.P., 2002. The snowball earth hypothesis: testing the limits of global change. Terra Nova 14, 129–155.

Hoffman, P.F., Kaufman, A.J., Halverson, G.P., Schrag, D.P., 1998. A Neoproterozoic snowball earth. Science, 281, 1342-1346.

Hoffman, P. F., Halverson, G. P., Domack, E. W., Husson, J. M., Higgins, J. A., Schrag, D. P., 2007. Are basal Ediacaran (635Ma) post-glacial 'cap dolostones' diachronous? Earth and Planetary Science Letters 258, 114–131.

Hofmann, H.J., 1966. Ordovician paleocurrents near Cincinnati, Ohio. The Journal of Geology 74, 868-890.

Hofmann, H.J., Pearson, D.A.B., Wilson, B.H., 1980. Stromatolites and fenestral fabric in early Proterozoic Huronian Supergroup, Ontario. Canadian Journal of Earth Sciences 17, 1351-1357.

Houston, R.S., Lanthier, L.R., Karlstrom, K.E., Sylvester, G., 1981. Paleoproterozoic diamictite of southern Wyoming. In: Hambrey, M.J., Harland, W.B. (Eds.), Earth's Pre-Pleistocene Glacial Record. Cambridge University Press, New York, 795–799.

Hrabar, S.V., Cressman, E.R., Potter, P.E., 1971. Crossbedding of the Tanglewood Limestone Member of the Lexington Limestone (Ordovician) of the Blue Grass region of Kentucky. B.Y.U. Geology Studies 18, 99-114.

Huang, J., Chu, X., Jiang, G., Feng, L., Chang, H. 2011. Hydrothermal origin of elevated iron, manganese and redox-sensitive trace elements in the ca. 635Ma Doushantuo cap carbonate. Journal of the Geological Society of London 168, 805–815.

Jakes, P., Taylor, S.R., 1974. Excess Eu content in Precambrian rocks and continental evolution. Geochimica et Cosmochimica Acta 38, 739-745.

James, N.P., Narbonne, G.M., Kyser, T.K., 2001. Late Neoproterozoic cap carbonates: Mackenzie Mountains, northwestern Canada: precipitation and global glacial meltdown. Canadian Journal of Earth Sciences 38, 1229–1262.

Jarvis, K.E., Gray, A.L., McCurdy, E., 1989. Avoidance of spectral interference on europium in inductively coupled plasma mass spectrometry by sensitive measurement of the doubly charged ion. Journal of Analytical Atomic Spectrometry 4, 743–747.

Jiang, G., Kennedy, M.J., Christie-Blick, N., 2003. Stable isotopic evidence for methane seeps in Neoproterozoic postglacial cap carbonates. Nature 426, 822–826.

Jiang, G., Kennedy, M.J., Christie-Blick, N., Wu, H., Zhang, S., 2006a. Stratigraphy, sedimentary structures, and textures of the Late Neoproterozoic Doushantuo cap carbonate in South China. Journal of Sedimentary Research 76, 978–995.

Jiang, G., Shi, X., Zhang, S., 2006b. Methane seeps, methane hydrate destabilization, and the late Neoproterozoic postglacial cap carbonates. Chinese Science Bulletin 51, 1152–1173.

Jiang, G., Kaufman, A.J., Christie-Blick, N., Zhang, S., Wu, H., 2007. Carbon isotope variability across the Ediacaran Yangtze platformin South China: implications for a large surface to deep ocean δ13C gradient. Earth and Planetary Science Letters 261, 303–320.

Johannesson, K.H., Hawkins Jr., D.L., Cortés, A., 2006. Do Archean chemical sediments re- cord ancient seawater rare earth element patterns? Geochimica et Cosmochimica Acta 70, 871–890.

Johnson, H.D., 1978. Shallow siliciclastic seas, *in* Sedimentary environments and facies. H.G. Reading (Ed.) Elsevier, New York, 207-258.

Jolly, W.T., 1987. Geology and geochemistry of Huronian rhyolites and low-Ti continental tholeiites from the Thessalon region, central Ontario. Canadian Journal of Earth Sciences 24, 1360–1385.

Karlstrom, K.E., Flurkey, A.J., Houston, R.S., 1983. Stratigraphy and depositional setting of the Proterozoic Snowy Pass Supergroup, southeastern Wyoming: record of an early Proterozoic Atlantic-type cratonic margin. Geological Society of America Bulletin 94 (11), 1257-1274.

Kasemann, S.A., Prave, A.R., Fallick, A.E., Hawkesworth, C.J., Hoffmann, K.H., 2010. Neoproterozoic ice ages, boron isotopes, and ocean acidification: Implications for a snowball Earth. Geology 38, 775–778.

Kasting, J.F., Shuhei, Ono, 2006. Palaeoclimates: the first two billion years. Philosophical Transactions of the Royal Society B 361, 917–929.

Kaufman, A.J., Johnston, D.T., Farquhar, J., Masterson, A.L., Lyons, T.W., Bates, S., Anbar, A.D., Arnold, G.L., Garvin, J., Buick, R., 2007. Late Archean biospheric oxygenation and atmospheric evolution. Science 317, 1900–1903.

Kawabe, I., Kitahara, Y., Naito, K., 1991. Non-chondritic yttrium/holmium ratio and lanthanide tetrad effect observed in pre-Cenozoic limestones. Geochemical Journal 25, 31-44.

Kazmierczak, J. and Goldring, R., 1978. Subtidal flat-pebble conglomerate from the Upper Devonian of Poland: a multiprovenant high-energy product. Geological Magazine 115, 359–366.

Ketchum, K.Y., Heaman, L.M., Bennett, G., Hughes, D.J., 2013. Age, petrogenesis and tectonic setting of the Thessalon volcanic rocks, Huronian Supergroup, Canada. Precambrian Research 233, 144-172.

Kennedy, M.J., 1996. Stratigraphy, sedimentology and isotopic geochemistry of Australian Neoproterozoic postglacial cap dolostones: deglaciation, $\delta^{13}C$ excursions and carbonate precipitation. Journal of Sedimentary Research 66, 1050–1064.

Kennedy, M.J., Christie-Blick, N., Sohl, L.E., 2001. Are Proterozoic cap carbonates and isotopic excursions a record of gas hydrate destabilization following Earth's coldest intervals? Geology 29, 443–446.

Kennedy, M.J., Runnegar, B., Prave, A.R., Hoffmann, K.H., Arthur, M.A., 1998. Two or four Neoproterozoic glaciations? Geology 26, 1059–1063.

Kennedy, W.J., Garrison, R.E., 1975. Morphology and genesis of nodular chalks and hardgrounds in the Upper Cretaceous of southern England. Sedimentology 22, 311–386.

King, L.H., Rokoengen, K., Fader, G.B.J., Gunleiksrud, T., 1991. Till-tongue stratigraphy. Geological Society of America Bulletin 103, 637-659.

Kirschvink, J.L., 1992. Late Proterozoic low-latitude global glaciation–The Snowball Earth. In: Schopf, J.W., Klein, C. (Eds.), The Proterozoic Biosphere. Cambridge University Press, Cambridge, 51–52.

Kirschvink, J.L., Kopp, R.E., 2008. Palaeoproterozoic ice houses and the evolution of oxygen-mediating enzymes: the cast for a late origin of photosystem II. Philosophical Transactions of the Royal Society B: Biological Sciences 363, 2755–2765.

Kirschvink, J.L., Gaidos, E.J., Bertani, L.E., Beukes, N.J., Gutzmer, J., Maepa, L.N., Steinberger, R.E., 2000. Paleoproterozoic snowball Earth: extreme climatic and geochemical global change and its biological consequences. Proceedings of the National Academy of Sciences of the United States of America 97, 1400-1405.

Klein, G. de V., 1967. Paleocurrent analysis in relation to modern marine sediment dispersal patterns. American Association of Petroleum Geologists Bulletin 51, 366-382.

Kopp, R.E., Kirschvink, J.L., Hilburn, I.A., Nash, C.Z., 2005. The Paleoproterozoic snowball Earth: A climate disaster triggered by the evolution of oxygenic photosynthesis. PNAS 102 (32), 11131-11136.

Krogh, T.E., Davis, D.W., Corfu, F., 1984. Precise U–Pb zircon and baddeleyite ages from the Sudbury area. In: Pye, E.G., Naldrett, A.J., Giblin, P.E. (Eds.), The Geology and Ore Deposits of the Sudbury Structure. Ontario Geological Survey, Toronto, ON, 431–446.

LaFontaine, D., 2012. Depositional environments of the Paleoproterozoic Espanola Formation with implications for post-Great Oxidation sedimentation conditions. Lakehead University, Department of Geology, 77p.

Lawrence, M.G., Greig, A., Collerson, K.D., Kamber, B.S., 2006. Rare Earth Element and Yttrium Variability in South East Queensland Waterways. Aquatic Geochemistry 12, 39–72.

Lawson, D. E., 1981. Distinguishing characteristics of diamictons at the margin of the Matanuska Glacier, Alaska. Annals of Glaciology 2, 78-84.

Le Blanc Smith, G., Eriksson, K.A., 1979. A fluvioglacial and glaciolacustrine deltaic depositional model for Permo-Carboniferous coals of the northeastern Karoo Basin, South Africa. Palaeogeography, Palaeoclimatology, Palaeoecology 27, 67-84.

Lee, Y.I. and Kim, J.C., 1992. Storm-influenced siliciclastic and carbonate ramp deposits, the Lower Ordovician Dumugol Formation, South Korea. Sedimentology 39, 951– 969.

Lemaitre, N., Bayon, G., Ondréas, H., Caprais, J.C., Freslon, N., Bollinger, C., Rouget, M.L., de Prunelé, A., Ruffine, L., Olu-Le Roy, K., Sarthou, G., 2014. Trace element behaviour at cold seeps and the potential export of dissolved iron to the ocean. Earth and Planetary Science Letters 404, 376–388.

Liu, X., Byrne, R.H., 1997. Rare earth and yttrium phosphate solubilities in aqueous solution. Geochimica et Cosmochimica Acta 61, 1625–1633.

Long, D.G.F., 1976. The Stratigraphy and Sedimentology of the Huronian (lower Aphebian) Mississagi and Serpent Formations. Digitized Theses. Paper 1042.

Long, D.G.F., 1978. Depositional environments of a thick Proterozoic sandstone: the (Huronian) Mississagi Formation of Ontario, Canada. Canadian Journal of Earth Science 15, 190-206.

Long, D.G.F., 2004. The tectonostratigraphic evolution of the Huronian basement and the subsequent basin fill: geological constraints on impact models of the Sudbury event. Precambrian Research 129, 203-223.

Long, D.G.F., 2009. The Huronian Supergroup. In: Rousell, D.H., Brown, G.H. (Eds.), A field guide to the Geology of Sudbury, Ontario. Ontario Geological Survey, Open File Report 6243, 14-30.

López-Gamundí, O., Sterren, A.F., Cisterna, G.A., (2016). Inter- and Intratill Boulder Pavements in the Carboniferous Hoyada Verde Formation of West Argentina: An insight on glacial advance/retreat fluctuations in Southwestern Gondwana. Palaeogeography, Palaeoclimatology, Palaeoecology. 447p.

Loyd, S.J., Marenco, P.M., Hagadorn, J.W., Lyons, T.W., Kaufman, A.J., Sour-Tovar, F., Corsetti, F.A., 2012. Sustained low marine sulfate concentrations from the Neo-proterozoic to the Cambrian: insights from carbonates of northwestern Mexico and eastern California. Earth and Planetary Science Letters 339 (340), 79–94.

Mackiewicz, N.E., Powell, R.D., Carlson, P.R., Molnia, B.F., 1984. Interlaminated ice-proximal glacimarine sediments in Muir Inlet, Alaska. Marine Geology 57, 113-147.

Manz, P.A., 1978. Bedforms produced by fine cohesionless granular and flakey sediments under subcritical water flows. Sedimentology 25, 83-103.

Markello, J.R. and Read, J.F., 1982. Upper Cambrian intra- shelf basin, Nolichucky Formation, southwest Virginia Appalachians. American Association of Petroleum Geologists Bulletin 66, 860–878.

Marlowe, J. I., 1968. Unconsolidated marine sediments in Baffin Bay. Journal of Sedimentary Petrology 38, 1065-1078.

Mawson, D., 1949. The Late Precambrian ice age and glacial record of the Bibliando Dome. Journal and Proceedings of the Royal Society of New South Wales 82, 150–174.

MacNaughton, R.B., Dalrymple, R.W., Narbonne, G.M., 1997. Early Cambrian braid-delta deposits, MacKenzie Mountains, north-western Canada. Sedimentology 44, 587-609.

McCormick, D.S., Grotzinger, J.P., 1993. Distinction of marine from alluvial facies in the Paleoproterozoic (1.9Ga) Burnside Formation, Kilohigok Basin, N.W.T., Canada. Journal of Sedimentary Petrology 63, 398-416.

McDowell, J.P., 1957. The sedimentary petrology of the Mississagi quartzite in the Blind River area. Ontario Department of Mines, Geological Circular 6, 31p.

McKee, E.D., Weir, G.W., 1953. Terminology for stratification and cross-stratification in sedimentary rocks. Geological Society of America Bulletin 64, 381-390.

McLennan, S.M., 1989. Rare earth elements in sedimentary rocks: influence of provenance and sedimentary processes. In: Lipin, B.R., McKay, G.A. (Eds.), Geochemistry and mineralogy of rare earth elements. Mineralogical Society of America Reviews in Mineralogy 21, 169–200.

McLennan, S.M., Bock, B., Hemming, S.R., Hurowitz, J.A., Lev, S.M., McDaniel, D.K., 2003. The roles of provenance and sedimentary processes in the geochemistry of sedimentary

rocks. In: Lentz, D.R. (Ed.), Geochemistry of Sediments and Sedimentary Rocks: Evolutionary Considerations to Mineral Deposit-forming Environments. Geological Association of Canada, GeoText 4, 7–38.

McLennan, S.M., Fryer, B.J., Young, G.M., 1979. The geochemistry of the carbonate- rich Espanola Formation (Huronian) with emphasis on the rare earth elements. Canadian Journal of Earth Sciences 16, 230-239.

McLennan, S.M., Hemming, S., McDaniel, D.K., Hanson, G.N., 1993. Geochemical approaches to sedimentation, provenance, and tectonics. Geological Society of America Special Paper 283, 21–39.

McLennan, S.M., Nance, W.B., Taylor, S.R., 1980. Rare earth element-thorium correlations in sedimentary rocks, and the composition of the continental crust. Geochimica et Cosmochimica Acta 44, 1833–1839.

McLennan, S.M., Taylor, S.R., Eriksson, K.A., 1983. Geochemistry of Archean shales from the Pilbara Supergroup, Western Australia. Geochimica et Cosmochimica Acta 47, 1211–1222.

McLennan, S., Taylor, S.R., McCulloch, M., Maynard, J., 1990. Geochemical and Nd-Sr isotopic composition of deep-sea turbidites: Crustal evolution and plate tectonic associations. Geochimica et Cosmochimica Acta 54, 2015–2050.

McLaughlin, P.I., Brett, C.E., Wilson, M.A., 2008. Hierarchy of sedimentary discontinuity surfaces and condensed beds from the middle Paleozoic of eastern North America: implications for cratonic sequence stratigraphy: dynamics of epeiric seas. Geological Association of Canada Special Paper 48, 175–200.

Meyer, E.E., Quicksall, A.N., Landis, J.D., Link, P.K., Bostick, B.C. 2012. Trace and rare earth elemental investigation of a Sturtian cap carbonate, Pocatello, Idaho: evidence for ocean redox conditions before and during carbonate deposition. Precambrian Research 192–195, 89–106.

Miall, A. D., 1983. Glaciomarine sedimentation in the Gowganda Formation (Huronian), northern Ontario. Journal of Sedimentary Petrology 53, 477-491.

Miall, A. D., 1985. Sedimentation on an early Proterozoic continental margin; the Gowganda Formation (Huronian), Elliot Lake area, Ontario, Canada. Sedimentology 2, 763-788.

Miall, A.D., 2000. Chapter 4: Facies Analysis. Principals of Sedimentary Basin analysis. Springer, Germany, Berlin, 141-248.

Miller, J.M.G., 1996. Glacial Sediments, in Sedimentary Environments: Processes, Facies, and Stratigraphy, Reading, H.G. (ed.), Blackwell Science, Oxford, 454-484.

Mills, P. C., 1983. Genesis and diagnostic value of soft-sediment deformation structures- A review. Sedimentary Geology 35, 83-104.

Mohanty, S.P., Barik, A., Sarangi, S., Sarkar, A., 2015. Carbon and oxygen isotope systematics of a Paleoproterozoic cap-carbonate sequence from the Sausar Group, Central India. Palaeogeography, Palaeoclimatology, Palaeoecology 417, 95-209.

Mosher, D.C., Piper, D.J.W., Vilks, G., Aksu, A.E., Fader, G.B., 1989. Evidence for Wisconsinian glaciations in the Verrill Canyong area, Scotian Slope. Quaternary Research 31, 27-40.

Mosher, D.C., Moran, K., Hiscott, R.N., 1994. Late Quaternary sediment, sediment mass-flow processes, and slope stability on the Scotian Slope. Sedimentology 41, 1039-1061.

Mount, J.F. and Kidder, D., 1993. Combined flow origin of edgewise intraclast conglomerates. Sellick Hill Formation (Lower Cambrian), South Australia. Sedimentology 40, 315–329.

Mrakovich, J.V., Coogan, A.H., 1974. Depositional environment of the Sharon Conglomerate Member of the Pottsville Formation in northeastern Ohio. Journal of Sedimentary Petrology 44, 1186-1199.

Muszynski, I., Birchfield, G.E., 1987. A coupled marine ice-stream—ice-shelf model. Journal of Glaciology 33, 3-15.

Myrow, P.M., Tice, L., Archuleta, B., Clark, B., Taylor, J.F., Ripperdan, R.L., 2004. Flat-pebble conglomerate: Its multiple origins and relationship to metre-scale depositional cycles. Sedimentology 51, 973–996.

Nagarajan, R., Madhavaraju, J., Armstrong-Altrin, J.S., Nagendra, R., 2011. Geochemistry of Neoproterozoic limestones of the Shahabad Formation, Bhima Basin, Karnataka, southern India. Geosciences Journal 15, 9-25.

Nance, W.B., Taylor, S.R., 1976. Rare earth patterns and crustal evolution, I. Australian post-Archean sedimentary rocks. Geochimica et Cosmochimica Acta 40, 1539-1551.

Nance W. B., Taylor S. R., 1977. Rare earth element patterns and crustal evolution – II. Archean sedimentary rocks from Kalgoorlie, Australia. Geochimica et Cosmochimica Acta 41, 225–231.

Neill, C.R., 1969. Bed forms in the lower Red Deer River, Alberta. Journal of Hydrology 7, 58-85.

Nesbitt, H.W., Young, G.M., 1982. Early Proterozoic climates and plate motions inferred from major element chemistry of lutites. Nature 299, 715–717.

Nitsche, F.O., Cunningham, A.P., Larter, R.D., Gohl, K., 2000. Geometry and development of glacial continental margin depositional systems in the Bellingshausen Sea. Marine Geology 62, 277-302.

Noble, S.R., Lightfoot, P.C., 1992. U–Pb baddeleyite ages of the Kearns and Triangle Mountain intrusions, Nipissing Diabase, Ontario. Canadian Journal of Earth Sciences 29, 1424–1429.

Nozaki, Y., Zhang, J., 1995. The rare earth elements and yttrium in the coastal/offshore mixing zone of Tokyo Bay waters and the Kuroshio. Biogeochemical Processes, Ocean Flux Western Pacific, 171–184.

Nozaki, Y., Zhang, J., Amakawa, H., 1997. The fractionation between Y and Ho in the marine environment. Earth and Planetary Science Letters 148, 329-340.

Nystuen, J. P., 1976. Facies and sedimentation of the Late Precambrian Moelv Tillite in the eastern part of the Sparagmite Region, southern Norway. Norges Geologiske Undersokelse 329, 1-70.

Obrochta, S.P., Duncan, D.S., Brooks, G.R., 2003. Hardbottom development and significance to the sediment-starved west-central Florida inner continental shelf. Sedimentary Geology 200, 291–306.

O'Hare, S., 2010. Sedimentological study of the glaciogenic Bruce Formation, of the Huronian Supergroup, in the north shore area, Ontario. HBSc Thesis, Lakehead University, Department of Geology, 111p.

Ore, H.T., 1964: Some criteria for recognition of braided stream deposits. Unvi. Wyoming, Dept. Geology, Contributions to Geology 3, 1-14.

Orton, G.J., Reading, H.G., 1993, Variability of deltaic processes in terms of sediment supply, with particular emphasis on grain size: Sedimentology 40, 475– 512.

Palonen, P.A., 1971. Stratigraphy and Depositional environment of the Mississagi Formation, Ontario; unpublished MSc thesis, University of Calgary, Calgary, Alberta.

Palonen, P.A., 1973. Paleogeography of the Mississagi Formation and lower Huronian cyclicity; *in* Huronian Stratigraphy and Sedimentation. Geological Association of Canada, Special Paper 12, 157-168.

Papineau, D., Mojzsis, S.J., Schmitt, A.K., 2007. Multiple sulfur isotopes from Paleoproterozoic Huronian interglacial sediments and the rise of atmospheric oxygen. Earth and Planetary Science Letters 255, 188–212.

Parviainen, E.A.U., 1973. The sedimentology of the Huronian Ramsay Lake and Bruce Formations, north shore of Lake Huron, Ontario, Ph.D thesis, University of Western Ontario, London, Ontario, 426p.

Paul, M. A., 1983. The supraglacial landsystem. In: N. Eyles (Editor), Glacial Geology: An Introduction for Engineers and Earth Scientists. Pergamon Press, Oxford, 71-90.

Pavlov, A.A., Kasting, J.F., Brown, L.L., 2000. Greenhouse warming by CH4 in the atmosphere of early Earth. Journal of Geophysical Research 105 (E5), 11981–11990.

Pettijohn, F.J., 1970. The Canadian Shield: a status report, *in* Symposium on Basins and Geosynclines of the Canadian Shield. Geological Survey of Canada, Paper 70-40, 329-355.

Pettijohn, F.J., 1975. Sedimentary Rocks; Harper and Row, New York, 628p.

Pienaar, P.J., 1963. Stratigraphy, petrology, and genesis of the Elliot Lake Group, Blind River, Ontario, including the uraniferous conglomerate. Geological Survey of Canada Bulletin 83, 140p.

Piepgras, D.J., Jacobsen, S.B., 1992. The behavior of rare earth elements in seawater; precise determination of variations in the North Pacific water column. Geochimica et Cosmochimica Acta 56 (5), 1851-1862.

Piper, D. J. W. and Normark, W. R., 1982. Acoustic interpretation of Quaternary sedimentation and erosion on the channelled upper Laurentian Fan, Atlantic margin of Canada. Canadian Journal of Earth Sciences 19, 1974-1984.

Piper, D. J. W. and Slatt, R. M., 1977. Late Quaternary clay-mineral distribution on the eastern continental margin of Canada. Geological Society of America Bulletin 88, 267-272.

Planavsky, N.J., McGoldrick, P., Scott, C.T., Li, C., Reinhard, C.T., Kelly, A.E., Chu, X., Bekker, A., Love, G.D., Lyons, T.W., 2011. Widespread iron-rich conditions in the mid-Proterozoic ocean. Nature 477, 448–451.

Plint, A.G., 2010. Wave- and storm-dominated shoreline and shallow-marine systems. In: James, N.P., Dalrymple, R.W. (Eds.), Facies Models 4. Geological Association of Canada, Newfoundland, Canada, 167-199.

Potter, P.E., 1967. Sand bodies and sedimentary environments: a review. American Association of Petroleum Geologists Bulletin 51, 337-365.

Powell, R. D., 1981. A model for sedimentation by tidewater glaciers. Annals of Glaciology 2, 129-134.

Powell, R.D., 1988. Processes and facies of temperate and sub-polar glaciers with tidewater fronts. Geological Society of America, Centennial Aunnual Meeting, Denver, Short Course Notes, 114.

Powell, R.D., 1990. Glaciomarine processes at grounding-line fans and their growth to ice-contact deltas, *in* Glacimarine Environments: Processes and Sediments, Dowdeswell, J.A., Scourse, J.D. (eds.), Special Publication Geological Society 53, 53-73.

Powell, R.D., Dawber, M., McInnes, J.N., Pyne, A.R., 1996. Observations of the grounding-line area at a floating glacier terminus. Annals of Glaciology 22, 217-223.

Prasad, N., Roscoe, S.M., 1996. Evidence of anoxic to oxic atmospheric change during 2.45–2.22 Ga from lower and upper sub-Huronian paleosols, Canada. Catena 27, 105–121.

Pretious, E. S., Blench, T., 1951. Final report of special observations of bed movement in Lower Fraser River at Ladner Reach during 1950 freshet. National Resource Council of Canada, Vancouver, B.C., Canada.

Purser, B.H., 1969. Syn-sedimentary marine lithification of Middle Jurassic limestones in the Paris basin. Sedimentology 12, 205-230.

Pye, K., 1987. Aeolian Dust and Dust Deposits; Academic Press, London, 334p.

Rasmussen, B., Bekker, A., Fletcher, I.R., 2013. Correlation of Paleoproterozoic glaciations based on U-Pb zircon ages for tuff beds in the Transvaal and Huronian Supergroups. Earth and Planetary Science Letters 382, 173-180.

Reineck, H.E., and Singh, I.B., 1973. Depositional sedimentary environments. Springer-Verlag, New York, New York, 439p.

Reineck H.E. and I.B. Singh, 1980. Depositional sedimentary environments. Springer, Berlin, 549p.

Richthofen, F., 1882. On the mode of origin of the loess; Geological Magazine 9, 293-305.

Rieu, R., Allen, P.A., Etienne, J.L., Cozzi, A., Wiechert, U., 2006. A Neoproterozoic glacially influenced basin margin succession and “atypical” cap carbonate associated with bedrock palaeovalleys, Mirbat area, southern Oman. Basin Research 18, 471–496.

Roberts, J.J., Boyd, R., 2004. Late Quaternary core stratigraphy of the northern New South Wales continental shelf. Australian Journal of Earth Science 51, 141–156.

Robertson, J.A., 1957a. District of Algoma Ontario. Ontario Department of Mines, Map 2001, Township 143.

Robertson, J.A., 1957b. District of Algoma Ontario. Ontario Department of Mines, Map 2002, Township 144.

Robertson, J.A., 1958a. District of Algoma Ontario. Ontario Department of Mines, Map 2003, Township 137.

Robertson, J.A., 1958b. District of Algoma Ontario. Ontario Department of Mines, Map 2004, Township 138.

Robertson, J.A., 1959a. District of Algoma Ontario. Ontario Department of Mines, Map 2014, Township 155.

Robertson, J.A., 1959b. District of Algoma Ontario. Ontario Department of Mines, Map 2015, Township 156.

Robertson, J.A., 1963a. District of Algoma Ontario. Ontario Department of Mines, Map 2113, Township 149.

Robertson, J.A., 1963b. District of Algoma Ontario. Ontario Department of Mines, Map 2114, Township 150.

Robertson, J.A., 1964. Geology of Scarfe, Mack, Cobden and Striker Townships, District of Algoma. Ontario Department of Mines Geological Report 20, 89p.

Robertson, J.A., 1965. Algoma District. Ontario Department of Mines, Map 2315, Lewis and Shedden Townships and parts of Indian Reserves No. 5 and No. 7.

Robertson, J.A., 1966. Victoria Township, District of Algoma. Ontario Department of Mines Preliminary Geological Map, 377.

Robertson, J.A., 1968. Geology of Township 149 and Township 150. Ontario Department of Mines Geological Report 57, 1-162.

Robertson, J.A., 1970. Geology of the Spragge area. Ontario Department of Mines Geological Report 76, 109p.

Robertson, J.A., 1973. A review of recently acquired geological data, Blind River-Elliot Lake area; *in* Huronian Stratigraphy and Sedimentation, G.M. Young (Ed.). Geological Association of Canada, Special Paper 12, 169-198.

Robertson, J.A., Abraham E.M., 1960. Algoma District. Ontario Department of Mines, Map 2028, Scarfe, Mack, Cobden, and Striker Townships.

Robertson, J.A., and Fraser, M., 1964. Lewis Township, District of Algoma. Ontario Department of Mines Preliminary Geological Map P 246.

Robertson, J.A., Card, K.D., Frarey, M.J., 1969. Committee on Huronian stratigraphy progress report. Canadian Journal of Earth Science 6, 335-336.

Rothman, D.H., Hayes, J.M., Summons, R.E., 2003. Dynamics of the Neoproterozoic carbon cycle. PNAS, USA 100, 8124–8129.

Rousell, D.H., Long, D.G.F., 1998. Are outliers of the Huronian Supergroup preserved in structures associated with the collapse of the Sudbury impact crater? Journal of Geology 106, 407-419.

Rust, B. R. and Romanelli, R., 1975. Late Quaternary subaquatic outwash deposits near Ottawa, Canada. In: A. V. Jopling and B. C. McDonald (Editors), Glaciofluvial and Glaciolacustrine

Sedimentation. Society of Economic Paleontologists and Mineralogists, Special Publication 23, 177-192.

Salvi, C., Busetti, M., Marinoni, L., Brambati, A., 2006. Late Quaternary glacial marine to marine sedimentation in the Pennell Trough (Ross Sea, Antarctica). Palaeogeography, Palaeoclimatology, Palaeoecology 231, 199-214.

Sarangi, S., Mohanty, S.P., Barik, A., 2017. Rare earth element characteristics of Paleoproterozoic cap carbonates pertaining to the Sausar Group, Central India: implications for ocean paleoredox conditions. Journal of Asian Earth Sciences 148, 31-50.

Savrda, C.E., 1995. Ichnologic applications in palaeoceanographic, palaeoclimatic and sea- level studies. PALAIOS 10, 565–577.

Schidlowski, M., Hayes, J.M., and Kaplan, I.R., 1983. Isotopic inferences of ancient biochemistries: carbon, sulfur, hydrogen, and nitrogen, in Schopf, J.W., ed., Earth's Earliest Biosphere: Its Origin and Evolution. Princeton University Press, Princeton, 149-187.

Schlager, W., James, N.P., 1978. Low-magnesian calcite limestones forming at the deep-seafloor, Tongue of the Ocean, Bahamas. Sedimentology 25, 675–702.

Schroder, S., Grotzinger, J.P., 2007. Evidence for anoxia at the Ediacaran-Cambrian boundary: the record of redox sensitive trace elements and rare earth elements in Oman. Journal of the Geological Society 164, 175–187.

Schumm, S.A., 1968. Speculations concerning paleo-hydrologic controls of terrestrial sedimentation. Geological Society of America Bulletin 79, 1573-1588.

Shackleton, J.S., 1962. Cross-strata of the Rough Rock (Millstone Grit Series) in the Pennines. Liverpool Manchr. Geological Journal 3, 109-118.

Shen, Y., Zhang, T., Chu, X., 2005. C-isotopic stratification in a Neoproterozoic postglacial ocean. Precambrian Research 137, 243–251.

Sheridan, R.E., 1981. Recent research on passive continental margins. Society of Economic Paleontologists and Mineralogists, Special Publication 32, 39-55.

Shields, G.A., 2005. Neoproterozoic cap car bonates: A critical appraisal of existing models and the plumeworld hypothesis. Terra Nova 17, 299–310.

Shields, G.A., Deynoux, M., Strauss, H., Paquet, H., and Nahon, D., 2007. Barite-bearing cap dolostones of the Taoudéni Basin, northwest Africa: Sedimentary and isotopic evidence for methane seepage after a Neoproterozoic glaciation. Precambrian Research 153, 209–235.

Shinn, E.A., 1969. Submarine lithification of Holocene carbonate sediments in the Persian Gulf. Sedimentology 12, 109–144.

Sholkovitz, E. R., Landing, W. M., Lewis, B. L., 1994. Ocean particle chemistry - the fractionation of rare-earth elements between suspended particles and seawater. Geochimica et Cosmochimica Acta 58, 1567–1579.

Schulz, K.J., Cannon, W.F., 2007. The Penokean orogeny in the Lake Superior region. Precambrian Research 157, 4–25.

Sekine, Y., Suzuki, K., Senda, R., Goto, K.T., Tajika, E., Tada, R., Goto, K., Yamamoto, S., Ohkouchi, N., Ogawa, N.O., Maruoka, T., 2011. Osmium evidence for synchronicity between a rise in atmospheric oxygen and Palaeoproterozoic deglaciation. Nature Communications 2, 502.

Sepkoski, J.J., 1982. Flat-pebble conglomerates, storm deposits, and the Cambrian bottom fauna. In: Cyclic Event and Stratification (Eds G. Einsele and A. Seilacher), Springer-Verlag, Berlin, 371–388.

Shen, Y., Zhang, T., Chu, X., 2005. C-isotopic stratification in a Neoproterozoic postglacial ocean. Precambrian Research 137, 243–251.

Shields, G., Webb, G., 2004. Has the REE Composition of Seawater Changed Over Geological Time? Chemical Geology 204, 103–107.

Shields, G.A., Deynoux, M., Strauss, H., Paquet, H., Nahon, D., 2007. Barite-bearing cap dolostones of the Taoudéni Basin, northwest Africa: Sedimentary and isotopic evidence for methane seepage after a Neoproterozoic glaciation. Precambrian Research 153, 209–235.

Simonson, B.M., Schubel, K.A., Hassler, S.W., 1993. Carbonate sedimentology of the early Precambrian Hamersley Group of Western Australia. Precambrian Research 60, 287–335.

Sims, P.K., Card, K.D., Lumbers, S.B., 1981. Evolution of early Proterozoic basins of the Great Lakes region; *in* Proterozoic Basins of Canada, Geological Survey of Canada, Paper 81-10, 379-397.

Smalley, I.J., 1971. 'In-Situ' theories of loess formation and the significance of the $CaCO_3$ content. Earth Science Review 7, 67-85.

Smalley, I.J. and Vita-Finzi, C., 1968. The formation of fine particles in sandy deserts and the nature of "desert" loess. Journal of Sedimentary Petrology, 38, 766-774.

Smalley, I.J., Jefferson, I.F., Dijkstra, T.A., and Derbyshire, E., 2000. Some major events in the development of the scientific study of loess. Earth-Science Reviews 54, 5-18.

Smith, N.D., Ashley, G.M., 1985. Proglacial lacustrine environment, *in* Ashley, G., Shaw, M., Smith, N.D. (eds.), Glacial Sedimentary Environments, Society of Economic Paleontologists and Mineralogists, Short Course 16, 135-216.

Soreghan, M.J., Soreghan, G.S., and Hamilton, M.A., 2000. Paleowinds inferred from detrital zircon geochronology of Upper Paleozoic loessite, western North America (Abst.); Geological Society of America, Annual Meeting, Reno.

Spencer, A.M., 1971. Late Precambrian glaciation in the North Atlantic region in Scotland. Geological Society, London, Memoirs 6, 1-48.

Stea, R.R., Piper, D.J.W., Fader, G.B.J., Boyd, R., 1998. Wisconsinian glacial and sea-level history of Maritime Canada and adjacent continental shelf: a correlation of land and sea events. Geological Society of America Bulletin 110, 821-845.

Stear, W.M., 1985. Comparison of the bedform distribution and dynamics of modern and ancient sandy ephemeral flood deposits in the southwestern Karoo region, South Africa. Sedimentary Geology 45, 209-230.

Stow, D., 1981. Laurentian fan: morphology, sediments, processes and growth pattern. American Association of Petroleum Geologists Bulletin 65, 375-393.

Stravers, J.A., Powell, R.D., 1997. Glacial debris flow deposits on the Baffin Island shelf: seismic facies architecture of till-tounge like deposits. Marine Geology 143, 151-167.

Strum, M., Matter, A., 1978. Turbidites and varves in Lake Brienz (Switzerland): deposition of clastic detritus by density currents. In: Matter, A., Tucker, M.E. (eds.), Modern and Ancient Lake Sediments: International Association of Sedimentologists, Special Publication No. 2, Blackwell, London, 145-168.

Suess, E., 2014. Marine cold seeps and their manifestations: geological control, biogeochemical criteria and environmental conditions. International Journal of Earth Sciences 103, 1889–1916.

Sumner, D.Y., Grotzinger, J.P., 2000. Late Archean aragonite precipitation: petrography, facies associations, and environmental significance. In: Grotzinger, J.P., James, N.P. (Eds.), Carbonate Sedimentation and Diagenesis in the Evolving Precambrian World, 67. SEPM Special Publication, 123–144.

Talling, P.J., Masson, D.G., Sumner, E.J., Malgesini, G., 2012. Subaqueous sediment density flows; depositional processes and deposit types. Sedimentology 59, 1937-2003.

Tang, H., Chen, Y., 2015. Global glaciations and atmospheric change at ca. 2.3 Ga. Geoscience Frontiers 4, 583-596.

Thompson, D.B., 1970. Sedimentation of the Triassic (Scythian) red pebbly sandstones in the Cheshire Basin and its margins. Geological Journal 7, 183-216.

Tsoar, H. and Pye, K., 1987. Dust transport and the question of desert loess formation. Sedimentology 34, 139-153.

Tungsheng, L., 1988. Loess in China, Springer-Verlag, Berlin, 224p.

Van Schmus, W.R., 1965. The geochronology of the Blind River-Bruce Mines area, Ontario. Journal of Geology 73, 755-780.

Vanyo, J.P., Awramik, S.M., 1982. Length of day obliquity of the ecliptic 850 Ma ago; preliminary results of a stromatolite growth model. Geophysical Research Letters 9, 1125-1128.

Vanyo, J.P., Awramik, S.M., 1985. Stromatolites and Earth-Sun-Moon dynamics. Precambrian Research 29, 121-142.

Vanyo, J.P., Hutchinson, R.A., Awramik, S.M., 1986. Heliotropism in microbial stromatolitic growths at Yellowstone National Park; geophysical inferences. Eos, Transactions, American Geophysical Union 67 (153), 155-156.

Veizer, J., 2003. Isotopic evolution of seawater on geological time scales: sedimentological perspective, in Lentz, D.R., ed., Geochemistry of Sediments and Sedimentary Rocks: Evolutionary Considerations to Mineral Deposit-Forming Environments: Geological Association of Canada, GeoText 4, 53-68.

Veizer, J., Clayton, R.N., Hinton, R.W., 1992. Geochemistry of Precambrian carbonates; IV, Early Paleoproterozoic (2.25 + or - 0.25 Ga) seawater. Geochimica et Cosmochimica Acta 56, 875-885.

Visher, G.S., 1965. Use of the vertical profile in environmental reconstruction. American Associatioon of Petroleum Geologists Bulletin 49, 41-61.

Visser, J.N.J., 1991. The paleoclimatic setting of the Late Proter- ozoic marine ice sheet in the Karoo Basin ofsouthern Africa. In: Anderson, J.B., Ashley, G.M. (Eds.), Glacial Marine Sedimentation: Paleoclimatic Significance. Geological Society of America Special Paper 261, 181–190.

Visser, J.N.J., Collinson, W.P. and Terblanche, J.C., 1984. The origin of soft-sediment deformation structures and related deposits in Permo-Carboniferous glacial and proglacial beds, South Africa. Journal of Sedimentary Petrology 54, 1183-1196.

Walker, R.G., 1984. Shelf and shallow marine sands. In: Facies models, R.G. Walker (Ed.). Geoscience Canada, Reprint Series 1, 141-170.

Walther, J. V., 2009. Essentials of geochemistry. Second edition. Jones and Bartlett Publishers, Sudbury, Mass. 797p.

Wang, J., Jiang, G., Xiao, S., Li, Q., Wei, Q., 2008. Carbon isotope evidence for widespread methane seeps in the ca. 635 Ma Doushantuo cap carbonate in south China. Geology 36, 347–350.

Webb, G.E., Kamber, B.S., 2000. Rare earth elements in Holocene reefal microbialites: a new shallow seawater proxy. Geochimica et Cosmochimica Acta 64, 1557–1565.

Williams, G.E., 1975. Late Precambrian glacial climate and the Earth's obliquity. Geological Magazine 112, 441–465.

Williams, G.E., Schmidt, P.W., 1997. Paleomagnetism of the Paleoproterozoic Gowganda and Lorrain Formations, Ontario: Low paleolatitude for Huronian glaciation. Earth and Planetary Science Letters 153, 157-169.

Williams, G.E., and Schmidt, P.W., 2018. Shuram–Wonoka carbon isotope excursion: Ediacaran revolution in the world ocean's meridional overturning circulation. Geoscience Frontiers 9, 391–402.

Williams, H., Hoffman, P.F., Lewry, J.F., Monger, J.W.H., Rivers, T., 1991. Anatomy of North America: thematic geologic portrayal of the continents. Tectonophysics 187, 117-134.

Wilson, M.D., 1985. Origin of Upper Cambrian flat pebble conglomerates in the Northern Powder River Basin, Wyoming. 7th SEPMCore Workshop. Golden, CO, 1–50.

Winker, C.D., Edwards, M.B., 1983. Nonstable progradational clastic shelf margins. Society of Economic Paleontologists and Mineralogists. Special Publication 33, 139-157.

Winsemann, L.D., Coleman, J.M., 1974. Mississippi River mouth processes: effluent dynamics and morphologic development. Journal of Geology 82, 751-788.

Withjack, M.O., Schlische, R.W., Olsen, P.E., 2002. Rift-basin structure and its influence on sedimentary systems. In: Renault, R.W., Ashley, G. (Eds.), Sedimentation in Continental Rifts. Society for Sedimentary Geology Special Publication 73, 57-81.

Ye, Q., Tong, J., Xiao, S., Zhu, S., An, Z., Tian, L., Hu, J., 2015. The survival of benthic macroscopic phototrophs on a Neoproterozoic Snowball Earth. Geology 43, 507-510.

Young, G.M., 1966. Huronian stratigraphy of the McGregor Bay area, Ontario: Relevance to the paleogeography of the Lake Superior region. Canadian Journal of Earth Science 3, 203-210.

Young, G.M., 1969. Geochemistry of early Proterozoic tillites and argillites of the Gowganda Formation, Ontario, Canada. Geochimica et Cosmochimica Acta 33, 483-492.

Young, G.M., 1972. Downward intrusive breccias in the Huronian Espanola Formation, Ontario, Canada. Canadian Journal of Earth Sciences 9, 756–762.

Young, G.M., 1973a. Origin of carbonate-rich Early Proterozoic Espanola Formation, Ontario, Canada. Geological Society of America Bulletin 84, 135–160.

Young, G.M., 1973b. Tillites and aluminous quartzites as possible time markers for Middle Precambrian (Aphebian) rocks of North America. In: Young, G.M. (Ed.), Huronian Stratigraphy and Sedimentation. The Geological Association of Canada, Special Paper 12, 97–127.

Young, G.M., 1981. Diamictites of the early Proterozoic Ramsey Lake and Bruce Formations, north shore of Lake Huron, Canada. In: Hambrey, M.J., Harland, W.B., (Eds.), Earth's pre-Pleistocene Glacial Record. Cambridge University Press, 813-816.

Young, G.M., 1988. Proterozoic plate tectonics, glaciations and iron-formations. Sedimentary Geology 58, 127-144.

Young, G.M., 2004. Earth's earliest extensive glaciations: tectonic setting and stratigraphic context of Paleoproterozoic glaciogenic deposits. In: Jenkins, G.S., McMenamin, M.A.S., McKay, C.P., Sohl, L. (Eds.), The Extreme Proterozoic: Geology, Geochemistry and Climate. American Geophysical Union, Washington, DC, Geophysical Monograph 146, 161-181.

Young, G.M., 2013a. Precambrian supercontinents, glaciations, atmospheric oxygenation, metazoan evolution and an impact that may have changed the second half of Earth history. Geoscience Frontiers 4, 247-261.

Young, G.M., 2013b. Climatic catastrophes in Earth history: two great Proterozoic glacial episodes. Geological Journal 48, 1-21.

Young, G.M., 2014. Contradictory correlations of Paleoproterozoic glacial deposits: Local, regional or global controls? Precambrian Research 247, 33-44.

Young, G.M., Jefferson, C.W., 1975. Late Precambrian shallow water deposits, Banks and Victoria Islands, Arctic Archipelago. Canadian Journal of Earth Science 12, 1734-1748.

Young, G.M., Nesbitt, H.W., 1985. The Gowganda Formation in the southern part of the Huronian outcrop belt, Ontario, Canada; stratigraphy, depositional environments and regional tectonic significance. Precambrian Research 29, 265-301.

Young, G. M., Long D.G.F., Fedo C.M., Nesbitt H.W., 2001. Paleoproterozoic Huronian basin: product of a Wilson cycle punctuated by glaciations and a meteorite impact. Sedimentary Geology 141-142, 233-254.

Zahnle, K., Claire, M., Catling, D., 2006. The loss of mass-independent fractionation in sulfur due to a Palaeoproterozoic collapse of atmospheric methane. Geobiology 4, 271–283.

Zolnai, A.I., Price, R.A., Helmstaedt, H., 1984. Regional cross section of the Southern Province adjacent to Lake Huron, Ontario: implications for the tectonic significance of the Murray Fault Zone. Canadian Journal of Earth Sciences 21, 447–456.

15.1 APPENDIX 1A:

MISSISSAGI FORMATION STRATIGRAPHIC SECTIONS

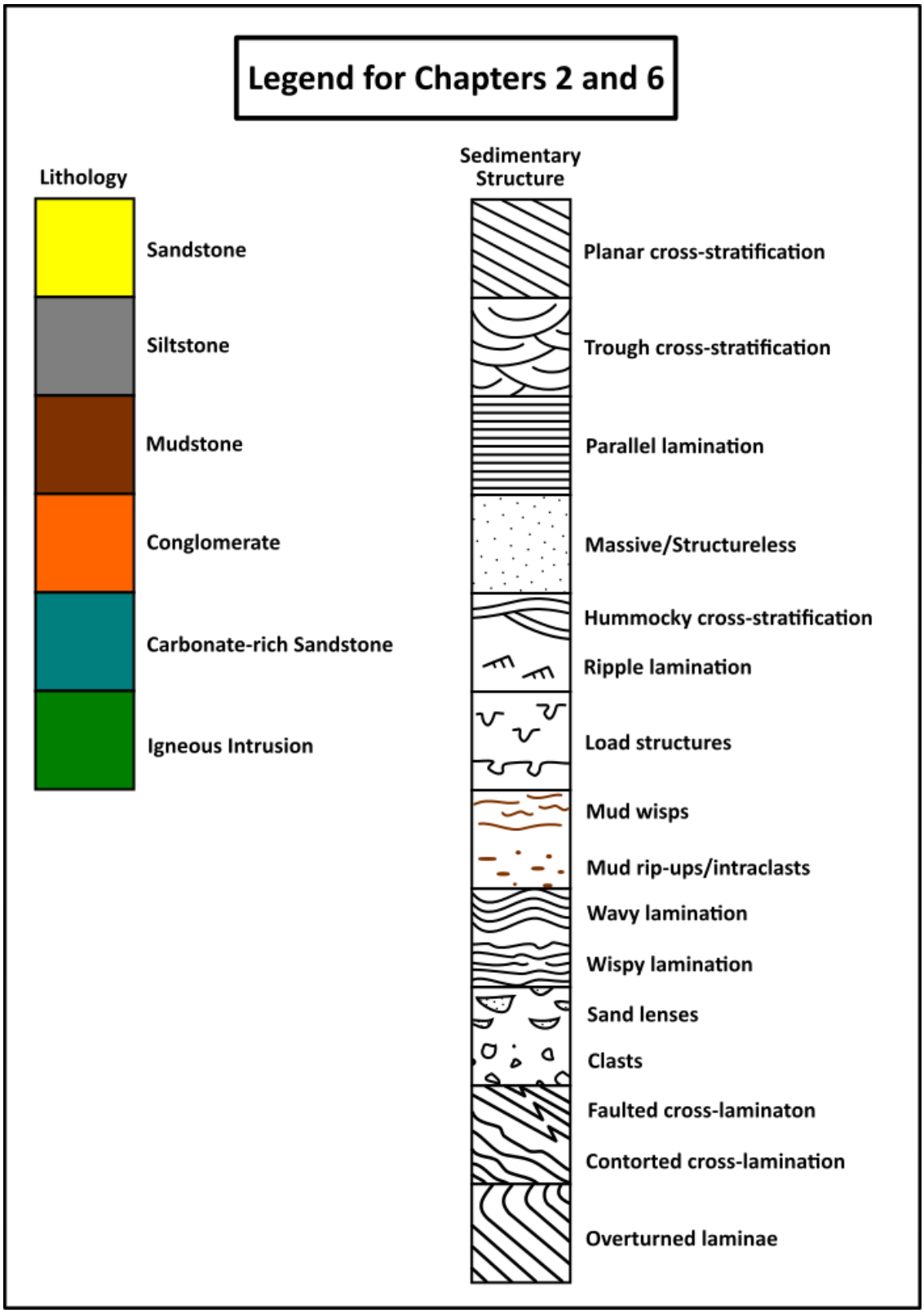

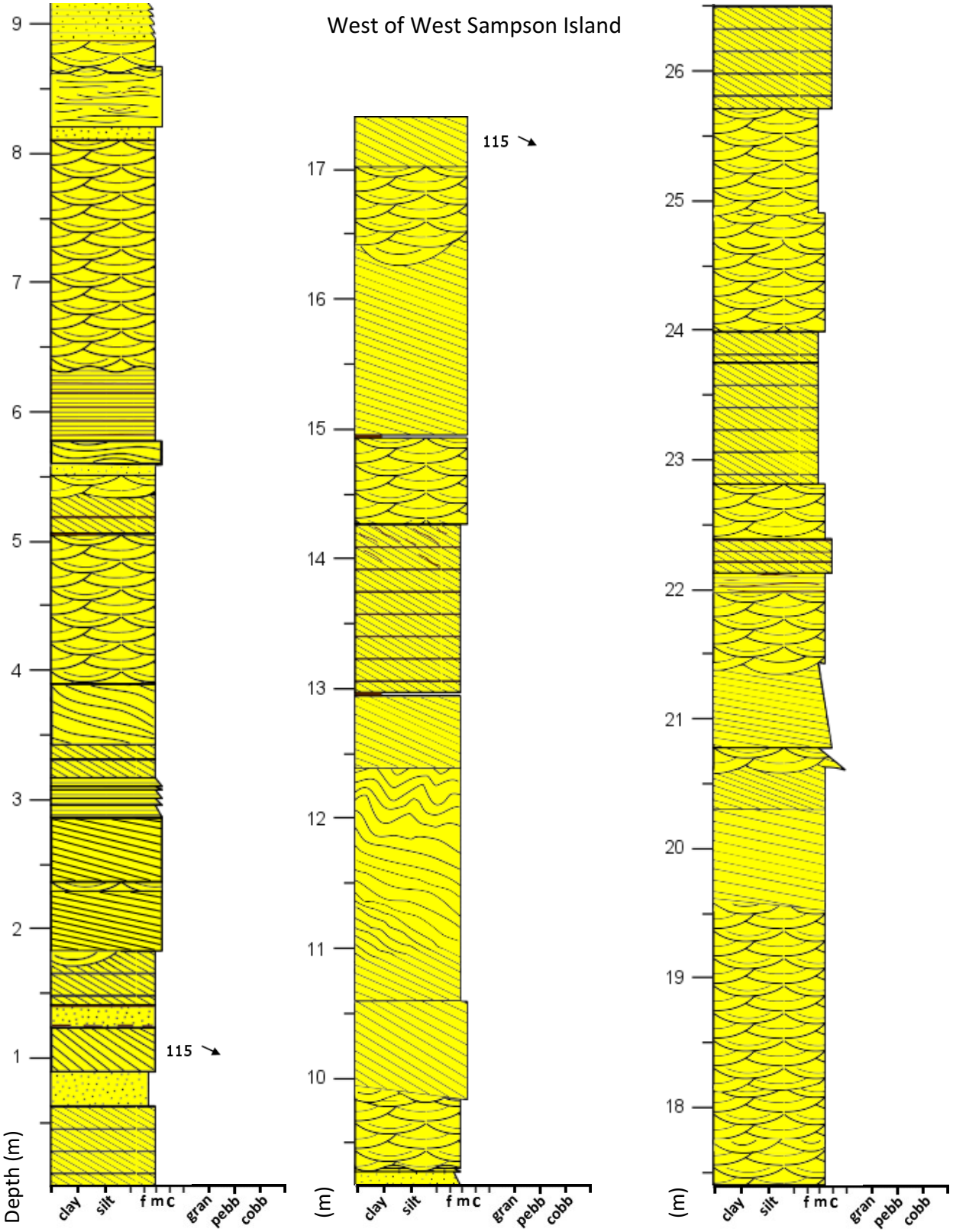
West of West Sampson Island
Depth (m)
9
8
7
6
5
4
3
2
1
115
clay
silt
f m c
gran
pebb
cobb
17
16
15
14
13
12
11
10
115
(m)
clay
silt
f m c
gran
pebb
cobb
26
25
24
23
22
21
20
19
18
(m)
clay
silt
f m c
gran
pebb
cobb

WEST OF WEST SAMPSON ISLAND

The stratigraphy of the upper Mississagi Formation west of West Sampson Island is typical in that it is dominated by planar and trough cross-stratified units. Planar cross-stratified units are large- to small-scale, formed from medium- and coarse-grained sands and can have laminae dipping at low angles. Large scale planar cross-stratified units sometimes show evidence of contortion and slumping within the upper parts of the foresets. Trough cross-stratification is the second most common unit, occurring as bundles and often erosively scouring underlying planar cross-stratified beds. The troughs are small- to medium-scale and sometimes have clay drapes and partings separating individual troughs within bundle sets. Some troughs display coarser bases that fine upwards into medium-grained sands but overall the typical grainsize of the trough cross-stratified beds is coarse- to medium-grained sands. Uncommon parallel lamination composed of medium- and coarse-grained sands forms between cross-stratified beds and can sometimes have laminae that are wavy to slightly contorted. Oftentimes the sorting within the parallel laminated units is poor and a change in grainsize is distinct between finer-grained and coarser-grained sands, or sands with a lower and higher concentration of silt and clay in the matrix. Small fining upwards beds are also a minor unit at this location and consist of coarse-grained sands to medium-grained sands that are poorly sorted. The exact contact with the overlying Bruce diamictite is submerged underwater and approximately 10m of stratigraphy is lost before encountering the overlying diamicitite to the south. Rare paleocurrent values collected from this location suggest a southeast direction of sediment transport.

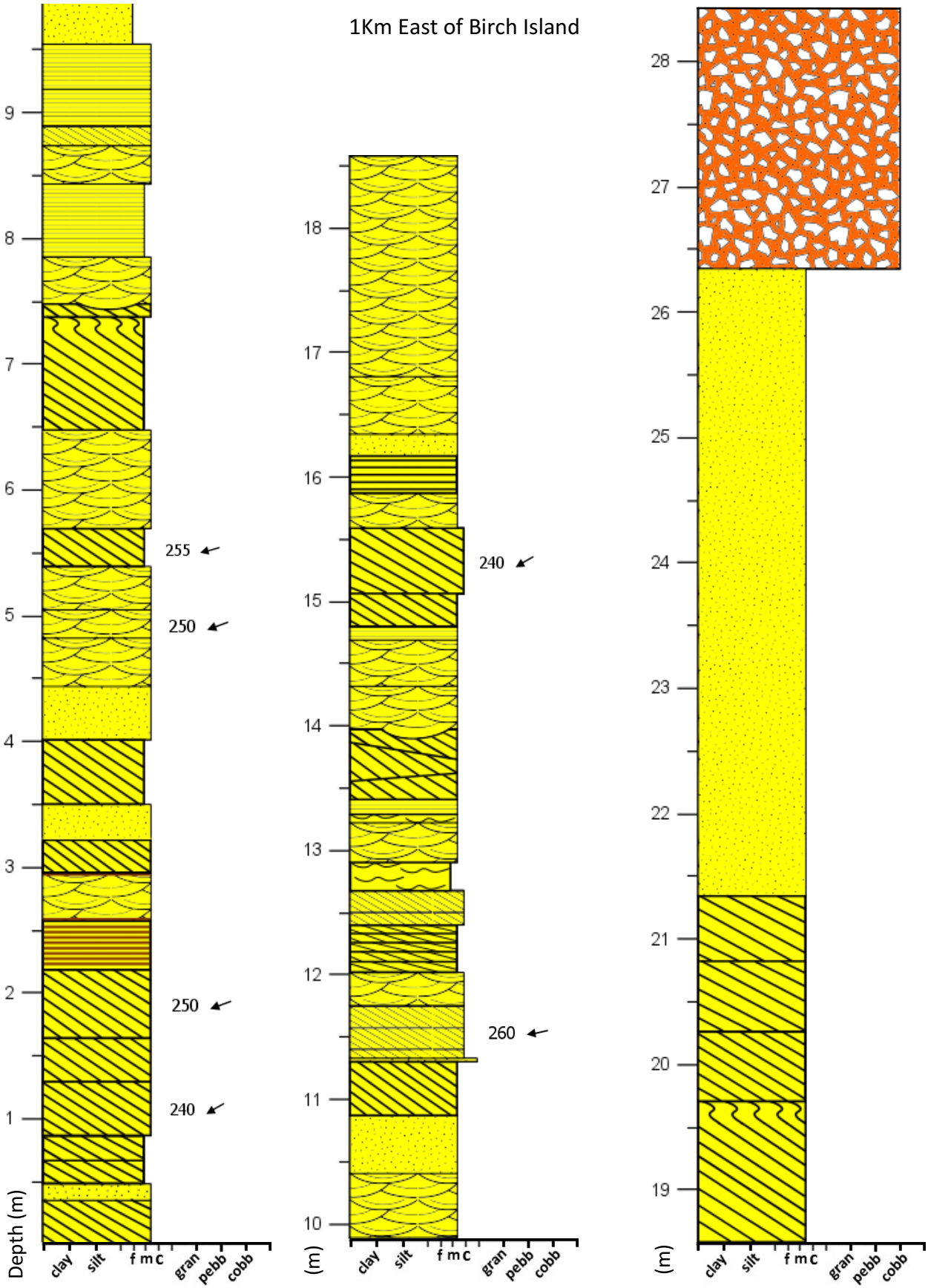
1Km East of Birch Island
Depth (m)
clay
silt
f m c
gran
pebb
cobb
255
250
250
240
240
260
(m)
(m)

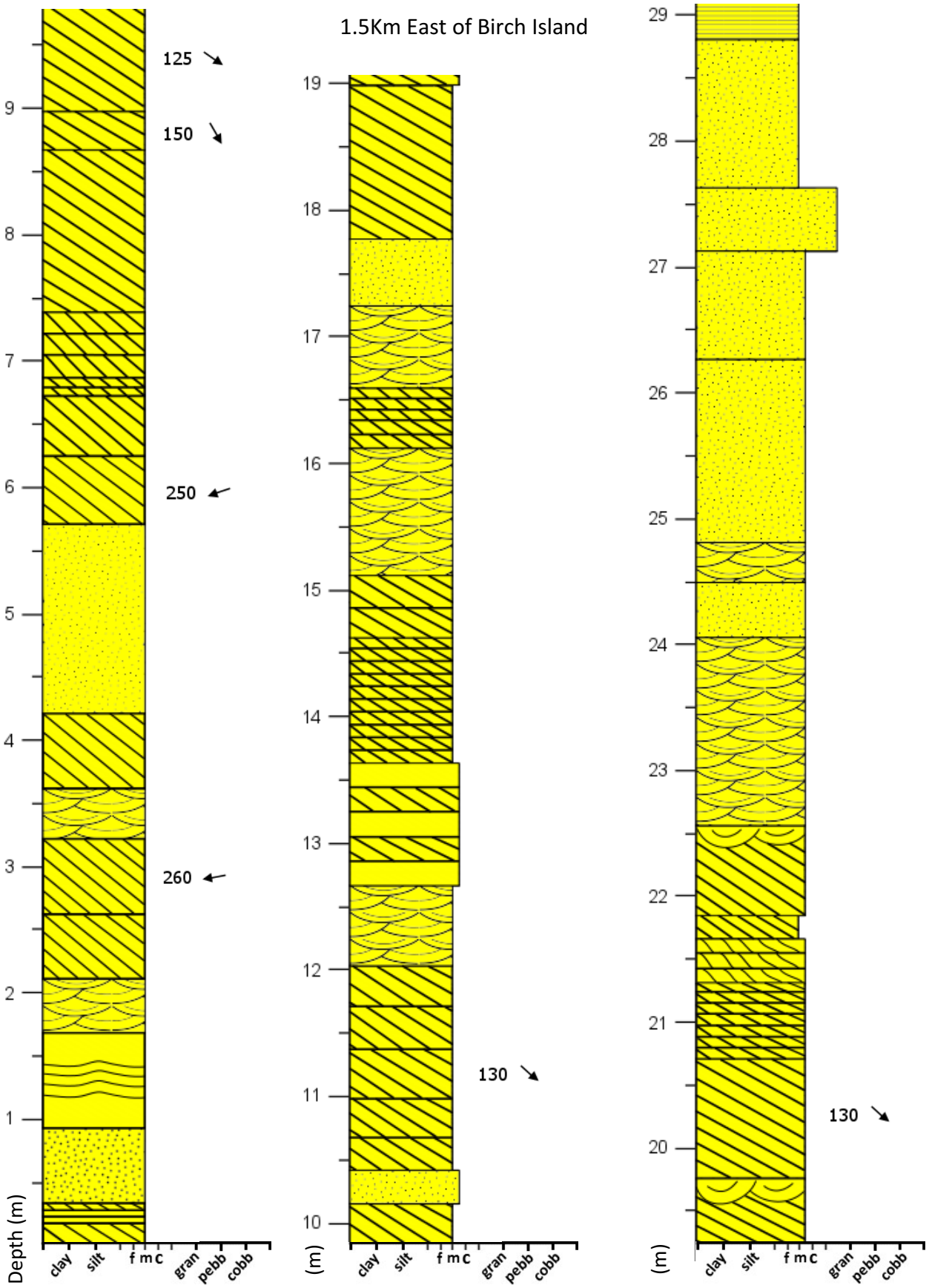
1.5Km East of Birch Island
125
150
250
260
130
130
Depth (m)
(m)
(m)
clay
silt
f m c
gran
pebb
cobb

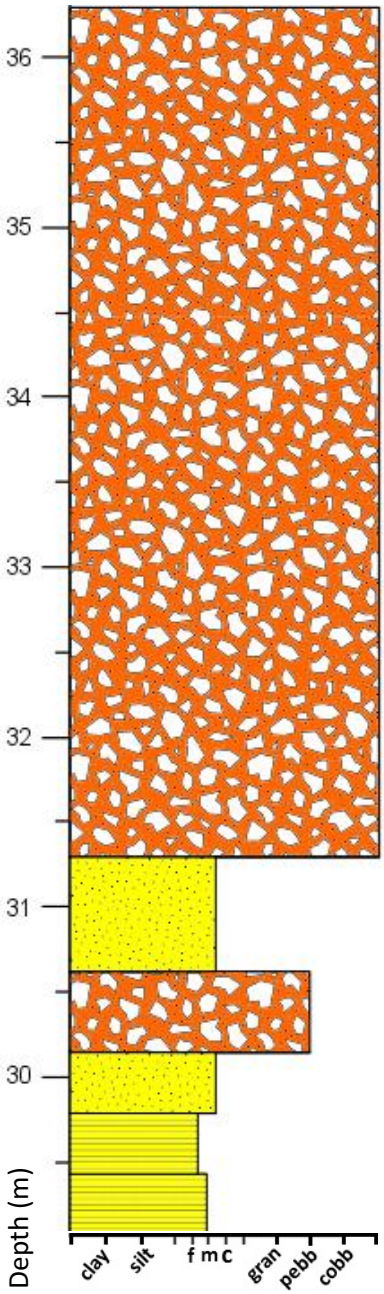
36
35
34
33
32
31
30
Depth (m)
clay
silt
f
m
c
gran
pebb
cobb

EAST OF BIRCH ISLAND

Two stratigraphic sections were logged on islands east from Birch Island with fairly similar features. Both sections were dominated by large-scale planar cross-stratification with some medium- to small-scale planar cross-stratification present as well. Grainsize of planar cross-stratified units is of medium- to coarse-grained sand. Some beds can be seen to pinch out laterally, and large-scale planar cross-stratified units can sometimes have evidence of internal slumping and contortion of laminae as well as rare clay drapes defining reactivation surfaces. Clay partings can also sometimes be observed separating beds. The second most common unit is small- to medium-scale trough cross-stratification of medium- to coarse-grained sands that typically occur as bundled sets of broad erosive scour fills. Occasionally, some troughs are coarser-grained at their base.

Parallel lamination and massive units are uncommon and parallel laminated beds consist of medium- to coarse-grained sands that are sometimes separated by silt and clay layers. Parallel laminated units are fine-grained or are wispy to wavy in appearance. Approaching the overlying Bruce diamictite at both outcrops, the Mississagi sandstones lose structure and become massive. At the outcrop further to the east there a noticeable decrease in sorting. Here the grainsize of the unit directly underlying the contact ranges from fine- to very coarse-grained sand, and has a noticeably higher concentration of silt and clay. At both outcrops the contact between the Mississagi and Bruce diamictite is sharp.

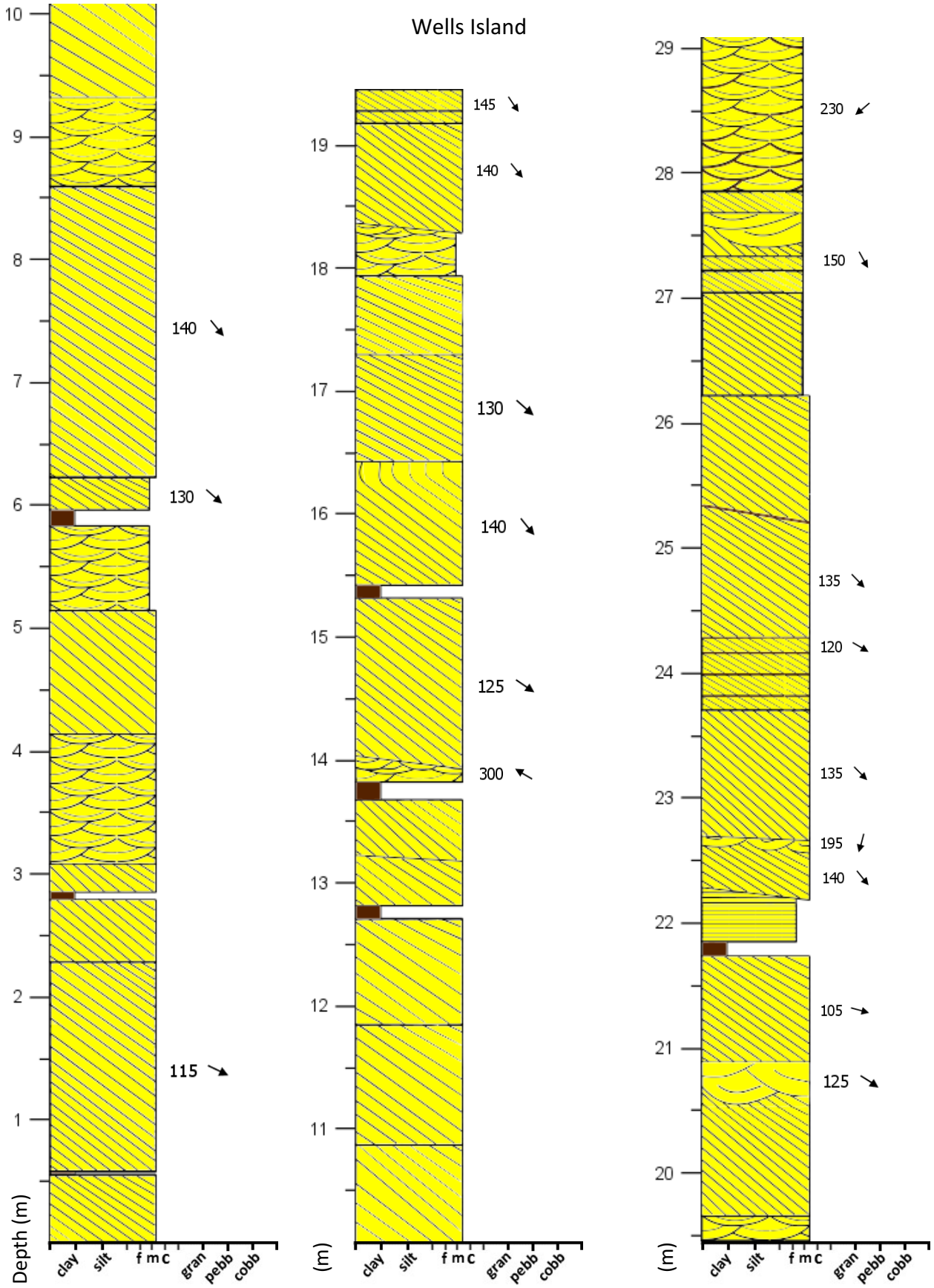
Wells Island
Depth (m)
(m)
(m)
clay
silt
f m c
gran
pebb
cobb
10
9
8
7
6
5
4
3
2
1
140
130
115
19
18
17
16
15
14
13
12
11
145
140
130
140
125
300
29
28
27
26
25
24
23
22
21
20
230
150
135
120
135
195
140
105
125

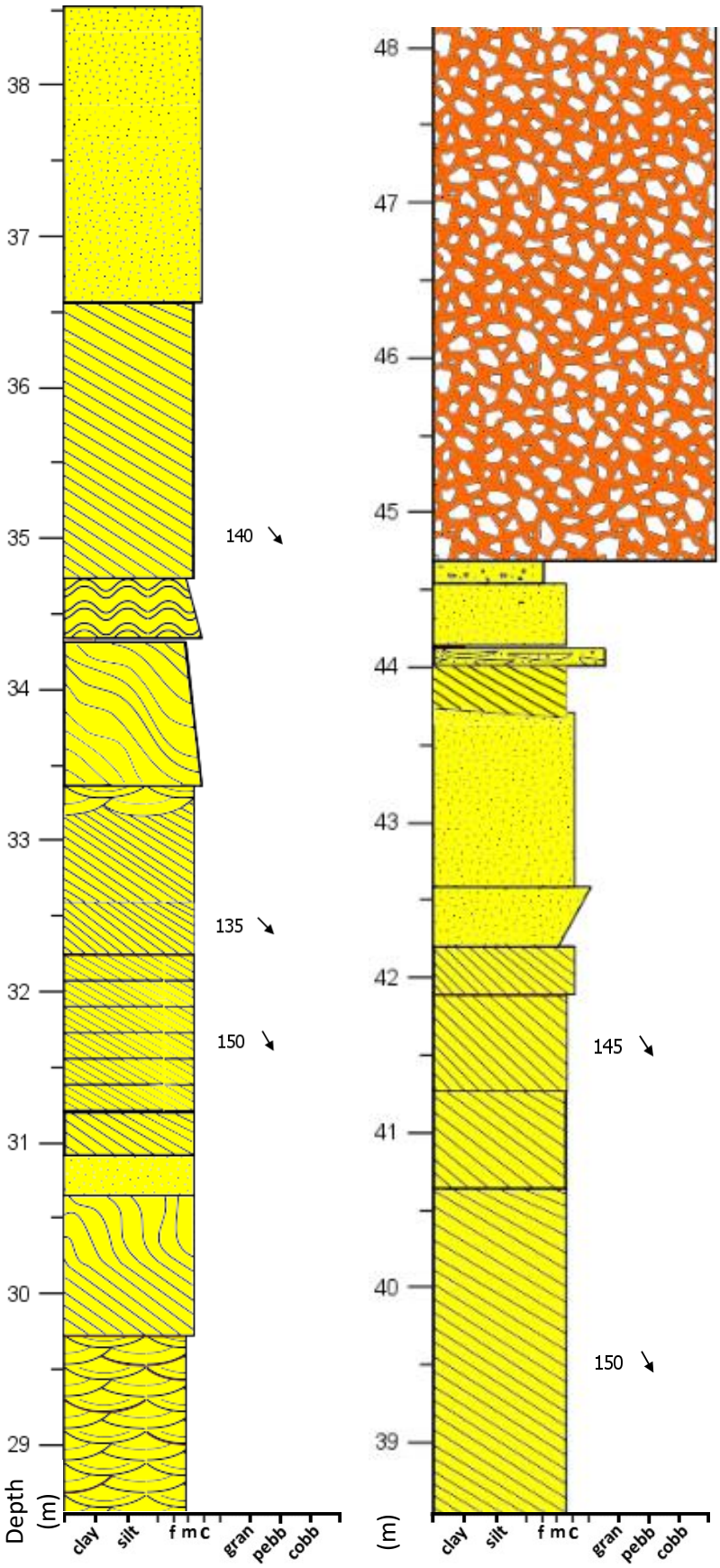
Depth (m)
38
37
36
35
34
33
32
31
30
29
140
135
150
clay
silt
f m c
gran
pebb
cobb
48
47
46
45
44
43
42
41
40
39
145
150
(m)
clay
silt
f m c
gran
pebb
cobb

WELLS ISLAND

At Wells Island the Mississagi Formation immediately below the Bruce is dominated by both planar cross-stratified and trough cross-stratified beds that show roughly unidirectional paleocurrent values, trending ESE to SSE. The planar cross-stratified beds are large-scale to rarely medium-scale and are separated by bundles of small-scale trough cross-stratified beds. Troughs will typically erosively scour into the planar cross-stratified bed that they overlie. Large-scale planar cross-stratified beds pinch out laterally in places and can be rarely separated by clay-rich layers up to 15cm thick. Clay-rich layers are also rarely present as mud drapes defining reactivation surfaces. One regressive climbing ripple was observed on a planar cross-stratified unit.

Grainsize of both planar and trough cross-stratified units is consistently medium- to coarse-grained, with some slightly finer-grained layers observed. The sequence contains one fine-grained sand to silt unit that is parallel laminated and erosively scoured into by a planar cross-stratified layer, which in turn is scoured by overlying trough cross-stratified beds. Soft-sediment deformation and slumping is common at the tops of planar cross-stratified beds, and in places the laminae may become overturned. Grainsize becomes much more variable approaching the contact with the Bruce Diamictite. Some layers are highly inequigranular and contain fine-grained sand to granules with rare pebbles up to 6mm in size. The unit directly underlying the contact with the diamictite is massive and is sharply overlain by a layer of fine-grained sandstone that hosts small dropstones.

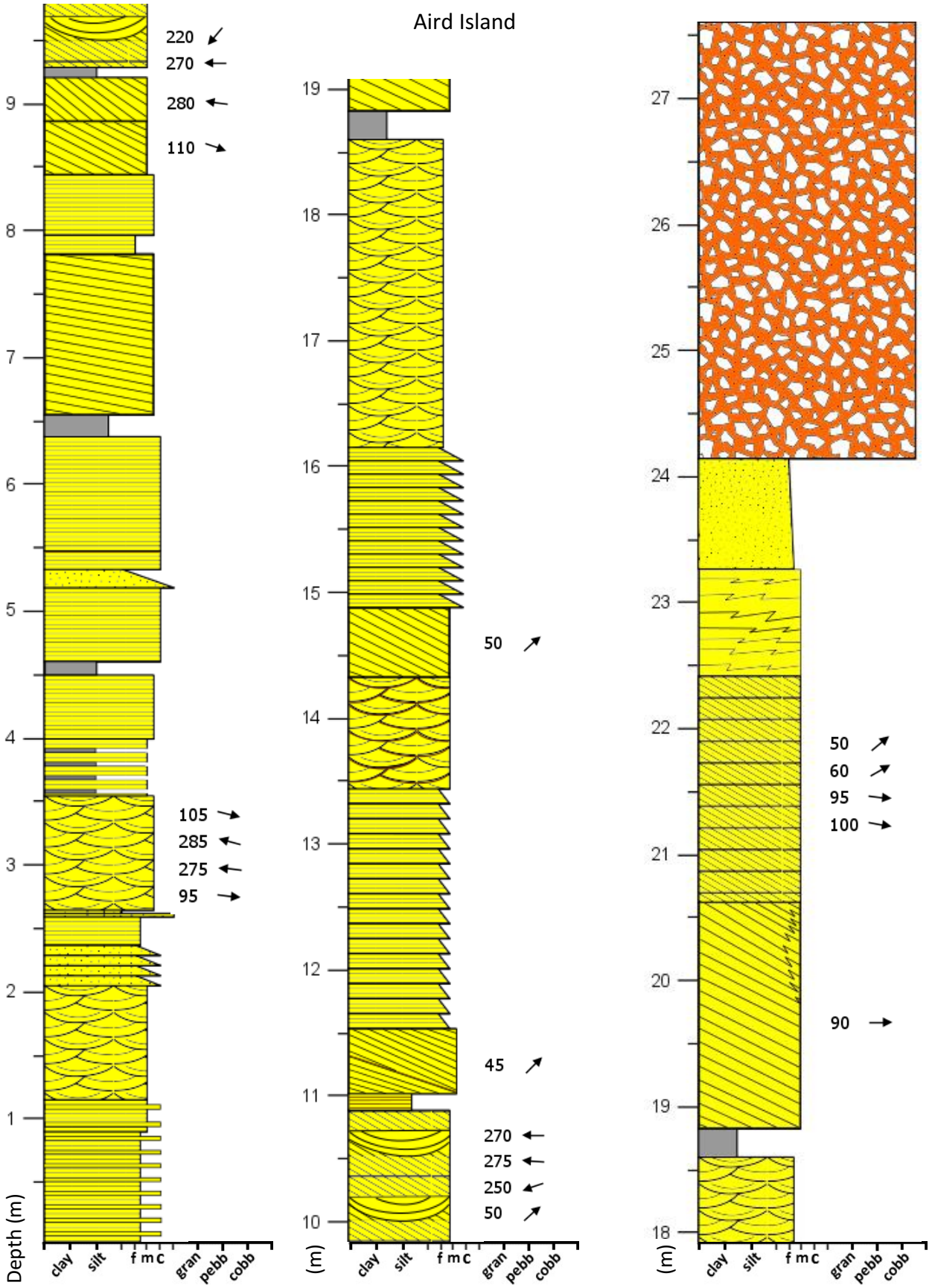
Aird Island
Depth (m)
(m)
(m)
clay
silt
f m c
gran
pebb
cobb
220
270
280
110
105
285
275
95
50
45
270
275
250
50
50
60
95
100
90

AIRD ISLAND

On Aird Island a stratigraphic section approximately 27.5m thick was logged of the contact between the upper Mississagi Formation and the overlying Bruce diamictite. The lithofacies present within the upper Mississagi at this contact are more variable than those encountered at other locations with planar and trough cross-stratification being present, as well as fining upwards units and parallel laminated units. Planar cross-stratification is large- to small-scale, composed of medium- to coarse-grained sands, and where small-scale it typically occurs in sets. Large-scale planar cross-stratified units can show internal reactivation surfaces and coarser grainsize at their bases. Approaching the contact with the Bruce, faulting of laminae in one large planar cross-stratified bed was observed, and the units immediately underlying the contact are massive or sheared in appearance. Trough cross-stratification is small- to medium-scale and also composed of medium- to coarse-grained sands. Troughs almost exclusively form bundles and scour into underlying planar cross-stratified units. Bidirectionality of paleocurrents can be observed within bundled sets of trough cross-stratification.

A feature unique to this location, relative to the other sections logged in this study, is the relatively common occurrence of fining upwards units and parallel lamination. Fining upwards units range in thickness from 8-10cm thick on average, up to 15cm in places, and typically occur in sets. They grade from medium-grained sand at their bases to silt and clay at their tops. While they often contain internal parallel lamination, they are sometimes massive with no internal structure visible. Parallel laminated units have a much more variable thickness, ranging from 1mm up to several cm. Lastly, clay-rich silt partings separate some units and are

typically bounded by planar and trough cross-stratified units as well as parallel laminated units. Paleocurrent directions for the stratigraphic sequence show two sets of bidirectional trends, one east-west, and another southwest-northeast. The northeast trend is stronger in influence than the others. Samples collected from the Mississagi Formation sandstone near the contact with the Bruce Formation, as well as from the Bruce diamictite immediately above the contact show a decrease in the sorting and an increase in the clay and silt content.

15.2 APPENDIX 1B

ESPANOLA FORMATION (DRILL CORE) STRATIGRAPHIC SECTIONS

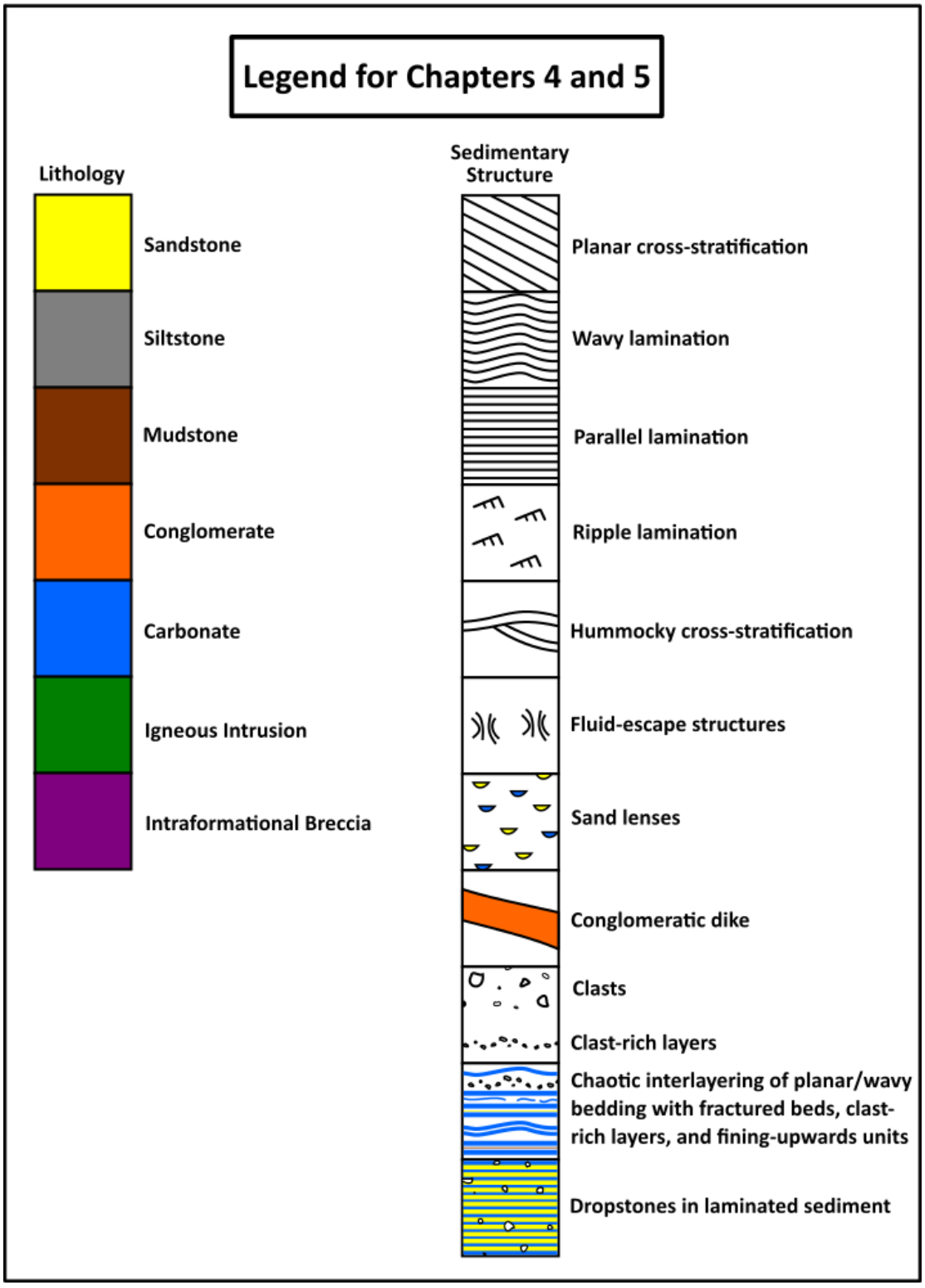

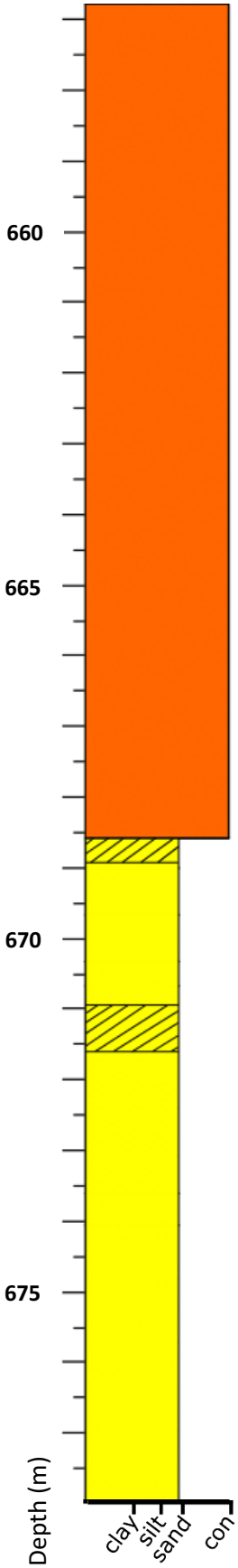
660
665
670
675
Depth (m)
clay
silt
sand
con

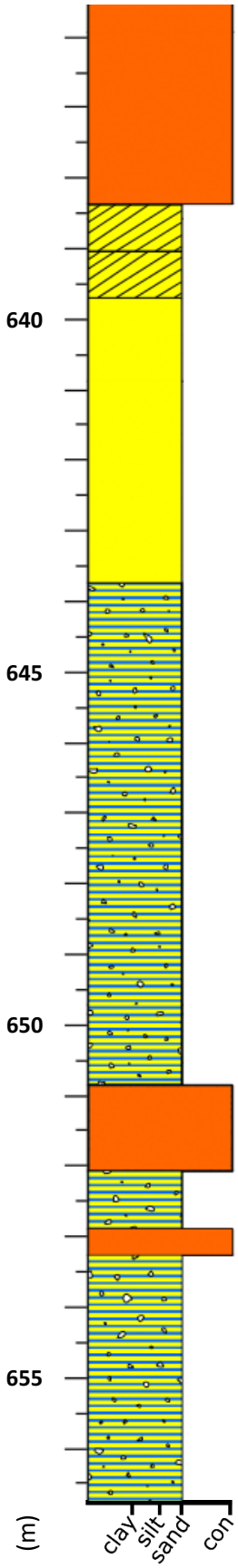
640
645
650
655
(m)
clay
silt
sand
con

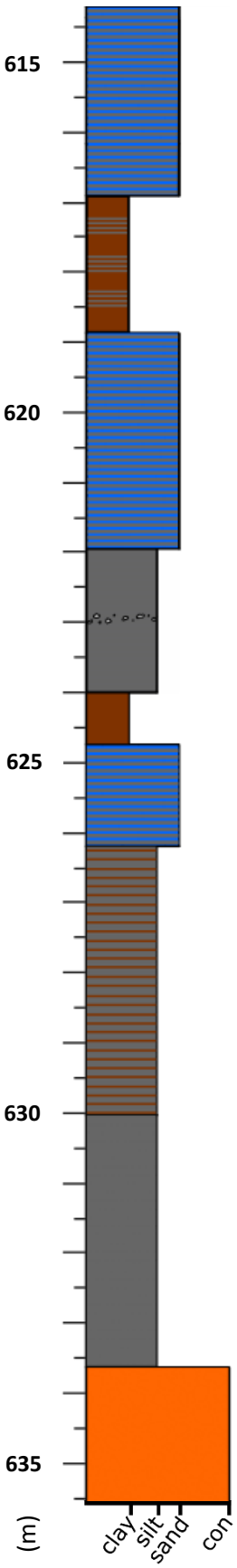
615
620
625
630
635
(m)
clay
silt
sand
con

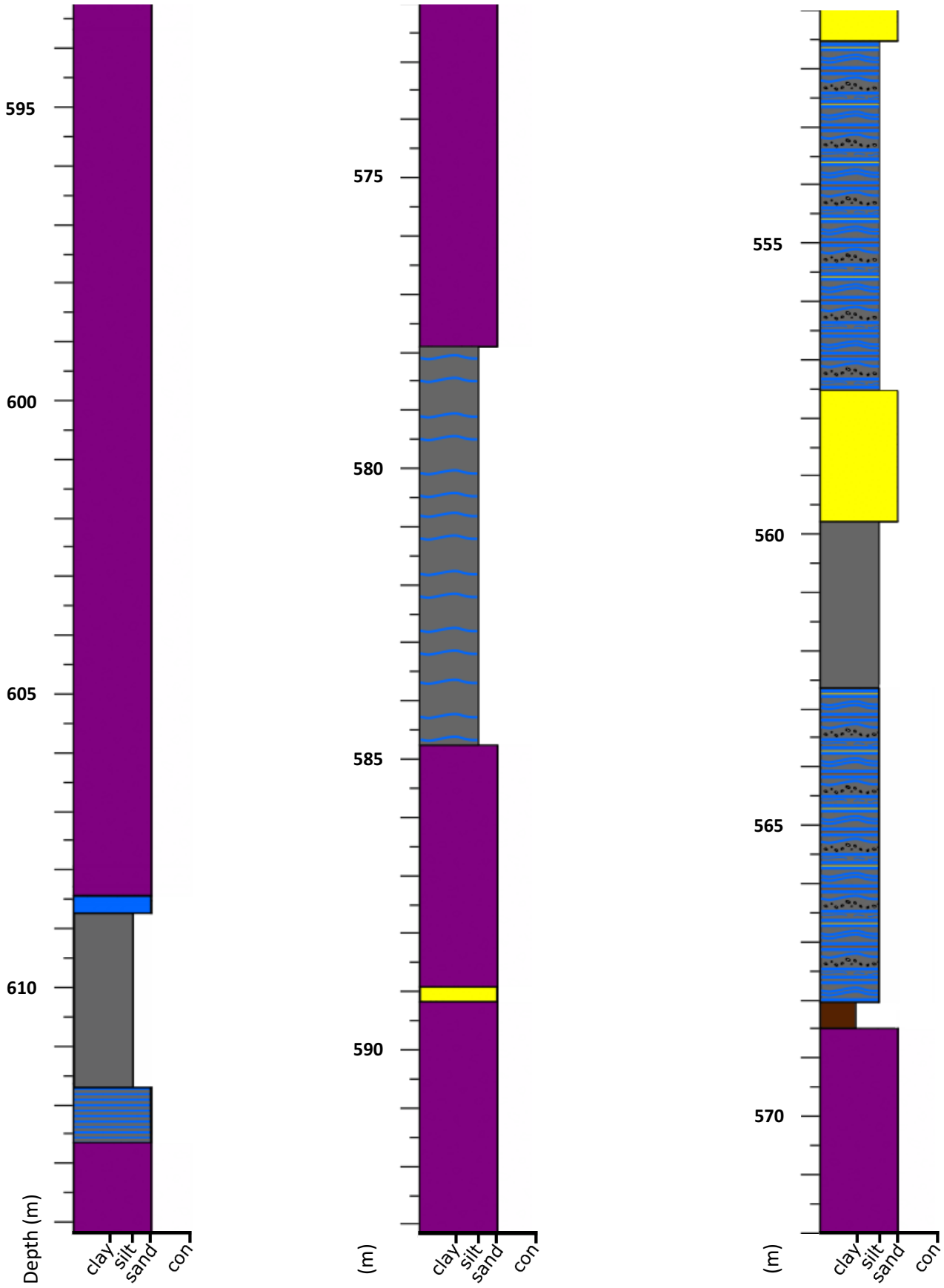
595
600
605
610
Depth (m)
clay
silt
sand
con
575
580
585
590
(m)
clay
silt
sand
con
555
560
565
570
(m)
clay
silt
sand
con

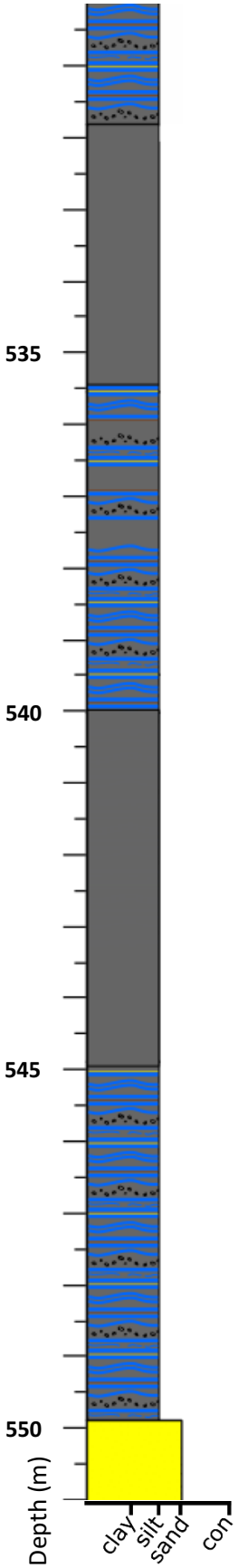
535
540
545
550
Depth (m)
clay
silt
sand
con

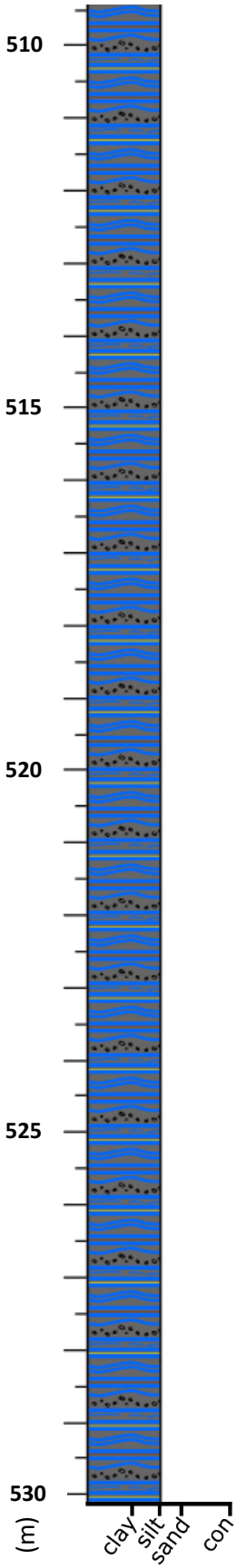
510
515
520
525
530
(m)
clay
silt
sand
con

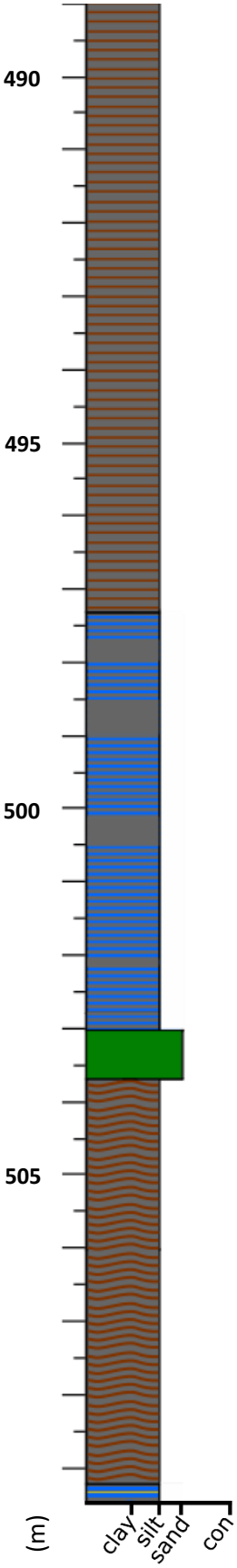
490
495
500
505
(m)
clay
silt
sand
con

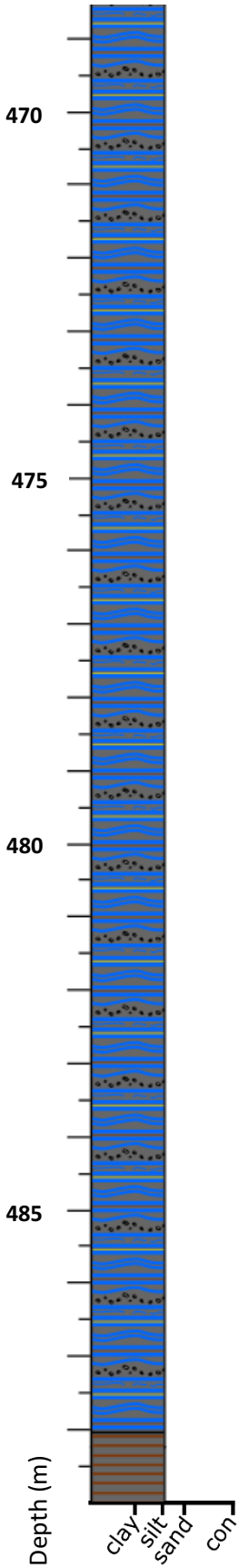
470
475
480
485
Depth (m)
clay
silt
sand
con

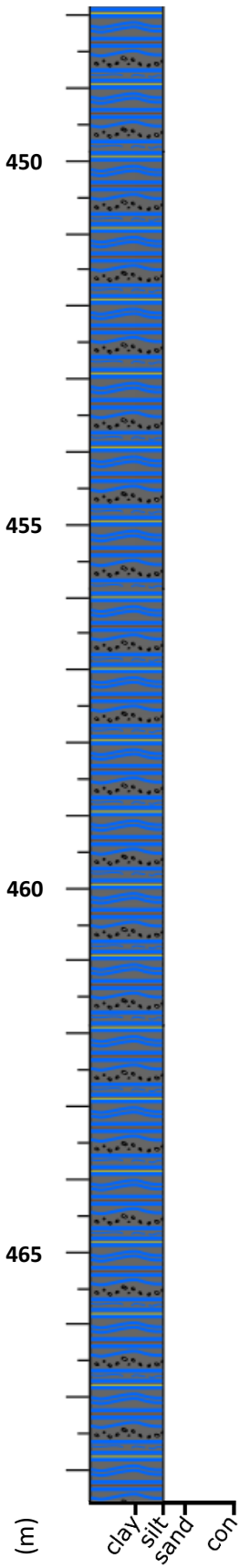
450
455
460
465
(m)
clay
silt
sand
con

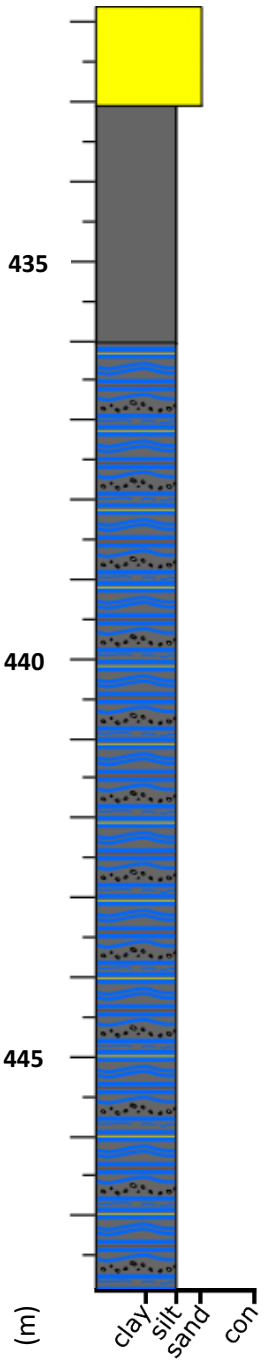
435
440
445
(m)
clay
silt
sand
con

DRILL HOLE E150-2

The Bruce Formation in drill hole E150-2 consists predominantly of massive sandy to silty diamictite that is grey in colour and has a variable clast content. Intermittently throughout the stratigraphy there are sections of massive fine-grained sandstone to siltstone that interbed with the diamictite and have no/little clasts. Approaching the contact with the Espanola Formation, these areas of clast-free fine-grained sand and siltstone begin to have sections of 1-10cm light orange weathering laminations. While typically parallel laminated, these light orange layers can also be highly contorted and disseminated to form 'mottled' patches. These light orange areas of stratigraphy have carbonate cements within them and react fairly strongly to HCl. Clast-rich areas of stratigraphy displace the clast-poor carbonate-rich areas, and in places, dropstones are visible displacing carbonate-rich laminae beneath them. The contact between the Bruce Formation and Espanola Formation is marked by a series of conglomerate beds and well-sorted medium-grained sandstone beds that are massive and cross-stratified. Directly above the contact the stratigraphy of the lower Espanola Formation is fairly typical and is dominated by interlaminated carbonate and siltstone. Parallel lamination is predominant but wavy to contorted lamination is common as well. Slump breccia is an accessory facies and mud laminae and wisps occur intermittently as well. Abundant intrusive breccia units break up the lower-middle stratigraphy of the Espanola Formation and these units have a broad range of angular clasts that have lithologies rendered from the various lithofacies associations of the Espanola Formation stratigraphy itself. In areas of primary stratigraphy that are between the breccias, siltstone and siliciclastic units predominate. Massive siltstone to fine-grained sandstone is the most common facies, with mud and carbonate laminae occasionally punctuating massive to

‘mushy’ and contorted appearing units. Moving upwards in stratigraphy, silt and fine-grained sandstone still predominate but carbonate units become more common again. Massive units and parallel lamination are the most common facies but lamination is usually very poorly preserved and lamination is often wavy to chaotic. Rip-up layers and fractured layers of siltstone are also very common. Soft-deformation in the form of load structures is present between siltstone and sandstone facies as well. The contact between the Espanola Formation and the Serpent Formation is obscure and is a very gradual transition during which there is a loss of the carbonate fraction.

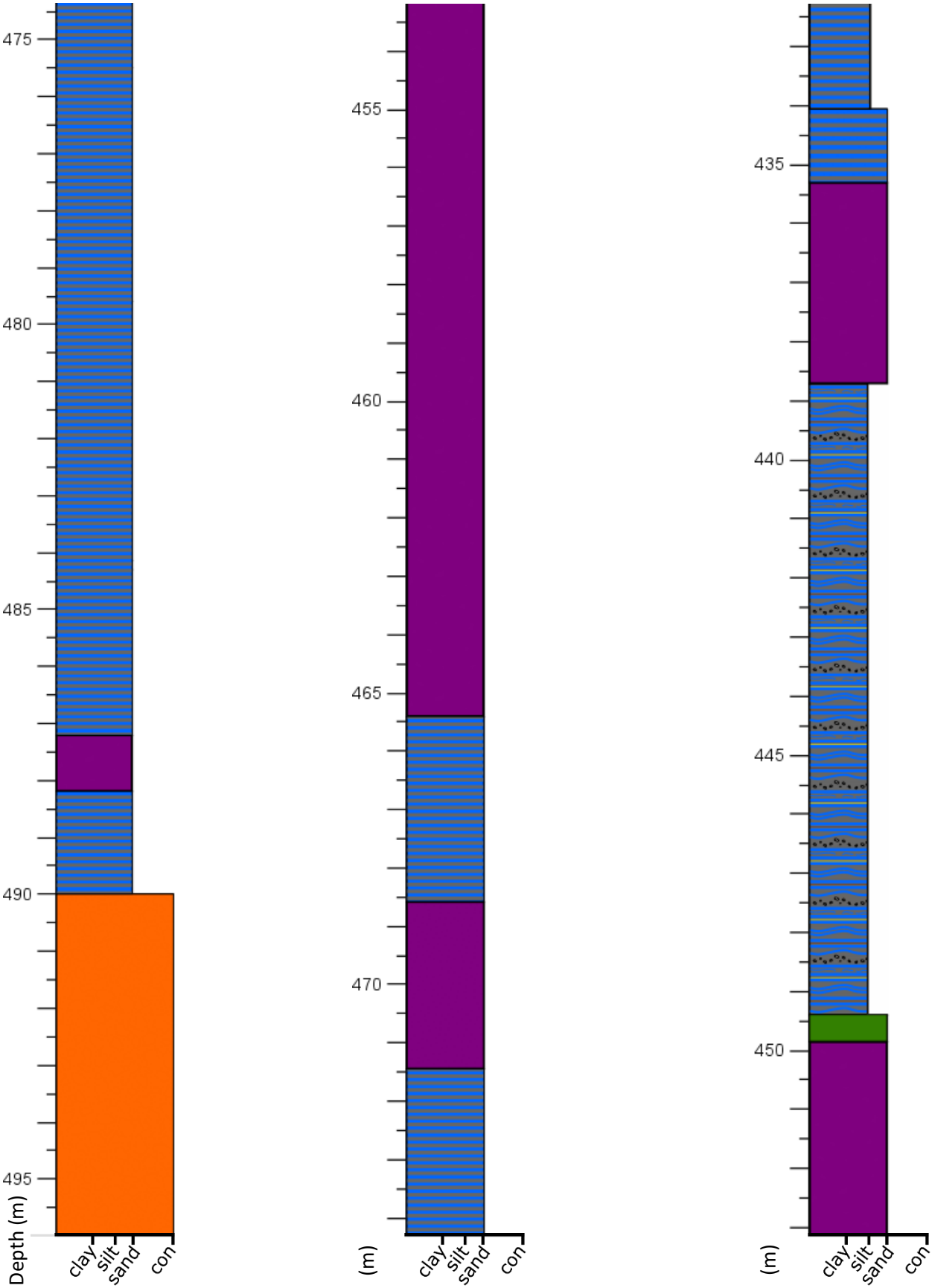
475
480
485
490
495
Depth (m)
clay
silt
sand
con
455
460
465
470
(m)
clay
silt
sand
con
435
440
445
450
(m)
clay
silt
sand
con

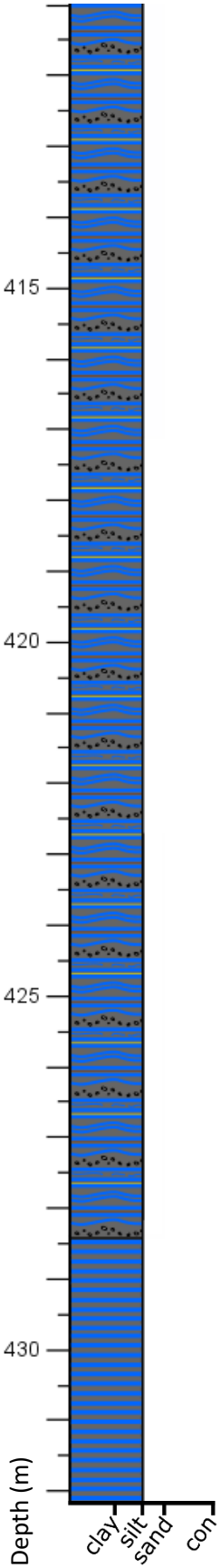
415
420
425
430
Depth (m)
clay
silt
sand
con

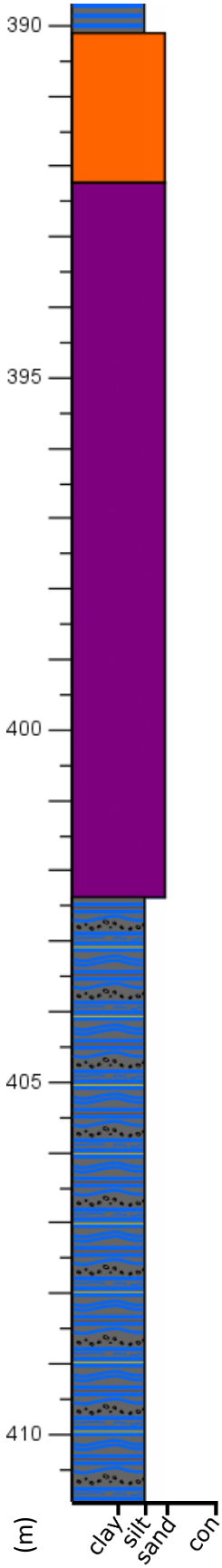
390
395
400
405
410
(m)
clay
silt
sand
con

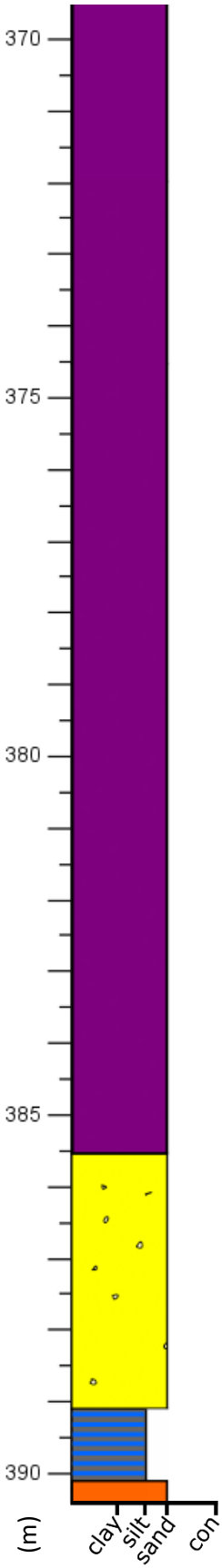
370
375
380
385
390
(m)
clay
silt
sand
con

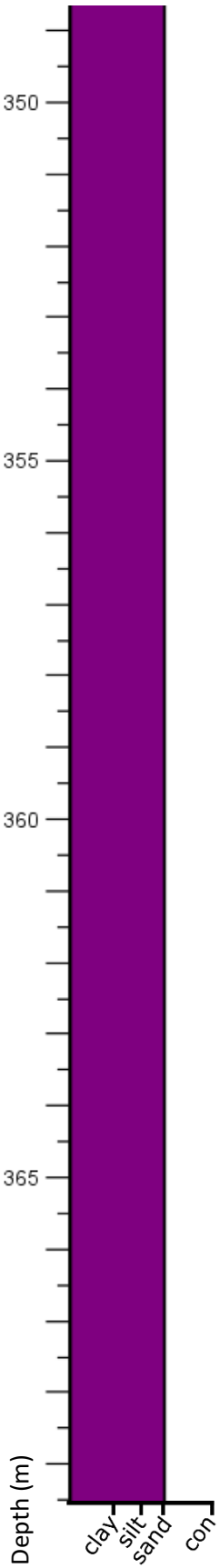
350
355
360
365
Depth (m)
clay
silt
sand
con

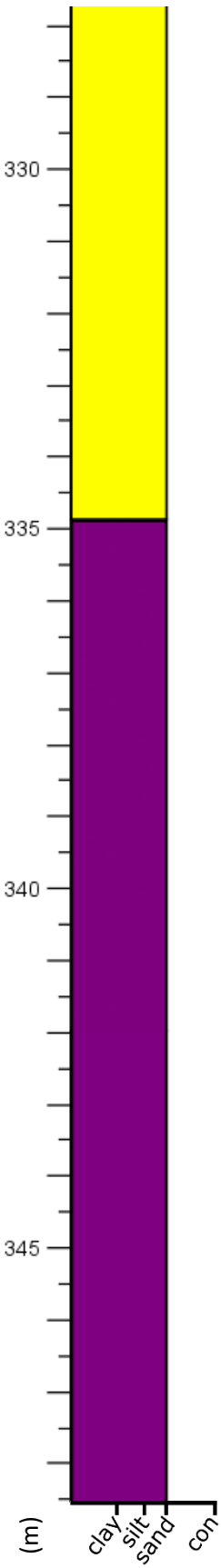
330
335
340
345
(m)
clay
silt
sand
con

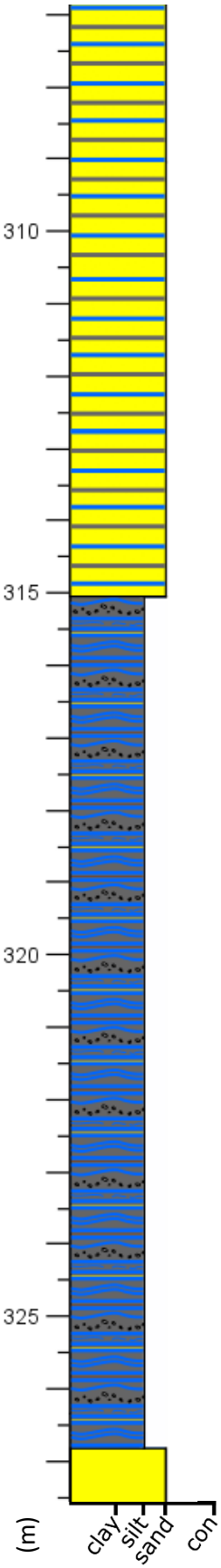
310
315
320
325
(m)
clay
silt
sand
con

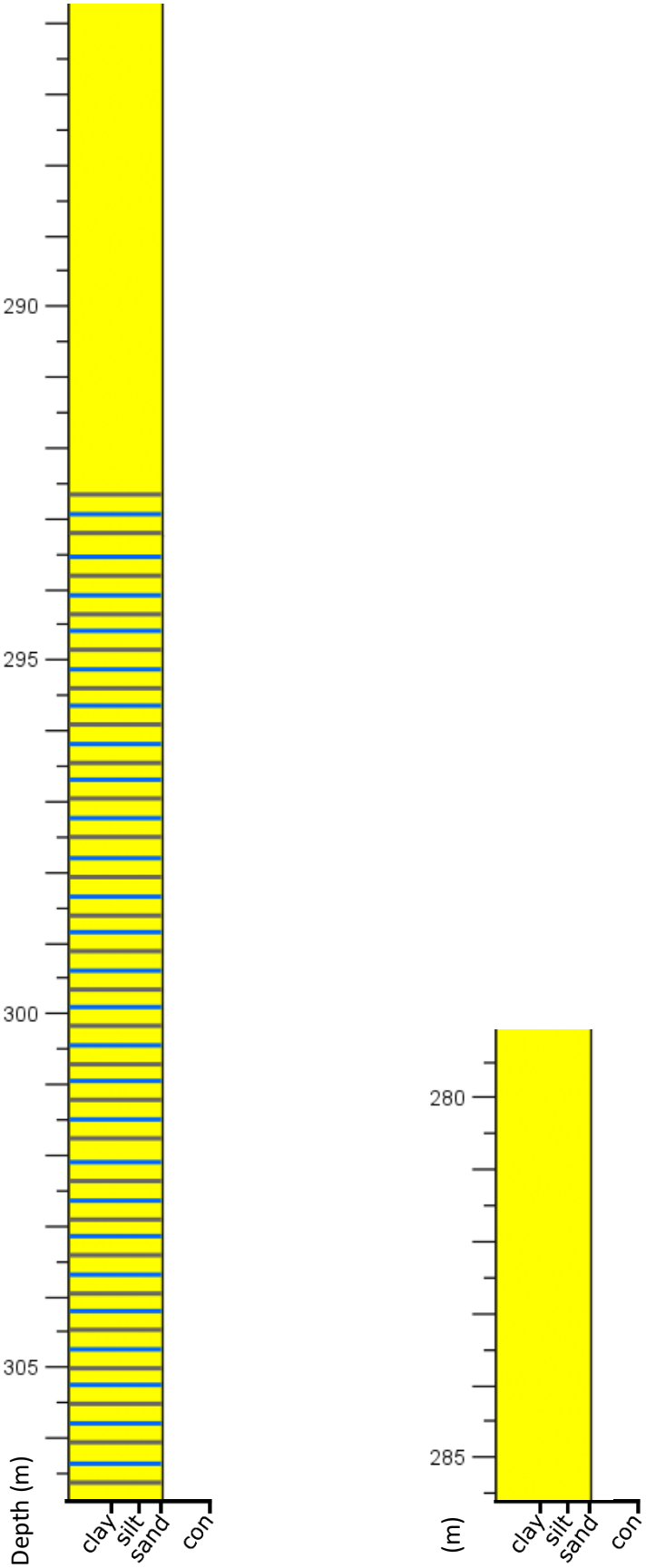
290
295
300
305
Depth (m)
clay
silt
sand
con
280
285
(m)
clay
silt
sand
con

DRILL HOLE 144-1

Within drill core H144-1 the Bruce Formation was only observed in part, as the contact between it and the adjacent Espanola Formation was missing. However, there is a minimum of 6m of Bruce diamictite with typical features of the both clast-rich, and matrix-rich diamictite facies occurring roughly interbedded with one another. The better sorted and more fine-grained beds have a lower clast content and contain red-brown carbonate-rich wisps to layers within them. These carbonate-rich layers range in thickness from 1mm up to 2cm and are often wavy to contorted. The presence of the carbonate-rich layers may indicate that these beds are a lateral equivalent to the laminated dropstone facies of drill hole E150-2. Both the clast-rich facies and the matrix-rich facies have a clast content that is dominated by white granite, with clasts being up to 8x5cm. The overlying Espanola Formation is of a typically interbedded to interlaminated fine- to medium-grained carbonate sand with grey and green layers of siltstone and mudstone. While this lithofacies is ubiquitous to the lower stratigraphy of the Espanola, there is an undetermined thickness of stratigraphy missing between it and the underlying Bruce diamictite. The lower stratigraphy, dominated by the interlaminated carbonate and siltstone lithofacies association, continues for another 50-60m in hole H144-1, however, stratigraphic thickness of this unit is greatly exaggerated by the presence of several beds of intrusive breccias, the thickest being ~15m. These intrusive breccias have sharp contacts with the adjacent facies, and contain abundant angular to subangular fragments of red weathered carbonate and green siltstone, suggesting that the material was sourced from higher up within the stratigraphy where both of these lithologies are more common. Aside from this, the interbedded to interlaminated carbonate and siltstone facies dominates the remainder of the

stratigraphy for the 50-60m. Layering ranges from parallel to commonly wavy and contorted, with layers of white carbonate sandstone that are 3mm-6cm thick, averaging 3-6cm thick. The siltstone layer thickness is highly more variable, ranging from 1mm up to 5cm. Siltstone is rarely the dominant lithology, and in these areas, carbonate sand is lens-like within massive to laminated siltstone. Contortion of the more carbonate-rich areas of the interlaminated to interbedded carbonate and siltstone facies also devolves in places into a slump breccia facies. Overlying the lower lithofacies associations of the Espanola, the stratigraphy becomes more dominated by the siliciclastic component, with the following 17m of stratigraphy being dominated by fine-grained sandstone and siltstone. Mudstone and medium-grained sand are accessory lithologies, and the lowermost 5-6m is finer-grained on average and contains abundant mud layers interbedded with fine-grained sand and siltstone. Thickness of the layers is typically 2-4cm and layers are often contorted. In comparison, the overlying 11-12m of stratigraphy is distinctly coarser-grained, and is dominated by fine- to medium-grained sandstone with abundant wisps to layers of siltstone. Approaching the upper contact of this lithofacies association, the sand takes on a white mottled appearance in places where there is a higher concentration of carbonate cement. The stratigraphy of the Espanola Formation above this area slowly transitions into facies that becomes richer in carbonate and carbonate-dominated units. The stratigraphy is still dominated by fine to medium-grained sandstone and siltstone, with abundant 1-3cm fining upwards units from sand into silt. Contacts between individual fining upwards beds are sharp and quite often irregular and erosive in appearance. Massive siltstone units are sometimes fractured and broken up and can contain lenses of sand, while sand-dominated areas contain rare layers of siltstone. The following 65m of stratigraphy

is once again cross-cut by massive intrusive breccias with only the rare appearance of primary stratigraphy in one area. A 2m thick conglomerate unit within the stratigraphy roughly fines upwards from a coarse-grained to medium-grained sand matrix with pebble-sized clasts of siltstone and white granite. This unit is overlain by interlayered siltstone with some sandstone, which in turn is overlain by a medium to fine-grained sandstone that becomes more poorly sorted approaching the upper contact and contains clasts of white granite up to 5x6cm in size. The remaining 55m of stratigraphy of Espanola Formation overlying the intrusive breccias is dominated by medium-grained white sand with a patchy appearance due to a high carbonate content, siltstone, and dark brown mud and carbonate-rich beds that range in thickness from 16-36cm with layered siltstone and sandstone between them. Sandstone-dominated areas contain layers of siltstone that are usually irregular and contorted with fragmentation of silt layers being common. Sandstone facies themselves are massive and do not contain lamination aside from the interlayering with the siltstone units, and occasional finer silt and mud laminations. The upper contact of the Espanola Formation with the overlying Serpent Formation is gradational, with an overall change to a predominance of medium-grained well sorted sand that is massive to layered in places, and a subsequent loss of the carbonate fraction.

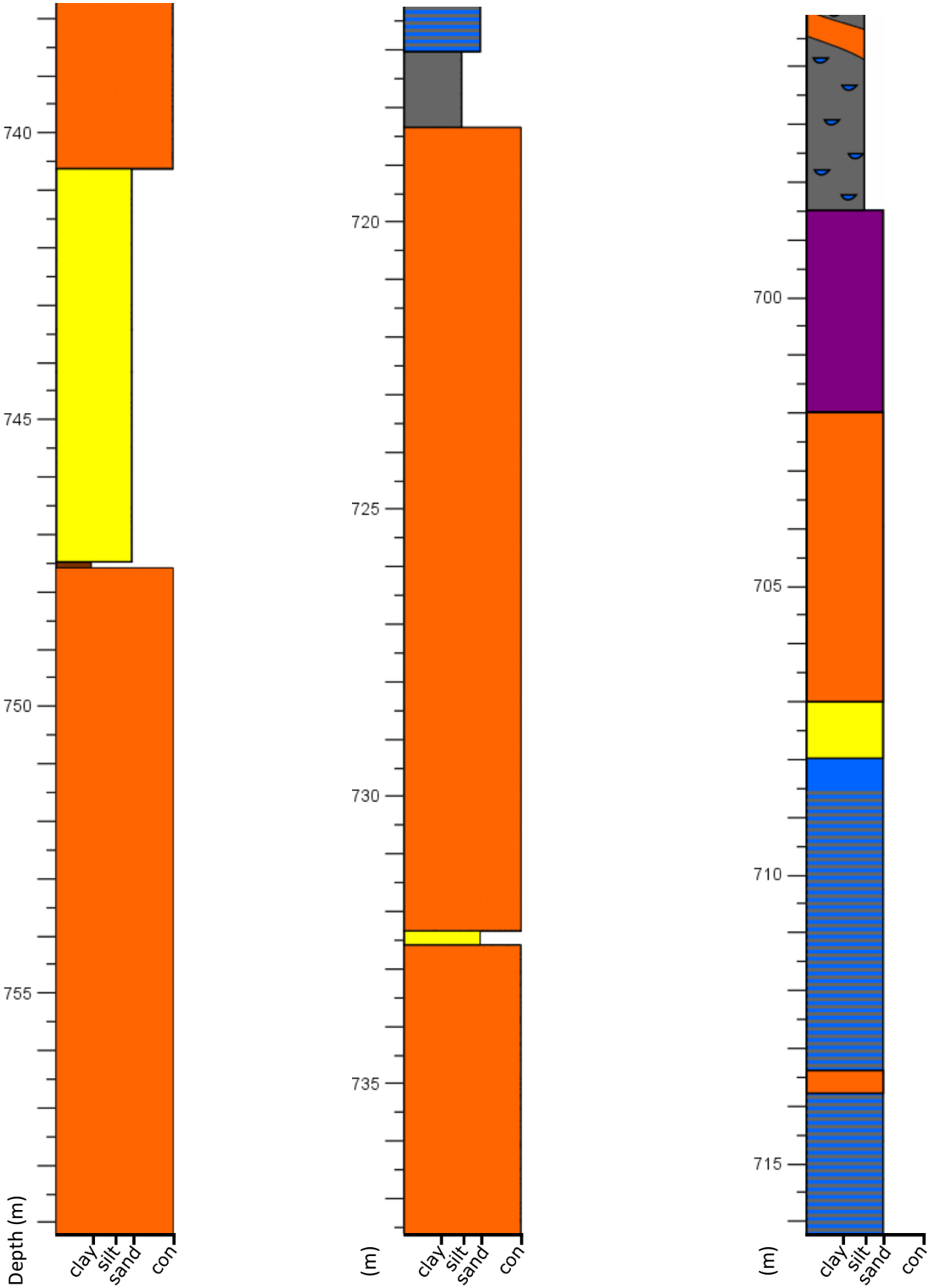
740
745
750
755
Depth (m)
clay
silt
sand
con
720
725
730
735
(m)
clay
silt
sand
con
700
705
710
715
(m)
clay
silt
sand
con

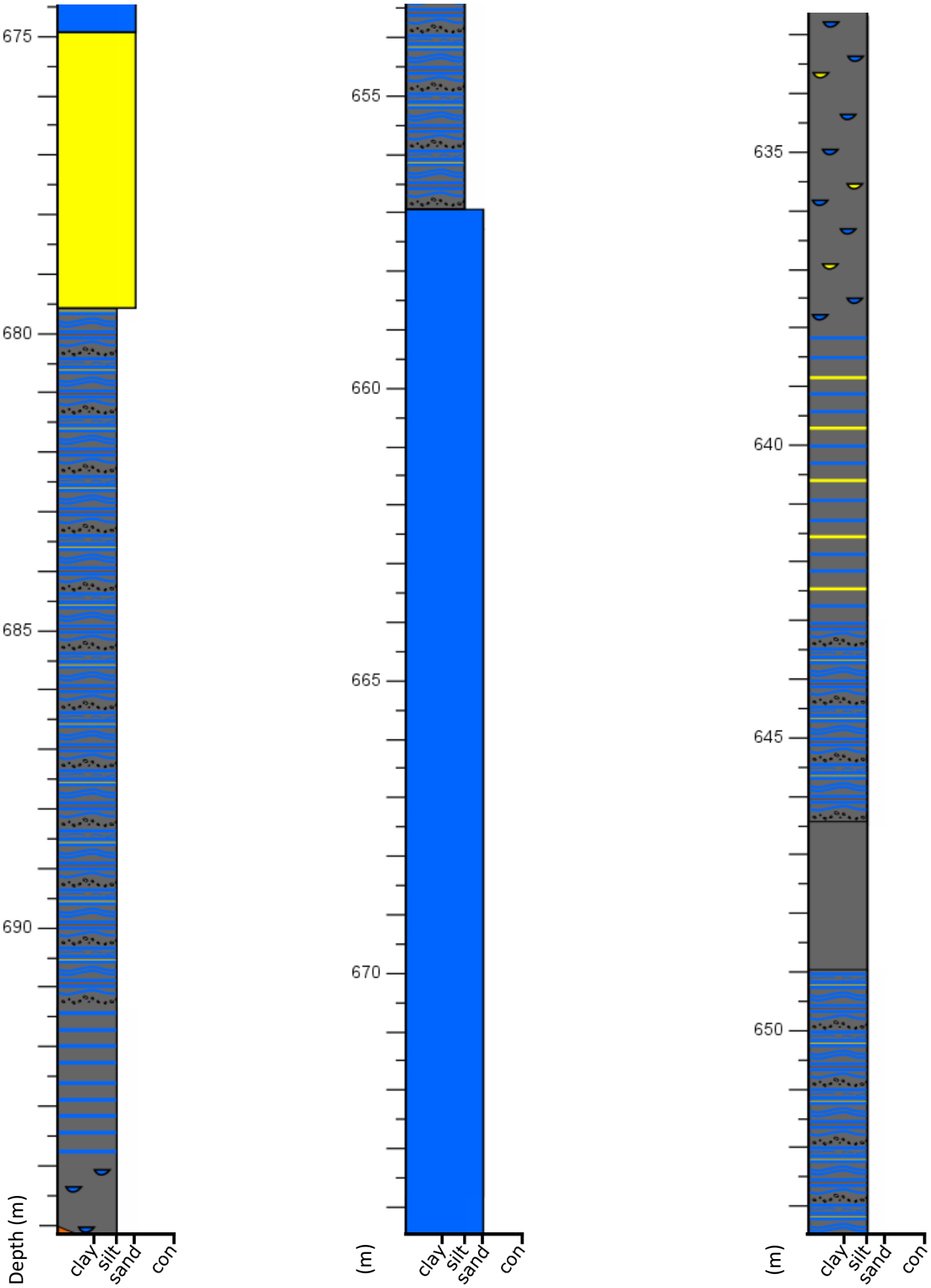
675
680
685
690
Depth (m)
clay
silt
sand
con
655
660
665
670
(m)
clay
silt
sand
con
635
640
645
650
(m)
clay
silt
sand
con

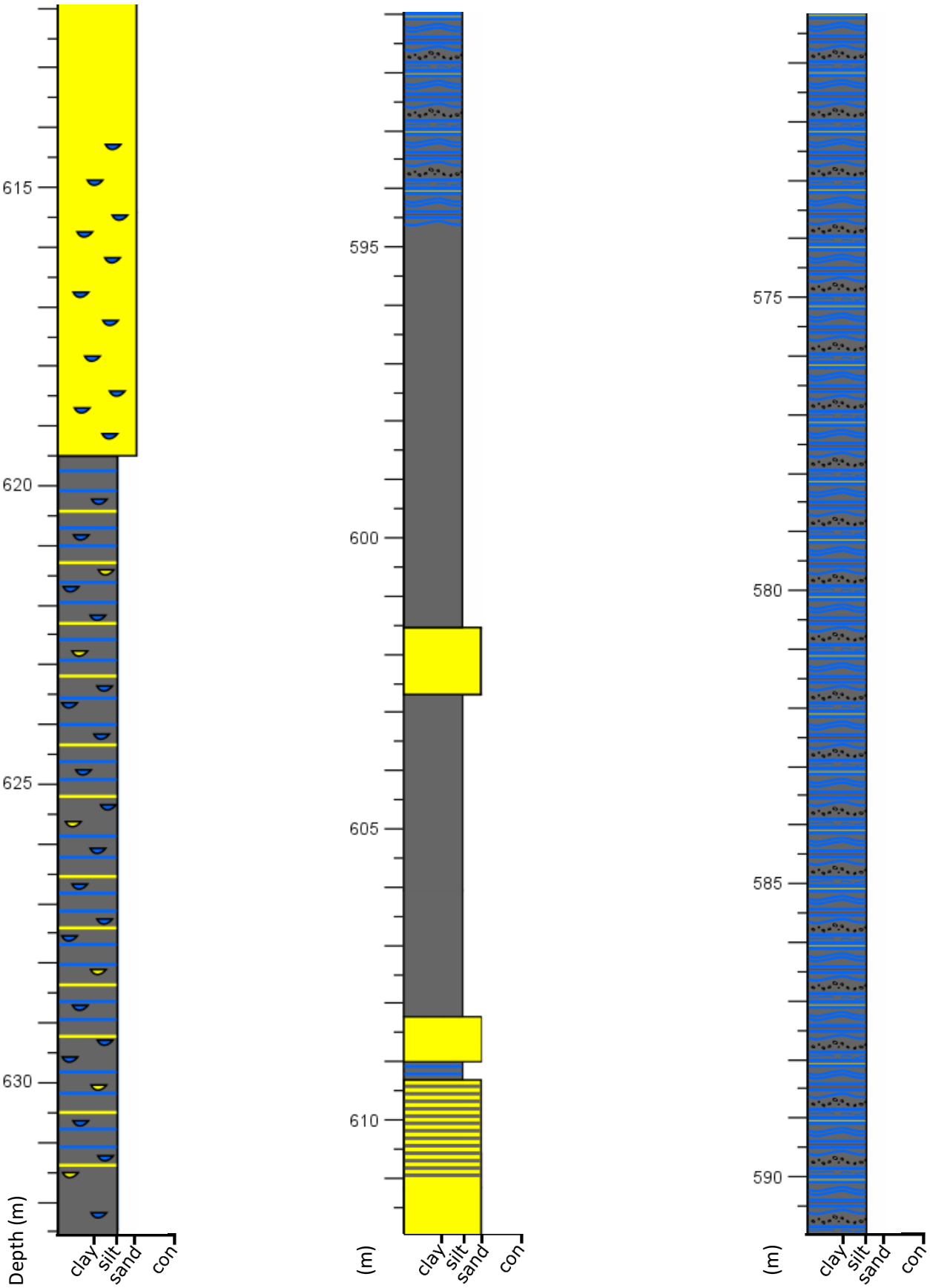
615
620
625
630
Depth (m)
clay
silt
sand
con
595
600
605
610
(m)
clay
silt
sand
con
575
580
585
590
(m)
clay
silt
sand
con

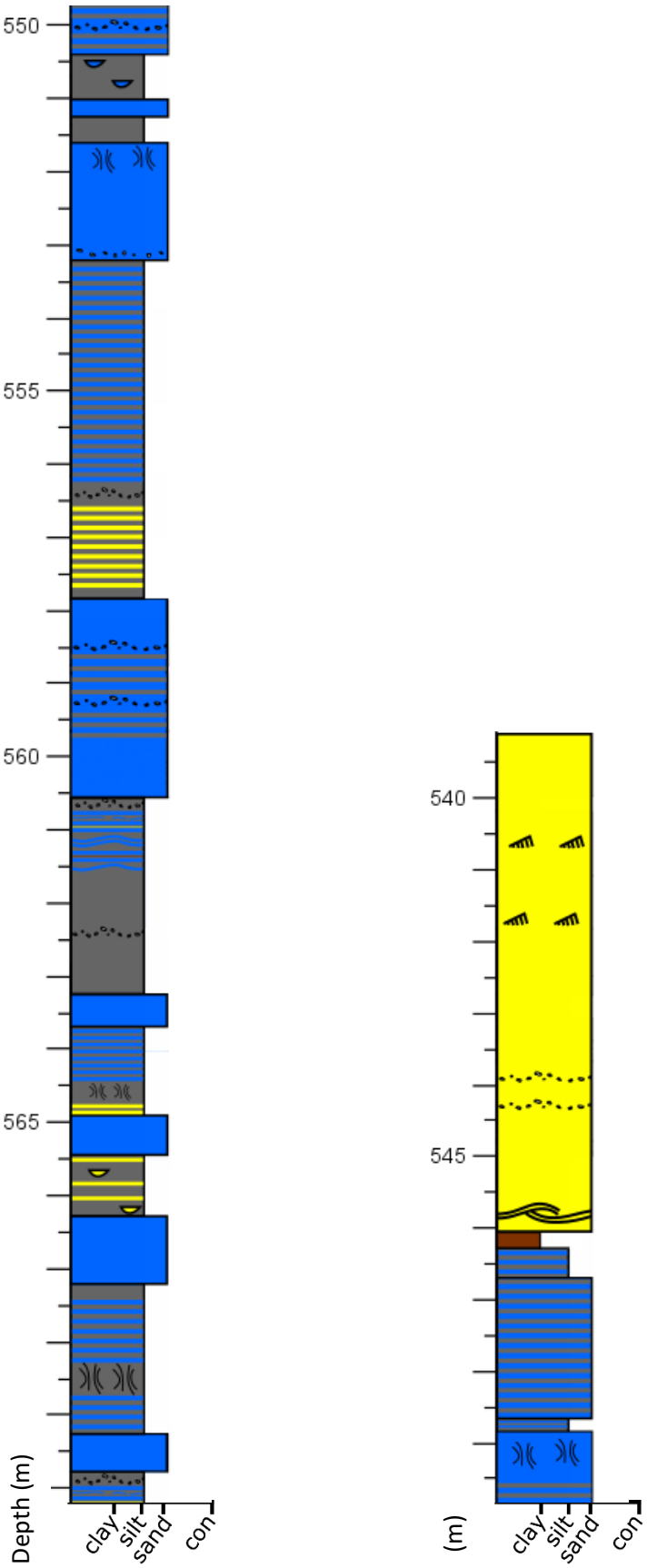
550
555
560
565
Depth (m)
clay
silt
sand
con
540
545
(m)
clay
silt
sand
con

DRILL HOLE E150-1

The Bruce Formation within drill core 150-1 is approximately 123m thick and is usually a grey colour with a fine- to coarse-grained poorly sorted sand matrix and a clast content dominated by rounded to subangular granite. Clast content is typically 1-5% but in places clast content increases to 50-70%. Overall the diamictite is massive and lacks internal structure or stratification but there is noticeable changes in the grainsize and sorting of the matrix. There is a general increase in the coarser sand to granule-sized matrix towards the base of the Bruce diamictite. Towards the top of the Bruce there are two sand layers, 341cm and 25cm thick that are well sorted and a white to light beige colour. The lower sand layer also contains a lower clay-rich layer approximately 10cm thick as well as rare internal mud wisps. The contacts of these sand beds are sharp with the surrounding diamictite.

The contact between the Bruce diamictite and the overlying Espanola Formation appears to be sharp and is marked by a change to a blue-grey to green siltstone layer. The siltstone layer may be approximately 150cm thick but is mostly missing due to oversampling. Directly overlying the siltstone is interbedded to interlaminated carbonate and siltstone ranging from parallel to heavily contorted in places. Rarely, the layering is crinkled and irregular. Following a sandstone and breccia unit that overlies the lower interlaminated carbonate and siltstone unit, there is a change to more predominantly siliciclastic units with varying amounts of carbonate. This section of stratigraphy, which constitutes the majority of the middle Espanola Formation, is dominated by siltstone with lesser sandstone and contains several facies including layered and massive units with lesser fining upwards beds that range in thickness from 1-3cm on average. Carbonate will form layers to lenses within the silt and are distinguishable primarily as white,

coarser-grained patches. Medium- to fine-grained sandstone lenses and layers are also commonly found within the siltstone-dominated facies and have variable amounts of carbonate cement. In places, fine- to medium-grained sandstone beds have a white 'mottled' appearance that is the result of the variable carbonate content. Mud also occurs as an accessory facies within the siliciclastic-dominated middle stratigraphy of the Espanola Formation and can form discrete mm-scale laminae within mud-rich silt units.

The upper stratigraphy is a gradational transition into siltstone and sandstone with carbonate-rich interbeds. Mud-rip up layers become fairly abundant and are usually ~1-3cm in thickness. Clasts often show no preferred orientation within these layers. Contacts between units become more irregular and erosive and are often marked by fractured surfaces. Contorted laminae, soft-sediment deformation, and water escape structures are all prevalent as well. There is also rare evidence of hummocky cross-lamination and ripple-lamination in fine-grained sandstone units, particularly approaching the contact with the Serpent Formation. The contact between the Espanola Formation and the Serpent Formation is a very broad and gradual transition during which there is a loss of carbonate-rich beds and overall increase in grainsize from fine-grained sand and siltstone to fine- and medium-grained sandstone.

15.3 APPENDIX 1C:

SERPENT FORMATION (AND UPPER ESPANOLA) STRATIGRAPHIC SECTIONS

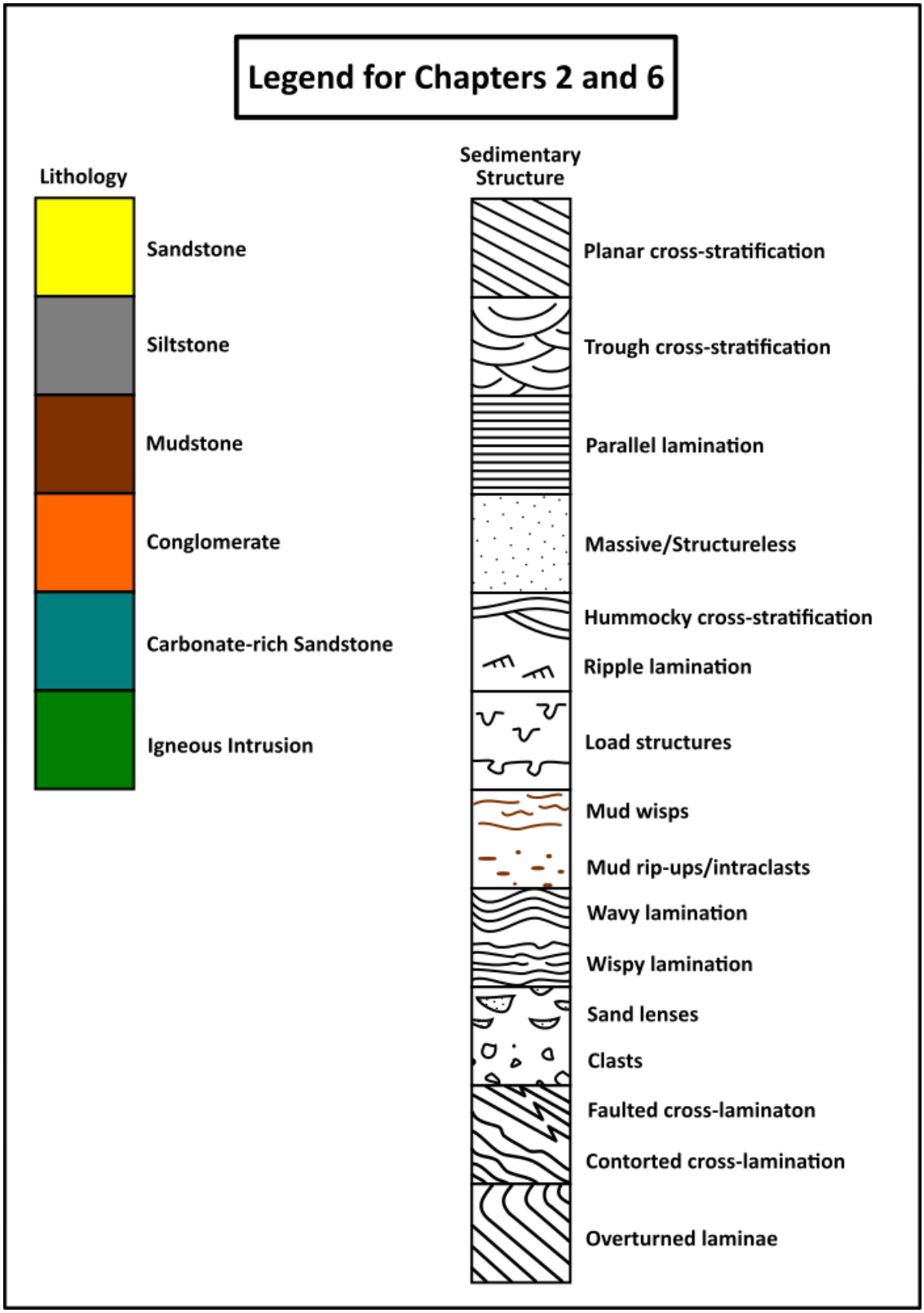

Aird Island

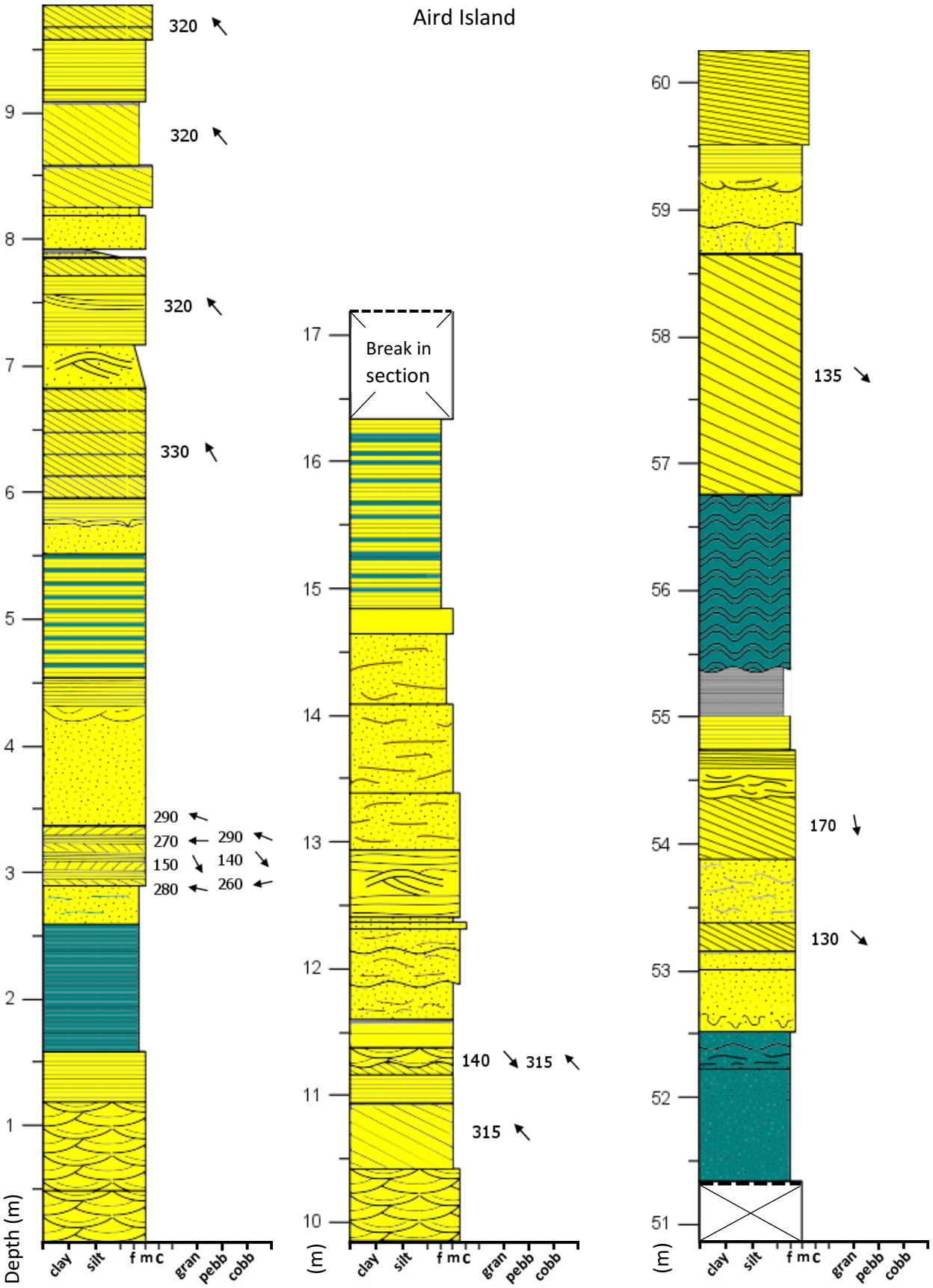
Depth (m)
clay
silt
f m c
gran
pebb
cobb
320
320
320
330
290
270
150
280
290
140
260
Break in section
140
315
315
(m)
135
170
130

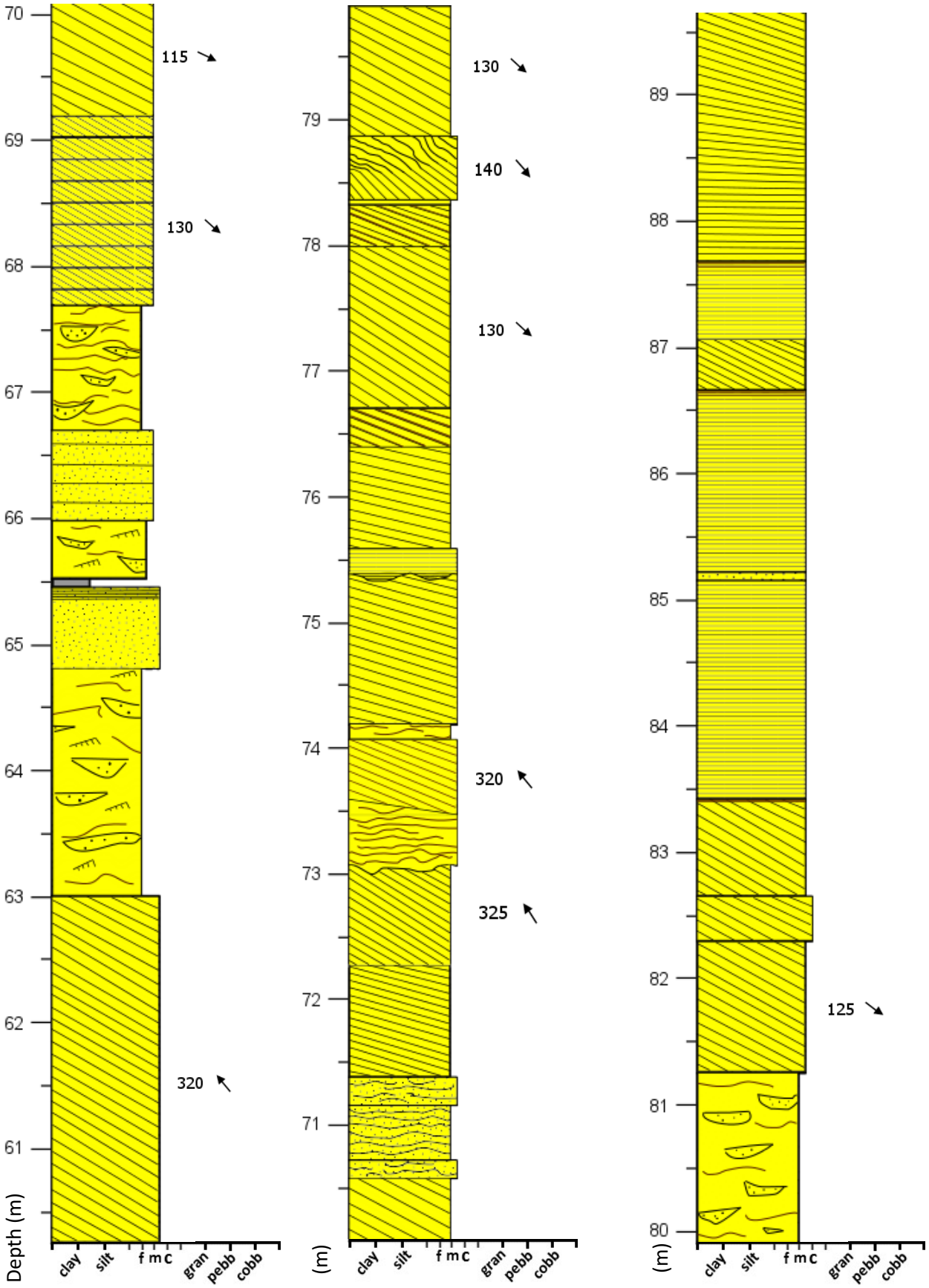
Depth (m)
70
69
68
67
66
65
64
63
62
61
115
130
320
clay
silt
f m c
gran
pebb
cobb
(m)
79
78
77
76
75
74
73
72
71
130
140
130
320
325
clay
silt
f m c
gran
pebb
cobb
(m)
89
88
87
86
85
84
83
82
81
80
125
clay
silt
f m c
gran
pebb
cobb

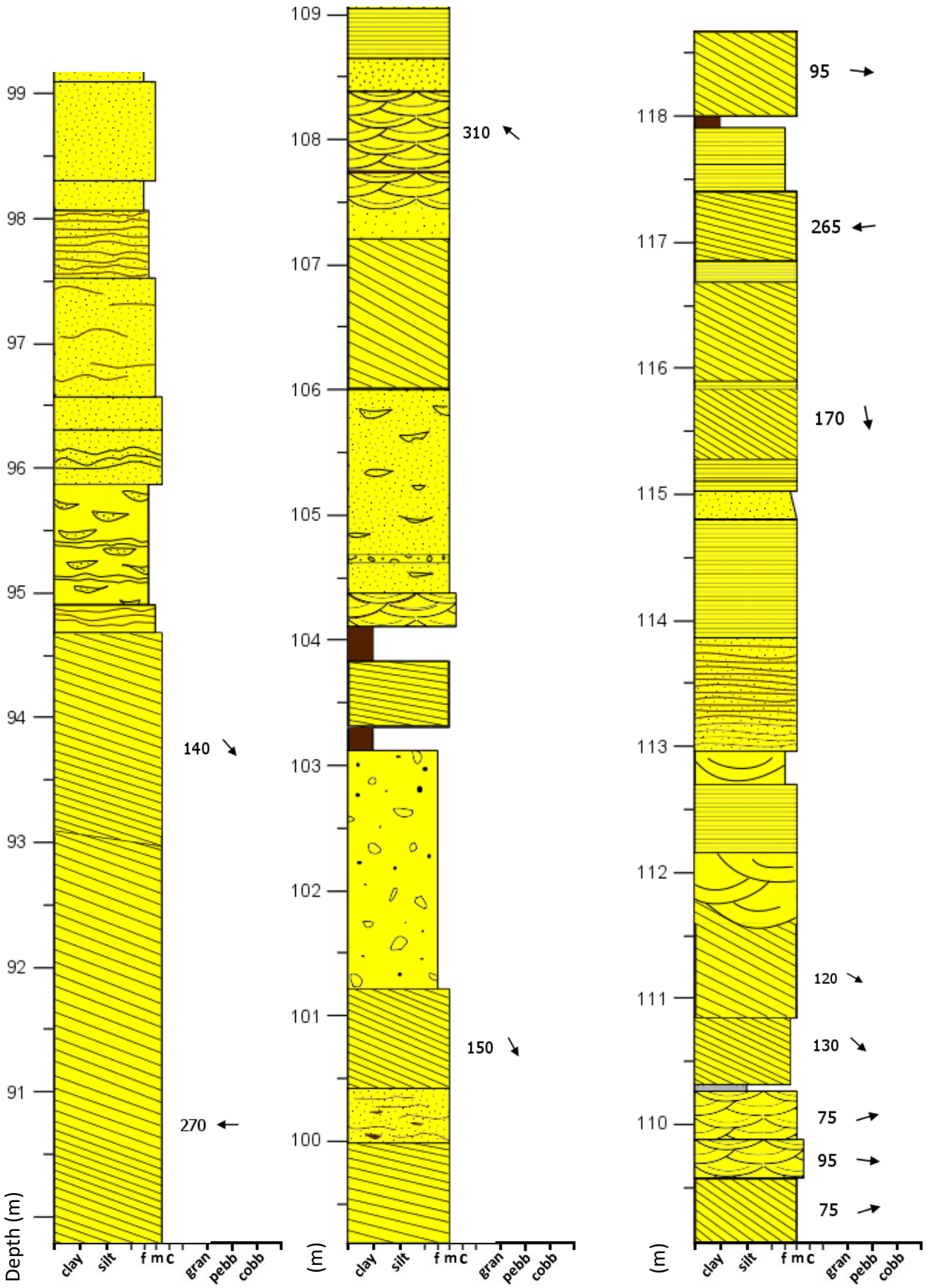
Depth (m)
99
98
97
96
95
94
93
92
91
140
270
clay
silt
f m c
gran
pebb
cobb
(m)
109
108
107
106
105
104
103
102
101
100
310
150
clay
silt
f m c
gran
pebb
cobb
(m)
118
117
116
115
114
113
112
111
110
95
265
170
120
130
75
95
75
clay
silt
f m c
gran
pebb
cobb

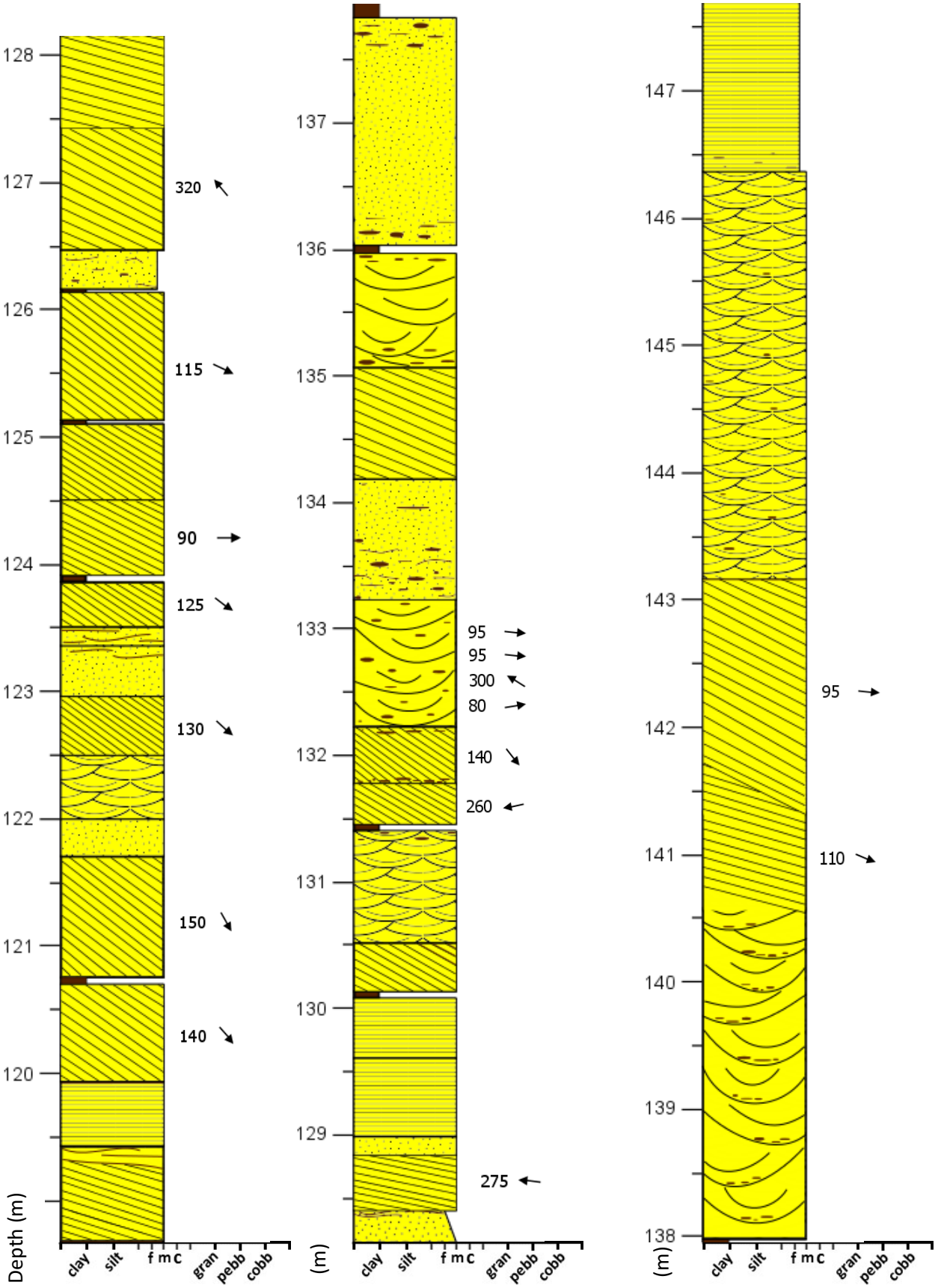
Depth (m)
128
127
126
125
124
123
122
121
120
320
115
90
125
130
150
140
clay
silt
f m c
gran
pebb
cobb
(m)
137
136
135
134
133
132
131
130
129
95
95
300
80
140
260
275
clay
silt
f m c
gran
pebb
cobb
(m)
147
146
145
144
143
142
141
140
139
138
95
110
clay
silt
f m c
gran
pebb
cobb

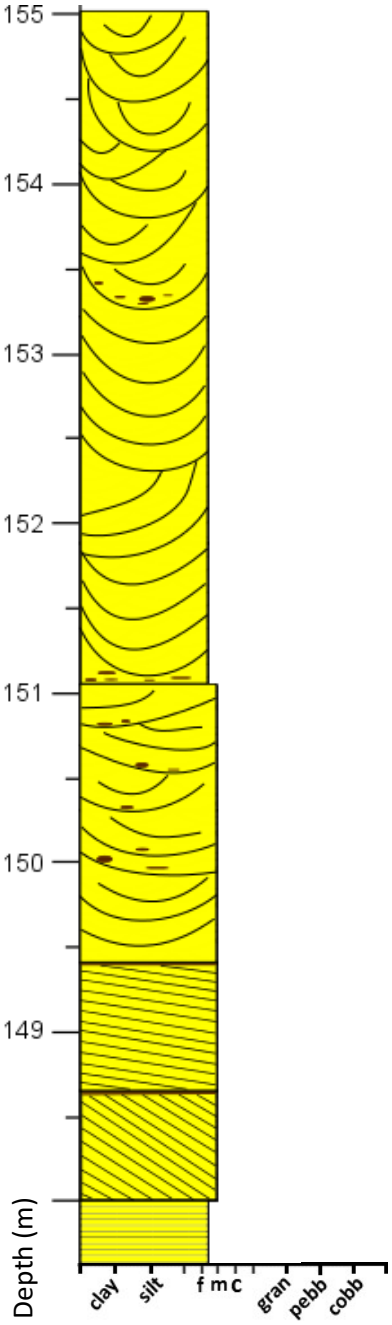

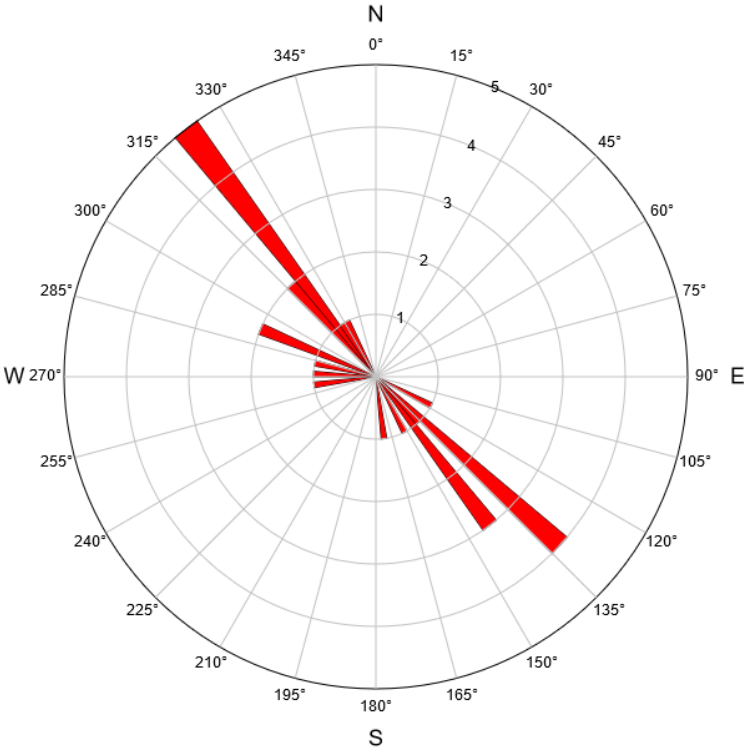

Paleocurrents 0-82m

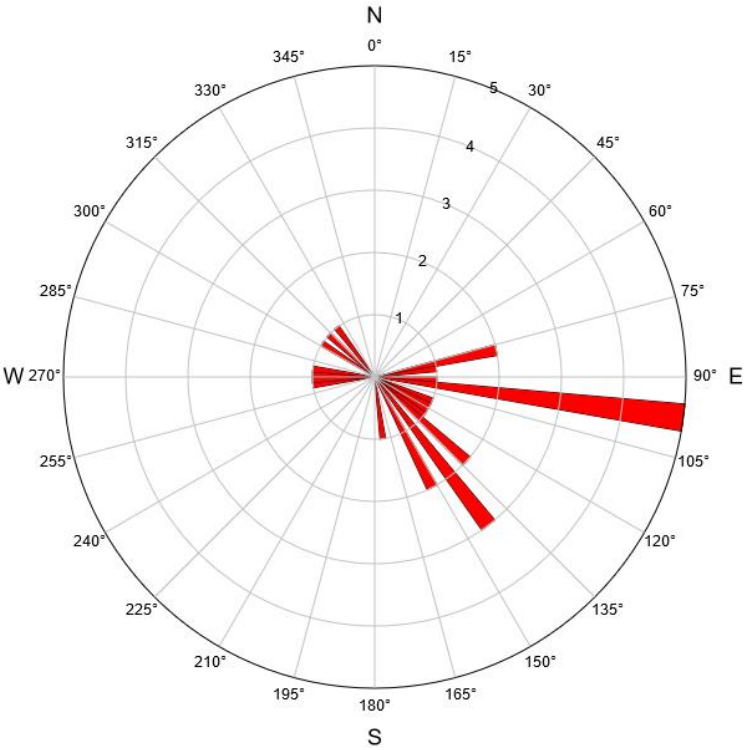

Paleocurrents 82-155m

AIRD ISLAND

A 155m section of outcrop was logged on an island located along the north shore of Lake Huron just south of Aird Island. The outcrop begins at the contact between the Espanola and Serpent and contains a transitional zone between the two in which carbonate-bearing siltier units alternate with coarser-grained sandstone units that lack carbonate in their matrix. The outcrop is dominated by large-scale planar cross-stratified units that are often low-angle and may be separated by slightly finer-grained horizontally laminated units. Rare muddy layers may separate individual planar cross-stratified beds or denote activation surfaces within beds themselves. There is a general upward increase in the abundance of trough cross-stratified bundles and coincident with this change is a shift from a more bidirectional paleocurrent direction to a more unidirectional current pattern. The lower half of the sedimentary sequence contains a broad range of sedimentary structures, including; hummocky cross-stratification, mud drapes, bidirectional planar cross-stratification, and wavy bedding. Rare bundles of small-scale trough cross-stratification exist between planar cross-stratified units. Paleocurrent data indicates a bidirectional NW and SE current pattern. Moving upwards in section, there is a general increase in the thickness of individual planar cross-stratified beds, with units as thick as 5m. Furthermore, there is also a trend from lower angle to higher angle near the tops of beds. The upper stratigraphy has a broad transition from being dominated by large-scale planar cross-stratified units, to a predominance of medium- to large-scale trough cross-stratified units. Mud wisps and mud rip-ups are present in many of the troughs, and particularly abundant at the base of some individual units.

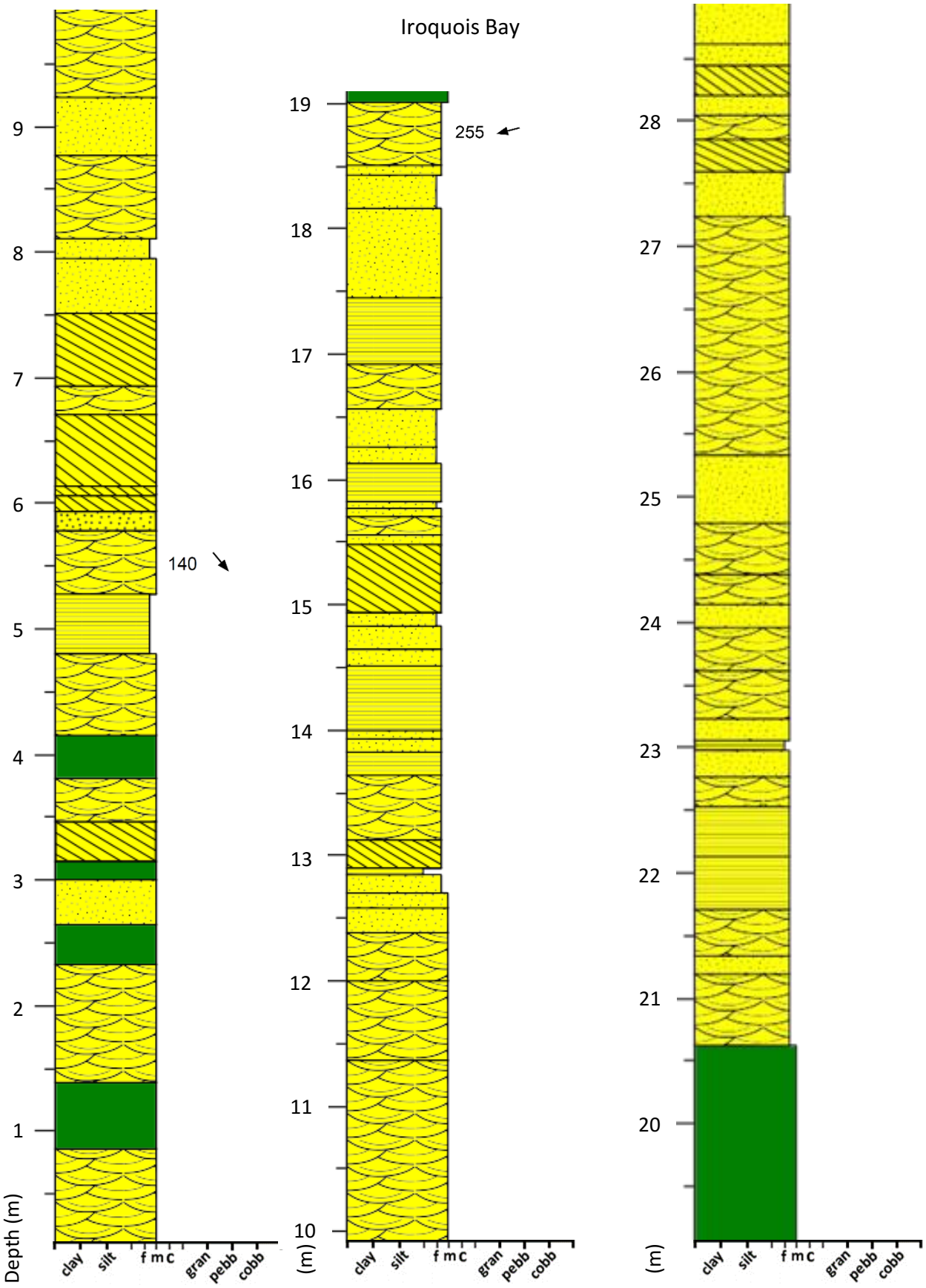
Iroquois Bay
Depth (m)
9
8
7
6
5
4
3
2
1
140
clay
silt
f m c
gran
pebb
cobb
19
18
17
16
15
14
13
12
11
10
(m)
255
clay
silt
f m c
gran
pebb
cobb
28
27
26
25
24
23
22
21
20
(m)
clay
silt
f m c
gran
pebb
cobb

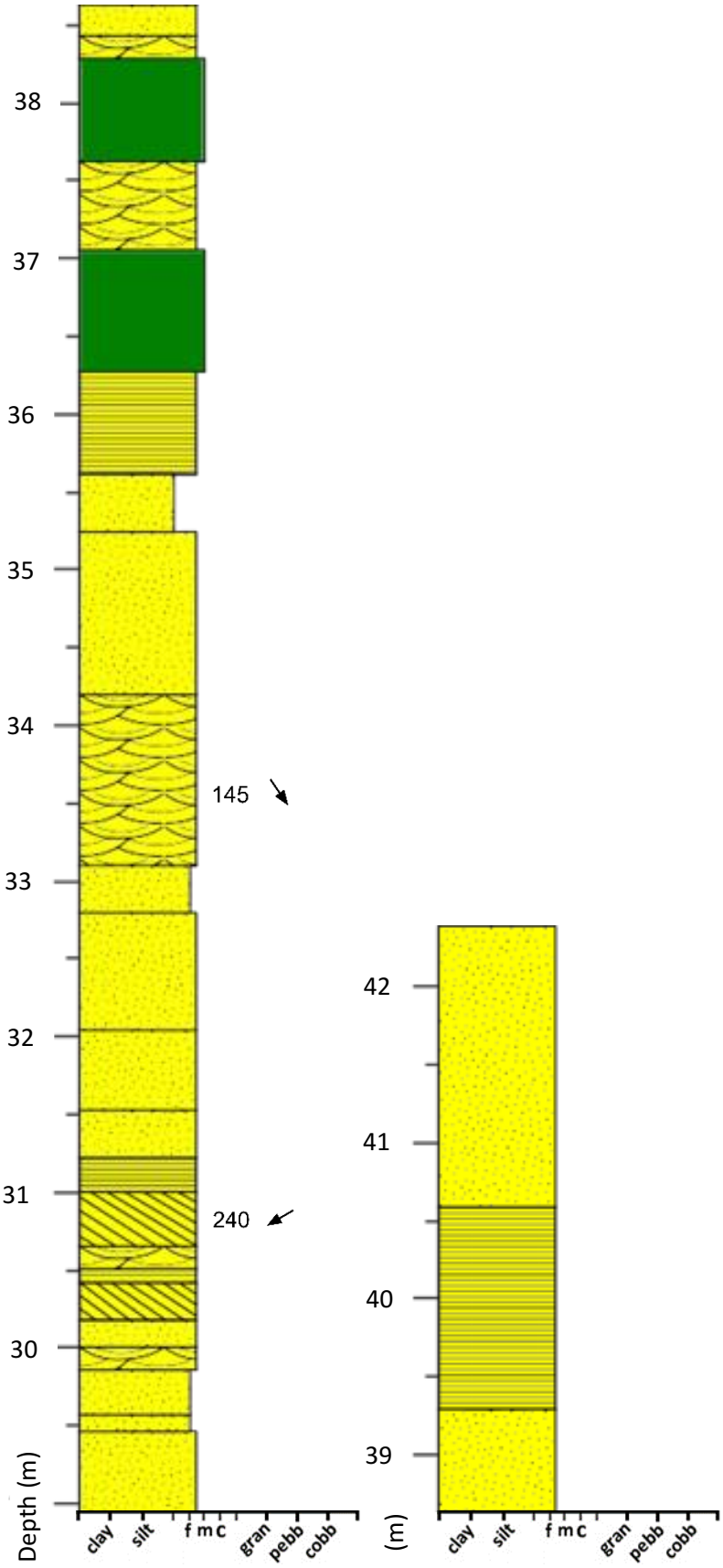
38
37
36
35
34
33
32
31
30
Depth (m)
145
240
clay
silt
f
m
c
gran
pebb
cobb
42
41
40
39
(m)
clay
silt
f
m
c
gran
pebb
cobb

IROQUOIS BAY

Immediately south-east of Iroquois Bay a ~42m section of the upper Espanola Formation into the lower Serpent Formation was logged. The most common facies within the transitional contact is small- to medium-scale, fine- to medium-grained trough cross-stratified sandstone. Troughs typically occur in sets of two or more and form bundles that erosively scour into the underlying beds. Rarely, mud wisps and laminae accentuate the base of some troughs. Small-scale to rarely medium-scale planar cross-stratification is also present and formed from fine- to medium-grained sand. These beds are less likely to form sets and more typically are separated by trough cross-stratification or massive fine- to medium-grained sandstones.

Another common facies within the transitional contact between the Espanola and Serpent Formations in the vicinity of Iroquois Bay is parallel laminated siltstone and sandstone. Lamination ranges from the mm-scale up to 2cm in places and has variable grainsizes but most commonly is between fine- to medium-grained sand and silt or mud. Rarely, silty and muddy parallel laminated beds may be slightly calcareous and often imparts more drastic recessive weathering in these units, but carbonate content is overall very low in this section of stratigraphy. Massive sandstone units are also fairly abundant but also include beds where layering or structure within a unit was obscured. However, these units are ~50cm thick on average and consist predominantly of relatively well-sorted fine- and medium-grained sand. The massive sandstone beds have sharp contacts with adjacent units and are typically laterally continuous but may in places be lens-shaped. At this location, igneous dykes also commonly intrude into the stratigraphy.

APPENDIX 2A – WHOLE ROCK REE

Sample #	La (ppm)	Ce (ppm)	Pr (ppm)	Nd (ppm)	Sm (ppm)	Eu (ppm)	Gd (ppm)	Tb (ppm)	Dy (ppm)	Ho (ppm)	Er (ppm)	Tm (ppm)	Yb (ppm)	Lu (ppm)
BHVO-2	14.783	36.778	5.251	24.239	5.811	2.042	6.917	0.998	5.171	0.944	2.578	0.331	2.058	0.292
8-44A	1.483	1.486	0.173	0.701	0.109	0.063	0.174	0.022	0.129	0.035	0.129	0.016	0.129	0.024
SR-16B	0.650	0.548	0.089	0.353	0.057	0.024	0.104	0.017	0.106	0.033	0.105	0.017	0.102	0.022
H91	25.080	51.948	6.033	22.306	4.159	1.054	4.632	0.630	3.418	0.684	2.091	0.298	1.945	0.298
17-6	17.576	34.115	3.950	14.916	2.900	0.847	3.342	0.461	2.365	0.444	1.282	0.167	1.054	0.158
E150-4	21.833	44.881	5.263	18.914	3.246	0.679	3.410	0.438	2.175	0.417	1.291	0.184	1.269	0.190
E152-7	20.073	41.683	4.785	17.377	3.062	0.750	3.205	0.409	2.163	0.435	1.394	0.212	1.425	0.224
E152-2	23.541	50.395	6.022	22.577	4.333	1.060	5.036	0.727	4.203	0.845	2.567	0.373	2.449	0.377
E152-9	42.736	88.393	10.394	39.826	7.383	1.389	8.322	0.994	4.549	0.789	2.579	0.367	2.608	0.391
E150-9	9.143	17.946	2.094	8.127	1.706	7.613	1.947	0.253	1.130	0.204	0.553	0.070	0.468	0.070
E150-5	23.659	49.344	5.763	21.379	3.745	0.847	4.133	0.541	2.781	0.544	1.661	0.238	1.546	0.236
144-3	9.862	16.043	2.026	7.614	1.299	0.323	1.665	0.217	1.012	0.203	0.555	0.079	0.526	0.084
E154-2	13.303	27.347	3.172	12.017	2.142	0.410	2.537	0.356	1.912	0.377	1.103	0.151	1.007	0.151
E150-7	20.702	44.171	4.977	17.988	3.180	0.817	3.340	0.429	1.991	0.365	1.005	0.138	0.839	0.121
E150-2	16.069	34.021	4.032	14.750	2.804	0.678	3.101	0.437	2.300	0.441	1.347	0.181	1.180	0.188
17-8	8.209	16.783	2.012	7.560	1.353	0.276	1.395	0.183	0.888	0.160	0.481	0.063	0.423	0.066
E152-10	53.417	109.453	12.790	47.570	8.603	1.706	9.720	1.187	5.248	0.983	3.159	0.448	3.118	0.492
E150-6	21.633	46.656	5.394	19.527	3.391	0.798	4.002	0.515	2.469	0.449	1.292	0.177	1.172	0.175
E152-5	48.228	97.836	11.484	42.426	7.396	1.574	8.234	1.103	5.568	1.078	3.284	0.452	3.028	0.484
E152-1	24.874	53.480	6.260	23.263	4.347	1.381	4.753	0.652	3.528	0.723	2.338	0.361	2.464	0.380
E152-3	55.841	116.580	13.691	50.106	8.704	1.728	9.307	1.196	5.905	1.109	3.371	0.474	3.212	0.503
E150-10	17.583	37.268	4.364	16.205	2.939	0.712	3.537	0.491	2.631	0.525	1.650	0.237	1.583	0.254
144-6	11.587	23.707	2.768	10.263	1.834	0.382	1.924	0.247	1.189	0.211	0.652	0.088	0.579	0.089
144-4	4.990	10.499	1.182	4.499	0.891	0.317	1.316	0.180	0.987	0.171	0.490	0.068	0.482	0.078
E150-3	17.210	36.718	4.119	15.250	2.945	0.823	3.615	0.469	2.528	0.477	1.478	0.211	1.436	0.221
E152-6	67.225	135.524	15.644	57.189	9.944	1.983	11.077	1.383	6.610	1.246	3.691	0.505	3.470	0.564
144-5	23.815	46.641	5.246	19.099	3.518	1.077	4.340	0.553	2.610	0.490	1.454	0.208	1.347	0.214

Sample #	La (ppm)	Ce (ppm)	Pr (ppm)	Nd (ppm)	Sm (ppm)	Eu (ppm)	Gd (ppm)	Tb (ppm)	Dy (ppm)	Ho (ppm)	Er (ppm)	Tm (ppm)	Yb (ppm)	Lu (ppm)
E154-1	25.003	52.975	6.208	22.888	4.089	0.903	4.985	0.655	3.451	0.671	2.116	0.281	2.009	0.303
E152-4	34.866	73.160	8.396	31.133	6.018	1.317	7.694	1.115	6.036	1.217	3.554	0.496	3.248	0.503
144-7	11.714	22.791	2.640	10.079	1.850	0.400	2.371	0.307	1.558	0.324	1.008	0.135	0.928	0.140
E152-8	10.175	22.079	2.684	10.827	2.416	1.242	3.093	0.420	1.945	0.344	0.983	0.142	1.060	0.160
17-7	24.768	47.304	5.358	20.453	3.897	1.266	5.183	0.725	3.620	0.662	1.921	0.263	1.715	0.265
E154-3	9.103	19.169	2.275	8.781	1.725	0.401	2.115	0.282	1.362	0.249	0.770	0.106	0.694	0.114
144-1	11.518	19.217	2.702	10.179	1.806	0.487	2.260	0.313	1.653	0.310	0.953	0.133	0.891	0.133
144-2	18.222	36.760	4.232	15.749	3.002	0.801	3.798	0.525	2.742	0.499	1.462	0.216	1.419	0.225
E150-8	24.846	51.224	5.904	21.995	3.977	1.015	4.581	0.628	3.353	0.666	2.045	0.279	1.890	0.280
17-9	17.892	34.216	3.784	13.342	2.074	0.510	2.693	0.330	1.462	0.271	0.802	0.103	0.695	0.112
17-22	13.930	29.654	3.492	13.578	2.572	0.498	3.182	0.422	2.119	0.432	1.310	0.193	1.293	0.200
E150-1	19.830	40.448	4.833	18.216	3.531	0.844	4.211	0.593	3.140	0.627	1.908	0.266	1.803	0.269
BHVO-2	14.091	34.720	5.077	23.543	5.681	1.948	6.495	0.934	4.988	0.909	2.403	0.307	1.857	0.265
8-44A	1.389	1.372	0.170	0.653	0.105	0.061	0.167	0.020	0.122	0.033	0.123	0.015	0.118	0.024
SR-16B	0.443	0.281	0.052	0.237	0.040	0.022	0.078	0.012	0.086	0.025	0.088	0.013	0.092	0.014
18-0-1	43.845	86.938	10.457	38.715	6.910	1.566	6.854	0.782	3.510	0.626	1.938	0.278	1.866	0.286
18-0-2	13.542	24.869	3.168	11.523	1.967	0.425	2.080	0.273	1.346	0.241	0.659	0.086	0.528	0.079
18-0-3	8.334	16.238	1.929	7.477	1.571	3.366	1.788	0.243	1.212	0.218	0.590	0.078	0.477	0.073
18-0-4	15.329	30.704	3.625	13.985	2.425	0.632	2.869	0.367	1.876	0.363	1.084	0.156	1.045	0.155
18-2-1	12.999	27.365	3.395	13.091	2.797	0.785	3.723	0.632	4.045	0.854	2.547	0.361	2.379	0.378
18-2-2	38.900	78.438	9.375	34.389	6.037	1.217	6.288	0.859	4.525	0.874	2.626	0.366	2.521	0.396
18-2-3	13.084	23.831	3.035	11.983	2.241	8.607	2.592	0.354	1.849	0.384	1.177	0.176	1.144	0.180
18-2-4	30.471	62.963	7.534	27.479	4.777	0.973	4.806	0.605	2.970	0.566	1.786	0.264	1.826	0.286
18-2-5	22.105	41.737	5.140	20.132	3.711	0.853	4.401	0.622	3.295	0.586	1.758	0.250	1.676	0.247
18-2-6	10.503	23.007	2.338	8.640	1.525	0.520	1.889	0.247	1.265	0.260	0.792	0.117	0.793	0.121
18-2-7	2.420	4.752	0.589	2.450	0.546	0.330	0.853	0.125	0.731	0.138	0.370	0.051	0.311	0.050
18-2-8	26.020	52.742	6.217	22.666	4.082	0.952	4.257	0.559	2.829	0.548	1.682	0.245	1.572	0.252
18-2-9	20.853	42.216	5.139	18.995	3.700	0.851	4.166	0.637	3.561	0.724	2.195	0.332	2.230	0.361

Sample #	La (ppm)	Ce (ppm)	Pr (ppm)	Nd (ppm)	Sm (ppm)	Eu (ppm)	Gd (ppm)	Tb (ppm)	Dy (ppm)	Ho (ppm)	Er (ppm)	Tm (ppm)	Yb (ppm)	Lu (ppm)
18-2-10	47.487	96.035	11.234	41.812	7.160	1.584	7.510	0.933	4.552	0.885	2.842	0.435	2.911	0.443
18-2-11	15.105	31.211	3.667	13.716	2.609	0.626	2.828	0.395	2.107	0.399	1.181	0.177	1.196	0.192
18-2-12	37.005	76.007	9.030	33.341	5.979	1.368	6.173	0.785	3.949	0.738	2.239	0.335	2.288	0.354
18-2-13	40.176	84.494	10.238	37.473	6.758	1.272	7.179	0.940	4.616	0.852	2.550	0.353	2.401	0.369
18-2-14	12.611	27.541	3.124	12.466	2.488	0.693	2.953	0.389	2.032	0.355	1.003	0.145	0.981	0.162
18-2-15	20.932	42.079	4.973	18.412	3.364	0.864	3.449	0.470	2.424	0.471	1.445	0.209	1.407	0.218
18-2-16	17.308	36.068	4.312	15.948	2.907	0.690	2.903	0.384	1.904	0.350	1.038	0.145	0.939	0.144
18-2-17	15.285	31.579	3.770	14.073	2.614	0.667	2.693	0.359	1.786	0.327	0.959	0.137	0.955	0.146
18-2-18	20.666	41.927	4.845	18.641	3.468	0.957	4.182	0.578	2.943	0.558	1.669	0.249	1.729	0.263
18-2-19	18.162	37.253	4.245	15.709	2.840	0.799	3.217	0.442	2.362	0.441	1.458	0.215	1.545	0.258
18-2-20	17.567	35.501	4.162	15.719	2.902	0.816	3.219	0.418	2.054	0.365	1.181	0.160	1.184	0.179
18-2-21	18.773	37.416	4.439	16.402	2.924	0.754	2.937	0.378	1.820	0.330	0.951	0.135	0.944	0.137
18-2-22	16.144	32.909	3.853	14.845	2.741	0.685	2.857	0.333	1.533	0.273	0.831	0.129	0.936	0.142
18-2-23	11.065	24.243	2.925	11.318	2.338	0.546	2.436	0.313	1.579	0.310	0.938	0.141	0.924	0.151
18-2-24	5.512	9.708	1.251	4.893	0.937	0.235	1.069	0.146	0.774	0.146	0.440	0.058	0.376	0.053
18-2-25	40.781	83.007	9.665	36.515	6.580	1.347	7.472	0.967	4.714	0.868	2.646	0.369	2.562	0.411
18-2-26	41.899	82.843	9.982	36.826	6.581	1.319	6.905	0.942	4.969	0.952	2.840	0.407	2.699	0.429
BHVO-2	14.331	35.951	5.130	23.617	5.736	1.999	6.603	0.964	5.110	0.897	2.417	0.310	1.895	0.278
8-44A	1.515	1.050	0.153	0.613	0.082	0.057	0.147	0.016	0.097	0.033	0.122	0.017	0.128	0.026
SR16-B	0.578	0.150	0.063	0.271	0.034	0.024	0.083	0.012	0.110	0.035	0.120	0.016	0.118	0.024
96	12.344	25.203	2.960	10.884	1.906	0.317	2.034	0.278	1.516	0.280	0.892	0.132	0.887	0.135
16	16.193	34.487	4.066	15.014	2.641	0.478	2.749	0.363	1.875	0.354	1.095	0.155	1.039	0.163
106	11.731	24.327	2.837	10.521	2.055	0.389	2.410	0.334	1.922	0.356	0.929	0.120	0.783	0.115
108	12.549	23.856	3.021	11.158	2.036	0.369	2.107	0.282	1.397	0.245	0.728	0.097	0.629	0.092
H111	11.521	23.197	2.748	10.131	1.809	0.337	1.908	0.257	1.355	0.253	0.742	0.107	0.682	0.107
H83	12.643	23.539	2.966	11.546	2.299	0.651	2.626	0.375	2.059	0.394	1.165	0.155	1.003	0.142
46	2.683	6.003	0.733	2.902	0.652	0.181	0.888	0.173	1.310	0.318	0.943	0.127	0.761	0.106
H84	17.562	36.923	4.314	15.787	2.711	0.620	2.827	0.375	1.906	0.342	1.037	0.148	0.971	0.143

Sample #	La (ppm)	Ce (ppm)	Pr (ppm)	Nd (ppm)	Sm (ppm)	Eu (ppm)	Gd (ppm)	Tb (ppm)	Dy (ppm)	Ho (ppm)	Er (ppm)	Tm (ppm)	Yb (ppm)	Lu (ppm)
14	10.815	25.038	2.847	10.604	1.893	0.257	1.863	0.241	1.141	0.201	0.619	0.087	0.611	0.100
H85	17.196	34.585	4.091	14.903	2.690	0.565	2.863	0.389	2.039	0.392	1.220	0.174	1.175	0.179
98	12.363	23.867	2.958	10.998	1.895	0.340	1.943	0.257	1.325	0.255	0.769	0.105	0.714	0.114
H92	28.109	57.321	6.706	24.881	4.376	0.920	4.484	0.617	3.276	0.645	2.097	0.324	2.279	0.375
110	9.153	19.481	2.308	8.722	1.856	0.548	2.275	0.327	1.710	0.308	0.915	0.116	0.780	0.109
54	2.528	5.604	0.757	3.363	1.046	0.562	1.550	0.271	1.514	0.290	0.788	0.099	0.652	0.095
H112	19.303	39.227	4.495	16.674	3.184	0.733	3.531	0.453	2.260	0.411	1.221	0.172	1.168	0.181
91	6.996	13.886	1.716	6.397	1.330	0.420	1.623	0.235	1.187	0.231	0.670	0.090	0.569	0.089
H81	9.963	20.445	2.350	8.773	1.707	0.472	1.894	0.248	1.220	0.214	0.644	0.088	0.621	0.098
H113	13.756	28.411	3.480	13.480	2.883	0.846	3.460	0.500	2.476	0.438	1.230	0.162	1.036	0.158
55	14.233	24.493	3.884	16.300	3.550	0.958	3.883	0.510	2.239	0.344	0.861	0.091	0.569	0.081
100	8.423	15.316	1.718	6.367	1.210	0.452	1.427	0.180	0.894	0.175	0.513	0.074	0.446	0.064
H89	18.906	39.569	4.571	16.631	3.258	0.727	3.945	0.565	3.002	0.601	1.785	0.243	1.564	0.243
80	2.430	5.047	0.590	2.187	0.440	0.186	0.482	0.063	0.312	0.059	0.176	0.025	0.178	0.029
50	1.806	3.338	0.461	1.850	0.389	0.120	0.568	0.109	0.740	0.172	0.464	0.059	0.337	0.047
104	6.407	12.927	1.439	5.162	0.906	0.162	1.145	0.159	0.843	0.159	0.441	0.055	0.354	0.055
H82	36.539	73.547	8.005	28.289	4.662	1.262	4.962	0.566	2.527	0.450	1.372	0.187	1.274	0.196
107	3.460	7.365	0.841	3.129	0.595	0.170	0.702	0.093	0.507	0.102	0.279	0.041	0.272	0.043
109	9.040	16.708	2.007	7.317	1.285	0.381	1.523	0.177	0.892	0.166	0.507	0.068	0.462	0.076
103	15.110	30.038	3.424	12.524	2.185	0.518	2.552	0.293	1.370	0.257	0.737	0.092	0.598	0.094

B.D. = below detection

APPENDIX 2B – PARTIAL REE

Sample #	La (ppm)	Ce (ppm)	Pr (ppm)	Nd (ppm)	Sm (ppm)	Eu (ppm)	Gd (ppm)	Tb (ppm)	Dy (ppm)	Ho (ppm)	Er (ppm)	Tm (ppm)	Yb (ppm)	Lu (ppm)
SR-22A	0.138	0.030	0.010	0.045	0.006	0.005	0.018	0.003	0.021	0.006	0.028	0.003	0.022	0.003
RL2-51	0.165	0.259	0.028	0.109	0.017	0.014	0.027	0.004	0.022	0.005	0.015	0.002	0.011	0.001
SR-22A	0.146	0.033	0.010	0.047	0.008	0.006	0.021	0.002	0.021	0.007	0.029	0.003	0.019	0.004
RL2-51	0.086	0.129	0.015	0.053	0.008	0.007	0.013	0.002	0.011	0.002	0.007	0.001	0.006	b.d.
144-6	1.357	3.208	0.436	1.948	0.450	0.098	0.473	0.064	0.296	0.050	0.135	0.016	0.112	0.016
E150-9	0.573	1.177	0.154	0.685	0.180	0.154	0.206	0.024	0.131	0.022	0.049	0.006	0.030	0.004
144-2	2.571	5.209	0.605	2.269	0.403	0.100	0.520	0.072	0.406	0.074	0.215	0.029	0.185	0.028
17-8	0.915	2.095	0.264	1.068	0.226	0.045	0.231	0.032	0.145	0.022	0.058	0.008	0.047	0.007
E150-2	1.097	2.246	0.271	1.077	0.176	0.024	0.201	0.022	0.105	0.020	0.061	0.009	0.067	0.014
E150-5	0.349	0.840	0.115	0.548	0.214	0.065	0.282	0.048	0.277	0.047	0.129	0.015	0.103	0.015
E150-8	1.117	2.457	0.326	1.459	0.439	0.125	0.646	0.105	0.612	0.119	0.320	0.041	0.249	0.034
E152-6	2.371	4.830	0.569	2.160	0.317	0.036	0.349	0.037	0.148	0.025	0.071	0.008	0.065	0.014
E150-4	0.543	1.341	0.199	0.950	0.358	0.114	0.507	0.084	0.507	0.099	0.262	0.037	0.228	0.033
E154-3	0.632	1.410	0.184	0.772	0.192	0.043	0.213	0.032	0.166	0.032	0.084	0.011	0.070	0.011
144-1	2.412	4.772	0.534	1.936	0.308	0.076	0.364	0.050	0.270	0.054	0.146	0.022	0.131	0.022
E152-5	2.062	4.171	0.493	1.902	0.262	0.029	0.267	0.031	0.118	0.022	0.083	0.014	0.117	0.029
E152-4	0.750	1.734	0.240	1.074	0.349	0.110	0.458	0.077	0.436	0.077	0.205	0.025	0.157	0.022
E150-1	0.525	1.251	0.181	0.857	0.327	0.103	0.487	0.088	0.519	0.102	0.310	0.044	0.259	0.039
144-4	2.128	4.451	0.526	2.046	0.408	0.125	0.535	0.078	0.426	0.071	0.184	0.026	0.168	0.025
E150-3	0.588	1.405	0.182	0.795	0.254	0.085	0.323	0.048	0.289	0.047	0.118	0.014	0.079	0.012
E152-8	0.752	1.646	0.216	0.930	0.221	0.075	0.255	0.031	0.136	0.024	0.068	0.011	0.089	0.017
E152-9	0.375	0.771	0.098	0.404	0.112	0.030	0.192	0.038	0.209	0.040	0.123	0.018	0.131	0.022
E152-1	1.821	3.706	0.431	1.608	0.236	0.030	0.261	0.028	0.118	0.020	0.055	0.006	0.036	0.006
17-9	1.390	2.835	0.343	1.351	0.267	0.058	0.288	0.035	0.160	0.027	0.076	0.009	0.061	0.008
17-22	4.370	9.278	1.116	4.287	0.804	0.133	0.847	0.112	0.558	0.094	0.290	0.041	0.249	0.035
E152-2	0.988	2.104	0.253	1.014	0.175	0.023	0.175	0.020	0.095	0.018	0.058	0.009	0.071	0.018
E154-1	0.706	1.555	0.186	0.716	0.105	0.015	0.105	0.013	0.046	0.007	0.025	0.003	0.029	0.005
E154-2	3.460	7.256	0.846	3.132	0.517	0.063	0.490	0.057	0.313	0.064	0.190	0.027	0.171	0.027
144-3	1.646	3.377	0.410	1.603	0.311	0.074	0.336	0.041	0.206	0.034	0.101	0.014	0.085	0.013

Sample #	La (ppm)	Ce (ppm)	Pr (ppm)	Nd (ppm)	Sm (ppm)	Eu (ppm)	Gd (ppm)	Tb (ppm)	Dy (ppm)	Ho (ppm)	Er (ppm)	Tm (ppm)	Yb (ppm)	Lu (ppm)
17-7	0.986	1.939	0.253	1.073	0.306	0.125	0.445	0.081	0.440	0.081	0.234	0.032	0.196	0.027
17-6	0.724	1.483	0.195	0.893	0.303	0.114	0.448	0.079	0.493	0.097	0.273	0.037	0.214	0.033
E152-10	0.220	0.462	0.063	0.273	0.086	0.025	0.151	0.030	0.191	0.039	0.110	0.018	0.124	0.023
E150-10	0.888	2.395	0.337	1.459	0.455	0.104	0.589	0.104	0.573	0.102	0.280	0.035	0.209	0.028
144-7	0.671	1.602	0.221	0.934	0.205	0.045	0.223	0.033	0.157	0.030	0.077	0.010	0.060	0.007
E150-6	1.650	3.957	0.532	2.286	0.663	0.176	0.836	0.132	0.733	0.127	0.330	0.039	0.244	0.032
144-5	0.360	0.776	0.099	0.421	0.112	0.036	0.180	0.031	0.187	0.034	0.093	0.012	0.090	0.014
H91	4.941	10.225	1.204	4.548	0.750	0.132	0.744	0.076	0.286	0.038	0.093	0.009	0.059	0.007
E152-3	2.847	6.012	0.726	2.838	0.402	0.047	0.422	0.044	0.180	0.032	0.105	0.015	0.117	0.029
E152-7	0.619	1.285	0.158	0.606	0.117	0.021	0.147	0.016	0.067	0.011	0.031	0.004	0.025	0.005
E150-7	1.224	2.740	0.353	1.490	0.382	0.112	0.487	0.075	0.379	0.070	0.183	0.024	0.137	0.019
SR-22A	0.960	0.740	0.110	0.500	0.073	0.039	0.140	0.018	0.140	0.043	0.150	0.021	0.140	0.026
RL2-51	0.824	1.458	0.170	0.675	0.111	0.056	0.139	0.023	0.140	0.031	0.111	0.020	0.111	0.022
98	0.372	0.699	0.084	0.343	0.063	0.010	0.084	0.010	0.054	0.012	0.031	0.003	0.025	0.003
H111	0.356	0.602	0.073	0.294	0.053	0.018	0.086	0.014	0.091	0.020	0.058	0.011	0.051	0.005
H89	8.716	17.128	2.016	7.891	0.964	0.146	1.273	0.177	1.102	0.281	1.070	0.208	1.755	0.453
H84	6.713	15.162	2.163	9.878	3.473	1.283	4.949	0.864	4.889	0.878	2.300	0.310	1.931	0.280
14	3.116	6.330	0.698	2.494	0.380	0.059	0.489	0.068	0.401	0.094	0.419	0.078	0.588	0.103
96	3.041	6.638	0.809	3.205	0.751	0.140	0.893	0.147	0.867	0.171	0.507	0.072	0.463	0.076
50	4.612	9.294	1.232	4.879	1.052	0.235	1.186	0.210	1.242	0.245	0.625	0.075	0.418	0.063
H82	7.098	15.147	1.987	8.632	2.722	1.010	3.955	0.744	4.357	0.786	2.002	0.253	1.552	0.220
H81	2.824	6.028	0.785	3.500	1.109	0.409	1.782	0.327	2.081	0.404	1.160	0.173	1.215	0.191
46	4.335	9.473	1.190	4.685	1.076	0.205	1.228	0.222	1.511	0.335	0.942	0.119	0.709	0.092
91	5.487	11.524	1.432	6.067	1.688	0.549	2.057	0.319	1.843	0.313	0.863	0.110	0.690	0.094
H83	2.366	5.250	0.772	3.583	1.192	0.366	1.507	0.261	1.674	0.329	0.925	0.129	0.801	0.110
106	5.543	12.369	1.485	5.692	1.262	0.275	1.681	0.276	1.571	0.283	0.744	0.101	0.595	0.088
H112	4.461	9.743	1.286	5.619	1.830	0.564	2.889	0.521	3.041	0.569	1.550	0.236	1.655	0.277
103	4.519	9.564	1.250	5.093	1.576	0.499	1.954	0.331	1.903	0.368	1.002	0.135	0.857	0.143
110	5.619	12.752	1.826	8.331	2.934	1.075	4.118	0.722	4.283	0.681	1.906	0.250	1.658	0.234

Sample #	La (ppm)	Ce (ppm)	Pr (ppm)	Nd (ppm)	Sm (ppm)	Eu (ppm)	Gd (ppm)	Tb (ppm)	Dy (ppm)	Ho (ppm)	Er (ppm)	Tm (ppm)	Yb (ppm)	Lu (ppm)
100	5.269	9.917	1.198	4.676	1.060	0.409	1.303	0.184	1.027	0.188	0.512	0.072	0.469	0.080
108	3.896	8.151	1.069	4.363	1.204	0.226	1.344	0.203	1.126	0.186	0.539	0.069	0.478	0.067
104	3.258	6.889	0.809	2.963	0.631	0.176	0.929	0.171	1.055	0.200	0.527	0.071	0.421	0.060
54	1.522	3.968	0.563	2.744	1.070	0.496	1.782	0.313	1.844	0.337	0.833	0.105	0.648	0.086
80	3.693	8.014	0.999	3.758	0.873	0.194	0.961	0.139	0.755	0.133	0.381	0.055	0.344	0.053
109	4.358	8.614	1.023	3.978	0.960	0.312	1.349	0.197	1.100	0.200	0.569	0.082	0.546	0.078
H113	5.371	12.896	1.779	7.891	2.423	0.780	3.056	0.514	2.858	0.487	1.310	0.172	1.146	0.162
107	3.190	6.830	0.808	3.059	0.629	0.163	0.773	0.138	0.823	0.161	0.467	0.068	0.409	0.064
55	25.733	54.983	7.018	28.437	6.396	1.609	6.658	0.928	4.415	0.634	1.456	0.181	1.154	0.140
H92	71.673	151.241	17.620	63.758	10.238	1.320	8.847	1.018	4.773	0.688	2.019	0.326	2.672	0.576
H85	1.193	2.674	0.394	1.810	0.719	0.238	1.264	0.252	1.600	0.337	1.019	0.148	1.006	0.158
92	3.041	6.962	0.947	3.920	1.162	0.405	1.483	0.238	1.419	0.276	0.746	0.098	0.556	0.086
17	2.631	4.298	0.473	1.792	0.287	0.050	0.341	0.046	0.301	0.069	0.240	0.043	0.310	0.055
16	2.044	3.420	0.371	1.376	0.193	0.028	0.203	0.027	0.152	0.037	0.151	0.032	0.288	0.052
8-44A	1.836	1.732	0.199	0.760	0.125	0.073	0.187	0.020	0.103	0.023	0.074	0.011	0.075	0.014
SR-16B	0.592	0.411	0.084	0.373	0.108	0.049	0.173	0.032	0.205	0.050	0.179	0.027	0.154	0.025
18-0-1	2.190	5.346	0.731	3.224	0.997	0.765	1.282	0.204	1.105	0.216	0.567	0.076	0.513	0.083
18-0-2	2.924	6.585	0.862	3.841	1.193	0.321	1.614	0.274	1.523	0.282	0.712	0.087	0.538	0.083
18-0-3	2.647	5.981	0.797	3.511	0.991	0.752	1.155	0.167	0.822	0.128	0.330	0.040	0.206	0.034
18-0-4	3.139	7.660	1.029	4.498	1.127	0.310	1.394	0.216	1.090	0.214	0.567	0.086	0.572	0.087
18-2-1	1.522	3.047	0.340	1.377	0.250	0.056	0.403	0.059	0.388	0.114	0.462	0.082	0.749	0.191
18-2-2	5.394	10.633	1.205	4.533	0.620	0.066	0.676	0.071	0.350	0.083	0.336	0.057	0.536	0.141
18-2-3	2.562	5.376	0.616	2.379	0.286	0.034	0.331	0.037	0.154	0.026	0.109	0.016	0.149	0.042
18-2-4	2.276	4.720	0.554	2.227	0.606	0.174	0.953	0.172	1.087	0.218	0.644	0.097	0.776	0.158
18-2-5	2.608	6.031	0.818	3.847	1.402	0.389	2.063	0.372	2.152	0.410	1.125	0.162	1.053	0.159
18-2-6	5.517	11.953	1.398	5.711	1.309	0.289	1.790	0.275	1.478	0.315	0.909	0.128	0.900	0.153
18-2-7	3.691	7.529	0.915	3.979	1.110	0.495	1.857	0.301	1.704	0.329	0.794	0.103	0.628	0.086
18-2-8	1.198	2.611	0.318	1.317	0.359	0.092	0.532	0.087	0.500	0.091	0.219	0.029	0.190	0.030
18-2-9	1.450	2.843	0.331	1.438	0.461	0.151	0.788	0.148	0.850	0.176	0.527	0.077	0.618	0.121
18-2-10	0.907	1.945	0.230	0.955	0.251	0.059	0.320	0.057	0.311	0.061	0.182	0.027	0.218	0.048

Sample #	La (ppm)	Ce (ppm)	Pr (ppm)	Nd (ppm)	Sm (ppm)	Eu (ppm)	Gd (ppm)	Tb (ppm)	Dy (ppm)	Ho (ppm)	Er (ppm)	Tm (ppm)	Yb (ppm)	Lu (ppm)
18-2-11	1.302	2.852	0.372	1.773	0.637	0.218	1.075	0.208	1.246	0.243	0.697	0.101	0.727	0.135
18-2-12	1.152	2.435	0.295	1.207	0.349	0.106	0.543	0.108	0.666	0.130	0.389	0.058	0.434	0.077
18-2-13	1.583	3.991	0.501	2.026	0.479	0.115	0.583	0.097	0.510	0.097	0.268	0.037	0.302	0.052
18-2-14	1.211	2.835	0.384	1.769	0.702	0.231	1.072	0.207	1.132	0.205	0.562	0.071	0.547	0.091
18-2-15	1.566	3.266	0.397	1.769	0.578	0.179	0.916	0.171	1.055	0.213	0.625	0.095	0.675	0.130
18-2-16	1.486	3.352	0.425	1.877	0.583	0.167	0.793	0.153	0.831	0.166	0.458	0.069	0.463	0.071
18-2-17	0.817	1.876	0.249	1.131	0.411	0.152	0.677	0.127	0.774	0.145	0.423	0.063	0.452	0.070
18-2-18	3.480	7.171	0.850	3.299	0.840	0.234	1.201	0.207	1.184	0.211	0.605	0.087	0.543	0.085
18-2-19	1.100	2.522	0.335	1.395	0.401	0.116	0.557	0.109	0.679	0.139	0.415	0.061	0.488	0.097
18-2-20	0.956	2.174	0.281	1.257	0.419	0.147	0.688	0.129	0.755	0.162	0.451	0.069	0.463	0.076
18-2-21	0.985	2.176	0.273	1.226	0.385	0.149	0.662	0.115	0.715	0.135	0.383	0.056	0.370	0.059
18-2-22	0.672	1.594	0.220	0.970	0.328	0.132	0.558	0.101	0.584	0.118	0.335	0.045	0.364	0.063
18-2-24	2.566	5.252	0.736	3.291	0.986	0.236	1.283	0.183	1.029	0.200	0.552	0.079	0.480	0.077
18-2-25	1.813	3.684	0.419	1.596	0.214	0.027	0.259	0.029	0.130	0.029	0.114	0.017	0.174	0.048
18-2-26	3.598	7.334	0.846	3.305	0.468	0.052	0.521	0.061	0.287	0.080	0.342	0.057	0.571	0.147

B.D. = Below Detection

APPENDIX 2C – WHOLE ROCK MAJORS

Sample #	Al_2O_3 (wt%)	BaO (wt%)	CaO (wt%)	Fe_2O_3 (wt%)	K_2O (wt%)	MgO (wt%)	MnO (wt%)	Na_2O (wt%)	P_2O_5 (wt%)	TiO_2 (wt%)
BHVO-2	11.790	0.013	9.921	9.647	0.448	5.832	0.138	2.339	0.227	2.111
8-44A	0.247	0.001	25.268	1.097	0.007	7.968	0.545	0.444	b.d.	0.004
SR16-B	0.114	0.002	29.105	0.107	0.006	0.400	0.102	0.346	b.d.	0.002
18-0-1	14.088	0.076	2.746	4.429	3.558	3.306	0.041	1.422	0.079	0.290
18-0-2	3.429	0.030	15.435	2.629	0.826	11.095	0.250	0.415	0.023	0.044
18-0-3	1.530	0.673	19.154	1.246	0.304	11.609	0.166	0.721	0.014	0.016
18-0-4	4.561	0.043	16.886	1.455	1.124	10.584	0.132	1.223	0.040	0.097
18-2-1	7.403	0.044	10.650	1.613	1.979	0.518	0.184	1.980	0.068	0.218
18-2-2	9.725	0.054	7.678	3.894	2.493	1.385	0.163	1.719	0.068	0.273
18-2-3	4.565	1.205	14.285	1.636	1.066	8.365	0.167	1.110	0.041	0.072
18-2-4	9.648	0.054	11.558	3.282	2.705	5.291	0.321	1.402	0.057	0.151
18-2-5	5.030	0.031	26.959	1.231	1.586	1.039	0.220	0.947	0.034	0.112
18-2-6	5.540	0.047	11.422	1.058	1.415	0.705	0.088	1.143	0.042	0.102
18-2-7	2.503	0.021	10.843	1.119	0.948	0.591	0.125	0.221	0.020	0.065
18-2-8	11.520	0.074	3.816	4.074	3.162	4.572	0.100	1.337	0.092	0.351
18-2-9	10.239	0.049	9.648	3.834	2.283	2.273	0.098	1.897	0.089	0.205
18-2-10	13.298	0.078	2.147	4.506	3.314	3.139	0.034	1.411	0.091	0.233
18-2-11	8.272	0.039	13.288	2.324	1.709	1.253	0.110	2.429	0.056	0.103
18-2-12	11.456	0.059	7.168	3.213	2.616	2.569	0.068	2.126	0.094	0.274
18-2-13	10.165	0.065	2.173	3.648	3.175	1.276	0.068	1.666	0.078	0.311
18-2-14	6.774	0.035	7.930	1.233	1.758	0.906	0.071	2.518	0.068	0.096
18-2-15	10.685	0.063	11.986	3.705	2.340	2.977	0.100	1.525	0.102	0.242
18-2-16	8.168	0.051	12.967	0.990	1.710	1.117	0.112	3.168	0.081	0.072
18-2-17	9.234	0.056	10.219	2.212	1.850	2.158	0.114	2.982	0.084	0.089
18-2-18	7.427	0.054	11.947	3.210	1.706	7.931	0.189	1.439	0.080	0.129
18-2-19	10.101	0.060	6.435	3.594	2.231	3.650	0.087	2.374	0.076	0.155
18-2-20	8.646	0.058	12.911	1.119	1.993	1.271	0.107	3.060	0.058	0.089
18-2-21	9.946	0.051	9.285	1.869	1.989	1.717	0.099	3.570	0.074	0.084
18-2-22	5.835	0.031	8.383	0.795	1.743	0.284	0.077	1.882	0.030	0.037

Sample #	Al_2O_3 (wt%)	BaO (wt%)	CaO (wt%)	Fe_2O_3 (wt%)	K_2O (wt%)	MgO (wt%)	MnO (wt%)	Na_2O (wt%)	P_2O_5 (wt%)	TiO_2 (wt%)
18-2-23	13.491	0.011	0.481	9.115	0.647	4.386	0.034	3.958	0.176	0.080
18-2-24	2.831	0.010	14.082	0.857	0.486	0.629	0.179	0.724	0.023	0.069
18-2-25	10.967	0.059	2.742	4.243	2.869	1.458	0.090	2.259	0.088	0.396
18-2-26	9.589	0.056	7.777	3.542	2.657	1.260	0.160	1.619	0.065	0.252
SR-16B	0.333	0.004	36.324	0.202	0.010	0.710	0.113	0.530	0.002	0.001
8-44A	0.286	0.000	25.906	1.144	0.005	9.227	0.589	0.451	0.003	0.008
BHVO-2	11.839	0.013	8.788	9.810	0.467	6.886	0.144	2.221	0.271	2.373
104	1.523	0.006	31.651	0.472	0.205	0.394	0.025	0.876	0.011	0.019
80	2.380	0.034	14.214	0.855	0.839	0.662	0.040	0.211	0.027	0.048
109	3.258	0.031	28.852	0.910	1.013	0.997	0.068	0.668	0.033	0.092
54	4.016	0.041	14.155	4.849	1.217	10.189	0.451	0.539	0.090	0.074
96	2.756	0.010	32.238	0.842	0.361	0.768	0.038	1.158	0.025	0.032
108	2.531	0.016	20.060	1.664	0.591	12.610	0.137	0.744	0.031	0.064
110	2.941	0.011	15.784	0.703	0.465	0.682	0.089	1.040	0.028	0.082
50	1.664	0.010	14.779	4.778	0.430	10.846	0.445	0.323	0.073	0.026
103	4.265	0.009	11.069	5.190	0.565	10.292	0.367	0.482	0.310	0.115
H113	4.284	0.020	29.440	1.320	0.784	1.157	0.221	1.306	0.157	0.112
106	1.886	0.005	32.294	1.055	0.173	0.988	0.077	0.763	0.020	0.045
14	2.830	0.007	19.822	0.710	0.162	1.012	0.027	1.528	0.027	0.089
107	2.013	0.014	19.945	0.749	0.491	0.502	0.021	0.473	0.021	0.044
100	1.997	0.012	20.894	3.077	0.642	9.871	0.368	0.594	0.083	0.039
H81	8.524	0.051	8.696	1.803	2.092	2.458	0.100	2.477	0.098	0.135
H84	5.615	0.019	15.683	2.705	0.600	13.154	0.222	0.728	0.050	0.085
H82	9.798	0.078	9.143	4.578	3.209	8.896	0.231	0.608	0.099	0.234
55	2.205	0.022	16.005	1.062	0.794	0.461	0.193	0.305	0.061	0.044
16	4.934	0.025	22.100	1.309	0.723	1.157	0.026	1.415	0.046	0.151
46	2.238	0.012	17.329	5.155	0.589	11.144	0.457	0.488	0.082	0.050
H85	5.546	0.003	27.201	2.811	0.191	7.659	0.222	0.578	0.055	0.052
H92	11.797	0.080	4.691	3.520	3.749	1.767	0.123	1.970	0.107	0.412
91	2.295	0.015	16.503	3.963	0.553	13.860	0.421	0.574	0.086	0.042

Sample #	Al_2O_3 (wt%)	BaO (wt%)	CaO (wt%)	Fe_2O_3 (wt%)	K_2O (wt%)	MgO (wt%)	MnO (wt%)	Na_2O (wt%)	P_2O_5 (wt%)	TiO_2 (wt%)
H89	8.158	0.057	2.797	2.524	2.747	1.018	0.087	1.411	0.073	0.282
H83	4.458	0.033	22.601	1.273	1.331	1.295	0.181	0.976	0.116	0.107
H112	9.919	0.047	11.088	2.702	2.337	2.429	0.107	1.802	0.100	0.263
H111	2.640	0.015	34.701	0.850	0.415	0.648	0.045	1.157	0.029	0.074
98	4.088	0.008	26.874	1.191	0.733	0.717	0.041	1.644	0.039	0.124
BHVO-2	12.370	0.013	9.828	9.680	0.449	5.666	0.137	2.700	0.234	1.430
8-44A	0.390	0.001	28.927	1.107	0.009	7.772	0.575	0.650	0.002	0.003
SR16B	0.353	0.002	35.223	0.174	0.008	0.429	0.105	0.622	0.004	0.002
H91	10.720	0.069	0.555	4.052	3.349	1.172	0.036	1.434	0.074	0.234
17-6	3.797	0.026	32.788	0.705	0.453	0.505	0.208	1.881	0.097	0.018
E150-4	5.400	0.008	21.550	2.539	0.238	8.054	0.194	0.796	0.041	0.030
E152-7	7.539	0.059	2.404	2.611	2.462	0.768	0.069	1.516	0.063	0.148
E152-2	8.757	0.056	5.170	2.917	2.616	0.971	0.107	1.474	0.077	0.179
E152-9	7.673	0.029	14.662	4.112	1.525	2.962	0.293	1.507	0.057	0.089
E150-9	1.101	1.210	19.917	1.213	0.266	11.619	0.161	0.628	0.011	0.012
E150-5	5.466	0.019	22.093	2.168	0.409	7.291	0.171	1.093	0.044	0.042
144-3	0.923	0.004	38.945	0.587	0.164	1.128	0.057	0.703	0.008	0.011
E154-2	1.603	0.010	39.085	0.520	0.260	0.346	0.051	1.107	0.009	0.020
E150-7	1.940	0.077	27.660	1.137	0.506	9.384	0.190	0.911	0.016	0.018
E150-2	2.747	0.009	20.782	2.137	0.233	9.762	0.231	0.642	0.017	0.016
17-8	1.984	0.015	33.838	0.951	0.454	2.155	0.048	0.592	0.018	0.021
E152-10	9.838	0.046	12.196	3.552	2.421	3.158	0.271	1.580	0.069	0.106
E150-6	3.015	0.028	21.123	1.524	0.744	11.361	0.164	0.993	0.019	0.031
E152-5	9.243	0.054	5.034	3.406	2.614	1.107	0.112	1.808	0.072	0.191
E152-1	15.918	0.117	0.268	4.410	5.303	2.339	0.025	1.237	0.143	0.335
E152-3	10.698	0.066	3.262	4.341	3.373	1.376	0.087	1.535	0.080	0.225
E150-10	5.430	0.038	16.278	1.844	1.338	10.717	0.128	1.052	0.043	0.065
144-6	2.127	0.011	30.536	1.368	0.406	6.058	0.104	1.083	0.016	0.022
144-4	1.200	0.012	21.490	0.526	0.411	0.321	0.028	0.406	0.011	0.019
E150-3	4.778	0.022	18.690	2.003	0.541	10.124	0.185	1.281	0.037	0.083

Sample #	Al_2O_3 (wt%)	BaO (wt%)	CaO (wt%)	Fe_2O_3 (wt%)	K_2O (wt%)	MgO (wt%)	MnO (wt%)	Na_2O (wt%)	P_2O_5 (wt%)	TiO_2 (wt%)
E152-6	10.324	0.072	3.421	3.669	3.537	1.053	0.080	1.459	0.078	0.204
144-5	6.244	0.049	8.128	1.693	1.682	1.141	0.068	1.223	0.047	0.062
E154-1	7.047	0.043	27.480	3.638	1.528	1.464	0.355	1.566	0.048	0.133
E152-4	8.933	0.057	4.361	2.809	2.710	0.865	0.097	1.671	0.067	0.193
144-7	1.454	0.010	34.397	1.384	0.384	5.305	0.089	0.847	0.010	0.012
E152-8	4.302	0.065	4.789	0.826	1.071	0.262	0.101	1.210	0.025	0.050
17-7	3.837	0.028	34.062	0.814	0.482	0.606	0.207	1.861	0.101	0.021
E154-3	1.598	0.009	39.225	0.572	0.201	0.368	0.042	1.165	0.010	0.022
144-1	2.586	0.012	29.640	0.820	0.467	0.452	0.043	0.935	0.022	0.038
144-2	2.204	0.014	35.853	0.622	0.488	0.330	0.045	1.042	0.017	0.023
E150-8	6.539	0.076	17.066	2.381	1.812	8.800	0.170	0.956	0.050	0.067
17-9	1.443	0.015	38.091	0.725	0.313	2.215	0.058	0.833	0.015	0.018
17-22	3.627	0.013	34.286	1.220	0.507	0.988	0.022	1.467	0.031	0.040
E150-1	4.275	0.013	24.462	1.959	0.335	5.375	0.178	0.752	0.031	0.066

B.D. = Below Detection

APPENDIX 2D – PARTIAL MAJORS

Sample #	Al_2O_3 (wt%)	BaO (wt%)	CaO (wt%)	Fe_2O_3 (wt%)	K_2O (wt%)	MgO (wt%)	MnO (wt%)	Na_2O (wt%)	P_2O_5 (wt%)	TiO_2 (wt%)
SR-16B	b.d.	0.001	9.193	0.014	0.001	0.085	0.024	0.001	b.d.	b.d.
8-44A	0.002	b.d.	17.795	0.442	0.002	3.627	0.293	0.004	b.d.	b.d.
SR-22A	0.001	0.001	25.046	0.146	0.001	0.675	0.122	0.006	b.d.	b.d.
RL2-51	0.004	b.d.	12.123	0.895	0.001	8.065	0.415	0.001	b.d.	b.d.
RL2-51	0.001	b.d.	15.169	1.069	b.d.	9.952	0.511	0.001	b.d.	b.d.
SR-22A	b.d.	0.001	16.358	0.154	b.d.	0.665	0.096	0.001	b.d.	b.d.
H81	0.009	b.d.	4.921	0.152	0.014	0.395	0.047	0.004	b.d.	b.d.
H82	0.015	b.d.	2.582	0.600	0.017	1.492	0.063	0.001	b.d.	b.d.
H83	0.007	b.d.	13.179	0.197	0.027	0.158	0.100	0.002	b.d.	b.d.
E150-10	0.016	0.002	12.335	0.985	0.013	8.045	0.109	0.006	b.d.	b.d.
E150-9	b.d.	0.049	13.585	0.109	0.003	9.030	0.131	0.002	b.d.	b.d.
E150-8	0.035	0.010	11.311	1.210	0.019	6.052	0.154	0.001	b.d.	b.d.
E150-7	0.012	0.013	15.095	0.784	0.004	7.365	0.143	0.008	b.d.	b.d.
E150-6	0.013	0.001	15.209	0.640	0.008	9.398	0.160	0.006	b.d.	b.d.
E150-5	0.041	b.d.	8.509	0.517	0.010	3.013	0.103	0.004	b.d.	b.d.
E150-4	0.030	0.001	11.521	0.605	0.009	3.193	0.146	0.004	b.d.	b.d.
E150-3	0.019	0.001	8.423	0.716	0.004	5.190	0.124	0.003	b.d.	b.d.
E150-2	0.080	0.001	1.571	0.118	0.036	0.036	0.030	0.003	b.d.	b.d.
H84	0.005	b.d.	4.833	0.106	0.008	0.659	0.044	0.002	b.d.	b.d.
H85	0.025	0.001	16.882	0.144	0.012	0.256	0.126	0.002	b.d.	b.d.
E150-1	0.030	0.002	11.479	0.290	0.021	1.160	0.108	b.d.	b.d.	b.d.
E152-10	0.056	b.d.	0.000	0.116	0.034	0.089	0.095	b.d.	b.d.	b.d.
E152-9	0.059	b.d.	4.813	0.146	0.035	0.100	0.108	b.d.	b.d.	b.d.
H92	0.031	0.001	3.002	0.078	0.056	0.041	0.063	0.004	b.d.	b.d.
H91	0.182	0.001	0.201	0.157	0.073	0.104	0.002	0.007	b.d.	b.d.
E152-8	0.024	0.002	2.167	0.044	0.015	0.021	0.053	0.005	b.d.	b.d.
E152-7	0.080	b.d.	0.398	0.109	0.019	0.044	0.009	0.001	b.d.	b.d.
E152-6	0.086	0.001	0.960	0.129	0.036	0.044	0.016	0.004	b.d.	b.d.
E152-5	0.086	0.001	2.281	0.130	0.043	0.040	0.045	0.004	b.d.	b.d.

Sample #	Al_2O_3 (wt%)	BaO (wt%)	CaO (wt%)	Fe_2O_3 (wt%)	K_2O (wt%)	MgO (wt%)	MnO (wt%)	Na_2O (wt%)	P_2O_5 (wt%)	TiO_2 (wt%)
E152-4	0.021	b.d.	12.674	1.261	0.006	7.050	0.204	0.003	b.d.	b.d.
H89	0.008	b.d.	1.343	0.023	0.021	0.015	0.028	0.003	b.d.	b.d.
E152-3	0.091	0.001	1.524	0.137	0.039	0.042	0.028	0.006	b.d.	b.d.
E152-2	0.079	0.001	1.915	0.113	0.032	0.054	0.034	0.004	b.d.	b.d.
E152-1	0.091	0.001	0.215	0.125	0.025	0.072	0.003	0.001	b.d.	b.d.
H113	0.012	0.001	0.000	0.224	0.013	0.173	0.139	0.003	b.d.	b.d.
H112	0.025	b.d.	6.602	0.128	0.028	0.118	0.059	0.003	b.d.	b.d.
E154-3	0.004	b.d.	19.698	0.181	0.002	0.141	0.022	0.002	b.d.	b.d.
E154-2	0.003	b.d.	19.066	0.190	0.005	0.109	0.026	b.d.	b.d.	b.d.
H111	0.001	b.d.	7.697	0.013	0.004	0.041	0.010	0.001	b.d.	b.d.
E154-1	0.021	b.d.	4.797	0.033	0.003	0.030	0.026	0.002	b.d.	b.d.
144-7	0.005	b.d.	9.134	1.000	0.002	4.202	0.050	0.001	b.d.	b.d.
144-6	0.006	b.d.	14.416	0.825	0.004	4.865	0.075	0.004	b.d.	b.d.
144-5	0.042	0.001	4.217	0.251	0.031	0.412	0.043	0.005	b.d.	b.d.
144-4	0.006	b.d.	17.290	0.275	0.003	0.181	0.018	b.d.	b.d.	b.d.
144-3	0.002	b.d.	16.532	0.287	0.003	0.761	0.028	0.001	b.d.	b.d.
144-2	0.005	b.d.	15.875	0.231	0.004	0.121	0.022	b.d.	b.d.	b.d.
144-1	0.012	b.d.	17.752	0.234	0.005	0.117	0.025	0.001	b.d.	b.d.
17-22	0.011	0.001	20.669	0.178	0.005	0.168	0.015	b.d.	b.d.	b.d.
17-9	0.007	b.d.	15.861	0.562	0.003	2.191	0.037	0.005	b.d.	b.d.
17-8	0.010	b.d.	8.283	0.511	0.003	1.909	0.027	b.d.	b.d.	b.d.
17-7	0.011	0.001	10.917	0.153	0.003	0.115	0.075	b.d.	b.d.	b.d.
17-6	0.008	b.d.	13.595	0.198	0.002	0.137	0.095	0.003	b.d.	b.d.
110	0.004	0.001	8.526	0.090	0.006	0.071	0.046	0.004	b.d.	b.d.
109	0.008	b.d.	16.329	0.185	0.017	0.191	0.038	0.002	b.d.	b.d.
108	0.009	b.d.	7.536	0.286	0.008	2.322	0.044	0.003	b.d.	b.d.
107	0.005	b.d.	20.084	0.211	0.006	0.131	0.014	0.002	b.d.	b.d.
106	0.004	b.d.	14.780	0.150	0.003	0.108	0.033	0.002	b.d.	b.d.
104	0.002	b.d.	24.303	0.279	0.004	0.217	0.019	0.002	b.d.	b.d.
103	0.022	b.d.	8.352	0.965	0.032	2.401	0.197	0.002	b.d.	b.d.

Sample #	Al_2O_3 (wt%)	BaO (wt%)	CaO (wt%)	Fe_2O_3 (wt%)	K_2O (wt%)	MgO (wt%)	MnO (wt%)	Na_2O (wt%)	P_2O_5 (wt%)	TiO_2 (wt%)
100	0.006	b.d.	8.354	0.897	0.008	2.632	0.154	0.001	b.d.	b.d.
98	0.029	b.d.	6.036	0.008	0.012	0.015	0.011	0.002	b.d.	b.d.
96	0.005	b.d.	11.486	0.072	0.005	0.060	0.014	0.001	b.d.	b.d.
92	0.017	b.d.	4.814	1.047	0.014	2.946	0.141	0.002	b.d.	b.d.
91	0.007	b.d.	3.556	0.587	0.007	2.124	0.100	0.003	b.d.	b.d.
80	0.009	0.001	19.479	0.225	0.010	0.233	0.035	0.002	b.d.	b.d.
55	0.011	b.d.	21.418	0.331	0.011	0.259	0.170	0.006	b.d.	b.d.
54	0.011	b.d.	4.468	1.237	0.013	2.527	0.151	0.001	b.d.	b.d.
50	0.007	b.d.	3.115	0.648	0.005	1.752	0.097	0.002	b.d.	b.d.
46	0.006	b.d.	4.003	1.031	0.007	2.164	0.123	0.002	b.d.	b.d.
17	0.003	b.d.	16.452	0.042	0.003	0.048	0.013	0.003	b.d.	b.d.
16	0.003	b.d.	14.374	0.028	0.002	0.024	0.012	0.002	b.d.	b.d.
14	0.002	b.d.	12.393	0.013	0.002	0.013	0.012	0.002	b.d.	b.d.
8-44A	b.d.	b.d.	7.162	0.127	b.d.	1.033	0.089	b.d.	b.d.	b.d.
SR-16B	0.003	0.001	12.869	0.049	b.d.	0.119	0.031	0.001	b.d.	b.d.
18-0-1	0.007	0.033	4.909	0.386	0.007	2.228	0.055	b.d.	b.d.	b.d.
18-0-2	0.010	0.002	4.373	0.420	0.005	2.138	0.062	b.d.	b.d.	b.d.
18-0-3	0.002	0.031	5.468	0.370	0.002	3.444	0.052	0.001	b.d.	b.d.
18-0-4	0.004	0.004	4.513	0.236	0.006	1.905	0.032	b.d.	b.d.	b.d.
18-2-1	0.012	b.d.	3.440	0.067	0.010	0.010	0.058	0.002	b.d.	0.001
18-2-2	0.011	b.d.	1.800	0.032	0.017	0.012	0.032	0.002	b.d.	b.d.
18-2-3	0.017	0.003	0.654	0.048	0.023	0.009	0.013	0.003	b.d.	b.d.
18-2-4	0.012	b.d.	3.271	0.190	0.024	0.495	0.081	b.d.	b.d.	b.d.
18-2-5	0.003	b.d.	8.809	0.102	0.013	0.069	0.080	b.d.	b.d.	b.d.
18-2-6	0.011	b.d.	11.088	0.138	0.008	0.097	0.065	b.d.	b.d.	0.001
18-2-7	0.006	0.001	11.568	0.214	0.018	0.115	0.091	0.002	b.d.	b.d.
18-2-8	0.017	b.d.	0.775	0.197	0.021	0.390	0.020	b.d.	b.d.	b.d.
18-2-9	0.014	b.d.	2.772	0.070	0.019	0.033	0.026	0.001	b.d.	b.d.
18-2-10	0.033	b.d.	0.737	0.042	0.021	0.025	0.008	b.d.	b.d.	b.d.
18-2-11	0.007	b.d.	3.728	0.059	0.013	0.033	0.030	b.d.	b.d.	b.d.

Sample #	Al_2O_3 (wt%)	BaO (wt%)	CaO (wt%)	Fe_2O_3 (wt%)	K_2O (wt%)	MgO (wt%)	MnO (wt%)	Na_2O (wt%)	P_2O_5 (wt%)	TiO_2 (wt%)
18-2-12	0.016	b.d.	2.276	0.088	0.014	0.053	0.019	b.d.	b.d.	b.d.
18-2-13	0.059	b.d.	0.924	0.090	0.019	0.052	0.011	0.013	b.d.	0.001
18-2-14	0.012	b.d.	3.982	0.071	0.011	0.065	0.034	0.002	b.d.	b.d.
18-2-15	0.014	b.d.	3.849	0.108	0.011	0.099	0.030	b.d.	b.d.	b.d.
18-2-16	0.009	b.d.	3.437	0.081	0.013	0.165	0.030	b.d.	b.d.	b.d.
18-2-17	0.005	b.d.	2.805	0.087	0.007	0.158	0.028	b.d.	b.d.	b.d.
18-2-18	0.021	0.001	3.558	0.492	0.021	1.934	0.062	0.006	b.d.	b.d.
18-2-19	0.011	b.d.	1.882	0.113	0.015	0.268	0.022	b.d.	b.d.	b.d.
18-2-20	0.006	b.d.	3.544	0.082	0.010	0.120	0.029	0.007	b.d.	b.d.
18-2-21	0.006	b.d.	2.838	0.096	0.006	0.140	0.027	0.003	b.d.	b.d.
18-2-22	0.005	b.d.	2.900	0.042	0.002	0.020	0.027	b.d.	b.d.	b.d.
18-2-23	0.055	b.d.	0.051	0.075	b.d.	0.042	0.001	0.004	b.d.	b.d.
18-2-24	0.002	b.d.	9.422	0.116	0.004	0.082	0.072	b.d.	b.d.	b.d.
18-2-25	0.016	b.d.	0.684	0.075	0.014	0.010	0.013	b.d.	b.d.	b.d.
18-2-26	0.014	b.d.	2.227	0.067	0.015	0.012	0.040	b.d.	b.d.	b.d.

B.D. = Below Detection

APPENDIX 2E – WHOLE ROCK MINORS

Sample #	Ba (ppm)	Cd (ppm)	Ce (ppm)	Cs (ppm)	Dy (ppm)	Er (ppm)	Eu (ppm)	Gd (ppm)	Hf (ppm)	Ho (ppm)	La (ppm)	Lu (ppm)	Mo (ppm)	Nb (ppm)
BHVO-2	132.106	0.160	35.951	0.096	5.110	2.417	1.999	6.603	5.646	0.897	14.331	0.278	3.938	18.085
8-44A	1.056	0.022	1.050	b.d.	0.097	0.122	0.057	0.147	1.455	0.033	1.515	0.026	0.315	0.032
SR-16B	48.708	0.086	0.150	0.006	0.110	0.120	0.024	0.083	0.568	0.035	0.578	0.024	0.132	0.050
96	100.647	0.060	25.203	0.429	1.516	0.892	0.317	2.034	1.724	0.280	12.344	0.135	0.158	0.697
16	236.547	0.048	34.487	0.282	1.875	1.095	0.478	2.749	2.163	0.354	16.193	0.163	0.612	4.651
106	49.518	0.080	24.327	0.240	1.922	0.929	0.389	2.410	2.137	0.356	11.731	0.115	0.766	1.456
108	170.845	0.045	23.856	1.190	1.397	0.728	0.369	2.107	1.844	0.245	12.549	0.092	0.226	1.872
H111	166.261	0.075	23.197	0.945	1.355	0.742	0.337	1.908	2.099	0.253	11.521	0.107	0.836	2.474
H83	298.221	0.096	23.539	5.150	2.059	1.165	0.651	2.626	1.828	0.394	12.643	0.142	0.703	1.623
46	131.628	0.033	6.003	0.313	1.310	0.943	0.181	0.888	1.677	0.318	2.683	0.106	0.106	0.394
H84	192.364	0.077	36.923	1.578	1.906	1.037	0.620	2.827	3.242	0.342	17.562	0.143	0.574	2.374
14	74.796	0.070	25.038	0.068	1.141	0.619	0.257	1.863	1.168	0.201	10.815	0.100	0.398	3.021
H85	32.418	0.073	34.585	1.364	2.039	1.220	0.565	2.863	3.429	0.392	17.196	0.179	0.487	1.183
98	90.295	0.072	23.867	0.875	1.325	0.769	0.340	1.943	3.137	0.255	12.363	0.114	0.825	4.294
H92	668.648	0.088	57.321	5.692	3.276	2.097	0.920	4.484	5.264	0.645	28.109	0.375	1.746	9.611
110	108.814	0.040	19.481	0.716	1.710	0.915	0.548	2.275	1.690	0.308	9.153	0.109	0.256	2.197
54	330.030	0.034	5.604	1.285	1.514	0.788	0.562	1.550	1.579	0.290	2.528	0.095	0.160	0.654
H112	332.966	0.072	39.227	3.729	2.260	1.221	0.733	3.531	3.005	0.411	19.303	0.181	0.848	4.720
91	111.784	0.035	13.886	0.903	1.187	0.670	0.420	1.623	0.985	0.231	6.996	0.089	0.072	0.569
H81	357.608	0.059	20.445	2.121	1.220	0.644	0.472	1.894	2.160	0.214	9.963	0.098	0.318	1.980
H113	144.277	0.078	28.411	0.934	2.476	1.230	0.846	3.460	2.572	0.438	13.756	0.158	0.607	1.921
55	181.200	0.064	24.493	0.689	2.239	0.861	0.958	3.883	0.455	0.344	14.233	0.081	6.343	0.462
100	99.691	0.018	15.316	0.670	0.894	0.513	0.452	1.427	1.341	0.175	8.423	0.064	0.195	0.581
H89	439.855	0.081	39.569	2.667	3.002	1.785	0.727	3.945	3.271	0.601	18.906	0.243	0.632	5.816
80	300.431	0.037	5.047	1.372	0.312	0.176	0.186	0.482	0.469	0.059	2.430	0.029	0.093	0.769
50	72.712	0.027	3.338	0.163	0.740	0.464	0.120	0.568	0.753	0.172	1.806	0.047	0.186	0.182
104	43.858	b.d.	12.927	0.192	0.843	0.441	0.162	1.145	0.756	0.159	6.407	0.055	0.166	0.377
H82	543.776	0.079	73.547	5.587	2.527	1.372	1.262	4.962	2.180	0.450	36.539	0.196	1.141	3.003
107	122.986	0.007	7.365	1.093	0.507	0.279	0.170	0.702	0.586	0.102	3.460	0.043	0.162	1.208

Sample #	Ba (ppm)	Cd (ppm)	Ce (ppm)	Cs (ppm)	Dy (ppm)	Er (ppm)	Eu (ppm)	Gd (ppm)	Hf (ppm)	Ho (ppm)	La (ppm)	Lu (ppm)	Mo (ppm)	Nb (ppm)
109	254.200	0.033	16.708	1.943	0.892	0.507	0.381	1.523	1.492	0.166	9.040	0.076	0.121	2.161
103	84.574	0.046	30.038	2.574	1.370	0.737	0.518	2.552	1.318	0.257	15.110	0.094	0.166	1.987
BHVO-2	279.373	0.325	34.720	0.209	4.988	2.403	1.948	6.495	5.396	0.909	14.091	0.265	3.752	16.556
8-44A	18.377	0.031	1.372	0.012	0.122	0.123	0.061	0.167	0.645	0.033	1.389	0.024	0.221	0.041
SR16-B	52.660	0.202	0.281	0.015	0.086	0.088	0.022	0.078	0.978	0.025	0.443	0.014	0.095	0.020
18-0-1	1997.583	0.238	86.938	23.003	3.510	1.938	1.566	6.854	5.241	0.626	43.845	0.286	1.118	5.036
18-0-2	749.955	0.077	24.869	2.641	1.346	0.659	0.425	2.080	1.284	0.241	13.542	0.079	0.140	0.669
18-0-3	21289.174	0.074	16.238	1.025	1.212	0.590	3.366	1.788	1.268	0.218	8.334	0.073	1.987	0.433
18-0-4	1131.821	0.140	30.704	5.439	1.876	1.084	0.632	2.869	4.834	0.363	15.329	0.155	0.396	2.561
18-2-1	1102.625	0.245	27.365	3.945	4.045	2.547	0.785	3.723	3.744	0.854	12.999	0.378	0.423	5.488
18-2-2	1040.755	0.464	78.438	5.241	4.525	2.626	1.217	6.288	4.043	0.874	38.900	0.396	0.863	7.549
18-2-3	51201.718	0.154	23.831	5.066	1.849	1.177	8.607	2.592	4.064	0.384	13.084	0.180	0.550	1.902
18-2-4	1221.893	0.247	62.963	9.679	2.970	1.786	0.973	4.806	5.113	0.566	30.471	0.286	0.935	3.707
18-2-5	851.477	0.178	41.737	8.821	3.295	1.758	0.853	4.401	4.395	0.586	22.105	0.247	0.138	3.052
18-2-6	1372.518	0.172	23.007	6.597	1.265	0.792	0.520	1.889	2.915	0.260	10.503	0.121	0.195	2.640
18-2-7	689.800	0.143	4.752	16.601	0.731	0.370	0.330	0.853	1.032	0.138	2.420	0.050	-0.011	1.597
18-2-8	1601.024	0.229	52.742	19.295	2.829	1.682	0.952	4.257	4.731	0.548	26.020	0.252	1.256	6.481
18-2-9	1241.895	0.208	42.216	11.988	3.561	2.195	0.851	4.166	6.528	0.724	20.853	0.361	1.082	5.509
18-2-10	2255.771	0.323	96.035	24.698	4.552	2.842	1.584	7.510	6.409	0.885	47.487	0.443	1.478	3.907
18-2-11	817.758	0.185	31.211	7.196	2.107	1.181	0.626	2.828	2.816	0.399	15.105	0.192	0.827	2.218
18-2-12	1836.644	0.264	76.007	19.050	3.949	2.239	1.368	6.173	5.410	0.738	37.005	0.354	1.272	5.277
18-2-13	1833.427	0.193	84.494	12.153	4.616	2.550	1.272	7.179	5.863	0.852	40.176	0.369	0.973	6.961
18-2-14	1007.224	0.086	27.541	6.751	2.032	1.003	0.693	2.953	4.129	0.355	12.611	0.162	0.377	2.115
18-2-15	1421.225	0.187	42.079	10.888	2.424	1.445	0.864	3.449	3.057	0.471	20.932	0.218	1.069	3.671
18-2-16	1325.880	0.101	36.068	10.392	1.904	1.038	0.690	2.903	3.637	0.350	17.308	0.144	0.631	1.180
18-2-17	1175.369	0.120	31.579	7.316	1.786	0.959	0.667	2.693	2.534	0.327	15.285	0.146	0.751	1.563
18-2-18	1261.529	0.155	41.927	13.008	2.943	1.669	0.957	4.182	3.663	0.558	20.666	0.263	0.886	1.938
18-2-19	1701.426	0.151	37.253	24.567	2.362	1.458	0.799	3.217	4.071	0.441	18.162	0.258	0.688	2.787
18-2-20	1609.781	0.109	35.501	12.421	2.054	1.181	0.816	3.219	3.188	0.365	17.567	0.179	0.311	1.453
18-2-21	1313.054	0.121	37.416	7.547	1.820	0.951	0.754	2.937	2.980	0.330	18.773	0.137	0.671	1.367

Sample #	Ba (ppm)	Cd (ppm)	Ce (ppm)	Cs (ppm)	Dy (ppm)	Er (ppm)	Eu (ppm)	Gd (ppm)	Hf (ppm)	Ho (ppm)	La (ppm)	Lu (ppm)	Mo (ppm)	Nb (ppm)
18-2-22	732.787	0.087	32.909	3.070	1.533	0.831	0.685	2.857	2.366	0.273	16.144	0.142	4.601	0.716
18-2-23	219.018	0.226	24.243	1.617	1.579	0.938	0.546	2.436	4.257	0.310	11.065	0.151	1.277	1.594
18-2-24	289.884	0.148	9.708	6.075	0.774	0.440	0.235	1.069	1.069	0.146	5.512	0.053	0.020	1.270
18-2-25	1613.093	0.332	83.007	9.549	4.714	2.646	1.347	7.472	6.189	0.868	40.781	0.411	0.890	6.888
18-2-26	1334.859	0.570	82.843	6.832	4.969	2.840	1.319	6.905	4.264	0.952	41.899	0.429	1.336	8.490
BHVO-2	14.639	b.d.	1.486	0.010	0.129	0.129	0.063	0.174	1.186	0.035	1.483	0.024	0.271	0.038
8-44A	53.456	0.197	0.548	0.016	0.106	0.105	0.024	0.104	1.032	0.033	0.650	0.022	0.237	0.035
SR-16B	1623.047	2.682	51.948	9.659	3.418	2.091	1.054	4.632	4.600	0.684	25.080	0.298	1.212	9.059
H91	1623.047	2.682	51.948	9.659	3.418	2.091	1.054	4.632	4.600	0.684	25.080	0.298	1.212	9.059
17-6	541.193	0.042	34.115	1.506	2.365	1.282	0.847	3.342	2.632	0.444	17.576	0.158	0.486	0.455
E150-4	189.207	0.043	44.881	2.557	2.175	1.291	0.679	3.410	3.590	0.417	21.833	0.190	0.504	0.978
E152-7	1523.921	0.227	41.683	6.723	2.163	1.394	0.750	3.205	3.882	0.435	20.073	0.224	2.942	5.498
E152-2	1485.194	0.351	50.395	7.251	4.203	2.567	1.060	5.036	4.910	0.845	23.541	0.377	0.944	7.628
E152-9	748.219	0.129	88.393	9.289	4.549	2.579	1.389	8.322	5.708	0.789	42.736	0.391	0.584	3.910
E150-9	41368.112	0.018	17.946	0.887	1.130	0.553	7.613	1.947	1.925	0.204	9.143	0.070	1.702	0.677
E150-5	505.816	0.072	49.344	3.883	2.781	1.661	0.847	4.133	4.245	0.544	23.659	0.236	0.433	1.844
144-3	132.280	0.084	16.043	1.439	1.012	0.555	0.323	1.665	2.177	0.203	9.862	0.084	0.210	0.549
E154-2	320.727	0.104	27.347	3.174	1.912	1.103	0.410	2.537	4.093	0.377	13.303	0.151	0.350	0.792
E150-7	1925.406	0.016	44.171	1.115	1.991	1.005	0.817	3.340	1.405	0.365	20.702	0.121	0.104	0.679
E150-2	252.839	0.016	34.021	1.585	2.300	1.347	0.678	3.101	2.320	0.441	16.069	0.188	0.237	0.591
17-8	351.357	0.032	16.783	1.857	0.888	0.481	0.276	1.395	1.432	0.160	8.209	0.066	0.495	0.784
E152-10	1223.193	0.240	109.453	13.357	5.248	3.159	1.706	9.720	7.666	0.983	53.417	0.492	1.080	4.110
E150-6	834.185	0.082	46.656	2.883	2.469	1.292	0.798	4.002	3.035	0.449	21.633	0.175	0.317	1.852
E152-5	1624.334	0.371	97.836	9.912	5.568	3.284	1.574	8.234	6.122	1.078	48.228	0.484	0.922	7.593
E152-1	2999.313	0.342	53.480	28.557	3.528	2.338	1.381	4.753	6.224	0.723	24.874	0.380	1.831	8.699
E152-3	2017.081	0.470	116.580	12.742	5.905	3.371	1.728	9.307	7.356	1.109	55.841	0.503	0.988	9.981
E150-10	1139.953	0.113	37.268	7.680	2.631	1.650	0.712	3.537	5.032	0.525	17.583	0.254	0.466	2.256
144-6	287.351	0.092	23.707	2.165	1.189	0.652	0.382	1.924	2.035	0.211	11.587	0.089	0.213	0.829
144-4	366.260	0.104	10.499	1.704	0.987	0.490	0.317	1.316	0.623	0.171	4.990	0.078	0.156	0.793
E150-3	628.353	0.185	36.718	2.416	2.528	1.478	0.823	3.615	5.143	0.477	17.210	0.221	0.199	4.287

Sample #	Ba (ppm)	Cd (ppm)	Ce (ppm)	Cs (ppm)	Dy (ppm)	Er (ppm)	Eu (ppm)	Gd (ppm)	Hf (ppm)	Ho (ppm)	La (ppm)	Lu (ppm)	Mo (ppm)	Nb (ppm)
E152-6	2387.782	0.289	135.524	13.863	6.610	3.691	1.983	11.077	7.360	1.246	67.225	0.564	1.015	8.982
144-5	1413.372	0.599	46.641	11.610	2.610	1.454	1.077	4.340	4.389	0.490	23.815	0.214	0.679	2.049
E154-1	1159.254	9.440	52.975	1.672	3.451	2.116	0.903	4.985	6.121	0.671	25.003	0.303	0.112	6.873
E152-4	1780.180	0.498	73.160	10.466	6.036	3.554	1.317	7.694	7.699	1.217	34.866	0.503	0.842	7.526
144-7	344.790	0.090	22.791	1.776	1.558	1.008	0.400	2.371	3.721	0.324	11.714	0.140	0.429	0.460
E152-8	1981.290	0.162	22.079	3.023	1.945	0.983	1.242	3.093	2.000	0.344	10.175	0.160	0.979	1.223
17-7	822.297	0.119	47.304	2.455	3.620	1.921	1.266	5.183	3.718	0.662	24.768	0.265	0.405	0.625
E154-3	281.466	0.083	19.169	0.862	1.362	0.770	0.401	2.115	3.877	0.249	9.103	0.114	0.436	1.058
144-1	385.812	0.118	19.217	2.123	1.653	0.953	0.487	2.260	2.149	0.310	11.518	0.133	0.333	1.564
144-2	544.928	0.130	36.760	2.212	2.742	1.462	0.801	3.798	4.432	0.499	18.222	0.225	1.283	0.953
E150-8	2519.659	0.122	51.224	9.185	3.353	2.045	1.015	4.581	4.670	0.666	24.846	0.280	0.243	1.772
17-9	490.330	b.d.	34.216	1.508	1.462	0.802	0.510	2.693	1.675	0.271	17.892	0.112	0.136	0.823
17-22	380.082	0.039	29.654	5.456	2.119	1.310	0.498	3.182	4.032	0.432	13.930	0.200	0.397	1.799
E150-1	466.510	0.850	40.448	7.508	3.140	1.908	0.844	4.211	4.623	0.627	19.830	0.269	0.303	3.093

Sample #	Nd (ppm)	Pb (ppm)	Pr (ppm)	Rb (ppm)	Sb (ppm)	Sm (ppm)	Sn (ppm)	Ta (ppm)	Tb (ppm)	Th (ppm)	Tm (ppm)	U (ppm)	W (ppm)	Y (ppm)	Yb (ppm)
BHVO-2	23.617	1.404	5.130	9.430	0.312	5.736	2.056	50.248	0.964	1.240	0.310	0.429	0.089	22.437	1.895
8-44A	0.613	b.d.	0.153	0.080	0.099	0.082	0.484	0.679	0.016	b.d.	0.017	0.057	6.213	3.810	0.128
SR-16B	10.884	1.217	2.960	19.450	0.285	1.906	0.998	2.577	0.278	2.440	0.132	0.880	3.869	7.898	0.887
96	10.884	1.217	2.960	19.450	0.285	1.906	0.998	2.577	0.278	2.440	0.132	0.880	3.869	7.898	0.887
16	15.014	1.460	4.066	22.216	0.778	2.641	1.562	15.247	0.363	5.003	0.155	1.974	5.014	9.513	1.039
106	10.521	4.334	2.837	10.324	0.191	2.055	0.477	6.193	0.334	2.037	0.120	0.858	3.240	10.686	0.783
108	11.158	1.304	3.021	34.300	0.892	2.036	1.013	11.596	0.282	2.535	0.097	0.966	4.118	6.860	0.629

Sample #	Nd (ppm)	Pb (ppm)	Pr (ppm)	Rb (ppm)	Sb (ppm)	Sm (ppm)	Sn (ppm)	Ta (ppm)	Tb (ppm)	Th (ppm)	Tm (ppm)	U (ppm)	W (ppm)	Y (ppm)	Yb (ppm)
H111	10.131	1.829	2.748	25.534	0.631	1.809	1.858	9.018	0.257	3.026	0.107	1.178	6.147	7.300	0.682
H83	11.546	8.043	2.966	72.522	1.319	2.299	1.294	5.472	0.375	4.169	0.155	1.436	10.111	11.721	1.003
46	2.902	b.d.	0.733	19.858	0.520	0.652	1.062	1.751	0.173	0.957	0.127	0.421	3.320	8.772	0.761
H84	15.787	3.116	4.314	31.760	1.285	2.711	1.803	7.930	0.375	6.130	0.148	1.916	5.397	10.074	0.971
14	10.604	1.800	2.847	5.329	0.393	1.893	1.601	9.071	0.241	2.851	0.087	1.286	5.289	5.656	0.611
H85	14.903	5.427	4.091	13.077	0.614	2.690	0.445	4.566	0.389	6.265	0.174	2.129	3.483	11.527	1.175
98	10.998	2.021	2.958	31.616	0.506	1.895	1.820	16.442	0.257	3.692	0.105	1.669	8.714	6.389	0.714
H92	24.881	5.796	6.706	147.161	1.344	4.376	2.396	35.733	0.617	14.725	0.324	4.160	8.163	17.431	2.279
110	8.722	2.054	2.308	22.659	0.587	1.856	0.845	13.356	0.327	3.717	0.116	1.251	17.247	8.320	0.780
54	3.363	b.d.	0.757	42.266	0.416	1.046	0.814	2.965	0.271	3.065	0.099	0.816	5.648	7.406	0.652
H112	16.674	6.606	4.495	80.440	1.378	3.184	1.710	18.796	0.453	9.245	0.172	2.776	6.926	10.929	1.168
91	6.397	6.820	1.716	20.466	1.204	1.330	1.201	2.586	0.235	1.828	0.090	0.654	1.921	6.693	0.569
H81	8.773	4.570	2.350	54.168	0.718	1.707	1.375	10.460	0.248	4.603	0.088	1.649	13.477	6.170	0.621
H113	13.480	9.597	3.480	29.958	1.247	2.883	1.469	8.183	0.500	3.732	0.162	2.473	6.440	12.807	1.036
55	16.300	1.302	3.884	27.806	0.270	3.550	0.583	1.452	0.510	0.951	0.091	1.091	1.791	8.516	0.569
100	6.367	10.329	1.718	29.926	0.727	1.210	0.354	2.180	0.180	1.413	0.074	0.642	1.362	5.653	0.446
H89	16.631	32.791	4.571	92.716	0.751	3.258	2.423	25.121	0.565	10.404	0.243	3.514	19.845	16.620	1.564
80	2.187	0.430	0.590	35.804	0.253	0.440	0.464	3.115	0.063	1.756	0.025	1.101	2.551	1.951	0.178
50	1.850	b.d.	0.461	11.435	0.051	0.389	0.384	0.384	0.109	0.670	0.059	0.277	6.022	4.615	0.337
104	5.162	b.d.	1.439	8.094	0.227	0.906	0.088	1.871	0.159	0.596	0.055	0.573	1.389	4.537	0.354
H82	28.289	4.405	8.005	141.033	0.910	4.662	2.060	10.692	0.566	8.419	0.187	2.133	22.249	11.929	1.274
107	3.129	b.d.	0.841	25.165	0.352	0.595	0.484	4.297	0.093	1.428	0.041	0.892	1.209	2.907	0.272
109	7.317	2.969	2.007	50.464	2.038	1.285	0.724	6.454	0.177	2.881	0.068	1.015	3.058	5.304	0.462
103	12.524	1.124	3.424	31.344	0.351	2.185	0.506	6.359	0.293	2.762	0.092	1.045	3.707	7.723	0.598
BHVO-2	23.543	3.467	5.077	18.071	0.465	5.681	1.794	1.254	0.934	1.153	0.307	0.430	0.466	20.277	1.857
8-44A	0.653	0.249	0.170	0.340	0.306	0.105	0.412	0.095	0.020	0.023	0.015	0.049	4.164	2.989	0.118
SR-16B	0.237	0.931	0.052	0.283	0.521	0.040	0.895	0.047	0.012	0.068	0.013	0.052	9.357	1.984	0.092

Sample #	Nd (ppm)	Pb (ppm)	Pr (ppm)	Rb (ppm)	Sb (ppm)	Sm (ppm)	Sn (ppm)	Ta (ppm)	Tb (ppm)	Th (ppm)	Tm (ppm)	U (ppm)	W (ppm)	Y (ppm)	Yb (ppm)
18-0-1	38.715	14.491	10.457	295.981	2.372	6.910	3.344	0.688	0.782	12.763	0.278	4.445	5.515	11.782	1.866
18-0-2	11.523	3.490	3.168	63.912	0.357	1.967	0.812	0.220	0.273	1.805	0.086	0.790	4.394	4.405	0.528
18-0-3	7.477	8.129	1.929	24.068	0.591	1.571	0.391	0.087	0.243	1.688	0.078	0.950	6.050	3.606	0.477
18-0-4	13.985	8.700	3.625	97.378	0.981	2.425	1.267	0.613	0.367	7.026	0.156	3.757	5.882	5.185	1.045
18-2-1	13.091	201.132	3.395	135.483	1.163	2.797	1.183	0.614	0.632	7.747	0.361	2.600	7.689	19.842	2.379
18-2-2	34.389	140.876	9.375	187.490	1.722	6.037	1.724	0.750	0.859	9.821	0.366	3.804	5.219	22.213	2.521
18-2-3	11.983	16.225	3.035	93.710	1.161	2.241	1.090	0.324	0.354	7.146	0.176	3.759	8.352	5.329	1.144
18-2-4	27.479	457.204	7.534	250.422	1.756	4.777	2.189	0.354	0.605	10.195	0.264	3.135	2.397	14.007	1.826
18-2-5	20.132	15.205	5.140	142.358	0.790	3.711	1.332	0.441	0.622	6.556	0.250	2.612	2.754	7.899	1.676
18-2-6	8.640	11.386	2.338	110.377	0.713	1.525	0.894	0.311	0.247	6.925	0.117	3.102	2.502	5.106	0.793
18-2-7	2.450	36.141	0.589	107.411	0.418	0.546	0.557	0.262	0.125	2.110	0.051	2.083	0.675	2.545	0.311
18-2-8	22.666	37.310	6.217	289.084	2.037	4.082	2.441	0.610	0.559	12.174	0.245	4.430	9.407	14.826	1.572
18-2-9	18.995	27.519	5.139	205.960	2.274	3.700	2.103	0.643	0.637	10.795	0.332	4.104	6.066	16.859	2.230
18-2-10	41.812	24.877	11.234	265.148	3.506	7.160	3.353	0.460	0.933	17.329	0.435	5.509	7.048	13.193	2.911
18-2-11	13.716	24.995	3.667	138.688	1.259	2.609	1.368	0.230	0.395	5.921	0.177	2.521	5.880	10.140	1.196
18-2-12	33.341	38.355	9.030	224.673	2.279	5.979	2.609	0.834	0.785	13.281	0.335	4.148	9.610	11.240	2.288
18-2-13	37.473	133.494	10.238	235.269	1.300	6.758	2.077	1.008	0.940	12.607	0.353	4.571	12.457	15.066	2.401
18-2-14	12.466	40.711	3.124	92.668	0.772	2.488	0.506	0.380	0.389	6.119	0.145	3.272	11.079	5.465	0.981
18-2-15	18.412	41.498	4.973	232.211	2.149	3.364	2.070	0.478	0.470	7.967	0.209	2.262	6.163	11.122	1.407
18-2-16	15.948	16.265	4.312	114.879	0.925	2.907	0.884	0.162	0.384	5.609	0.145	2.927	6.722	7.585	0.939
18-2-17	14.073	15.118	3.770	127.804	0.824	2.614	0.938	1.432	0.359	5.431	0.137	2.160	8.964	8.043	0.955
18-2-18	18.641	23.016	4.845	155.141	1.577	3.468	2.404	0.301	0.578	9.970	0.249	3.480	4.645	8.693	1.729
18-2-19	15.709	27.531	4.245	203.466	1.770	2.840	1.550	0.472	0.442	8.875	0.215	3.185	9.547	6.702	1.545
18-2-20	15.719	22.758	4.162	130.754	0.768	2.902	0.598	0.229	0.418	5.229	0.160	3.437	7.883	5.855	1.184
18-2-21	16.402	15.729	4.439	151.670	1.001	2.924	0.884	0.242	0.378	5.492	0.135	1.969	7.687	7.758	0.944
18-2-22	14.845	21.697	3.853	89.259	0.758	2.741	0.517	0.165	0.333	5.735	0.129	2.383	12.406	4.119	0.936
18-2-23	11.318	14.879	2.925	42.564	0.578	2.338	0.514	0.311	0.313	7.107	0.141	3.053	6.410	8.270	0.924

Sample #	Nd (ppm)	Pb (ppm)	Pr (ppm)	Rb (ppm)	Sb (ppm)	Sm (ppm)	Sn (ppm)	Ta (ppm)	Tb (ppm)	Th (ppm)	Tm (ppm)	U (ppm)	W (ppm)	Y (ppm)	Yb (ppm)
18-2-24	4.893	8.477	1.251	50.178	0.579	0.937	0.657	0.145	0.146	1.689	0.058	1.139	0.838	3.274	0.376
18-2-25	36.515	611.191	9.665	196.147	1.633	6.580	1.665	1.176	0.967	13.608	0.369	5.053	11.143	14.603	2.562
18-2-26	36.826	211.797	9.982	238.719	1.549	6.581	2.185	0.905	0.942	11.359	0.407	4.103	8.694	24.007	2.699
BHVO-2	24.239	2.845	5.251	19.020	0.578	5.811	1.878	1.263	0.998	1.406	0.331	0.493	0.440	21.994	2.058
8-44A	0.701	b.d.	0.173	0.428	0.350	0.109	0.354	0.087	0.022	0.051	0.016	0.065	4.520	3.045	0.129
SR-16B	0.353	1.088	0.089	0.467	0.379	0.057	0.837	0.038	0.017	0.078	0.017	0.059	2.338	2.409	0.102
H91	22.306	371.821	6.033	326.270	2.641	4.159	2.706	0.872	0.630	13.993	0.298	5.640	8.730	17.844	1.945
17-6	14.916	7.974	3.950	39.418	0.341	2.900	0.463	0.060	0.461	1.986	0.167	1.129	2.180	11.972	1.054
E150-4	18.914	6.945	5.263	25.548	1.315	3.246	0.652	0.093	0.438	5.168	0.184	1.767	2.427	10.056	1.269
E152-7	17.377	80.051	4.785	170.249	1.039	3.062	1.345	0.577	0.409	8.153	0.212	3.060	16.217	10.163	1.425
E152-2	22.577	211.934	6.022	207.442	1.710	4.333	2.227	0.834	0.727	11.397	0.373	3.717	10.625	19.552	2.449
E152-9	39.826	73.445	10.394	121.064	1.469	7.383	1.260	0.469	0.994	11.110	0.367	3.355	3.466	11.767	2.608
E150-9	8.127	12.273	2.094	15.866	0.501	1.706	0.389	0.129	0.253	1.895	0.070	1.012	5.065	3.339	0.468
E150-5	21.379	12.340	5.763	36.270	0.954	3.745	1.050	0.207	0.541	6.930	0.238	2.276	5.090	8.045	1.546
144-3	7.614	9.525	2.026	17.732	0.659	1.299	0.550	0.082	0.217	1.108	0.079	1.500	3.221	2.858	0.526
E154-2	12.017	13.152	3.172	28.453	1.301	2.142	0.493	0.142	0.356	1.878	0.151	0.834	3.131	5.151	1.007
E150-7	17.988	7.496	4.977	45.260	0.971	3.180	0.533	0.075	0.429	1.475	0.138	0.470	1.667	8.375	0.839
E150-2	14.750	3.919	4.032	22.400	0.790	2.804	0.658	0.078	0.437	1.976	0.181	0.624	1.410	8.967	1.180
17-8	7.560	10.925	2.012	39.780	0.554	1.353	0.761	0.100	0.183	1.627	0.063	0.796	1.993	3.541	0.423
E152-10	47.570	677.294	12.790	206.846	2.275	8.603	2.711	0.441	1.187	15.988	0.448	4.630	8.451	14.737	3.118
E150-6	19.527	6.524	5.394	65.176	1.152	3.391	0.916	0.256	0.515	2.742	0.177	1.001	3.640	6.204	1.172
E152-5	42.426	200.374	11.484	193.765	1.842	7.396	2.303	0.933	1.103	12.053	0.452	4.142	12.373	18.923	3.028
E152-1	23.263	8.876	6.260	427.023	1.871	4.347	4.568	0.728	0.652	15.635	0.361	5.653	6.291	14.196	2.464
E152-3	50.106	352.145	13.691	242.387	1.604	8.704	2.743	1.274	1.196	15.653	0.474	5.273	10.704	18.700	3.212
E150-10	16.205	8.121	4.364	120.946	1.419	2.939	1.431	0.321	0.491	7.208	0.237	2.843	5.245	7.185	1.583
144-6	10.263	5.548	2.768	39.053	0.677	1.834	0.694	0.084	0.247	1.898	0.088	0.823	2.007	4.978	0.579
144-4	4.499	9.834	1.182	40.167	0.287	0.891	0.583	0.104	0.180	1.604	0.068	0.957	3.946	2.914	0.482

Sample #	Nd (ppm)	Pb (ppm)	Pr (ppm)	Rb (ppm)	Sb (ppm)	Sm (ppm)	Sn (ppm)	Ta (ppm)	Tb (ppm)	Th (ppm)	Tm (ppm)	U (ppm)	W (ppm)	Y (ppm)	Yb (ppm)
E150-3	15.250	13.281	4.119	48.403	0.737	2.945	1.371	0.462	0.469	8.822	0.211	3.157	4.090	8.350	1.436
E152-6	57.189	295.660	15.644	288.112	2.863	9.944	2.854	1.165	1.383	17.308	0.505	6.174	12.958	18.922	3.470
144-5	19.099	28.912	5.246	162.413	1.491	3.518	1.742	0.284	0.553	9.504	0.208	4.032	9.492	7.780	1.347
E154-1	22.888	875.520	6.208	89.075	3.381	4.089	2.074	0.824	0.655	11.473	0.281	3.665	2.086	10.444	2.009
E152-4	31.133	136.035	8.396	217.452	1.580	6.018	2.384	1.135	1.115	16.743	0.496	6.350	16.465	19.735	3.248
144-7	10.079	13.849	2.640	48.635	1.445	1.850	0.519	0.076	0.307	2.133	0.135	1.136	5.193	6.298	0.928
E152-8	10.827	12.560	2.684	75.246	0.678	2.416	0.504	0.206	0.420	5.045	0.142	1.917	10.150	5.214	1.060
17-7	20.453	25.969	5.358	42.620	1.289	3.897	0.713	0.174	0.725	3.832	0.263	1.937	5.532	11.438	1.715
E154-3	8.781	13.679	2.275	18.792	1.247	1.725	0.562	0.123	0.282	2.216	0.106	1.220	1.956	4.224	0.694
144-1	10.179	8.409	2.702	42.869	0.773	1.806	0.692	0.240	0.313	2.760	0.133	1.400	17.390	4.125	0.891
144-2	15.749	12.438	4.232	52.579	1.509	3.002	1.188	0.165	0.525	3.434	0.216	3.445	5.197	7.316	1.419
E150-8	21.995	8.611	5.904	154.704	1.594	3.977	1.835	0.247	0.628	8.213	0.279	2.910	3.125	10.339	1.890
17-9	13.342	34.411	3.784	37.290	2.588	2.074	0.509	0.132	0.330	2.075	0.103	1.076	4.877	4.139	0.695
17-22	13.578	11.111	3.492	53.268	0.924	2.572	0.674	0.247	0.422	4.909	0.193	2.359	3.482	5.920	1.293
E150-1	18.216	20.695	4.833	45.119	1.094	3.531	12.391	0.432	0.593	6.134	0.266	2.152	3.643	8.759	1.803

B.D. = Below Detection

APPENDIX 2F - PARTIAL MINORS

Sample #	Ba (ppm)	Cd (ppm)	Ce (ppm)	Cs (ppm)	Dy (ppm)	Er (ppm)	Eu (ppm)	Gd (ppm)	Hf (ppm)	Ho (ppm)	La (ppm)	Lu (ppm)	Mo (ppm)	Nb (ppm)
SR-16B	32.185	0.060	0.096	0.000	0.059	0.059	0.017	0.047	0.001	0.018	0.285	0.008	0.007	b.d.
8-44A	2.255	0.035	1.198	0.000	0.108	0.098	0.060	0.152	0.001	0.031	1.333	0.019	0.022	b.d.
SR-22A	7.395	0.020	0.030	0.000	0.021	0.028	0.005	0.018	0.000	0.006	0.138	0.003	b.d.	b.d.
RL2-51	2.575	0.029	0.259	0.002	0.022	0.015	0.014	0.027	b.d.	0.005	0.165	0.001	0.003	b.d.
RL2-51	b.d.	0.036	0.129	0.047	0.011	0.007	0.007	0.013	b.d.	0.002	0.086	0.000	0.003	b.d.
SR-22A	9.306	0.003	0.033	b.d.	0.021	0.029	0.006	0.021	b.d.	0.007	0.146	0.004	b.d.	b.d.
H81	24.518	0.096	6.028	0.113	2.041	1.146	0.416	1.849	b.d.	0.404	2.824	0.191	0.057	0.001
H82	78.391	0.096	15.147	0.038	4.418	2.027	1.016	4.086	b.d.	0.786	7.098	0.220	0.109	b.d.
H83	14.830	0.078	5.250	0.061	1.665	0.936	0.375	1.567	b.d.	0.329	2.366	0.110	0.007	0.003
E150-10	26.074	0.008	2.395	0.016	0.573	0.280	0.104	0.589	0.012	0.102	0.888	0.028	0.006	b.d.
E150-9	619.680	0.004	1.177	0.008	0.131	0.049	0.154	0.206	b.d.	0.022	0.573	0.004	0.004	b.d.
E150-8	146.507	0.017	2.457	0.021	0.612	0.320	0.125	0.646	0.008	0.119	1.117	0.034	b.d.	b.d.
E150-7	142.905	0.046	2.740	0.003	0.379	0.183	0.112	0.487	0.007	0.070	1.224	0.019	0.004	b.d.
E150-6	11.276	0.014	3.957	0.007	0.733	0.330	0.176	0.836	0.014	0.127	1.650	0.032	b.d.	b.d.
E150-5	5.221	0.036	0.840	0.050	0.277	0.129	0.065	0.282	0.001	0.047	0.349	0.015	b.d.	b.d.
E150-4	8.481	0.019	1.341	0.090	0.507	0.262	0.114	0.507	0.005	0.099	0.543	0.033	b.d.	b.d.
E150-3	8.590	0.016	1.405	0.020	0.289	0.118	0.085	0.323	0.006	0.047	0.588	0.012	b.d.	b.d.
E150-2	7.030	0.038	2.246	0.029	0.105	0.061	0.024	0.201	b.d.	0.020	1.097	0.014	b.d.	b.d.
H84	86.085	0.163	15.162	0.035	4.919	2.351	1.278	5.017	0.011	0.878	6.713	0.280	0.128	0.005
H85	17.640	0.105	2.674	0.150	1.576	1.024	0.240	1.287	0.007	0.337	1.193	0.158	0.006	b.d.
E150-1	40.778	0.027	1.251	0.082	0.519	0.310	0.103	0.487	0.011	0.102	0.525	0.039	0.001	b.d.
E152-10	4.822	0.005	0.462	0.067	0.191	0.110	0.025	0.151	0.003	0.039	0.220	0.023	b.d.	b.d.
E152-9	4.437	0.009	0.771	0.076	0.209	0.123	0.030	0.192	0.001	0.040	0.375	0.022	0.002	b.d.
H92	152.087	0.140	151.241	0.316	4.215	2.217	1.311	10.097	b.d.	0.688	71.673	0.576	0.074	0.004
H91	16.266	0.020	10.225	0.077	0.286	0.093	0.132	0.744	0.004	0.038	4.941	0.007	b.d.	b.d.
E152-8	36.470	0.000	1.646	0.034	0.136	0.068	0.075	0.255	0.002	0.024	0.752	0.017	0.001	b.d.

Sample #	Ba (ppm)	Cd (ppm)	Ce (ppm)	Cs (ppm)	Dy (ppm)	Er (ppm)	Eu (ppm)	Gd (ppm)	Hf (ppm)	Ho (ppm)	La (ppm)	Lu (ppm)	Mo (ppm)	Nb (ppm)
E152-7	3.921	b.d.	1.285	0.032	0.067	0.031	0.021	0.147	0.002	0.011	0.619	0.005	0.000	b.d.
E152-6	10.574	0.001	4.830	0.032	0.148	0.071	0.036	0.349	b.d.	0.025	2.371	0.014	0.000	b.d.
E152-5	12.810	b.d.	4.171	0.039	0.118	0.083	0.029	0.267	b.d.	0.022	2.062	0.029	b.d.	b.d.
E152-4	2.757	0.039	1.734	0.031	0.436	0.205	0.110	0.458	0.006	0.077	0.750	0.022	b.d.	b.d.
H89	101.299	0.156	17.128	0.208	1.025	1.189	0.161	1.444	b.d.	0.281	8.716	0.453	0.073	b.d.
E152-3	14.323	0.013	6.012	0.035	0.180	0.105	0.047	0.422	0.003	0.032	2.847	0.029	0.003	b.d.
E152-2	7.388	0.038	2.104	0.023	0.095	0.058	0.023	0.175	0.002	0.018	0.988	0.018	0.003	b.d.
E152-1	8.507	0.112	3.706	0.024	0.118	0.055	0.030	0.261	0.001	0.020	1.821	0.006	0.002	0.001
H113	16.743	0.106	12.896	0.022	2.814	1.345	0.794	3.205	0.034	0.487	5.371	0.162	0.035	0.002
H112	37.895	0.169	9.743	0.094	3.031	1.586	0.573	3.010	0.180	0.569	4.461	0.277	0.062	0.002
E154-3	1.763	0.016	1.410	0.025	0.166	0.084	0.043	0.213	b.d.	0.032	0.632	0.011	b.d.	b.d.
E154-2	5.074	0.017	7.256	0.021	0.313	0.190	0.063	0.490	0.006	0.064	3.460	0.027	0.001	0.025
H111	10.729	0.018	0.602	0.005	0.088	0.063	0.016	0.099	b.d.	0.020	0.356	0.005	0.007	b.d.
E154-1	5.749	0.188	1.555	0.025	0.046	0.025	0.015	0.105	0.001	0.007	0.706	0.005	b.d.	b.d.
144-7	2.113	0.019	1.602	0.004	0.157	0.077	0.045	0.223	0.004	0.030	0.671	0.007	b.d.	b.d.
144-6	7.291	0.012	3.208	0.005	0.296	0.135	0.098	0.473	0.003	0.050	1.357	0.016	b.d.	b.d.
144-5	10.427	0.286	0.776	0.048	0.187	0.093	0.036	0.180	0.004	0.034	0.360	0.014	b.d.	b.d.
144-4	4.596	0.005	4.451	0.002	0.426	0.184	0.125	0.535	0.007	0.071	2.128	0.025	b.d.	b.d.
144-3	6.529	0.035	3.377	0.005	0.206	0.101	0.074	0.336	0.003	0.034	1.646	0.013	b.d.	b.d.
144-2	7.479	0.008	5.209	0.003	0.406	0.215	0.100	0.520	0.003	0.074	2.571	0.028	b.d.	b.d.
144-1	1.644	0.033	4.772	0.004	0.270	0.146	0.076	0.364	0.001	0.054	2.412	0.022	b.d.	b.d.
17-22	12.174	0.001	9.278	0.005	0.558	0.290	0.133	0.847	0.011	0.094	4.370	0.035	0.005	b.d.
17-9	3.041	0.028	2.835	0.005	0.160	0.076	0.058	0.288	0.004	0.027	1.390	0.008	b.d.	b.d.
17-8	6.528	0.014	2.095	0.004	0.145	0.058	0.045	0.231	b.d.	0.022	0.915	0.007	b.d.	b.d.
17-7	12.603	0.007	1.939	0.003	0.440	0.234	0.125	0.445	0.007	0.081	0.986	0.027	b.d.	b.d.
17-6	5.885	0.124	1.483	0.004	0.493	0.273	0.114	0.448	0.010	0.097	0.724	0.033	b.d.	b.d.
110	70.920	0.096	12.752	0.037	4.124	1.932	1.092	4.301	0.013	0.681	5.619	0.234	0.106	0.003

Sample #	Ba (ppm)	Cd (ppm)	Ce (ppm)	Cs (ppm)	Dy (ppm)	Er (ppm)	Eu (ppm)	Gd (ppm)	Hf (ppm)	Ho (ppm)	La (ppm)	Lu (ppm)	Mo (ppm)	Nb (ppm)
109	18.682	0.043	8.614	0.031	1.036	0.572	0.313	1.422	0.023	0.200	4.358	0.078	0.008	b.d.
108	19.511	0.023	8.151	0.023	1.113	0.546	0.228	1.421	b.d.	0.186	3.896	0.067	0.018	0.001
107	10.658	0.021	6.830	0.008	0.823	0.469	0.164	0.852	b.d.	0.161	3.190	0.064	0.008	0.001
106	5.476	0.052	12.369	0.009	1.556	0.756	0.280	1.797	0.026	0.283	5.543	0.088	0.021	b.d.
104	4.571	0.031	6.889	0.002	1.052	0.529	0.171	1.005	0.011	0.200	3.258	0.060	0.014	b.d.
103	19.173	0.060	9.564	0.141	1.885	1.033	0.498	2.050	0.018	0.368	4.519	0.143	0.022	0.002
100	13.094	0.046	9.917	0.005	0.986	0.523	0.402	1.396	b.d.	0.188	5.269	0.080	0.082	b.d.
98	9.299	0.030	0.699	0.029	0.055	0.035	0.013	0.095	0.013	0.012	0.372	0.003	0.276	0.012
96	16.621	0.029	6.638	0.006	0.844	0.519	0.141	0.987	b.d.	0.171	3.041	0.076	0.024	0.002
92	29.125	0.027	6.962	0.013	1.461	0.736	0.407	1.562	b.d.	0.276	3.041	0.086	0.077	0.001
91	25.644	0.069	11.524	0.051	1.785	0.878	0.543	2.133	0.010	0.313	5.487	0.094	0.013	0.001
80	27.888	0.056	8.014	0.009	0.742	0.394	0.200	1.047	0.001	0.133	3.693	0.053	0.003	b.d.
55	9.536	0.055	54.983	0.006	4.207	1.554	1.621	7.220	0.044	0.634	25.733	0.140	0.097	b.d.
54	21.781	0.047	3.968	0.013	1.794	0.839	0.491	1.792	b.d.	0.337	1.522	0.086	0.028	b.d.
50	8.111	0.080	9.294	0.008	1.254	0.643	0.234	1.302	b.d.	0.245	4.612	0.063	b.d.	0.003
46	9.169	0.016	9.473	0.014	1.513	0.933	0.208	1.356	b.d.	0.335	4.335	0.092	0.044	b.d.
17	4.936	0.020	4.298	0.005	0.275	0.262	0.050	0.381	b.d.	0.069	2.631	0.055	0.006	0.008
16	6.264	0.019	3.420	0.004	0.145	0.156	0.026	0.242	b.d.	0.037	2.044	0.052	0.016	0.008
14	9.774	0.041	6.330	0.009	0.375	0.416	0.065	0.534	0.067	0.094	3.116	0.103	0.062	0.007
8-44A	3.972	b.d.	1.732	0.025	0.103	0.074	0.073	0.187	b.d.	0.023	1.836	0.014	b.d.	0.005
SR-16B	58.364	b.d.	0.411	0.054	0.205	0.179	0.049	0.173	b.d.	0.050	0.592	0.025	b.d.	0.010
18-0-1	3178.655	b.d.	5.346	0.125	1.105	0.567	0.765	1.282	0.058	0.216	2.190	0.083	0.012	0.009
18-0-2	205.189	b.d.	6.585	0.127	1.523	0.712	0.321	1.614	0.001	0.282	2.924	0.083	0.015	0.001
18-0-3	3015.074	b.d.	5.981	0.028	0.822	0.330	0.752	1.155	b.d.	0.128	2.647	0.034	0.292	0.002
18-0-4	338.753	0.529	7.660	0.115	1.090	0.567	0.310	1.394	0.030	0.214	3.139	0.087	0.053	0.011
18-2-1	12.925	b.d.	3.047	0.180	0.388	0.462	0.056	0.403	b.d.	0.114	1.522	0.191	0.044	0.019
18-2-2	23.327	b.d.	10.633	0.401	0.350	0.336	0.066	0.676	b.d.	0.083	5.394	0.141	b.d.	0.009

Sample #	Ba (ppm)	Cd (ppm)	Ce (ppm)	Cs (ppm)	Dy (ppm)	Er (ppm)	Eu (ppm)	Gd (ppm)	Hf (ppm)	Ho (ppm)	La (ppm)	Lu (ppm)	Mo (ppm)	Nb (ppm)
18-2-3	25.989	b.d.	5.376	0.280	0.154	0.109	0.034	0.331	b.d.	0.026	2.562	0.042	0.030	0.007
18-2-4	25.656	b.d.	4.720	0.383	1.087	0.644	0.174	0.953	0.035	0.218	2.276	0.158	0.011	0.010
18-2-5	16.825	b.d.	6.031	0.358	2.152	1.125	0.389	2.063	0.030	0.410	2.608	0.159	0.032	0.016
18-2-6	42.771	b.d.	11.953	0.244	1.478	0.909	0.289	1.790	0.031	0.315	5.517	0.153	0.003	0.002
18-2-7	64.448	b.d.	7.529	0.908	1.704	0.794	0.495	1.857	0.021	0.329	3.691	0.086	b.d.	0.012
18-2-8	27.216	b.d.	2.611	0.257	0.500	0.219	0.092	0.532	0.009	0.091	1.198	0.030	0.027	0.008
18-2-9	25.139	b.d.	2.843	0.418	0.850	0.527	0.151	0.788	b.d.	0.176	1.450	0.121	0.130	0.004
18-2-10	35.752	0.326	1.945	0.181	0.311	0.182	0.059	0.320	b.d.	0.061	0.907	0.048	0.066	b.d.
18-2-11	17.074	b.d.	2.852	0.393	1.246	0.697	0.218	1.075	0.007	0.243	1.302	0.135	0.039	0.002
18-2-12	16.627	b.d.	2.435	0.292	0.666	0.389	0.106	0.543	0.024	0.130	1.152	0.077	0.019	0.002
18-2-13	25.575	0.636	3.991	0.176	0.510	0.268	0.115	0.583	0.005	0.097	1.583	0.052	b.d.	0.038
18-2-14	20.119	b.d.	2.835	0.779	1.132	0.562	0.231	1.072	0.004	0.205	1.211	0.091	0.005	0.001
18-2-15	24.339	b.d.	3.266	0.153	1.055	0.625	0.179	0.916	0.003	0.213	1.566	0.130	b.d.	b.d.
18-2-16	16.058	b.d.	3.352	0.910	0.831	0.458	0.167	0.793	0.003	0.166	1.486	0.071	0.021	0.003
18-2-17	11.219	b.d.	1.876	0.345	0.774	0.423	0.152	0.677	b.d.	0.145	0.817	0.070	b.d.	0.003
18-2-18	48.919	b.d.	7.171	0.682	1.184	0.605	0.234	1.201	0.003	0.211	3.480	0.085	0.093	b.d.
18-2-19	19.489	b.d.	2.522	0.590	0.679	0.415	0.116	0.557	b.d.	0.139	1.100	0.097	b.d.	0.005
18-2-20	15.776	b.d.	2.174	0.377	0.755	0.451	0.147	0.688	b.d.	0.162	0.956	0.076	b.d.	b.d.
18-2-21	19.823	b.d.	2.176	0.251	0.715	0.383	0.149	0.662	b.d.	0.135	0.985	0.059	b.d.	0.080
18-2-22	5.772	b.d.	1.594	0.077	0.584	0.335	0.132	0.558	b.d.	0.118	0.672	0.063	0.164	b.d.
18-2-23	4.092	b.d.	0.621	0.311	0.052	0.011	0.022	0.095	b.d.	0.006	0.279	b.d.	0.006	b.d.
18-2-24	16.047	b.d.	5.252	0.315	1.029	0.552	0.236	1.283	0.021	0.200	2.566	0.077	b.d.	0.005
18-2-25	16.729	b.d.	3.684	0.171	0.130	0.114	0.027	0.259	0.082	0.029	1.813	0.048	0.008	0.012
18-2-26	18.995	b.d.	7.334	0.171	0.287	0.342	0.052	0.521	0.010	0.080	3.598	0.147	b.d.	0.017

Sample #	Nd (ppm)	Pb (ppm)	Pr (ppm)	Rb (ppm)	Sb (ppm)	Sm (ppm)	Sn (ppm)	Ta (ppm)	Tb (ppm)	Th (ppm)	Tm (ppm)	U (ppm)	W (ppm)	Y (ppm)	Yb (ppm)
SR-16B	0.124	b.d.	0.021	0.062	0.001	0.018	0.156	b.d.	0.007	0.026	0.008	0.007	0.146	2.213	0.049
8-44A	0.595	0.149	0.142	0.045	0.006	0.088	0.134	b.d.	0.019	b.d.	0.013	0.014	0.222	4.302	0.090
SR-22A	0.045	b.d.	0.010	0.004	b.d.	0.006	0.003	b.d.	0.003	0.003	0.003	b.d.	b.d.	0.820	0.022
RL2-51	0.109	0.163	0.028	0.005	b.d.	0.017	0.008	0.125	0.004	0.006	0.002	b.d.	4.768	0.342	0.011
RL2-51	0.053	b.d.	0.015	0.031	b.d.	0.008	0.006	1.048	0.002	0.002	0.001	b.d.	12.097	0.167	0.006
SR-22A	0.047	b.d.	0.010	0.001	b.d.	0.008	0.019	b.d.	0.002	0.001	0.003	b.d.	b.d.	0.762	0.019
H81	3.564	9.479	0.785	10.085	0.163	1.132	0.135	0.001	0.327	0.317	0.173	0.529	0.301	15.735	1.192
H82	8.622	11.484	1.987	11.742	0.155	2.764	0.149	b.d.	0.744	0.766	0.253	0.278	b.d.	29.197	1.556
H83	3.614	5.455	0.772	6.333	0.072	1.225	0.004	0.000	0.261	0.139	0.129	0.098	0.072	13.374	0.790
E150-10	1.459	0.857	0.337	0.536	0.035	0.455	0.020	0.143	0.104	0.164	0.035	0.034	b.d.	2.121	0.209
E150-9	0.685	0.686	0.154	0.216	b.d.	0.180	b.d.	b.d.	0.024	0.011	0.006	0.003	b.d.	0.630	0.030
E150-8	1.459	1.131	0.326	0.915	0.057	0.439	b.d.	b.d.	0.105	0.136	0.041	0.026	b.d.	3.056	0.249
E150-7	1.490	0.748	0.353	0.098	0.007	0.382	0.015	0.114	0.075	0.039	0.024	0.013	b.d.	1.456	0.137
E150-6	2.286	4.495	0.532	0.350	0.003	0.663	0.013	0.091	0.132	0.110	0.039	0.019	b.d.	2.373	0.244
E150-5	0.548	0.694	0.115	0.729	0.009	0.214	b.d.	b.d.	0.048	0.103	0.015	0.015	b.d.	1.176	0.103
E150-4	0.950	1.614	0.199	0.910	0.017	0.358	b.d.	b.d.	0.084	0.105	0.037	0.028	b.d.	2.330	0.228
E150-3	0.795	0.867	0.182	0.326	0.009	0.254	0.010	0.052	0.048	0.103	0.014	0.020	b.d.	1.181	0.079
E150-2	1.077	6.593	0.271	1.429	0.014	0.176	b.d.	b.d.	0.022	0.103	0.009	0.167	b.d.	0.539	0.067
H84	9.970	10.970	2.163	5.166	0.143	3.480	0.231	0.002	0.864	0.704	0.310	0.367	0.513	34.489	1.853
H85	1.814	11.007	0.394	2.807	0.039	0.739	0.030	0.002	0.252	0.205	0.148	0.083	0.005	9.035	0.994
E150-1	0.857	2.290	0.181	2.592	0.033	0.327	0.018	0.115	0.088	0.109	0.044	0.039	b.d.	2.482	0.259
E152-10	0.273	30.925	0.063	1.939	0.042	0.086	0.008	0.048	0.030	0.071	0.018	0.036	b.d.	0.865	0.124
E152-9	0.404	4.798	0.098	2.186	0.043	0.112	0.006	0.240	0.038	0.012	0.018	0.033	8.490	0.971	0.131
H92	64.734	14.782	17.620	48.541	0.290	10.306	0.090	0.000	1.018	7.965	0.326	1.034	0.013	17.135	2.615
H91	4.548	11.404	1.204	3.307	0.005	0.750	0.013	0.031	0.076	0.058	0.009	0.187	b.d.	0.825	0.059
E152-8	0.930	0.840	0.216	1.208	0.031	0.221	0.012	0.029	0.031	0.109	0.011	0.112	b.d.	0.601	0.089

Sample #	Nd (ppm)	Pb (ppm)	Pr (ppm)	Rb (ppm)	Sb (ppm)	Sm (ppm)	Sn (ppm)	Ta (ppm)	Tb (ppm)	Th (ppm)	Tm (ppm)	U (ppm)	W (ppm)	Y (ppm)	Yb (ppm)
E152-7	0.606	3.249	0.158	1.031	0.006	0.117	0.013	0.037	0.016	0.010	0.004	0.052	b.d.	0.284	0.025
E152-6	2.160	7.185	0.569	2.223	0.019	0.317	0.002	b.d.	0.037	0.126	0.008	0.124	b.d.	0.660	0.065
E152-5	1.902	15.579	0.493	2.328	0.021	0.262	0.002	b.d.	0.031	0.271	0.014	0.141	b.d.	0.663	0.117
E152-4	1.074	0.683	0.240	0.367	0.008	0.349	0.008	0.080	0.077	0.046	0.025	0.008	b.d.	2.018	0.157
H89	7.781	21.797	2.016	56.466	0.781	1.057	b.d.	b.d.	0.177	0.409	0.208	1.161	b.d.	12.867	1.794
E152-3	2.838	20.567	0.726	2.240	0.031	0.402	0.018	0.075	0.044	0.288	0.015	0.187	b.d.	0.789	0.117
E152-2	1.014	10.013	0.253	1.307	0.015	0.175	0.010	0.105	0.020	0.179	0.009	0.088	b.d.	0.481	0.071
E152-1	1.608	13.266	0.431	1.444	0.013	0.236	0.015	0.593	0.028	0.115	0.006	0.136	b.d.	0.491	0.036
H113	8.067	17.389	1.779	1.527	0.127	2.445	0.141	0.003	0.514	0.276	0.172	0.331	0.223	14.249	1.129
H112	5.724	22.097	1.286	8.964	0.276	1.908	0.069	0.010	0.521	1.485	0.236	0.487	0.046	15.671	1.620
E154-3	0.772	0.504	0.184	0.121	0.000	0.192	b.d.	b.d.	0.032	0.044	0.011	0.002	b.d.	0.739	0.070
E154-2	3.132	0.683	0.846	0.480	0.011	0.517	0.013	0.297	0.057	0.187	0.027	0.010	b.d.	1.457	0.171
H111	0.293	b.d.	0.073	1.102	0.016	0.052	0.034	b.d.	0.014	b.d.	0.011	0.028	0.179	1.022	0.055
E154-1	0.716	39.509	0.186	0.140	0.041	0.105	0.008	0.072	0.013	0.072	0.003	0.042	b.d.	0.202	0.029
144-7	0.934	0.359	0.221	0.073	0.003	0.205	0.004	0.036	0.033	0.050	0.010	0.015	b.d.	0.690	0.060
144-6	1.948	1.765	0.436	0.171	0.021	0.450	0.007	b.d.	0.064	0.059	0.016	0.015	b.d.	1.218	0.112
144-5	0.421	0.827	0.099	0.977	0.009	0.112	0.007	0.067	0.031	0.048	0.012	0.114	b.d.	0.706	0.090
144-4	2.046	1.020	0.526	0.090	0.005	0.408	0.009	0.078	0.078	0.149	0.026	0.017	b.d.	1.744	0.168
144-3	1.603	6.655	0.410	0.135	0.020	0.311	0.013	0.078	0.041	0.040	0.014	0.045	b.d.	0.894	0.085
144-2	2.269	1.535	0.605	0.235	0.002	0.403	0.006	b.d.	0.072	0.120	0.029	0.092	b.d.	1.852	0.185
144-1	1.936	1.118	0.534	0.210	0.003	0.308	0.001	b.d.	0.050	0.158	0.022	0.001	b.d.	1.283	0.131
17-22	4.287	1.803	1.116	0.273	0.022	0.804	0.020	0.087	0.112	0.152	0.041	0.072	b.d.	2.207	0.249
17-9	1.351	0.428	0.343	0.081	0.000	0.267	0.009	0.018	0.035	0.052	0.009	0.016	b.d.	0.689	0.061
17-8	1.068	0.494	0.264	0.157	0.002	0.226	0.003	b.d.	0.032	0.078	0.008	0.021	b.d.	0.560	0.047
17-7	1.073	1.963	0.253	0.104	0.025	0.306	0.013	0.069	0.081	0.030	0.032	0.029	b.d.	2.050	0.196
17-6	0.893	1.429	0.195	0.082	0.009	0.303	0.011	0.098	0.079	0.020	0.037	0.025	b.d.	2.133	0.214
110	8.304	9.173	1.826	4.274	0.104	2.805	0.155	0.006	0.722	0.633	0.250	0.266	0.461	29.607	1.593

Sample #	Nd (ppm)	Pb (ppm)	Pr (ppm)	Rb (ppm)	Sb (ppm)	Sm (ppm)	Sn (ppm)	Ta (ppm)	Tb (ppm)	Th (ppm)	Tm (ppm)	U (ppm)	W (ppm)	Y (ppm)	Yb (ppm)
109	4.054	4.803	1.023	2.437	0.010	0.959	0.012	b.d.	0.197	0.386	0.082	0.050	0.023	5.913	0.531
108	4.443	0.763	1.069	1.521	0.013	1.233	0.055	b.d.	0.203	0.260	0.069	0.067	b.d.	7.217	0.468
107	3.073	1.517	0.808	0.710	0.016	0.631	0.044	b.d.	0.138	0.409	0.068	0.065	0.010	6.573	0.416
106	5.779	4.555	1.485	0.336	0.005	1.292	0.041	0.004	0.276	0.241	0.101	0.047	0.094	8.323	0.591
104	2.986	2.365	0.809	0.172	0.004	0.634	0.085	0.002	0.171	0.228	0.071	0.047	0.105	5.499	0.416
103	5.260	3.064	1.250	16.188	0.024	1.546	0.078	0.002	0.331	0.251	0.135	0.145	0.165	15.018	0.858
100	4.817	24.048	1.198	1.075	0.085	1.075	0.036	b.d.	0.184	0.243	0.072	0.093	b.d.	6.275	0.473
98	0.339	1.522	0.084	9.597	0.048	0.071	0.049	b.d.	0.010	b.d.	0.003	0.072	b.d.	0.553	0.031
96	3.252	1.456	0.809	0.613	0.005	0.751	0.015	0.001	0.147	0.042	0.072	0.032	0.009	4.741	0.473
92	4.004	9.616	0.947	3.204	0.085	1.179	0.028	b.d.	0.238	0.523	0.098	0.190	0.026	10.771	0.557
91	6.035	15.431	1.432	2.588	0.307	1.701	0.142	0.000	0.319	0.302	0.110	0.136	b.d.	9.477	0.646
80	3.829	4.732	0.999	0.932	0.011	0.864	0.018	b.d.	0.139	0.227	0.055	0.058	0.024	5.385	0.344
55	28.905	5.180	7.018	0.639	0.006	6.572	0.060	0.005	0.928	0.521	0.181	0.131	0.064	17.560	1.103
54	2.811	1.777	0.563	2.393	0.027	1.087	0.030	b.d.	0.313	1.020	0.105	0.209	0.213	8.454	0.614
50	4.953	b.d.	1.232	1.870	0.002	1.086	0.097	b.d.	0.210	0.499	0.075	0.056	b.d.	9.160	0.423
46	4.579	b.d.	1.190	3.379	b.d.	1.109	0.029	b.d.	0.222	0.138	0.119	0.077	b.d.	12.675	0.704
17	1.812	0.368	0.473	0.193	0.015	0.291	0.047	b.d.	0.046	0.229	0.043	0.121	0.051	2.134	0.306
16	1.349	0.331	0.371	0.260	0.013	0.189	0.045	b.d.	0.027	0.126	0.032	0.066	0.141	1.564	0.289
14	2.573	0.307	0.698	0.168	0.016	0.428	0.160	0.004	0.068	0.271	0.078	0.236	0.241	3.139	0.576
8-44A	0.760	b.d.	0.199	0.474	0.010	0.125	b.d.	b.d.	0.020	b.d.	0.011	7.171	b.d.	3.566	0.075
SR-16B	0.373	2.298	0.084	0.355	0.012	0.108	b.d.	b.d.	0.032	0.057	0.027	1.732	b.d.	3.875	0.154
18-0-1	3.224	1.558	0.731	3.967	0.229	0.997	b.d.	0.003	0.204	0.405	0.076	10.633	b.d.	6.529	0.513
18-0-2	3.841	b.d.	0.862	3.093	0.015	1.193	b.d.	b.d.	0.274	0.158	0.087	2.522	b.d.	8.940	0.538
18-0-3	3.511	b.d.	0.797	0.910	0.132	0.991	b.d.	0.004	0.167	0.152	0.040	3.991	b.d.	4.660	0.206
18-0-4	4.498	3.874	1.029	2.773	0.283	1.127	b.d.	0.008	0.216	0.444	0.086	2.176	6.508	6.273	0.572
18-2-1	1.377	36.899	0.340	6.226	0.191	0.250	b.d.	b.d.	0.059	0.335	0.082	11.953	b.d.	4.380	0.749
18-2-2	4.533	28.870	1.205	12.697	0.125	0.620	b.d.	b.d.	0.071	0.950	0.057	1.594	b.d.	2.713	0.536

Sample #	Nd (ppm)	Pb (ppm)	Pr (ppm)	Rb (ppm)	Sb (ppm)	Sm (ppm)	Sn (ppm)	Ta (ppm)	Tb (ppm)	Th (ppm)	Tm (ppm)	U (ppm)	W (ppm)	Y (ppm)	Yb (ppm)
18-2-3	2.379	9.712	0.616	14.452	0.103	0.286	b.d.	0.011	0.037	0.471	0.016	1.945	b.d.	0.700	0.149
18-2-4	2.227	148.629	0.554	17.564	0.149	0.606	b.d.	0.014	0.172	0.235	0.097	2.852	b.d.	6.261	0.776
18-2-5	3.847	5.049	0.818	9.964	0.082	1.402	b.d.	0.003	0.372	0.290	0.162	7.529	0.802	11.938	1.053
18-2-6	5.711	6.414	1.398	4.882	0.096	1.309	b.d.	b.d.	0.275	0.444	0.128	6.031	1.287	9.727	0.900
18-2-7	3.979	17.814	0.915	14.295	0.098	1.110	b.d.	0.001	0.301	0.174	0.103	4.720	b.d.	10.712	0.628
18-2-8	1.317	4.394	0.318	10.223	0.102	0.359	b.d.	b.d.	0.087	0.422	0.029	2.174	b.d.	2.631	0.190
18-2-9	1.438	4.646	0.331	10.948	0.129	0.461	b.d.	b.d.	0.148	0.716	0.077	2.435	b.d.	5.244	0.618
18-2-10	0.955	9.850	0.230	8.543	0.068	0.251	b.d.	b.d.	0.057	0.469	0.027	0.621	b.d.	1.472	0.218
18-2-11	1.773	7.879	0.372	8.538	0.136	0.637	b.d.	b.d.	0.208	0.375	0.101	7.660	b.d.	7.145	0.727
18-2-12	1.207	6.992	0.295	7.492	0.108	0.349	b.d.	b.d.	0.108	0.311	0.058	3.352	b.d.	3.894	0.434
18-2-13	2.026	3.832	0.501	7.299	0.080	0.479	b.d.	b.d.	0.097	0.404	0.037	2.611	0.901	2.513	0.302
18-2-14	1.769	7.805	0.384	9.268	0.122	0.702	b.d.	b.d.	0.207	0.409	0.071	3.047	b.d.	6.361	0.547
18-2-15	1.769	22.898	0.397	5.909	0.157	0.578	0.281	b.d.	0.171	0.355	0.095	0.000	0.087	6.116	0.675
18-2-16	1.877	3.107	0.425	10.327	0.133	0.583	b.d.	0.001	0.153	0.441	0.069	5.981	b.d.	4.955	0.463
18-2-17	1.131	2.633	0.249	5.238	0.096	0.411	b.d.	0.010	0.127	0.115	0.063	3.684	b.d.	4.249	0.452
18-2-18	3.299	5.655	0.850	13.944	0.174	0.840	b.d.	b.d.	0.207	0.476	0.087	2.843	b.d.	6.667	0.543
18-2-19	1.395	5.465	0.335	12.635	0.088	0.401	b.d.	b.d.	0.109	0.240	0.061	5.346	1.955	3.608	0.488
18-2-20	1.257	2.437	0.281	7.014	0.062	0.419	b.d.	b.d.	0.129	0.074	0.069	2.835	b.d.	4.767	0.463
18-2-21	1.226	1.020	0.273	4.048	0.068	0.385	b.d.	b.d.	0.115	0.115	0.056	5.376	b.d.	3.967	0.370
18-2-22	0.970	2.165	0.220	0.944	0.120	0.328	b.d.	b.d.	0.101	0.176	0.045	5.252	b.d.	3.371	0.364
18-2-23	0.343	b.d.	0.083	2.170	b.d.	0.087	b.d.	0.005	0.012	0.115	b.d.	6.585	b.d.	b.d.	b.d.
18-2-24	3.291	4.651	0.736	4.223	0.100	0.986	b.d.	0.007	0.183	0.199	0.079	1.876	b.d.	6.704	0.480
18-2-25	1.596	25.391	0.419	9.919	0.134	0.214	b.d.	b.d.	0.029	0.253	0.017	7.334	b.d.	0.770	0.174
18-2-26	3.305	18.589	0.846	10.368	0.102	0.468	b.d.	b.d.	0.061	0.492	0.057	3.266	b.d.	2.835	0.571

B.D. = Below Detection